

Ph.D. Thesis

Nonlinear Model Predictive Control for Oil Reservoirs Management

Andrea Capolei

Technical University of Denmark
Department of Applied Mathematics and Computer Science
Building 303B, Matematiktorvet, DK-2800 Kongens Lyngby, Denmark
IMM-PhD-2013-315



Technical University of Denmark
Department of Applied Mathematics and Computer Science
Building 303B, Matematiktorvet, DK-2800 Kongens Lyngby, Denmark
Phone +45 45253031
compute@compute.dtu.dk
www.compute.dtu.dk
IMM-PhD-2013-315

Preface

This thesis was prepared at the Department of Applied Mathematics and Computer Science (DTU Compute) and the Center for Energy Resources Engineering (CERE), Technical University of Denmark (DTU), in partial fulfillment of the requirements for receiving the Ph.D. degree in applied mathematics.

The work presented in this thesis was carried out from May 2010 to August 2013. During the period January-February 2012, I was visiting researcher at Center for Integrated Operations in Petroleum Industry (IO Center) at NTNU (Trondheim, Norway) under the supervision of prof. Bjarne Foss.

The PhD research project presented in this thesis is fully financed by the Danish Research Council for Technology and Production Sciences. FTP Grant no. 274-06-0284. The project was supervised by John Bagterp Jørgensen.

A handwritten signature in black ink, appearing to read 'Andrea Capolei', with a stylized, cursive script.

Andrea Capolei

Lyngby, 31-July-2013

to my wife, Elena.

Summary

The current world average recovery factor from oil fields is widely agreed to be about 30 – 35%. An increase of 10% point of this recovery factor would bring about 500 billion of oil barrels, sufficient to meet 16 years of current global production. To realize this potential production increase, the research community is working on improving current feedback model-based optimal control technologies.

The topic of this thesis is production optimization for water flooding in the secondary phase of oil recovery. We developed numerical methods for nonlinear model predictive control (NMPC) of an oil field. The controller consists of

- A model based optimizer for maximizing some predicted financial measure of the reservoir (e.g. the net present value).
- A parameter and state estimator.
- Use of the moving horizon principle for data assimilation and implementation of the computed control input.

The optimizer uses gradient-based optimization and the required gradients are computed by the adjoint method. We propose the use of efficient high order implicit time integration methods for the solution of the forward and the adjoint equations of the dynamical model. The Ensemble Kalman filter is used for data assimilation. Further, we studied the use of robust control strategies in both open-loop, i.e. without measurement feedback, and closed-loop, i.e. with measurement feedback, configurations.

This thesis has three main original contributions:

1. The first contribution in this thesis is to improve the computationally expensive gradient computation by using high-order ESDIRK (Explicit Singly Diagonally Implicit Runge-Kutta) temporal integration methods and continuous adjoints. The high order integration scheme allows larger time steps and therefore faster solution times. We compare gradient computation by the continuous adjoint method to the discrete adjoint method and the finite-difference method. We demonstrate that the optimization algorithm can be accelerated by using the continuous time adjoint equations. This is the first time in the literature that the higher order continuous adjoint and higher order discrete adjoint methods have been investigated for oil production optimization.
2. The second contribution of this thesis is the application of the Robust Optimization strategy in both open-loop (i.e. without measurement feedback) and closed-loop (i.e. with measurement feedback). In the oil industry, Robust Optimization has been suggested to compensate for inherent geological uncertainties in an oil field. In robust optimization of an oil reservoir, the water injection and production borehole pressures are computed such that the predicted net present value of an ensemble of permeability field realizations is maximized. In our study, the permeability field is the uncertain parameters. We compare the performance of the RO strategy to a certainty equivalent optimization strategy, based on the ensemble mean of the permeability field realizations as its permeability field, and to a reactive strategy. In open-loop, for the case studied, the reactive strategy performed better than the open-loop RO strategy. These observations are non-trivial, as previous literature suggests that the open-loop RO strategy performs better than the reactive strategy. Simulations indicate that the inferior performance of the open-loop RO strategy compared to the reactive strategy is due to the inability of the RO strategy to efficiently encompass ensembles with very different and conflicting optimal control trajectories. Hence, we propose a modified RO strategy that allow shut in of uneconomical wells. The modified RO strategy performs significantly better than the other open-loop strategies and the reactive strategy. Finally, this is the first time in literature that the RO optimization has been investigated in closed-loop. Surprisingly, for the case studied, the closed-loop certainty equivalent strategy yields a higher NPV than the closed-loop RO strategy. The uncertainty reduction of the permeability field estimate due to data assimilation explains the good performance of the closed-loop certainty equivalent optimization strategy. Consequently, in closed-loop, the increased computational effort of the RO strategy compared to the certainty equivalent strategy is not justified for the particular case studied in this paper.
3. The third contribution of this thesis is a mean-variance method for risk mitigation in production optimization of oil reservoirs. We introduce a return-risk bicriterion objective function for the profit-risk tradeoff. With this objective function we link the optimization problem in production optimization to the Markowitz portfolio optimization problem in finance or to the the robust design problem in topology optimization. In this study we focus on open-loop configuration, i.e.

without measurement feedback. We demonstrate that a return-risk bi-criterion objective function is a valuable tool for the profit-risk tradeoff. If combined with the previous contribution, this result trigger the necessity of comparing the closed-loop CE strategy with the closed-loop MV strategy.

The thesis consists of a summary report and a collection of five research papers written during the period May 2010 to August 2013. Three papers are published in conference proceedings, one paper is published in *Computational Geosciences* journal and another paper is submitted to *Journal of Petroleum Science and Engineering*.

Summary (Danish)

På nuværende tidspunkt er den gennemsnitlige indvindingsgrad af verdens oliefelter bredt accepteret til at ligge omkring 30-35%. En forøgelse af indvindingsgraden på 10% vil resultere i omkring 500 milliarder tønder olie; svarende til 16 års udvinding ved nuværende produktion på verdensplan. For at realisere denne potentielle produktionsforøgelse arbejder forskningsmiljøerne på at forbedre nuværende feedback modelbaserede optimale reguleringsteknologier.

Denne afhandling omhandler produktionsoptimering ved vandinjektion i anden fase af olieudvindingen. Vi har udviklet numeriske metoder til non-lineær modelprædiktiv regulering (NMPC) af et oliefelt. Regulatoren består af

- En modelbaseret optimeringsalgoritme til at maximere en given prædikeret økonomisk målestok (f.eks. nuværende netto værdi).
- En parameter og tilstandsestimator.
- Brug af 'moving horizon' princippet til databehandling og implementation af regulatorinput

Optimeringsalgoritmen bruger gradientbaseret optimering, og de krævede grader beregnes ved 'adjoint method'. Vi anbefaler anvendelsen af effektive højordens implicite tidsintegrationsmetoder til løsningen af the forward and adjoint equations for den dynamiske model. Ensemble Kalman filter anvendes til databehandling. Vi har yderligere undersøgt anvendelsen af robuste reguleringsstrategier i både åben sløjfe, dvs. uden feedback fra de målte variable, og lukket sløjfe, dvs. med feedback fra de målte variable

3 hovedelementer udgør denne afhandling:

1. Første element i denne afhandling er at effektivisere den beregningsmæssigt dyre gradientberegning ved anvendelse af højjordens ESDIRK (EksPLICIT Singular Diagonalt Implicit Runge-Kutta) tidsmæssig integration samt continuous adjoints. Højjordens integrationsmetoden muliggør længere tidsskridt og dermed hurtigere beregningstider. Vi sammenligner gradientberegning ved continuous adjoint method to discrete adjoint method samt med Finite Difference metoden. Vi viser, at optimeringsalgoritmen kan gøres hurtigere ved brug af continuous time adjoint equations.
2. Andet element i denne afhandling omhandler anvendelsen af robust optimering i både åben sløjfe (dvs. uden feedback fra målte variable) og i lukket sløjfe (dvs. med feedback fra målte variable). Inden for olieindustrien er robust optimering blevet foreslået som en måde at kompensere for de geologiske unøjagtigheder i et oliefelt. Ved robust optimering af et oliereservoir beregnes trykket ved vandinjektions- samt produktionsbrøndene således, at den prædikterede netto værdi af et ensemble af feltets permeabilitetsrepræsentationer maksimeres. I vores studie udgør feltets permeabilitet usikkerhedsparametren. Vi sammenligner ydelsen af den robuste optimeringsstrategi med en given tilsvarende optimeringsstrategi, hvor feltets permeabilitet beregnes baseret på et gennemsnit over et ensemble af feltets permeabilitetsrepræsentationer, samt til en reaktiv strategi.
3. Det tredje bidrag til denne afhandling er en 'mean-variance' metode for risiko nedsættelse modvirkning i produktions optimering af olie reservoirer. Vi introducerer en retur-risiko bi-kriterium objektiv funktion for fortjeneste risiko tradeoff. Med denne objektiv funktion, linker vi optimeringens problemet i produktions optimering til Markowitz portefølje optimerings problemet i finans eller til det robuste designproblem i topologi optimering. I dette studie fokuserer vi på open-loop konfiguration, dvs. uden maling(s) feedback tilbagemelding.

Denne afhandling består et resume' samt en artikkelsamling bestående af 5 artikler skrevet i perioden maj 2010 til august 2013. 3 artikler er udgivet som conferenceartikler, en er udgivet i tidsskriftet Computational Geosciences Journal og endnu en er i forberedelsesfasen til indsendelse og en anden artikel er indsendt til Journal of Petroleum Science and Engineering.

Glossary

List of abbreviations

The following abbreviations are used in this thesis:

AD	Automatic Differentiation
BFGS	Broyden-Fletcher-Goldfarb-Shanno
BHP	Bottom-hole pressure
CE	Certainty equivalent
CLRM	Closed-loop Reservoir Management
EnKF	Ensemble Kalman Filter
EOR	Enhanced Oil Recovery
ESDIRK	Explicit Singly Diagonally Implicit Runge-Kutta
KKT	Karush-Kuhn-Tucker
mD	milli Darcy
MPC	Model Predictive Control
MV	Mean-variance
NMPC	Nonlinear Model Predictive Control
NPV	Net Present Value
NO	Nominal
PDE	Partial Differential Equation
RK	Runge-Kutta
RO	Robust Optimization
SQP	Sequential Quadratic Programming

Contents

Preface	i
Summary	v
Summary (Danish)	ix
1 Introduction	1
1.1 Reservoir Simulation	2
1.2 Closed-loop Reservoir Management	3
1.2.1 Model Based Optimization	4
1.2.2 Data Assimilation	5
1.3 Production Optimization under Uncertainty	6
1.4 Contribution	7
1.5 Thesis Organization	10
2 Preliminaries	13
2.1 Reservoir Model	13
2.1.1 Two Phase Flow Model	14
2.1.2 Wells	17
2.2 Gradient based Optimization	18
2.2.1 Control Parametrization	19
2.2.2 Input Constraints	20
2.2.3 Single Shooting Optimization	20
2.3 Parameter Estimation with the Ensemble Kalman Filter (EnKF)	21
2.3.1 Basic Ensemble Kalman Filter	21
2.3.2 Performance Metrics	24
3 ESDIRK Integration methods	27
3.1 ESDIRK Methods	28

4	Gradients Computations	31
4.1	Forward Sensitivities	32
4.1.1	Discrete Sensitivity Equations	33
4.1.2	Convergence- and Error-Control	35
4.2	Continuous Adjoint Method	36
4.2.1	Solving the Adjoint Equations	37
4.2.2	Continuous Extension	38
4.3	Discrete Adjoint Method	39
4.3.1	Solving the Discrete System	40
4.4	Case Study I: Production Optimization for a Conventional Oil Field	42
4.4.1	Discussion of the Results	44
4.4.2	Summary	47
5	Production Optimization under Uncertainty	53
5.1	Optimal Control Problem	54
5.1.1	Control Constraints	55
5.1.2	Certainty-Equivalent, Robust, and Mean-Variance Optimization	56
5.2	Key Performance Indicators	57
5.2.1	Profit, Risk and Market Solution	58
5.2.2	Cumulative Productions Indicators	59
5.2.3	Uncertain Parameters	60
5.2.4	Optimizer	60
5.3	Case Study II: Robust Optimization Performances	62
5.3.1	Open-Loop Optimization	63
5.3.2	Closed-Loop optimization	68
5.3.3	Summary	70
5.4	Case study III: Mean-Variance Optimization	85
5.4.1	Description of the Test Cases	86
5.4.2	Test Case I	87
5.4.3	Test Case II	92
5.4.4	Summary	94
6	Concluding Remarks and Recommendations for Further Work	97
A	Useful Results	101
A.1	ESDIRK Coefficients	101
A.2	Proof of Proposition 1.	104
A.3	Proof of Proposition 4.	106
A.4	Derivatives $\frac{\partial R_{j,i}}{\partial X_{j,l}}$	107
A.5	Computation of the MV Objective and its Gradients	108
B	Paper I	111
C	Paper II	119

CONTENTS**xvii**

D Paper III	127
E Paper IV	149
F Paper V	173
Bibliography	191

CHAPTER 1

Introduction

More than 9 billion people are expected to live on Earth by 2050, up from 7 billion today. As living standards improve for many across the world and more people buy their first refrigerators, computers or cars, energy use will rise. Total global energy demand could rise by up to 80% by mid-century from its level in 2000. Despite up to 50% of the world's energy mix could come from renewables and nuclear in 2050, fossil fuels (i.e. coal, oil and natural gas) will still be main sources of energy. Global proved oil reserves at the end of 2012 are sufficient to meet about 52 years of global production and the number of new significant oil fields found per year is decreasing [1]. Further, the current world average recovery factor from oil fields is widely agreed to be 30 – 35%. Increasing this recovery with 10% point would bring about 500 billion of oil barrels, sufficient to meet 16 years of global production. To realize this potential production increase, the research community is working on improving current oil recovery techniques.

Oil is generally found in sandstones and limestones, beneath the earth surface. The rock containing the oil is called the reservoir rock. An important rock property for oil extraction is the porosity, i.e. the fraction of the rock that can be occupied by the fluids. Another important property is the permeability, which describes the ability of the rock to transmit fluids through interconnected pores. A suitable reservoir rock must be porous, permeable, and contain enough oil to make it economically feasible for the operating company to drill and produce oil. After the exploration phase, where reservoirs are identified and wells are drilled, oil fields are developed in two or three

phases. In the primary phase, the reservoir pressure is large enough to make the oil flow to the production wells. In the secondary phase, water must be injected to maintain pressure and move the oil towards the producers. In some cases, a tertiary phase known as enhanced oil recovery is considered. Enhanced oil recovery includes technologies such as in situ combustion, surfactant flooding, polymer flooding, and steam flooding [2]. After the secondary phase, typically the oil recovery is somewhere between 10% and 50% [3, 4].

In this thesis we describe numerical techniques from system and control theory to improve the oil recovery process in the secondary phase. Specifically, we focus on:

- Reservoir simulation
- Closed-loop reservoir management
- Production Optimization under Uncertainty

1.1 Reservoir Simulation

Reservoir simulation is the simulation of the flow of fluids (typically, oil, water, and gas) through porous media under the wells' control (usually well's bottom hole pressure or liquid rate). Mathematically, the model description is given through a system of nonlinear partial differential equations (PDEs). After spatial and temporal discretization, these PDEs are reduced to a system of nonlinear equations. The state of the reservoir (pressure, saturation, fluid composition, rock properties) is updated in time by solving this system of nonlinear equations. There are a number of different mathematical reservoir models as well as different discretization techniques. In this thesis, we use the method of lines to discretize the reservoir equations, i.e. we first discretize the equations in space and then in time. However, we describe in detail only the time discretization. The space discretization is done in the same way as described in [5], to which we refer for further details. For temporal integration we propose a high order temporal integration method (Explicit Singly Diagonally Implicit Runge-Kutta, ESDIRK) for forward computation of the initial value problem and for backward solution of the associated continuous-time and discrete-time adjoints. Conventional practice by commercial reservoir simulators is limited to the use of first order temporal implicit or semi-implicit integrators for the initial value problem and the adjoints. [6–8] introduce high order ESDIRK methods in two phase reservoir simulation and production optimization based on the discrete adjoints. However, they use only first order (implicit Euler) adjoint computation. We extend that work by using a high order scheme also for gradient computation. Further, we consider the use of the continuous adjoint for gradient computation. A high order scheme allows larger steps and therefore faster solution of the reservoir model equations.

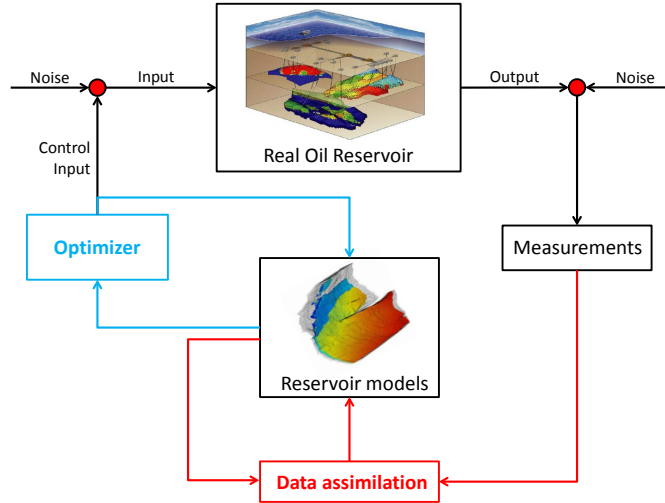


Figure 1.1: Closed loop reservoir management

In our study, we consider two reservoir models:

1. A slightly compressible two phase flow. We implement a Matlab reservoir simulator based on finite volume discretization in space and ESDIRK discretization in time. With this model we show the opportunity to exploit efficient high order time integration schemes and its adjoint gradient computation.
2. An incompressible two phase flow implemented in the MRST reservoir simulator [9, 10]. We use this simulator in combination with a code, developed by [10], that compute discrete adjoint gradients. With this second model we study the closed-loop reservoir management and the mean-variance optimization concepts. These two concepts are further explained in the subsequent sections.

1.2 Closed-loop Reservoir Management

In the oil industry, closed-loop reservoir management (CLRM) has been suggested to maximize oil recovery or a financial measure such as the net present value of a given oil reservoir [11–22]. Fig. 1.1 illustrates the components in closed-loop reservoir management. The controller consists of model based data assimilation (red box and arrows in Fig. 1.1), also known as a parameter and state estimator, and a model based optimizer (blue box and arrows in Fig. 1.1) for maximizing the oil recovery or some predicted

financial measure such as the net present value. The inputs to the controller are production measurements, forecasts of the oil price, the interest rate, and the operating unit costs. Based on these inputs the controller computes water injection trajectories as well as borehole pressure trajectories. Only the first part of these trajectories are implemented in the real oil reservoir. As new measurements become available, the process is repeated. The parameters and the states of the model are re-estimated using the data assimilation component. These filtered states and parameters are used in the model based optimization for computation of optimal trajectories for the manipulated variables, and the first part of the trajectories are implemented. This form of control is also known as Nonlinear Model Predictive Control (NMPC) [23–29]. A key difference of NMPC applied to reservoir management with traditional process control applications, is the size of the model describing the system. In reservoir management, spatial discretization of the partial differential equation (PDE) system describing the flow results in a system of differential equations that is much larger (sizes of $10^4 - 10^7$ are common in oil problems) than the systems typically encountered in process control applications. The large-scale nature of the closed-loop reservoir management problem requires special numerical techniques for the data assimilation [30] as well as the optimization [31, 32].

1.2.1 Model Based Optimization

In CLRM, model based optimization is called production optimization. Production optimization aims to find the optimal control input that maximize a performance index, e.g. net present value or oil recovery, for the life time of the oil reservoir. The control input for oil reservoirs can be well rates, bottom-hole pressures (bhp), and valve/choke settings.

Litterature studies show that in conventional waterflooding of an oil field, optimal control strategies may enable higher oil recovery than with a conventional reactive strategy in which producers are closed based on water breakthrough. There are different optimization methods available in the oil litterature. A first classification consists in considering global optimization methods (e.g. simulated annealing, swarm-based optimization algorithms) versus nonlinear programming methods. Nonlinear programming methods cannot guarantee to find a global optimum since they aim to find a local optimum. However, due to the large computational costs of the global optimization methods, nonlinear programming methods are most used in practice. Among the nonlinear programming methods we can differentiate between derivative-free methods and gradient based methods. When the gradients are available from the reservoir simulator, the gradient based methods are more efficient compared to the derivative free methods [33]. In gradient based methods, gradients can be computed by a perturbation method (e.g. finite difference method), by the adjoint method or by an ensemble-based method [34, 35]. The perturbation method perturbs the simulator computation around a nominal value. This method is computational expensive and affected by numerical

noise. Computing the gradient using the adjoint method is more laborious because requires knowledge of the internal of a simulator. The ensemble-based computation is a more recent approach that promises to be a good compromise among computational cost, quality of the gradient computation, and ease of implementation.

Once the gradients are available, we need to choose the optimization method to use. In this work we will to a large extent use existing state of art optimization packages (i.e. Knitro, Matlab's `fmincon`). We also implement a sequential quadratic programming (SQP) algorithm with line-search and BFGS approximation of the Hessian [36].

1.2.2 Data Assimilation

Data assimilation is the process of reconstructing, in the presence of uncertainties, unknown reservoir's quantities based on the available measurements such as production data, well logs or seismic data. Usually fluid and rock properties such as permeability, porosity, saturation, pressure and fault location are estimated.

Data assimilation techniques are mostly used in fields like meteorology [37], oceanography [37], groundwater flow [38] and reservoir simulation [39]. There are two different approaches to data assimilation: the variational approach and the sequential approach. The variational approach uses optimization techniques that aim to minimize a distance between measured data and forecasts from the model. This is done by adjusting initial conditions and/or parameters [40–42]. The most known sequential approach is Kalman filtering [43]. Kalman filtering is an effective tool for solving uncertain linear models. A recent development of the Kalman filter, the Ensemble Kalman Filter (EnKF) has gained a lot of attention in the reservoir community. The EnKF method is a Monte Carlo implementation of the Kalman filter [44]. EnKF uses an ensemble of prior models and updates them every time a new measurement is available. When all the ensemble members are updated, a new prediction of the reservoir's performance can be estimated. Data assimilation by the EnKF is a popular method for history matching as well as closed-loop reservoir management [11, 13, 14, 16, 45]. In [46], different data assimilation and optimization methods are tested on the synthetic "Brugge field" to maximize its NPV. The three best results are all obtained by methods using an EnKF for data assimilation. The literature available on the EnKF in petroleum engineering is rather large and mature. Data assimilation using the ensemble Kalman filter has been reviewed by [47–49] and [30, 50, 51] provide overviews of filtering techniques. A review of various issues of the EnKF, including sampling error because of small ensembles, covariance localization (limiting the influence of the observations to the state variables that are located spatially close to them), filter divergence, and model error, is given in [48] and [47]. [52] describes the necessity of introducing a confirming step to ensure consistency of the updated static and dynamic variables with the flow equations, while [47] discusses the reduction of the ensemble size with a resam-

pling scheme. The problem of ensemble collapse is discussed in [53]. [54] considers a way to handle model constraints within the EnKF. [55] investigates an update step that preserves multi-point statistics and not only two point-statistics.

In this thesis we implement an EnKF algorithm in Matlab to do parameter estimation.

1.3 Production Optimization under Uncertainty

When we approximate the real reservoir behaviour by using a numerical model, we should keep in mind two important aspects of the approximation that we are doing. First of all, not all the physics occurring in a real reservoir can be modelled in an appropriate way. In general, many simplifications are imposed on the model, to make the problem computationally tractable. Secondly, there is usually a large uncertainty in the parameter values of the simulation model. Geophysical and fluid properties (e.g. reservoir structure, the initial fluid contacts, the values of permeabilities, porosities, fault transmissibilities, etc.), as well as the amount of hydrocarbons present in the reservoir are poorly known. These reservoir related parameters are assumed to be known in conventional production optimization algorithms [12–14, 18, 21, 22, 56, 57]. However, neglecting the uncertainties leads to results produced by numerical reservoir models that contradict the data gathered from the real field. It is then difficult to make decisions based only on the output of a numerical model. In the oil industry, Robust Optimization (RO) [56, 58] has been suggested to compensate for the inherent geological uncertainties in an oil field. In RO of an oil reservoir, the water injection and production borehole pressures (bhp) are computed such that the expected net present value (NPV) of an ensemble of realizations of the permeability field is maximized. In conventional production optimization, the nominal net present value (NPV) of the oil reservoir is maximized (to compute the NPV, nominal values for the model's parameters are taken). In certainty equivalent production optimization, the expected reservoir model parameters are used in the maximization. The purpose of the robust production optimization is to (indirectly) mitigate the significant uncertainties in the parameters of the reservoir model. However, by the certainty equivalent and the robust production optimization methods, the trade-off between expected profit (NPV) and risk (variance of the NPV) is not addressed directly. Compared to a certainty equivalent optimization which uses a single realization of the reservoir model, in RO the risk is reduced because we model the uncertainty with an ensemble of realizations of the reservoir model. Fig. 1.2 illustrates risk versus expected return (mean) for different optimization and operation strategies. This is a sketch that shows the qualitative behaviour of the results in this thesis. As it is evident, certainty equivalent optimization and RO strategy indicate that a significant risk (variance in the NPV) is associated with these strategies. The implication is that the RO strategy may improve current operation, but you cannot be sure due to the significant risk arising from the uncertain reservoir model. This is

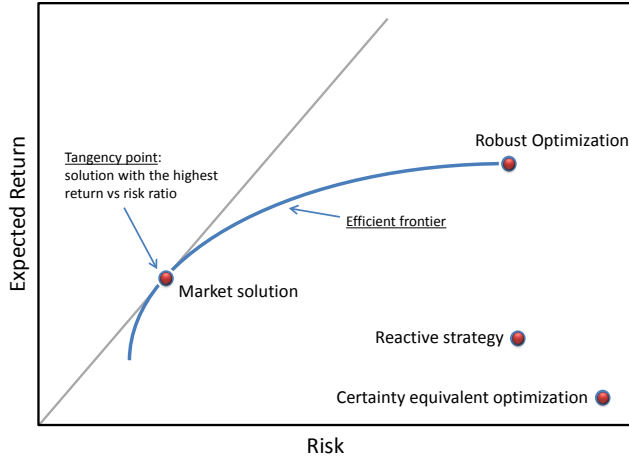


Figure 1.2: A sketch of the trade-off between risk and expected return in different optimization methods implemented in the optimizer for model based production optimization.

probably one of the reasons that NMPC for CLRM has not been widely adopted in the operation of oil reservoirs. The optimization problem in production optimization can be compared in some sense to Markowitz portfolio optimization problem in finance [59, 60] or to robust design in topology optimization [61, 62]. The key to mitigate risk is to optimize a bi-criterion objective function including both expected return (NPV) and risk (variance of NPV) for the ensemble of possible reservoir models. In this way, we can use a single parameter to compute an efficient frontier (the blue Pareto curve in Fig. 1.2) of risk and expected return. One limit of this efficient frontier represents the robust optimization, while the other limit is the minimum risk minimum return solution. By proper balancing the risk and the return in the bi-criterion objective function, we can tune the optimizer in the controller such that an optimal ratio of return vs risk is obtained (such a solution is called the Market solution in Fig. 1.2).

1.4 Contribution

In this section we describe the three main contributions of this thesis, putting them in perspective with current state-of-art research.

1. *Efficient High Order Forward and Adjoint Gradients Computation by ESDIRK Methods*

To compute the gradient of the objective function in a single shooting optimization method, [63] introduces the discrete adjoint of a generic Runge-kutta method to solve an optimal control problem governed by ODEs. [64] shows that such discrete adjoint has the same order and linear stability as the forward integrator. He also points out that the calculation of gradients by reverse automatic differentiation leads to the discrete adjoint approach. [4] provide an overview of gradient computation using the discrete adjoint. [12] and [65] explain and demonstrate gradient computation by the adjoint equations based on the implicit Euler discretization. [66] describes the continuous adjoint method and studies the stability of the continuous adjoint system. [67] suggest the continuous-time high order adjoint equations for gradient computation in production optimization. [6–8] introduce high order ESDIRK methods in two phase reservoir simulation and production optimization based on the implicit Euler discrete adjoints. The high order scheme allows larger steps and therefore faster solution of the reservoir model equations. [21] apply high order continuous-time adjoint based on ESDIRK to a conventional oil field case study. [68] compare gradients computed by discrete and continuous adjoints for problems arising in aerodynamics. They conclude that the gradients computed from continuous adjoints is accurate enough to be used in optimization algorithms. Since computation of gradients based on continuous time adjoints is faster than gradients based on discrete adjoints, this conclusion implies that the gradient computations can be accelerated by using the continuous time adjoint equations.

The novel contribution in this thesis is that we formulate and compare the adjoint gradient computation of high order ESDIRK methods. Using the ESDIRK method, the continuous adjoint method is able to use a time grid different than the time grid used in the forward integration. So it can compute the sensitivities much faster than the discrete adjoint method and the finite-difference method. Computational experiments (See section 4.4) show that when the time steps are controlled in a certain range, the continuous adjoint method produces gradients sufficiently accurate for the optimization algorithm and somewhat faster than the discrete adjoint method.

2. *Study of Open-loop and Closed-loop Robust Optimization Strategies*

In the model based optimization part of CLRM, a traditional choice is to use methods based on one realization, usually the ensemble mean from the EnKF. To reduce the risk arising from uncertainty in the geological description, [58] proposes to optimize the expectation of net present value over a set of reservoir models using a gradient based method. This procedure is referred to as robust optimization (RO). In open-loop simulations, [58] compares the results of the RO procedure to two alternative approaches: a nominal optimization (NO) and a reactive control approach. They find that RO yields a much smaller variance than the alternatives. Moreover the RO strategy significantly improves the expected NPV over the alternative methods (on average 9.5% higher than using reactive-control and 5.9% higher than the average of NO strategies). [34, 45, 69]

do closed-loop reservoir management using an EnKF for data assimilation and robust optimization with a gradient-free ensemble based optimization scheme for the model based optimization. [34] reports that an ensemble based optimization results in a NPV improvement of 22% compared to a reactive strategy. However, they do not compare the closed-loop robust strategy to a closed-loop certainty equivalent strategy.

In general, for open-loop implementations, previous test case studies presented in the literature, show that a traditional robust optimization strategy (RO) gives a higher expected NPV with lower NPV standard deviation than a conventional reactive strategy. We present and study a test case (see section 5.3) where the opposite happen: The reactive strategy gives a higher expected NPV with a lower NPV standard deviation than the RO strategy. To improve the RO strategy, we propose a modified robust optimization strategy (modified RO) that can shut in uneconomical producer wells. This strategy inherits the features of both the reactive and the RO strategy. Simulations reveal that the modified RO strategy results in operations with larger returns and less risk than the reactive strategy, the RO strategy, and the certainty equivalent strategy. The returns are measured by the expected NPV and the risk is measured by the standard deviation of the NPV.

To our knowledge, there is no closed-loop application of the gradient-based robust optimization strategy as implemented in [58] available in the literature. Furthermore, the CLRM literature misses an open-loop as well as a closed-loop comparison of the performance of an ensemble based optimization scheme [34] or a gradient-based robust optimization scheme [58] with a certainty equivalent optimization strategy based on the ensemble mean. In this thesis we partially fill this gap and do CLRM comparing a RO strategy [58] to three alternative approaches: a reactive strategy, a nominal strategy, and a certainty equivalent strategy. By using feedback, the ensemble of permeability fields converge to a point such that the RO strategy becomes equivalent to the certainty equivalent strategy based on the ensemble mean. The RO is more expensive computationally than the certainty equivalent strategy. In Section 5.3 we use a case study to compare the RO strategy in both open-loop and closed-loop configurations to other strategies.

3. *Return-risk Mitigation in Production Optimization* In Chapter 5 we address the problem of including the risk management in a standard robust gradient based optimization algorithm. We introduce a mean-variance model to the oil problem by adding a variance term to the robust objective function. In the oil literature, previous efforts to explicitly include a risk measure in the objective function did not give any insight on the risk-return relationship. In [70] they improve the sweep efficiency by equalizing the arrival time of the waterfront at all producers using multiple geologic realizations. They address geological uncertainty in terms of two forms of objective functions: 1) a stochastic form which includes the expected value and the standard deviation combined with a risk coefficient

and 2) a min-max form which minimizes the worst case scenario. [71] propose the use of a multi-objective optimization strategy. They optimize the sum of three different objective functions. Each objective function consist of a weighted combination of expected value and standard deviation. However, in both these works the relation between risk and the expected value or how to choose the adversion factors are not clear. A main contribution of this thesis is to demonstrate, that a return-risk bi-criterion objective function is a valuable tool for the profit-risk tradeoff. We do this for the open loop optimization and do not consider the effect of feedback (see Section 5.4).

1.5 Thesis Organization

This thesis is divided into 6 chapters and 6 appendices.

- *Chapter 1* - In this chapter we give the background and motivation behind the project
- *Chapter 2* - This chapter provides preliminary materials for the next chapters. We describe the oil reservoir models used in this work, we formulate the constrained optimal control problem involved in the oil production optimization problem and we describe the ensemble Kalman filter i.e. the data assimilation method used in this thesis for parameter estimation.
- *Chapter 3* - In this chapter we describe our implementation of the ESDIRK method for time integration of the reservoir model and for computation of the objective function.
- *Chapter 4* - In this chapter we describe sensitivity computation using continuous and the discrete ESDIRK adjoint methods. For completeness, we present also the forward sensitivity computation using ESDIRK. Finally, we present a case study where the continuous adjoint and the discrete adjoint methods are compared in a production optimization study.
- *Chapter 5* - In this chapter we deal with production optimization under uncertainty. We formulate a mean-variance objective function for the oil problem and demonstrate that RO is a special extreme case of this objective function. Finally, we present two case studies.

In the first case study we compare both the open-loop and the closed loop performances of the CE and the RO strategies.

In the second case study we investigate and compare the performance of the mean-variance optimization to a certainty equivalent optimization, a reactive

control strategy, and RO. In this second case study we consider only open-loop excerpts of the solution.

- *Chapter 6* - Concluding remarks and recommendation for further work are given in this chapter.
- *Appendix A* - This appendix reports the ESDIRK coefficients and some useful results used in this thesis.
- *Appendix B - F* - These appendices report three published conference papers, one journal paper published in Computational Geosciences journal and one journal paper submitted to *Journal of Petroleum Science and Engineering*. The material presented in the papers and in the thesis overlap to some extent. However, they are complementary, since both contain details that are not presented elsewhere.

CHAPTER 2

Preliminaries

This chapter provides preliminary materials for the next chapters. We describe the oil reservoir models used in this work, we formulate the constrained optimal control problem involved in the oil production optimization problem, and we describe the ensemble Kalman filter for parameter or state estimation.

This chapter is based on [21, 56].

2.1 Reservoir Model

An oil reservoir is a porous medium that contains a mixture of hydrocarbons and water. In general, the hydrocarbon part consists of many components but a common simplification is to assume a three phase (oil, gas, water) description known as the black oil model [72–74]. In this thesis, we assume that the reservoirs are in the secondary recovery phase (waterflooding) where the pressures are above the bubble point pressure of the oil phase. Therefore, two-phase immiscible flow, i.e. flow without mass transfer between the two phases, is a reasonable assumption. In this section we present two reservoir models used in this thesis. The first reservoir model is a slightly compressible two-phase flow. We developed an oil reservoir simulator in the same way as described in [5]. The second model is an incompressible two phase flow. We do

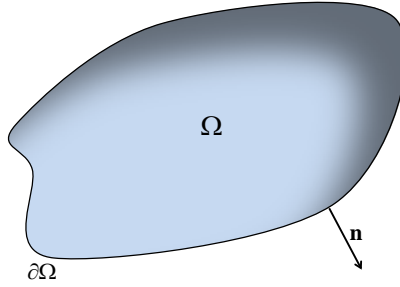


Figure 2.1: Porous media domain Ω

not develop an oil reservoir simulator for this second reservoir model. Instead, we use the MRST [9] reservoir simulator. In both reservoir models we assume incompressible rocks, constant porosity, no gravity effects or capillary pressure, no-flow boundaries, and isothermal conditions.

2.1.1 Two Phase Flow Model

The two-phase flow is described by a mass conservation equation and by the Darcy's law [73]. Let $\Omega \subset \mathbb{R}^d$ ($d \leq 3$) be a porous medium domain with frontier $\partial\Omega$ and let \mathbf{n} be the outward pointing unit normal on the boundary as depicted in Fig. 2.1. The mass conservation of water ($l \equiv w$) and oil ($l \equiv o$)

$$\frac{\partial}{\partial t} C_l(P_l, S_l) = -\nabla \cdot F_l(P_l, S_l) + \tilde{Q}_l, \quad l \in \{w, o\}, \quad \mathbf{r} \in \Omega \quad (2.1)$$

states that the difference in mass flowing out of a unit volume per unit time, $\nabla \cdot F_l(P_l, S_l)$ $\left[\frac{Kg}{m^3s} \right]$, plus the mass added or extracted through an external source/sink (well), \tilde{Q}_l , must be equal to the accumulation of mass per unit of time and volume, $\frac{\partial}{\partial t} C_l$.

In (2.1), $F_l = \rho_l(P_l) \mathbf{u}_l(P_l, S_l)$ $\left[\frac{Kg}{m^2s} \right]$ is the flux of phase l , \mathbf{u}_l $\left[\frac{m}{s} \right]$ is the velocity of phase l , $C_l = \phi \rho_l(P_l) S_l$ is the mass concentration of phase l , S_l is the saturation of the phase l defined as the proportion of the pore space occupied by the respective phase, ϕ is the porosity defined as the ratio of aggregated pore space to the volume of the entire rock, ρ_l is the density of phase l , and P_l is the pressure of phase l . The well terms \tilde{Q}_l are

given by

$$\tilde{Q}_w = \sum_{i \in \mathcal{I}, \mathcal{P}} \rho_w \cdot q_{w,i} \cdot \delta(\mathbf{r} - \mathbf{r}_i) \quad (2.2a)$$

$$\tilde{Q}_o = \sum_{i \in \mathcal{P}} \rho_o \cdot q_{o,i} \cdot \delta(\mathbf{r} - \mathbf{r}_i) \quad (2.2b)$$

where \mathcal{I} and \mathcal{P} are the set of injector and producer wells, respectively, $\delta(\mathbf{r} - \mathbf{r}_i)$ $[\frac{1}{m^3}]$ is the Dirac's delta function, $q_{w,i}$ $[\frac{m^3}{s}]$ and $q_{o,i}$ are the volumetric water and oil rates at well i .

Darcy's law

$$\mathbf{u}_l(P_l, S_l) = -\mathbf{K} \lambda_l \left(\nabla P_l - \rho_l(P_l) g \nabla z \right) \quad (2.3)$$

with the boundary condition

$$\mathbf{u}_l \cdot \mathbf{n} = 0, \quad l \in \{w, o\}, \quad x \in \partial\Omega \quad (2.4)$$

gives the macroscopic phase velocity.

In (2.3), $\lambda_l = \frac{k_{rl}(S_l)}{\mu_l}$ is the mobility of phase l , k_{rl} $[-]$ is the relative permeability of phase l , μ_l $[Pa \cdot s]$ denotes the viscosity of phase l , g $[\frac{m}{s^2}]$ is the gravitational acceleration, z $[m]$ denotes depth, and \mathbf{K} $[m^2]$ stands for the absolute permeability tensor. The absolute permeability represents the ability to flow or transmit fluids through a rock when a single phase is present in the rock. In general the permeability tensor \mathbf{K} is a full 3×3 matrix. However, in practical applications, the orientation of the coordinate system can be aligned with geological layering in the reservoir such that the permeability tensor \mathbf{K} becomes a diagonal matrix:

$$1D: \mathbf{K} = k, \quad 2D: \mathbf{K} = \begin{pmatrix} k_x & 0 \\ 0 & k_y \end{pmatrix}, \quad 3D: \mathbf{K} = \begin{pmatrix} k_x & 0 & 0 \\ 0 & k_y & 0 \\ 0 & 0 & k_z \end{pmatrix} \quad (2.5)$$

The saturations and the pressure of the two phases are linked by the relations [73] :

$$S_w + S_o = 1 \quad (2.6)$$

$$P_o - P_w = P_c(S_w) \quad (2.7)$$

P_c $[Pa]$ is the oil-water capillary pressure, which depends on the water saturation S_w . The densities are assumed to be linear functions of the pressures [72, 73]

$$\rho_l = \rho_l(P_l) = \rho_l^0 (1 + c_l(P_l - P_l^0)) \quad l \in \{w, o\} \quad (2.8)$$

where ρ_l^0 and P_l^0 are densities and pressures references and c_l is the compressibility of phase l .

In this thesis, we consider only 2D flows and isotropic permeability fields (i.e. $k_x = k_y = k$). Also gravity forces and capillary pressure are ignored i.e. $P_o = P_w = P$. Then combining (2.1) for each of phases l with (2.2) and (2.3), the 2D slightly compressible two-phase flow system used in this thesis takes the form:

$$\frac{\partial}{\partial t} (\phi \rho_w(P) S_w) = \nabla \cdot (\rho_w(P) \lambda_w \mathbf{K} \nabla P) + \sum_{i \in \mathcal{I}, \mathcal{D}} \rho_w \cdot q_{w,i} \cdot \delta(\mathbf{r} - \mathbf{r}_i) \quad (2.9a)$$

$$\frac{\partial}{\partial t} (\phi \rho_o(P) S_o) = \nabla \cdot (\rho_o(P) \lambda_o \mathbf{K} \nabla P) + \sum_{i \in \mathcal{D}} \rho_o \cdot q_{o,i} \cdot \delta(\mathbf{r} - \mathbf{r}_i) \quad (2.9b)$$

Incompressible Two-Phase Flow

In case of an incompressible reservoir, the governing equations can be represented by pressure and saturation equations [73].

The pressure equation is described as

$$\begin{aligned} \mathbf{u} &= -\lambda_t \mathbf{K} \nabla P, & \nabla \cdot \mathbf{u} &= \sum_{i \in \mathcal{I}, \mathcal{D}} q_i \cdot \delta(\mathbf{r} - \mathbf{r}_i) & \text{in } \Omega \\ \mathbf{u} \cdot \mathbf{n} &= 0 & \text{on } \partial\Omega \end{aligned} \quad (2.10)$$

where $\mathbf{u} = \mathbf{u}_w + \mathbf{u}_o$ is the Darcy velocity (total velocity), $q_i [\frac{m^3}{s}]$ is the volumetric well rate, and $\lambda_t = \lambda_w + \lambda_o$ is the total mobility, which in this setting is the sum of the water and oil mobility functions.

The saturation equation is given by

$$\phi \frac{\partial}{\partial t} S_w + \nabla \cdot (f_w(S_w) \mathbf{u}) = \sum_{i \in \mathcal{I}, \mathcal{D}} q_{w,i} \cdot \delta(\mathbf{r} - \mathbf{r}_i) \quad (2.11)$$

$f_w(S_w)$ is the water fractional flow which is defined as

$$f_w(S_w) = \frac{\lambda_w}{\lambda_t} \quad (2.12)$$

Fig. 2.2 illustrates the water fractional flow as function of the water saturation.

Relative Permeabilities

When more phases are flowing simultaneously, they interfere with each other. To take this effect into account, the concept of relative permeabilities is introduced. They represent the additional resistance to flow of a phase caused by the presence of the other phase. They are considered to be functions of water saturation only. Their values are derived based on laboratory measurements performed on core samples taken from a

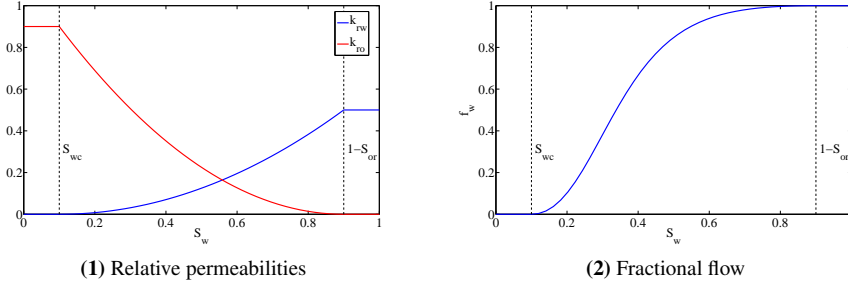


Figure 2.2: Typical clipped relative permeabilities and fractional flow curves.

real reservoir. However, in this thesis, the Corey model [72, 73] is used to describe the relationship between relative permeabilities and water saturation:

$$k_{rw} = k_{rw}^0 S^{n_w} \quad (2.13a)$$

$$k_{ro} = k_{ro}^0 (1 - S)^{n_o} \quad (2.13b)$$

and

$$S = \frac{S_w - S_{wc}}{(1 - S_{or} - S_{wc})} \quad (2.14a)$$

k_{rw}^0 and k_{ro}^0 are the end-point relative permeabilities for the oil and water respectively. n_o and n_w are the Corey exponents. S_{or} is the residual oil saturation and S_{wc} is the connate water saturation. Fig. 2.2 shows typical clipped relative permeability curves.

2.1.2 Wells

Wells are implemented using the Peaceman well model [75]

$$q_i = -\lambda_t W I_i (p_i - p_i^{bhp}) \quad (2.15)$$

p_i^{bhp} is the wellbore pressure, and $W I_i$ is the Peaceman well-index. The volumetric water flow rates at injection and production wells are

$$q_{w,i} = q_i \quad i \in \mathcal{I} \quad (2.16a)$$

$$q_{w,i} = f_w q_i \quad i \in \mathcal{P} \quad (2.16b)$$

The volumetric oil flow rates at production wells are

$$q_{o,i} = (1 - f_w) q_i \quad i \in \mathcal{P} \quad (2.17)$$

At time t , the cumulative oil production, $Q_o(t)$ [m^3], and the cumulative water injection, $Q_w(t)$ [m^3], are

$$Q_o(t) = \int_0^t \sum_{i \in \mathcal{D}} q_{o,i} dt \quad (2.18)$$

$$Q_w(t) = \int_0^t \sum_{i \in \mathcal{I}} q_i dt \quad (2.19)$$

Spatial Discretization

The slightly compressible reservoir model is developed in the same way as implemented in [5]. [5] use a first order spatial discretization consisting of a finite volume (FV) discretization of the equations (2.9) combined with a two point flux approximation (TPFA) of the fluxes F_l . The resulting discretized equations are integrated in time using an ESDRIK method. The incompressible reservoir model is implemented in the MRST [9] reservoir simulator. Also MRST uses a first order spatial discretization method. The pressure and saturation equations, (2.10) and (2.11), are first discretized by the FV method with TPFA and then solved sequentially (explicit-pressure and implicit-saturation).

In general, after spatial discretization, both reservoir models used in this thesis reduce to an initial value problem (IVP) in the general form [5]

$$x(t_a) = x_0 \quad (2.20a)$$

$$\frac{d}{dt} g(x(t)) = f(x(t), u(t), \theta), \quad t \in [t_a, t_b], \quad (2.20b)$$

$x(t)$ is the state vector consisting of the pressures and saturations of each reservoir's grid block, $u(t)$ is the control vector consisting of wells bhp or wells liquid rates and θ is a parameter vector. We will use this IVP formulation in the next section to define the constrained optimal control problem that we solve in oil production optimization.

2.2 Gradient based Optimization

In this section, we present the continuous-time constrained optimal control problem and its transcription by the single shooting method to a finite dimensional constrained optimization problem. First we present the continuous-time optimal control problem. Then we parametrize the control function using piecewise constant basis functions. Finally, we convert the problem into a constrained optimization problem using the single shooting method.

Consider the continuous-time constrained optimal control problem in the Bolza form [76, 77]

$$\max_{x(t), u(t)} J = \hat{\Phi}(x(t_b)) + \int_{t_a}^{t_b} \Phi(x(t), u(t)) dt \quad (2.21a)$$

subject to

$$x(t_a) = x_0 \quad (2.21b)$$

$$\frac{d}{dt} g(x(t)) = f(x(t), u(t), \theta), t \in [t_a, t_b], \quad (2.21c)$$

$$u(t) \in \mathcal{U}(t) \quad (2.21d)$$

$x(t) \in \mathbb{R}^{n_x}$ is the state vector, $u(t) \in \mathbb{R}^{n_u}$ is the control vector and θ is a parameter vector in an uncertain space Θ (in our case the permeability field). The time interval $I = [t_a, t_b]$ as well as the initial state, x_0 , are assumed to be fixed. (2.21c) represents the dynamic model and includes systems described by index-1 differential algebraic equations (DAE). (2.21d) represents linear constraints on the input values, e.g. $u_{\min} \leq u(t) \leq u_{\max}$ and some constraints related to the rate of movement that are dependent on the input parametrization. In our formulations, we do not allow nonlinear state or output constraints, see e.g. [57] for a discussion of output constraints.

2.2.1 Control Parametrization

Let T_s denote the sample time such that an equidistant mesh can be defined as

$$t_a = t_0 < \dots < t_S < \dots < t_N = t_b \quad (2.22)$$

with $t_j = t_a + jT_s$ for $j = 0, 1, \dots, N$. We use a piecewise constant representation of the control function on this equidistant mesh, i.e. we approximate the control vector for every subinterval $[t_j, t_{j+1}]$ by the zero-order-hold parametrization

$$u(t) = u_j, u_j \in \mathbb{R}^{n_u}, t_j \leq t < t_{j+1}, j \in \mathcal{N} \quad (2.23)$$

with

$$\mathcal{N} = \{0, 1, \dots, N-1\}. \quad (2.24)$$

With this discretization we can introduce the discretized control vector

$$\bar{u} = \begin{bmatrix} u_0 \\ u_1 \\ \vdots \\ u_{N-1} \end{bmatrix} \quad (2.25)$$

2.2.2 Input Constraints

The input constraints (2.21d) include bound constraints $u_{\min} \leq u_k \leq u_{\max}$. In the discrete problem using the zero-order-hold parametrization, we also include rate of movement constraints in the form $\Delta u_{\min} \leq \Delta u_k \leq \Delta u_{\max}$ with $\Delta u_k = u_k - u_{k-1}$.

2.2.3 Single Shooting Optimization

We use a single shooting algorithm [21, 78] for solution of (2.21). Alternatives are multiple-shooting [79, 80] and collocation methods [81]. Despite the fact that multiple-shooting and collocation methods offer better convergence properties than the single shooting method [79–81], their application in production optimization is restricted by the large state dimension of production optimization problems. The use of multiple shooting is prevented by the need for computation of state sensitivities. The collocation method do not allow for adaptive time stepping and would need to solve huge-scale optimization problems. In the single shooting optimization algorithm, we define the function

$$\begin{aligned} \psi(\bar{u}, x_0, \theta) = & \left\{ J = \int_{t_a}^{t_b} \Phi(x(t), u(t)) dt + \hat{\Phi}(x(t_b)) : \quad x(t_0) = x_0, \right. \\ & \left. \frac{d}{dt} g(x(t)) = f(x(t), u(t), \theta), t_a \leq t \leq t_b, \quad u(t) = u_k, t_k \leq t < t_{k+1}, k \in \mathcal{N} \right\} \end{aligned} \quad (2.26)$$

such that (2.21) can be approximated with the finite dimensional constrained optimization problem [82]

$$\max_{\bar{u}} \quad \psi = \psi(\bar{u}, x_0, \theta) \quad (2.27a)$$

$$s.t. \quad c(\bar{u}) \geq 0 \quad (2.27b)$$

We use gradient based methods [10] for solution of (2.27). To compute the required gradients of the objective function (2.26) with respect to the control vector parameters, i.e. $\partial \psi / \partial u_k$, $k \in \mathcal{N}$ we use the adjoint method. In Chapter 4 we describe how to compute adjoint gradients using ESDIRK methods.

In solving (2.27), a gradient based method seek to converge to a solution where the Karush-Kuhn-Tucker (KKT) [82, 83] conditions hold. A solution u^* , which yields optimal states x^* , of the optimization problem (2.27) is said to satisfy the KKT conditions

if there exist a Lagrange multiplier vector $\mu^* \in \mathbb{R}^{n_c}$, with components μ_i^* , such that

$$\begin{aligned} \nabla_{\bar{u}} \psi(\bar{u}, x_0) + \nabla_{\bar{u}} c(u^*) \mu^* &= 0 \\ c(u^*) &\geq 0 \\ \mu_i^* &\geq 0 \quad i = 1, \dots, n_c \\ \mu_i^* \cdot c(u^*)_i &= 0 \quad i = 1, \dots, n_c \end{aligned} \quad (2.28)$$

To solve the KKT equations (2.28) we use different optimizers. For the case study presented in Section 4.4, we developed a quasi-Newton implementation of Powell's Sequential Quadratic Programming (SQP) method with linesearch for stepsize selection and BFGS update of the Hessian. The method is described in [36]. For the case studies presented in Section 5.3 and Section 5.4 we use two commercial optimization software packages: Knitro [84] and Matlab's `fmincon` function [85]. Both of these software have two main solvers, which are based on state-of-art active-set and interior-point methods. When using Knitro as well as `fmincon`, we select an interior point method since we experience the lowest computation times with this method. Further details on the optimizers are given in the case studies.

2.3 Parameter Estimation with the Ensemble Kalman Filter (EnKF)

We use the Ensemble Kalman filter (EnKF) for estimating the permeability field. The estimation is based on production data measurements. The EnKF is a Monte Carlo implementation of the Kalman filter [23, 43, 86, 87] using an ensemble of n_d realizations to represent the necessary first and second moments (means and covariances). In this section we describe the EnKF.

Consider the discrete time system

$$x_{k+1} = F(x_k, u_k, \theta) \quad (2.29a)$$

$$y_k = G(x_k, u_k) + v_k \quad v_k \sim N(0, R) \quad (2.29b)$$

2.3.1 Basic Ensemble Kalman Filter

(2.29a) includes the states, x , and the parameters, θ . Therefore, we form the augmented state space model

$$x_{k+1} = F(x_k, u_k, \theta_k) \quad (2.30a)$$

$$\theta_{k+1} = \theta_k \quad (2.30b)$$

and apply the EnKF to the dynamic equation (2.30) and the measurement equation (2.29b). In the EnKF all means and covariances are represented by samples of the stochastic variables. Therefore, the initial mean and covariance of the augmented states, $[x_k, \theta_k]$, are represented by

$$\left\{ x_{0|0}^i, \theta_{0|0}^i \right\}_{i=1}^{n_d} = \left\{ x_0, \theta_{0|0}^i \right\}_{i=1}^{n_d} \quad (2.31)$$

It should be noted that the initial states, x_0 , in our case are assumed to be known exactly. Only the parameters, θ , are uncertain. Index i refers to each of the n_d members of the ensemble, i.e. each realization.

In the following, we describe the algorithm for discrete time instant k . In general, at discrete time instant k , both the states and the parameters from the previous instant, $k-1$, are uncertain. This is denoted

$$\left\{ x_{k-1|k-1}^i, \theta_{k-1|k-1}^i \right\}_{i=1}^{n_d} \quad k = 1, 2, \dots \quad (2.32)$$

In the EnKF, the one-step prediction step is conducted by passing each ensemble member through the dynamics (2.30) such that for $i = 1, 2, \dots, n_d$

$$x_{k|k-1}^i = F(x_{k-1|k-1}^i, u_{k-1}, \theta_{k-1|k-1}^i), \quad (2.33a)$$

$$\theta_{k|k-1}^i = \theta_{k-1|k-1}^i, \quad (2.33b)$$

where the previous input, u_{k-1} , is known. Then the output, $z_{k|k-1}^i$, and the measurement, $y_{k|k-1}^i$, at discrete time k may be computed as

$$z_{k|k-1}^i = G(x_{k|k-1}^i, u_{k-1}) \quad i = 1, 2, \dots, n_d \quad (2.34a)$$

$$y_{k|k-1}^i = z_{k|k-1}^i + v_k^i \quad i = 1, 2, \dots, n_d \quad (2.34b)$$

To obtain the correct covariances of the state estimates in the EnKF, it is important that each ensemble member, $y_{k|k-1}^i$, contain measurement noise, $v_{k|k-1}^i$ [88]. It should also be noted that u_{k-1} is used in the evaluation of G in (2.34a). The explanation for the use of u_{k-1} is that we use a zero-order-hold representation of $u(t)$, i.e. $u(t) = u_{k-1}$ for $t_{k-1} \leq t < t_k$, and that we assume the measurement is conducted at time $t_k^- = \lim_{t < t_k} t$. Then, at time t_k , the EnKF and optimal control computations are conducted infinitely fast such the next decisions, $u(t) = u_k$ for $t_k \leq t < t_{k+1}$, can be implemented at time t_k .

The innovation, e_k^i , for each ensemble member is computed using the actual measurement, y_k , and the predicted measurement

$$e_k^i = z_{k|k-1}^i - y_k \quad i = 1, 2, \dots, n_d \quad (2.35a)$$

$$e_k^i = y_k - y_{k|k-1}^i = -e_k^i - v_k^i \quad i = 1, 2, \dots, n_d \quad (2.35b)$$

In these equations, y_k is the actual measurement and therefore a deterministic variable. In the EnKF, the realized trajectory of the system and an ensemble of different state trajectories are considered. In the derivation of the standard Kalman filter [23, 86, 87], it is the other way around. A (infinite) number of system realizations are considered, while the filter is represented by one deterministic trajectory (the mean).

The optimal linear estimator conditioned on the innovations are [86]

$$x_{k|k}^i = x_{k|k-1}^i + K_{x,k} e_k^i \quad i = 1, 2, \dots, n_d \quad (2.36a)$$

$$\theta_{k|k}^i = \theta_{k|k-1}^i + K_{\theta,k} e_k^i \quad i = 1, 2, \dots, n_d \quad (2.36b)$$

with the Kalman filter gains computed as

$$K_{x,k} = \langle x_{k|k-1}, e_k \rangle \langle e_k, e_k \rangle^{-1} \quad (2.37a)$$

$$K_{\theta,k} = \langle \theta_{k|k-1}, e_k \rangle \langle e_k, e_k \rangle^{-1} \quad (2.37b)$$

using the covariances

$$\langle x_{k|k-1}, e_k \rangle = \langle x_{k|k-1}, \boldsymbol{\varepsilon}_k \rangle \quad (2.38a)$$

$$\langle \theta_{k|k-1}, e_k \rangle = \langle \theta_{k|k-1}, \boldsymbol{\varepsilon}_k \rangle \quad (2.38b)$$

$$\langle e_k, e_k \rangle = \langle \boldsymbol{\varepsilon}_k, \boldsymbol{\varepsilon}_k \rangle + \langle v_k, v_k \rangle \approx \langle \boldsymbol{\varepsilon}_k, \boldsymbol{\varepsilon}_k \rangle + R \quad (2.38c)$$

The Kalman gains may be based on direct computation of the empirical estimates ($\langle x_{k|k-1}, e_k \rangle$, $\langle \theta_{k|k-1}, e_k \rangle$, $\langle e_k, e_k \rangle$) or the relations in (2.38). We choose to base the computations on (2.38). The approximate first moments (means) are computed as

$$\hat{z}_{k|k-1} = E \{ \hat{z}_{k|k-1} \} \approx \frac{1}{n_d} \sum_{i=1}^{n_d} z_{k|k-1}^i$$

$$\hat{\boldsymbol{\varepsilon}}_k = E \{ \boldsymbol{\varepsilon}_k \} \approx \frac{1}{n_d} \sum_{i=1}^{n_d} \boldsymbol{\varepsilon}_k^i = \hat{z}_{k|k-1} - y_k$$

$$\hat{x}_{k|k-1} = E \{ x_{k|k-1} \} \approx \frac{1}{n_d} \sum_{i=1}^{n_d} x_{k|k-1}^i$$

$$\hat{\theta}_{k|k-1} = E \{ \theta_{k|k-1} \} \approx \frac{1}{n_d} \sum_{i=1}^{n_d} \theta_{k|k-1}^i$$

and the approximate second moments (covariances) computed by

$$\langle x_{k|k-1}, \boldsymbol{\varepsilon}_k \rangle \approx \frac{1}{n_d - 1} \sum_{i=1}^{n_d} (x_{k|k-1}^i - \hat{x}_{k|k-1}) (\boldsymbol{\varepsilon}_k^i - \hat{\boldsymbol{\varepsilon}}_k)'$$

$$\langle \theta_{k|k-1}, \boldsymbol{\varepsilon}_k \rangle \approx \frac{1}{n_d - 1} \sum_{i=1}^{n_d} (\theta_{k|k-1}^i - \hat{\theta}_{k|k-1}) (\boldsymbol{\varepsilon}_k^i - \hat{\boldsymbol{\varepsilon}}_k)'$$

$$\langle \boldsymbol{\varepsilon}_k, \boldsymbol{\varepsilon}_k \rangle \approx \frac{1}{n_d - 1} \sum_{i=1}^{n_d} (\boldsymbol{\varepsilon}_k^i - \hat{\boldsymbol{\varepsilon}}_k) (\boldsymbol{\varepsilon}_k^i - \hat{\boldsymbol{\varepsilon}}_k)'$$

The result of (2.36) in this procedure is an ensemble

$$\left\{ x_{k|k}^i, \theta_{k|k}^i \right\}_{i=1}^{n_d} \quad k = 1, 2, \dots \quad (2.41)$$

representing the states and parameters at time k given measurements up until time k . Using this ensemble, a robust optimization may be performed or various statistics such as the mean may be computed.

(2.36) may result in non-physical updates. Therefore, we modify the EnKF such that the ensemble (2.41) satisfies physical constraints, e.g. that the permeabilities are in certain ranges. To mitigate such effects, we clip the solution according to the constraints

$$\theta_{k|k}^i := \begin{cases} \theta_{\min} & \theta_{k|k}^i < \theta_{\min} \\ \theta_{k|k}^i & \theta_{\min} \leq \theta_{k|k}^i \leq \theta_{\max} \\ \theta_{\max} & \theta_{k|k}^i > \theta_{\max} \end{cases} \quad (2.42)$$

and compute the filtered states, $\hat{x}_{k|k}^i$, by solving the dynamic model equations

$$x_{j+1|k}^i = F(x_{j|k}^i, u_j, \theta_{k|k}^i), \quad x_{0|k}^i = x_0, \quad j = 0, 1, \dots, k-1 \quad (2.43)$$

for each ensemble member, $i \in \{1, \dots, n_d\}$, using the clipped parameter estimates computed by (2.42). In this way, state updates consistent with the model is guaranteed [52]. In particular, this eliminates the possibility of nonphysical states (nonphysical pressures and saturations). The computational load can potentially be reduced by only doing the initial-value simulation when the estimated saturation and pressure changes passes a certain threshold [34]. The modifications (2.42) and (2.43) provides the ensemble (2.41) that is used for the optimal control computations and for the initiation of the EnKF at the next time step. Finally it should be mentioned that, the choice of the ensemble size, n_d , in the EnKF is a topic of research itself[89]. It affects the performance of the filter. In reservoir engineering an ensemble size of 100 is a common choice based on experience [14], [90]. However, this number is problem dependent and in some cases good results can also be obtained using ensembles with fewer members [90].

2.3.2 Performance Metrics

To measure the convergence of the Kalman filter estimates, we consider the mean standard deviation

$$\sigma_k = \sqrt{\frac{1}{n_p} \left(\frac{1}{n_d - 1} \sum_{i=1}^{n_d} \left\| \theta_{k|k}^i - \hat{\theta}_{k|k} \right\|_2^2 \right)} \quad (2.44)$$

of the parameters in the parameter vector, $\theta_{k|k}$. σ_k measures the ensemble spread. We also consider the root-mean-square-error of the parameter estimates compared to the true parameters, θ^0 :

$$RMSE_k = \frac{\|\hat{\theta}_{k|k} - \theta^0\|_2}{\sqrt{n_p}} \quad (2.45)$$

θ_k can be computed for real as well as synthetic cases, while $RMSE_k$ can only be computed for synthetic cases in which the true parameters, θ^0 , are available.

In the ideal case, the spread (2.44) should converge to a number related to the measurement noise and the root-mean-square-error (2.45) should converge to 0. In practice, (2.45) will not converge to zero due to e.g. factors like model-plant mismatch. Cases with divergence of the root-mean-square-error may indicate that the ensemble is too small to represent the true uncertainty.

CHAPTER 3

ESDIRK Integration methods

This chapter is based on [79].

In this section, we describe our implementation of the ESDIRK method. This implementation of ESDIRK is used to integrate a dynamical model in the general form

$$x(t_a) = x_0 \tag{3.1a}$$

$$\frac{d}{dt}g(x(t)) = f(x(t), u(t)), \quad t \in [t_a, t_b], \tag{3.1b}$$

as well as the objective function $\psi(\{u_k\}_{k=0}^{N-1}, x_0)$ in (2.26). Note that for notational simplicity we ignore the θ parameter because it is assumed to be fixed during the time integration.

ESDIRK methods are special implicit Runge-Kutta methods that are computationally efficient and often constructed such that they have an embedded error estimator and are both A- and L-stable as well as stiffly accurate [91–93]. This implies that they can be applied for solving stiff systems as well as index-1 differential algebraic equation systems. For problems with frequent discontinuities, such that in zero-order-hold parametrized optimal control problems, ESDIRK methods have been reported to outperform multi-step methods such as BDF for problems in which medium- to high-accuracy solutions are required [93–95]. [96] develops ESDIRK methods of order 1–3 with embedded error estimators, i.e. ESDIRK1(2), ESDIRK2(3) and ESDIRK3(4),

that are A- and L-stable as well as stiffly accurate. [97, 98] implement the ESDIRK3(4) with approximate computation of the sensitivities for ODEs and index-1 DAEs. [99] first shows how to solve a systems of differential equations in the form (3.1) by a fully implicit Runge-kutta (IRK) method using an efficient inexact newton method. [8] propose to use ESDIRK method to intergrate a reservoir model in the form (3.1).

In the oil community, it is believed that high order methods in the time domain are not needed because of the big uncertainty in the parameters and because of the significant non-smoothness of the solutions. Despite this, we believe that the greater accuracy of these methods is beneficial in improving convergence during the optimization process. Furthermore, high order methods are ideal in combination with a predictive step-size controller, that can significantly speed-up the integration process compared to conventional heuristic step-size algorithms.

3.1 ESDIRK Methods

Computation of $\psi(\{u_k\}_{k=0}^{N-1}, x_0)$ consists of two major operations: 1) For each integration step we first compute the model states $x(t)$ solving the initial value problem (3.1), 2) and then we compute, using the same quadrature points, the value of the Lagrange term (3.2)

$$\bar{\psi}(t) := \int_{t_a}^t \Phi(x(t), u(t)) dt \quad t_a \leq t \leq t_b. \quad (3.2)$$

in the cost function (2.21a). Let \tilde{t}_n denote the integration times chosen by the step size controller in the integrator. Each integration step size, h_n , is chosen such that it is smaller than or equal to the sample time, T_s . Therefore, one sample interval contains many integration steps. Fig. 3.1 illustrates this. We consider ESDIRK methods with s stages that are designed to be stiffly accurate and with an embedded error estimator [96, 97]. The numerical solution of the IVP (2.21c) by such ESDIRK method may in each integration step $[\tilde{t}_n, \tilde{t}_{n+1}]$ be denoted [7, 79]

$$T_1 = \tilde{t}_n, \quad T_i = \tilde{t}_n + c_i h_n \quad (3.3a)$$

$$X_1 = x_n, \quad u = u(\tilde{t}_n) \quad (3.3b)$$

$$\phi_i(\{X_j\}_{j=1}^{i-1}, u) = g(X_1) + h_n \sum_{j=1}^{i-1} a_{ij} f(X_j, u) \quad (3.3c)$$

$$g(X_i) = \phi_i(\{X_j\}_{j=1}^{i-1}, u) + h_n \gamma f(X_i, u) \quad (3.3d)$$

$$x_{n+1} = X_s \quad (3.3e)$$

$$e_{n+1} = h_n \sum_{j=1}^s d_i f(X_j, u) \quad (3.3f)$$

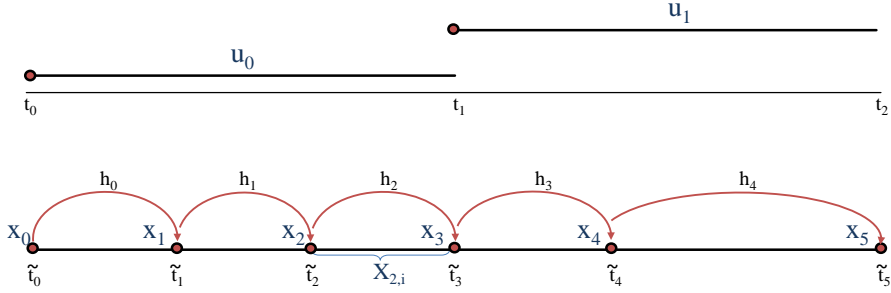


Figure 3.1: State and control input time-discretization. The figure shows a time horizon divided in 5 integration steps with 2 control steps. $X_{2,i}$ denotes the ESDIRK inner stages X_i in the integration step $[\tilde{t}_2, \tilde{t}_3]$.

with $i = 2, \dots, s$. X_i denotes the numerical solution at time T_i for $i \in \{1, \dots, s\}$. x_{n+1} is the numerical solution at time $\tilde{t}_{n+1} = \tilde{t}_n + h_n$. e_{n+1} is the estimated error of the numerical solution, i.e. $\|e_{n+1}\| \approx \|g(x_{n+1}) - g(x(\tilde{t}_{n+1}))\|$.

Subsequent to solution of (3.3), we compute the numerical solution of the cost function (3.2)

$$\bar{\psi}(\tilde{t}_{n+1}) = \bar{\psi}(\tilde{t}_n) + h_n \sum_{i=1}^s b_i \Phi(X_i, u) \quad (3.4)$$

When $\tilde{t}_{n+1} = t_b$, we add the Mayer term of (2.21a) such that

$$\Psi(\{u_k\}_{k=0}^{N-1}, x_0) = \Psi(t_b) = \bar{\psi}(t_b) + \hat{\Phi}(x(t_b)) \quad (3.5)$$

The main computational effort in the ESDIRK method is solution of the implicit equations (3.3d) using a Newton based method. (3.3d) is solved by sequential solution of

$$R_i(X_i) := [g(X_i) - h_n \gamma f(X_i, u)] - \phi_i(\{X_j\}_{j=1}^{i-1}, u) = 0 \quad (3.6)$$

for $i = 2, \dots, s$. (3.6) is solved using an inexact Newton method. Each iteration in the inexact Newton method for solution of (3.6) may be denoted

$$M \Delta X_i^{[l]} = -R_i(X_i^{[l]}) \quad (3.7a)$$

$$X_i^{[l+1]} = X_i^{[l]} + \Delta X_i^{[l]} \quad (3.7b)$$

The iteration matrix, M , is an approximation

$$M \approx \mathbf{J}(X_i^{[l]}) \quad (3.8)$$

to the Jacobian of the residual function

$$\mathbf{J}_i(X_i) = \frac{\partial R_i}{\partial X_i}(X_i) = \frac{\partial g}{\partial x}(X_i) - h_n \gamma \frac{\partial f}{\partial x}(X_i, u) \quad (3.9)$$

In this thesis we only consider direct methods for solution of the linear system (3.7). This implies that a sparse LU factorization is used for the factorization of the iteration matrix. The iteration matrix, M , and its LU factorization is updated adaptively by monitoring the convergence rate of the inexact Newton iterations. Convergence of the inexact Newton iteration is measured by

$$\|R_i(X_i^{[l]})\| = \max_{j \in \{1, \dots, n_x\}} \frac{|(R_i(X_i^{[l]}))_j|}{\max\{\text{atol}_j, \text{rtol}_j g_j(X_i^{[l]})\}} < \tau \quad (3.10)$$

where atol is the absolute tolerance and rtol is the relative tolerance. Steps are accepted if this measure of the residual is smaller than $\tau \approx 10^{-2}$. In case of divergence or slow convergence, the iterations are terminated, the step size, h_n , is decreased, and the Jacobian of the iteration matrix is re-evaluated and factorized. As explained in e.g. [7] and [79], the controller adjusts the temporal step sizes such that the error estimate satisfies a norm similar to the norm used in (3.10).

CHAPTER 4

Gradients Computations

This chapter is based on [19, 79].

The easiest way to implement computation of gradients is to use finite-difference methods [82]. These methods are easy to implement because they treat the oil reservoir simulator as a black box. However, due to the large number of state and control variables in oil problems, these methods become prohibitive. Another way to compute gradients is to use the sensitivity equations [100], which is still quite expensive. In fact, both of these methods have a time complexity of $O(n_u)$ objective function evaluations (2.26), where n_u is the dimension of the control input u . In this thesis we use the adjoint method to compute the gradients, which requires two times the evaluation of the objective function regardless of the dimension of control input. In order to validate the adjoint-gradient implementation, we compare the gradients produced by the adjoint methods against those from the finite difference computation.

In this chapter we discuss both the continuous and the discrete ESDIRK adjoint computation for a model in the form (3.1). For completeness, we also present the forward sensitivity computation for this kind of model equations. Finally, we present a case study where continuous adjoint, discrete adjoint, and finite difference computations are compared in a production optimization study. Simulations show that the continuous adjoint method produces gradients sufficiently accurate for the optimization algorithm and somewhat faster than the discrete adjoint method.

This is the first time in the literature that the higher order continuous adjoint and higher order discrete adjoint methods have been investigated for oil production optimization.

4.1 Forward Sensitivities

The contribution of this section is exact numerical computation of the sensitivities in differential equations (3.1) based on ESDIRK1(2), ESDIRK2(3) and ESDIRK3(4). The sensitivities are computed using the staggered corrector approach [97, 100] and an efficient inexact Newton algorithm that reuses the factorization of the iteration matrix. In this thesis we do not use forward sensitivities in the solution of the production optimization problem because of their higher computational effort compared to the adjoint method. Nevertheless, in this Section we present gradient computation using forward sensitivities because in [79] we use the solution of the differential equation (3.1) and its forward sensitivities in a multiple-shooting algorithm for constrained optimal control.

By introducing input and state sensitivities

$$\begin{aligned} S_{u_k}(t) &= \frac{\partial}{\partial u_k} x(t; x_0, \{u_j\}_{j=0}^{N-1}) \\ S_{x_0}(t) &= \frac{\partial}{\partial x_0} x(t; x_0, \{u_j\}_{j=0}^{N-1}) \end{aligned} \quad (4.1)$$

and considering that (2.23) implies

$$\frac{\partial u}{\partial u_k}(t) = \begin{cases} I & t_k \leq t < t_{k+1} \\ 0 & \text{otherwise} \end{cases}, \quad (4.2)$$

the gradients, $\partial\psi/\partial u_k$ and $\partial\psi/\partial x_0$, may be computed as

$$\begin{aligned} \frac{\partial\psi}{\partial u_k} &= \frac{\partial\hat{\Phi}}{\partial x} S_{u_k}(t_b) + \int_{t_a}^{t_b} \left(\frac{\partial\Phi}{\partial u} \frac{\partial u}{\partial u_k}(t) + \frac{\partial\Phi}{\partial x} S_{u_k}(t) \right) dt \quad k = 0, 1, \dots, N-1 \\ \frac{\partial\psi}{\partial x_0} &= \frac{\partial\hat{\Phi}}{\partial x} S_{x_0}(t_b) + \int_{t_a}^{t_b} \left(\frac{\partial\Phi}{\partial x} S_{x_0}(t) \right) dt \end{aligned} \quad (4.3)$$

in which $x(t)$ is computed by solution of (3.1). $S_{u_k}(t)$ satisfies

$$S_{u_k}(t) = 0, \quad t \leq t_k \quad (4.4a)$$

$$\begin{aligned} \frac{\partial}{\partial t} \left(\frac{\partial g}{\partial x}(x(t)) S_{u_k}(t) \right) &= \frac{\partial f}{\partial x}(x(t), u(t)) S_{u_k}(t) \\ &+ \frac{\partial f}{\partial u}(x(t), u(t)) \frac{\partial u}{\partial u_k}(t), \quad t \geq t_k \end{aligned} \quad (4.4b)$$

and $S_{x_0}(t)$ satisfies

$$S_{x_0}(t_a) = I \quad (4.5a)$$

$$\frac{\partial}{\partial t} \left(\frac{\partial g}{\partial x}(x(t)) S_{x_0}(t) \right) = \frac{\partial f}{\partial x}(x(t), u(t)) S_{x_0}(t) \quad (4.5b)$$

(4.36), (4.4) and (4.5) may be derived from (2.26) by taking the derivatives with respect to x_0 and u_k , using the chain rule and the Schwartz theorem.

4.1.1 Discrete Sensitivity Equations

The ESDIRK method is used in a staggered-corrector fashion to integrate the sensitivity equations (4.4) and (4.5) at the same quadrature points used for integration of the initial value problem (3.1).

In each integration step $[\tilde{t}_n, \tilde{t}_{n+1}]$, subsequent to the solution of (3.3), we compute the state sensitivities using the ESDIRK method by solution of

$$\bar{S}_{x_0,1} = S_{x_0,n} \quad (4.6a)$$

$$\Theta_{x,i} = \frac{\partial g}{\partial x}(X_1) \bar{S}_{x_0,1} + h_n \sum_{j=1}^{i-1} a_{ij} \frac{\partial f}{\partial x}(X_j, u) \bar{S}_{x_0,j} \quad (4.6b)$$

$$\frac{\partial g}{\partial x}(X_i) \bar{S}_{x_0,i} = \Theta_{x,i} + h_n \gamma \frac{\partial f}{\partial x}(X_i, u) \bar{S}_{x_0,i} \quad (4.6c)$$

$$S_{x_0,n+1} = \bar{S}_{x_0,s} \quad (4.6d)$$

for $i = 2, \dots, s$. The computationally expensive step in these computations is solution of the linear system of equations (4.6c)

$$R_{x,i}(\bar{S}_{x_0,i}) = J(X_i) \bar{S}_{x_0,i} - \Theta_{x,i} = 0 \quad (4.7)$$

with $J(X_i)$ defined by (3.9).

Similarly, the parameter sensitivities are computed using the ESDIRK method by solu-

tion of

$$\bar{S}_{u_k,1} = S_{u_k,n} \quad (4.8a)$$

$$\begin{aligned} \Theta_{u_k,i} &= \frac{\partial g}{\partial x}(X_1)\bar{S}_{u_k,1} \\ &+ h_n \sum_{l=1}^{i-1} a_{il} \left(\frac{\partial f}{\partial x}(X_l, u)\bar{S}_{u_k,l} + \frac{\partial f}{\partial u}(X_l, u) \frac{\partial u}{\partial u_k}(T_l) \right) \end{aligned} \quad (4.8b)$$

$$+ h_n \gamma \frac{\partial f}{\partial u}(X_i, u) \frac{\partial u}{\partial u_k}(T_i)$$

$$\frac{\partial g}{\partial x}(X_i)\bar{S}_{u_k,i} = \Theta_{u_k,i} + h_n \gamma \frac{\partial f}{\partial x}(X_i, u)\bar{S}_{u_k,i} \quad (4.8c)$$

$$S_{u_k,n+1} = \bar{S}_{u_k,s} \quad (4.8d)$$

for $i = 2, \dots, s$. The computationally expensive step in these computations is the solution of the linear system of equations (4.8c)

$$R_{u_k,i}(\bar{S}_{u_k,i}) = J(X_i)\bar{S}_{u_k,i} - \Theta_{u_k,i} = 0 \quad (4.9)$$

with $J(X_i)$ defined by (3.9).

Subsequent to solution of (4.6) and (4.8), we compute the numerical solution of (4.3) using the same quadrature points, i.e.

$$\begin{aligned} \frac{\partial \Psi}{\partial u_k}(\tilde{t}_{n+1}) &= \frac{\partial \Psi}{\partial u_k}(\tilde{t}_n) + h_n \sum_{i=1}^s \left(\frac{\partial \Phi}{\partial u} \frac{\partial u}{\partial u_k}(\tilde{t}_n) + \frac{\partial \Phi}{\partial x}(T_i)\bar{S}_{u_k,i} \right) \quad k = 0, 1, \dots, N-1 \\ \frac{\partial \Psi}{\partial x_0}(\tilde{t}_{n+1}) &= \frac{\partial \Psi}{\partial x_0}(\tilde{t}_n) + h_n \sum_{i=1}^s \left(\frac{\partial \Phi}{\partial x}(T_i)\bar{S}_{x_0,i} \right) \end{aligned} \quad (4.10)$$

When $\tilde{t}_{n+1} = t_b$, we add the gradient of the Mayer term comparing in (4.3), such that

$$\begin{aligned} \frac{\partial \Psi}{\partial u_k}(\{u_j\}_{j=0}^{N-1}, x_0) &= \frac{\partial \Psi}{\partial u_k}(\tilde{t}_b) + \frac{\partial \hat{\Phi}}{\partial x} S_{u_k}(t_b) \\ \frac{\partial \Psi}{\partial x_0}(\{u_j\}_{j=0}^{N-1}, x_0) &= \frac{\partial \Psi}{\partial x_0}(\tilde{t}_b) + \frac{\partial \hat{\Phi}}{\partial x} S_{x_0}(t_b) \end{aligned} \quad (4.11)$$

The linear system of equations (4.7) and (4.9) may be solved in identical ways. Therefore, we only discuss the solution of the state sensitivity equation (4.7) in the following. It is implied that the parameter sensitivity equation (4.9) is solved in a similar way.

(4.7) is solved using an inexact Newton method that employs that the LU-factors of an approximation, M , of the Jacobian matrix, $J(X_i)$, are already available. The steps in

this inexact Newton procedure may be denoted

$$M\Delta\bar{S}_{x_0,i}^{[l]} = -R_{x,i}(\bar{S}_{x_0,i}^{[l]}) \quad (4.12a)$$

$$\bar{S}_{x_0,i}^{[l+1]} = \bar{S}_{x_0,i}^{[l]} + \Delta\bar{S}_{x_0,i}^{[l]} \quad (4.12b)$$

where M is the already factorized matrix (3.8). These factors are used in the solution of (4.12a).

Convergence of the inexact Newton iteration is measured by

$$\|R_{x,i}(\bar{S}_{s_k,i}^{[l]})\| < \tau \quad (4.13)$$

using the norm defined by (3.10) columnwise. The tolerances specified for the differential equations (3.1) may be different from the tolerances specified for the sensitivity equations.

4.1.2 Convergence- and Error-Control

The ESDIRK method computes the sensitivities using a staggered-corrector approach [100]. First, the method solves for the state equations. Only when they have converged it solves the sensitivity equations. The method is implemented such that it satisfies the internal-numerical-differentiation principle [101]. Satisfaction of this principle is achieved by converging the discrete-time sensitivity equations (4.6) and (4.8) and keeping the same step size as used in the state equations. Consequently, no error estimation is needed in the sensitivity computations.

The step size controller for the state equations (3.3) is based on the error estimator embedded in the ESDIRK method. We use a predictive step size controller [102]. The convergence in the inexact Newton iterations is monitored by observing the ratio

$$\alpha_{l+1} = \frac{\|R_i^{l+1}\|}{\|R_i^l\|} \quad (4.14)$$

with R_i^l being the relevant residual at iteration l and $\|\cdot\|$ being the norm defined by (3.10). In case of divergence ($\alpha_{l+1} > 1$) the step size is reduced and the computations at the current step are repeated.

The initial guesses of the solution to the residual equations are obtained using an explicit Euler step from either the previous converged solution or the first stage value.

4.2 Continuous Adjoint Method

In this section, we describe a continuous-time adjoint based method for computation of the gradients $\frac{\partial \psi}{\partial u_k}$ $\frac{\partial \psi}{\partial x_0}$ of the objective function (2.26).

PROPOSITION 1 (GRADIENTS BASED ON CONTINUOUS ADJOINTS) *Consider the function $\psi = \psi(\{u_k\}_{k=0}^{N-1}; x_0)$ defined by (2.26).*

The gradients, $\partial \psi / \partial u_k$ and $\partial \psi / \partial x_0$, may be computed as

$$\frac{\partial \psi}{\partial u_k} = \int_{t_k}^{t_{k+1}} \left(\frac{\partial \Phi}{\partial u} - \lambda^T \frac{\partial f}{\partial u} \right) dt \quad k = 0, 1, \dots, N-1 \quad (4.15a)$$

$$\frac{\partial \psi}{\partial x_0} = -\lambda^T(t_a) \frac{\partial g}{\partial x}(t_a) \quad (4.15b)$$

in which $x(t)$ is computed by solution of (2.21b)-(2.21c) and $\lambda(t)$ is computed by solution of the adjoint equations

$$\frac{d\lambda^T}{dt} \frac{\partial g}{\partial x} + \lambda^T \frac{\partial f}{\partial x} - \frac{\partial \Phi}{\partial x} = 0 \quad (4.16a)$$

$$\frac{\partial \hat{\Phi}}{\partial x}(x(t_b)) + \lambda^T(t_b) \frac{\partial g}{\partial x}(x(t_b)) = 0 \quad (4.16b)$$

PROOF. See Appendix A.2.

REMARK 2 (COMPUTATION USING ESDIRK) *$x(t)$ is computed using the ESDIRK method applied to (2.21b)-(2.21c) and integrating forwards. This gives the approximations $x_n \approx x(t_n)$. This solution is stored. The same ESDIRK method is applied for computation of $\lambda(t)$ by solving (4.16) integrating backwards in time, see Fig. 4.1. A continuous extension of $x(t)$, see section 4.2.2, is used to compute approximations $\lambda(t)$ in the backward quadrature points. Finally, (4.15a) is integrated using the backward quadrature points used to compute $\lambda(t)$.*

REMARK 3 (GRADIENTS COMPUTED BY CONTINUOUS ADJOINTS) *The gradients computed using the continuous adjoints are not the exact gradients, $\partial \psi / \partial u_k$, when the involved differential equations and integrals are computed by discretization using the ESDIRK method. However, they can be made sufficiently precise for the optimizer such that they do not affect the convergence [68]. The advantage of the continuous adjoint equations (4.16) is that they can be solved faster than the adjoint equations for the discretized system (3.3)-(3.5).*

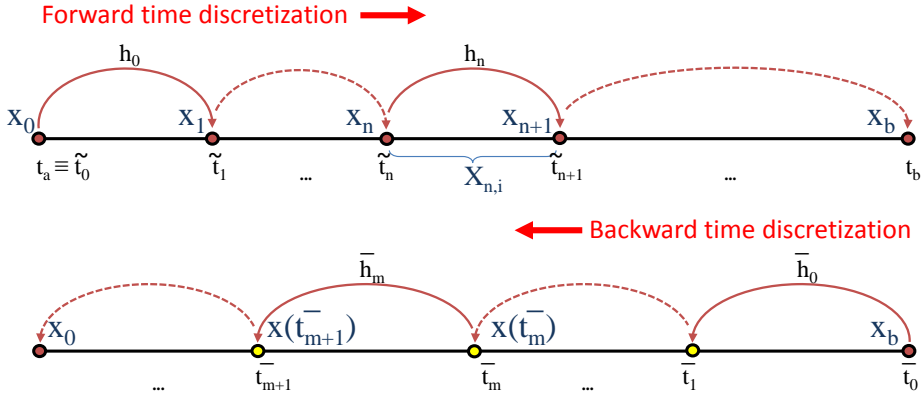


Figure 4.1: Forward and Backward time discretizations.

4.2.1 Solving the Adjoint Equations

Usually, integration software is written to integrate forward in time. Our ESDIRK methods are also implemented in that way. To integrate the linear equations (4.16), we introduce the change of variables

$$t = t_b + t_a - \bar{t} \quad (4.17)$$

$$\bar{\lambda}(\bar{t}) = \lambda(t_b + t_a - \bar{t}) \quad (4.18)$$

such that the transpose of (4.16) becomes

$$A(\bar{t}) \frac{d\bar{\lambda}}{d\bar{t}} - B(\bar{t})\bar{\lambda} + C(\bar{t}) = 0 \quad (4.19a)$$

$$D(t_a) + A(t_a)\bar{\lambda}(t_a) = 0 \quad (4.19b)$$

where

$$A(\bar{t}) = \nabla_x g(x(t_b + t_a - \bar{t})) \quad (4.20)$$

$$B(\bar{t}) = \nabla_x f(x(t_b + t_a - \bar{t}), u(t_b + t_a - \bar{t})) \quad (4.21)$$

$$C(\bar{t}) = \nabla_x \Phi(x(t_b + t_a - \bar{t}), u(t_b + t_a - \bar{t})) \quad (4.22)$$

$$D(\bar{t}) = \nabla_x \hat{\Phi}(x(t_b + t_a - \bar{t})) \quad (4.23)$$

We integrate this system (4.19) forward in $\bar{t} \in [t_a, t_b]$. The solution of system (4.19) by an s -stage, stiffly accurate, Runge-Kutta ESDIRK method may in each integration step

$[\bar{t}_{n-1}, \bar{t}_n]$ be denoted [103]

$$A(\bar{t}_{n-1})\dot{Y}_1 - B(\bar{t}_{n-1})\bar{\lambda}_{n-1} + C(\bar{t}_{n-1}) = 0 \quad (4.24a)$$

$$\begin{aligned} [A(\bar{t}_{n-1} + c_i\bar{h}_{n-1}) - \bar{h}_{n-1}\gamma B(\bar{t}_{n-1} + c_i\bar{h}_{n-1})]\dot{Y}_i &= B(\bar{t}_{n-1} + c_i\bar{h}_{n-1})[\bar{\lambda}_{n-1} + \\ &+ \bar{h}_{n-1} \sum_{j=1}^{i-1} a_{ij}\dot{Y}_j] - C(\bar{t}_{n-1} + c_i\bar{h}_{n-1}) \end{aligned} \quad (4.24b)$$

with $i = 2, \dots, s$ where

$$\dot{Y}_i \approx \frac{d\bar{\lambda}}{d\bar{t}}(\bar{t}_{n-1} + c_i\bar{h}_{n-1}) \quad (4.25)$$

$$Y_i = \bar{\lambda}_{n-1} + \bar{h}_{n-1} \sum_{j=1}^s a_{ij}\dot{Y}_j \approx \bar{\lambda}(\bar{t}_{n-1} + c_i\bar{h}_{n-1}) \quad (4.26)$$

$$\bar{\lambda}_n = \bar{\lambda}_{n-1} + \bar{h}_{n-1} \sum_{j=1}^s b_j\dot{Y}_j \approx \bar{\lambda}(\bar{t}_n) \quad (4.27)$$

The main computational effort in solving the adjoint equations using the ESDIRK method is to solve the linear equations (4.24).

4.2.2 Continuous Extension

When we solve the system (4.19) using the ESDIRK solver, we need a numerical approximation of the state vector $x(t)$ in temporal points \bar{T}_i that in general are not the same as the quadrature points T_i of the forward integration in (3.3). To compute this approximation we use a continuous extension. The numerical approximation to $x(\bar{t}_n + h_n\theta)$ for $\theta \in [0, 1]$ is given by [96, 97]

$$x(\bar{t}_n + h_n\theta) = x_n + h_n \sum_{i=1}^s \bar{b}_i(\theta) \bar{f}(X_i, u) \quad (4.28a)$$

X_i are the stage values of solving the system (3.3) in $t \in [\bar{t}_n, \bar{t}_{n+1}]$ and

$$\bar{f}(X_i, u) = \left[\frac{\partial g}{\partial x}(X_i) \right]^{-1} f(X_i, u). \quad (4.29)$$

$\bar{b}_i(\theta)$ is a matrix function [96, 97]

$$\bar{b}_i(\theta) = \sum_{k=1}^q \bar{b}_{i,k} \theta^k \quad (4.30)$$

where q is the order of the continuous extension. Further, the continuous extension used is of the same order as the forward integration method (except the extension for ESDIRK34 that is one order lower [96, 97]).

4.3 Discrete Adjoint Method

In this section, we describe a discrete adjoint based method to compute the gradients of the cost function with respect to the control vector parameters, $\partial\psi/\partial u_k$ for $k \in \mathcal{N}$. In the following, we use \bar{N} to indicate the total number of (forward) integration steps. Let $X_{j,i}$ denote the i -th stage values in the integration step $[\tilde{t}_j, \tilde{t}_{j+1}]$, see Fig. 3.1, such that we have

$$\begin{aligned} X_{0,1} &\equiv x_0, & t &= t_a = \tilde{t}_0 \\ X_{j,i}, & & t &\in [\tilde{t}_j, \tilde{t}_{j+1}] \\ X_{j+1,1} &\equiv X_{j,s}, & t &= \tilde{t}_{j+1} \quad \forall j \in \{0, \dots, \bar{N}-2\} \\ X_{\bar{N}-1,s}, & & t &= t_b = \tilde{t}_{\bar{N}} \\ \tilde{u}_j &\equiv u(\tilde{t}_j) = u_k & & \text{for some } k \in \mathcal{N}. \end{aligned} \quad (4.31)$$

With this notation, the ESDIRK discretization of (2.26) is

$$\begin{aligned} \psi(\{u_k\}_{k=0}^{N-1}, x_0) &= \left\{ J = \hat{\Phi}(X_{\bar{N}-1,s}) + \sum_{j=0}^{\bar{N}-1} \sum_{i=1}^s h_j b_i \Phi(X_{j,i}, \tilde{u}_j) : \right. \\ &\left. R_{j,i}(\{X_{j,l}\}_{l=1}^i, \tilde{u}_j) = 0 \quad j \in \{0, \dots, \bar{N}-1\}, i \in \{2, \dots, s\} \right\} \end{aligned} \quad (4.32)$$

and

$$\begin{aligned} R_{j,i} &= g(X_{j,i}) - \phi_{j,i}(\{X_{j,l}\}_{l=1}^{i-1}, \tilde{u}_j) - h_j \gamma f(X_{j,i}, \tilde{u}_j) \\ \phi_{j,i}(X_{j,1}, \dots, X_{j,i-1}, \tilde{u}_j) &= g(X_{j,1}) + h_j \sum_{l=1}^{i-1} a_{il} f(X_{j,l}, \tilde{u}_j). \end{aligned} \quad (4.33)$$

Introduce the vectors $\bar{x} \in \mathbb{R}^{(\bar{N}(s-1)) \cdot n_x}$, $\bar{R} \in \mathbb{R}^{(\bar{N}(s-1)) \cdot n_x}$, and $\bar{u} \in \mathbb{R}^{N \cdot n_u}$ by

$$\bar{x} = \begin{bmatrix} X_{0,2} \\ \vdots \\ X_{0,s} \\ X_{1,2} \\ \vdots \\ X_{\bar{N}-2,s} \\ X_{\bar{N}-1,2} \\ \vdots \\ X_{\bar{N}-1,s} \end{bmatrix}, \quad \bar{u} = \begin{bmatrix} u_0 \\ u_1 \\ \vdots \\ u_{N-1} \end{bmatrix}, \quad \bar{R} = \begin{bmatrix} R_{0,2} \\ \vdots \\ R_{0,s} \\ R_{1,2} \\ \vdots \\ R_{\bar{N}-2,s} \\ R_{\bar{N}-1,2} \\ \vdots \\ R_{\bar{N}-1,s} \end{bmatrix}, \quad (4.34)$$

Then we can rewrite the problem (2.27) in the compact form

$$\max_{\bar{u}} \quad \psi(x_0, \bar{u}) = \left\{ J(x_0, \bar{x}, \bar{u}) : \bar{R}(x_0, \bar{x}, \bar{u}) = 0 \right\} \quad (4.35a)$$

$$s.t. \quad \bar{u} \in \mathcal{U} \quad (4.35b)$$

$\bar{R}(x_0, \bar{x}, \bar{u}) = 0$ is the discretized dynamical model (2.21b)-(2.21c) in residual form. The relation $\bar{R}(x_0, \bar{x}, \bar{u}) = 0$ and the vectors x_0 and \bar{u} determine the state vector \bar{x} .

This leads to the following proposition for computation of the discrete adjoints.

PROPOSITION 4 (GRADIENTS BASED ON DISCRETE ADJOINTS) *Consider the function $\psi = \psi(\bar{u}; x_0)$ defined in (4.35).*

The gradients, $\partial\psi/\partial\bar{u}$, $\partial\psi/\partial x_0$, may be computed as

$$\begin{aligned} \frac{\partial\psi}{\partial\bar{u}} &= \frac{\partial J}{\partial\bar{u}} + \lambda^T \frac{\partial\bar{R}}{\partial\bar{u}} \\ \frac{\partial\psi}{\partial x_0} &= \frac{\partial J}{\partial x_0} + \lambda^T \frac{\partial\bar{R}}{\partial x_0} \end{aligned} \quad (4.36)$$

in which \bar{x} is computed by solution of $\bar{R}(x_0, \bar{x}, \bar{u}) = 0$ and λ is computed by solution of the discrete adjoint equations

$$\lambda^T \frac{\partial\bar{R}}{\partial\bar{x}} = - \frac{\partial J}{\partial\bar{x}} \quad (4.37a)$$

PROOF. See Appendix A.3.

4.3.1 Solving the Discrete System

Due to the special block structure of $\frac{\partial\bar{R}}{\partial\bar{x}}$, the solution of the discrete adjoint equations (4.37) is computed backward. Define the vector λ as

$$\lambda = \begin{bmatrix} \lambda_{0,2} \\ \vdots \\ \lambda_{0,s} \\ \lambda_{1,2} \\ \vdots \\ \lambda_{\bar{N}-2,s} \\ \lambda_{\bar{N}-1,2} \\ \vdots \\ \lambda_{\bar{N}-1,s} \end{bmatrix} \quad (4.38)$$

We compute λ by computing its subvectors in the reverse order, i.e. $\lambda_{\bar{N}-1,s}, \dots, \lambda_{\bar{N}-1,2}, \dots, \lambda_{0,2}, \lambda_{0,0}$. The last subvector, $\lambda_{\bar{N}-1,s}$, is computed by

$$\lambda_{\bar{N}-1,s}^T \cdot \frac{\partial R_{\bar{N}-1,s}}{\partial X_{\bar{N}-1,s}} = -\frac{\partial J}{\partial X_{\bar{N}-1,s}} \quad (4.39)$$

which is equivalent to the expression

$$\lambda_{\bar{N}-1,s}^T \cdot \left(\frac{\partial g}{\partial x}(X_{\bar{N}-1,s}) - h_{\bar{N}-1} \gamma \frac{\partial f}{\partial x}(X_{\bar{N}-1,s}, u_N) \right) = - \left(\frac{\partial \hat{\Phi}}{\partial x}(X_{\bar{N}-1,s}) + h_{\bar{N}-1} b_s \frac{\partial \Phi}{\partial x}(X_{\bar{N}-1,s}, u_N) \right) \quad (4.40)$$

Subsequently, the remaining subvectors, $\lambda_{k,j}$ and $\lambda_{k-1,s}$, are computed by marching backwards

$$\lambda_{k,s-j}^T \cdot \frac{\partial R_{k,s-j}}{\partial X_{k,s-j}} = -\frac{\partial J}{\partial X_{k,s-j}} - \sum_{i=1}^j \lambda_{k,s-j+i}^T \cdot \frac{\partial R_{k,s-j+i}}{\partial X_{k,s-j}} \quad (4.41a)$$

$$\lambda_{k-1,s}^T \cdot \frac{\partial R_{k-1,s}}{\partial X_{k-1,s}} = -\frac{\partial J}{\partial X_{k-1,s}} - \sum_{i=1}^{s-1} \lambda_{k,i+1}^T \cdot \frac{\partial R_{k,i+1}}{\partial X_{k-1,s}} \quad (4.41b)$$

for $k \in \{\bar{N}-1, \dots, 1\}$ and $j \in \{1, \dots, s-2\}$. For $k=0$ and $j \in \{1, \dots, s-2\}$ we compute $\lambda_{0,s-1}, \dots, \lambda_{0,2}$ by solving

$$\lambda_{0,s-j}^T \cdot \frac{\partial R_{0,s-j}}{\partial X_{0,s-j}} = -\frac{\partial J}{\partial X_{0,s-j}} - \sum_{i=1}^j \lambda_{0,s-j+i}^T \cdot \frac{\partial R_{0,s-j+i}}{\partial X_{0,s-j}} \quad (4.42a)$$

Finally, we can rewrite (4.36) as

$$\begin{aligned} \frac{\partial \psi}{\partial u_k} &= \sum_{j:u(\bar{t}_j) \equiv u_k} \left(h_j \sum_{l=1}^s b_l \frac{\partial \Phi}{\partial u}(X_{j,l}, u_k) + \sum_{i=2}^s \lambda_{j,i}^T \frac{\partial R_{j,i}}{\partial \tilde{u}_j}(\{X_{j,r}\}_{r=1}^i, u_k) \right) \\ \frac{\partial \psi}{\partial x_0} &= h_0 b_1 \frac{\partial \Phi}{\partial x_0}(x_0, u_0) + \lambda_{0,2}^T \frac{\partial g}{\partial x_0}(x_0) \end{aligned} \quad (4.43)$$

The derivatives, $\frac{\partial R_{j,i}}{\partial X_{j,l}}$, $\frac{\partial R_{j,i}}{\partial \tilde{u}_j}$, are provided in Appendix A.3.

Note In the special case that $s=2$, e.g. in ESDIRK12, we don't have to solve the equations (4.41a) and (4.42).

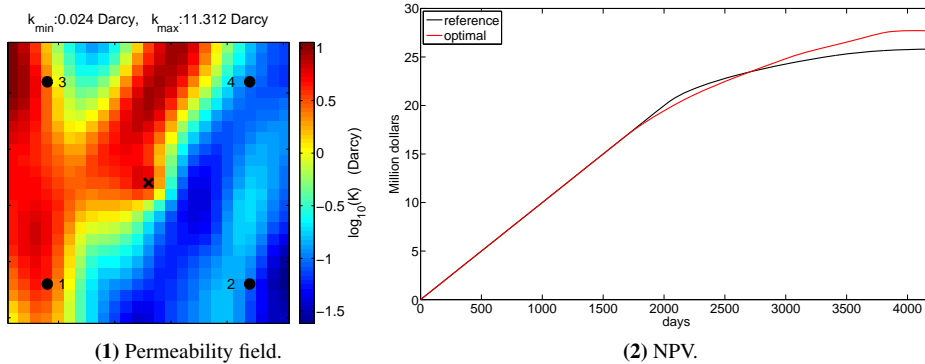


Figure 4.2: **Left:** Permeability field with the location of the wells. A circle indicates the location of an injector and a cross indicates the location of a producer. **Right:** The net present value (NPV) computed using ESDIRK3(4) and the discrete adjoint.

4.4 Case Study I: Production Optimization for a Conventional Oil Field

In this section, we apply our algorithm for constrained optimal control problems to production optimization in a conventional horizontal oil field that can be modeled as a slightly compressible two phase flow in a porous medium (2.9). This test case is taken from [21]. The reservoir size is $450 \text{ m} \times 450 \text{ m} \times 10 \text{ m}$. By spatial discretization this reservoir is divided into $25 \times 25 \times 1$ grid blocks. The configuration of injection wells and producers as well as the permeability field is illustrated in Fig. 4.21. As indicated in Fig. 4.21, the four injectors are located in the corners of the field, while the single producer is located in the center of the field.

The specification of the two phase oil model consists of the injector ($i \in \mathcal{I}$) and the producer ($i \in \mathcal{P}$) locations, the permeability parameters indicated in Fig. 4.21, and the parameters listed in Table 5.1. The initial reservoir pressure is 400 atm everywhere in the reservoir. The initial water saturation is 0.1 everywhere in the reservoir. This implies that initially the reservoir has a uniform oil saturation of 0.9.

The discounted stage cost function (see (2.21a))

$$\Phi(t) = \Phi(x(t), u(t)) = -\frac{1}{(1+b)^{t/365}} \sum_{j \in \mathcal{P}} (r_o(1-f_w) - f_w r_w) q_j(t) \quad (4.44)$$

accounts for the value of the oil produced minus the processing cost of the produced

4.4 Case Study I: Production Optimization for a Conventional Oil Field 43

Table 4.1: Parameters for the two phase model and the discounted state cost function (4.44).

Symbol	Description	Value	Unit
ϕ	Porosity	0.2	-
c_r	Rock compressibility	0	Pa ⁻¹
ρ_o	Oil density (400 atm)	800	kg/m ³
ρ_w	Water density (400 atm)	1000	kg/m ³
c_o	Oil compressibility	10 ⁻⁵	1/atm
c_w	Water compressibility	10 ⁻⁵	1/atm
μ_o	Dynamic oil viscosity	2 · 10 ⁻³	Pa · s
μ_w	Dynamic water viscosity	1 · 10 ⁻³	Pa · s
S_{or}	Residual oil saturation	0.1	-
S_{ow}	Connate water saturation	0.1	-
n_o	Corey exponent for oil	1.5	-
n_w	Corey exponent for water	1.4	-
P_{init}	Initial reservoir pressure	400	atm
S_{init}	Initial water saturation	0.1	-
r_o	Oil price	100	USD/m ³
r_w	Water production cost	20	USD/m ³

water. In this cost function, we have neglected the processing cost of injected water as well as the effect of pressure on injecting water. b is the discount factor. The fractional flow of water, $f_w = \lambda_w / (\lambda_w + \lambda_o)$, indicates the relative flow of water. $\lambda_w = \rho_w k k_{rw} / \mu_w$ and $\lambda_o = \rho_o k k_{ro} / \mu_o$ are the water and oil mobilities, respectively. In the problems considered, we do not have any cost-to-go terms, i.e. $\hat{\Phi}(t_b) = 0$. The optimizer maximizes the net present value by manipulating the injection of water at the injectors and by manipulation of the total fluid production (oil and water) at the producers. Hence, the manipulated variable at time period $k \in \mathcal{N}$ is $u_k = \{\{q_{w,i,k}\}_{i \in \mathcal{I}}, \{q_{i,k}\}_{i \in \mathcal{P}}\}$ with \mathcal{I} being the set of injectors and \mathcal{P} being the set of producers. For $i \in \mathcal{I}$, $q_{w,i,k}$ is the injection rate (m³/day) of water in time period $k \in \mathcal{N}$ at injector i . For $i \in \mathcal{P}$, $q_{i,k}$ is the total flow rate (m³/day) at producer i in time period $k \in \mathcal{N}$. Therefore, at producer $i \in \mathcal{P}$, the water flow rate is $q_{w,i,k} = f_w q_{i,k}$ and the oil flow rate is $q_{o,i,k} = (1 - f_w) q_{i,k}$.

There are bound constraints in the production optimization problem because the water injected at injectors and the production at the producers must both be positive and because each production facility has a maximum flow capacity. In the considered problem we have

$$|q_{i,k} - q_{i,k-1}| \leq 5 \quad i \in \mathcal{I} \cup \mathcal{P}, k \in \mathcal{N} \quad (4.45a)$$

$$-q_{\max} \leq q_{i,k} \leq 0 \quad i \in \mathcal{P}, k \in \mathcal{N} \quad (4.45b)$$

The maximum flow capacity, q_{\max} , is the same for all injectors and producers in this

case study. The rate of change for all injectors and producers are $|q_{i,k} - q_{i,k-1}| \leq 5$ for $i \in \mathcal{I} \cup \mathcal{P}$ and $k \in \mathcal{N}$. Since the injection of oil is zero, $q_{o,i,k} = 0$ for $i \in \mathcal{I}$, we get $|q_{w,i,k} - q_{w,i,k-1}| \leq 5$ for $i \in \mathcal{I}$ and $k \in \mathcal{N}$. This leads to the rate of movement constraints. In addition we use a voidage replacement constraint [4, 12]

$$\sum_{i \in \mathcal{I}} q_{i,k} = \sum_{i \in \mathcal{I}} q_{w,i,k} = - \sum_{i \in \mathcal{P}} q_{i,k} \quad k \in \mathcal{N} \quad (4.46)$$

and enforce a constant total injection, $\sum_{i \in \mathcal{I}} q_{w,i,k} = q_{\max}$ for $k \in \mathcal{N}$. This translates into constraints of the type (2.27b). By the total injection constraint, the optimization problem reduces to a problem of redistributing the flows among the injectors.

The prediction and control horizon is $t_b = 4200$ days and the sampling period is $T_s = 120$ days. Hence the prediction and control horizon correspond to $N = 35$ periods. With a total injection at each time period of $q_{\max} = 100 \text{ m}^3/\text{day}$, these specifications corresponds to injection of 1.05 pore volume during operation of the reservoir. A reference case with a constant injection of $25 \text{ m}^3/\text{day}$ from each injector is considered. A prediction horizon of 4270 days is optimal in the reference case for a total injection of $100 \text{ m}^3/\text{day}$. We consider the case of no discount, i.e. $b = 0$.

Fig. 4.2(2) illustrates the net present value for the base case scenarios as well as the optimized scenarios. The plot of NPV demonstrates that the NPV is lower than the base case NPV at some time during the production. At the end of the production, the optimized NPV increases with 7.2% compared to the reference case.

4.4.1 Discussion of the Results

The ESDIRK methods that we refer to in this case study are ESDIRK1(2), ESDIRK2(3) and ESDIRK3(4). They are first, second, and third order accurate methods, respectively. Their embedded error estimator is one order higher than the order of the advancing method. ESDIRK1(2) is the implicit Euler integration scheme with an embedded error estimator of order two.

Firstly, we test the gradient computation using the continuous adjoint, the discrete adjoint and the central finite differences. These methods produce gradients of comparable numerical values. We compare the gradients computed by the continuous adjoint method and the finite difference method to adjoints computed by the discrete adjoint method. We do this by computing the relative error with respect to the gradient computed by the discrete adjoint method. Finally, Table 4.2 provides computational statistics of ESDIRK3(4) method. It reveals that for increasing stepsizes \bar{h} of the adjoint integration, the continuous adjoint method is significantly faster than the discrete adjoint method (which is based on a fixed forward integration step h).

Secondly, we report the optimization results of the test case introduced in the previous section. Table 4.3 reports the computational statistics of the optimization process. We

find that there is a benefit in using the continuous adjoint method because the optimization algorithm requires less time and the value of the net present values is comparable with the one obtained by using the discrete adjoint. Finally, the optimal trajectories are compared.

In all the examples in this work, we use a fixed stepsize, $h = 4$ days, for the forward integration. We tried also smaller stepsizes $h = 0.5, 1, 2$ days finding similar qualitative results. Using a bigger stepsize, e.g. $h = 5$ days, was not possible because of a failure in the convergence of the equation solver (3.3). We solve (3.3) using absolute and relative tolerances in (3.10) equal to 10^{-8} . The perturbation used for the central finite difference method is $\delta u = 10^{-4}$.

Gradient Computation Results

Fig. 4.3(1) shows the gradients, $\frac{\partial \psi}{\partial u_k}$, computed using the different methods. The different gradients are comparable and by visual inspection we see no difference. Fig. 4.3(2) reports the relative error of the gradient, $\frac{\partial \psi}{\partial u_k}$, computed using the finite difference and the continuous adjoint methods with respect to the gradients computed by the discrete adjoint method. In general, the error increases as the adjoint stepsize, \bar{h} , increases; this is particular noticeable for the last control step. Different injectors have different relative errors. Injector 4 has the largest relative error, i.e. 80%. This error occurs in the last control step. Large differences in the last control step was also noted in [67]. They computed the continuous adjoint based on the implicit Euler method. [67] also show that the explanation for this large error between the continuous adjoint method and the discrete adjoint is in the different boundary conditions. Thus the Lagrange multipliers obtained by the two methods differ in general and so will be the corresponding gradients of the objective.

Table 4.2 reports computational statistics for gradient computations using ESDIRK3(4). We note that using the continuous adjoint, the time, T_{adj} , spend for gradient computation is inversely proportional to the continuous adjoint step-size, \bar{h} . Using the same step size, $h = \bar{h}$, the continuous adjoint method uses more computation time, t_{adj} , than the discrete adjoint method. This is due to the increased time spend in computing the continuous extension.

Using the others ESDIRK methods, 1(2)-3(4), we get similar tables. However there is an issue in our implementation. Using the continuous ESDIRK1(2) adjoint method, we do not need to solve both linear systems in (4.24) in each step. It is enough to solve only (4.24b) as we don't need \dot{Y}_1 to compute $Y_2 = \bar{\lambda}_n$ for ESDIRK1(2). This gives a penalty in using the continuous adjoint with ESDIRK1(2). In a future implementation, we will tailor the method for ESDIRK1(2) such that we avoid this penalty.

Table 4.2: Computational statistics for the gradient computation. h : forward integration step size. \bar{h} : continuous adjoint stepsize. t_{adj} : time to compute the gradient with the adjoint method scaled with respect to the forward integration time. T_{adj} : time to compute the gradient with the continuous adjoint method scaled with respect to the time to compute the gradient with the adjoint method using $\bar{h} = 4$.

	ESDIRK	$h[day]$	$\bar{h}[day]$	t_{adj}	T_{adj}
discrete adjoint	3(4)	4	–	1.37	–
continuous adjoint	3(4)	4	4	1.70	1
	3(4)	4	12	0.58	0.33
	3(4)	4	120	0.06	0.03

Optimization Results

The optimizer chosen for this case study is an SQP solver, see Section 2.2.3. We use the following stopping criteria for our SQP algorithm. An optimal solution is reported if the KKT conditions are satisfied to within a relative and absolute tolerance of 10^{-6} . The current best but non-optimal iterate is also returned in case of failure in the line search procedure, i.e. if the line search uses more than 20 iterations. Finally, the current best but non-optimal iterate is also returned in case of a relative change in the cost function less than 10^{-10} or if the number of SQP iterations exceeds 100. For the current case, we have never experienced that the SQP algorithm uses more than 100 iterations.

Table 4.3 reports computational statistics for the optimization process. We note that the NPVs computed using ESDIRK3(4) are bigger than the NPVs computed using ESDIRK1(2). Also the NPVs computed by the discrete adjoints are bigger than the ones computed using the continuous adjoint (with the same ESDIRK scheme). For both ESDIRK1(2) and ESDIRK3(4), we note that using the continuous adjoint with the biggest stepsize $\bar{h} = 20$ days, the computation time $T/T_{discr,RK12}$ is reduced by a factor of about three. Furthermore, we note that using the continuous adjoint based on ESDIRK3(4) with $\bar{h} = 20$, the computation time is halved when compared to using the ESDIRK1(2) method with the discrete adjoint gradient computation. This is indicated by $T/T_{discr,RK12}$ in Table 4.3.

Fig. 4.4(1) and Fig. 4.4(2) report the optimal water injection rates using the different adjoint methods based on ESDIRK1(2) and ESDIRK3(4), respectively. We note that when $h = \bar{h} = 4$, the trajectories agree for all times and visually we see no differences. Increasing \bar{h} produces a change in the solution and this change is more marked in the last control steps. This is in agreement with the results of Fig. 4.3(2). We note that

4.4 Case Study I: Production Optimization for a Conventional Oil Field 47

Table 4.3: Computational statistics for the optimization process. h : forward integration stepsize (in days). \bar{h} : continuous adjoint stepsize (in days). SQP: Number of iterations in the SQP-algorithm. QP: Number of KKT-matrix factorizations in the interior-point QP-solver. LS: Number of line searches and call to the ESDIRK algorithm. $T/T_{d.,RK12}$: time to compute the optimal solution scaled to the time to compute the optimal solution using the ESDIRK1(2) discrete gradient. $T/T_{d.,RK34}$: time to compute the optimal solution scaled to the time to compute the optimal solution using the ESDIRK3(4) discrete gradient.

RK	Adj.	h	\bar{h}	SQP	QP	LS	$T/T_{d.,RK12}$	$T/T_{d.,RK34}$	NPV [\$]
1(2)	discr.	4	–	84	1248	111	1	–	27.661.373
	cont.	4	4	62	894	129	0.94	–	27.661.351
	cont.	4	12	42	552	74	0.50	–	27.659.895
	cont.	4	120	25	272	45	0.27	–	27.598.463
3(4)	discr.	4	–	66	938	92	1.42	1	27.672.877
	cont.	4	4	66	945	134	1.85	1.30	27.672.870
	cont.	4	12	69	998	106	1.32	0.93	27.672.875
	cont.	4	120	38	507	58	0.57	0.40	27.667.576

the solutions computed using continuous adjoints are closer to the solution computed by discrete adjoints for EDSIRK3(4) than for ESDIRK1(2). This is due to the higher accuracy of the EDSIRK3(4) method compared to the ESDIRK1(2) method.

Fig. 4.5(1) and Fig. 4.5(2) report the NPVs as function of the SQP iteration number. We note that in general the different methods converge to similar numerical values. As reported in Table 4.3, they converge with a different rate (i.e. they use a different number of iterations). Increasing the step size, \bar{h} , the NPV decreases and this decrease is greater for ESDIRK1(2) than ESDIRK3(4).

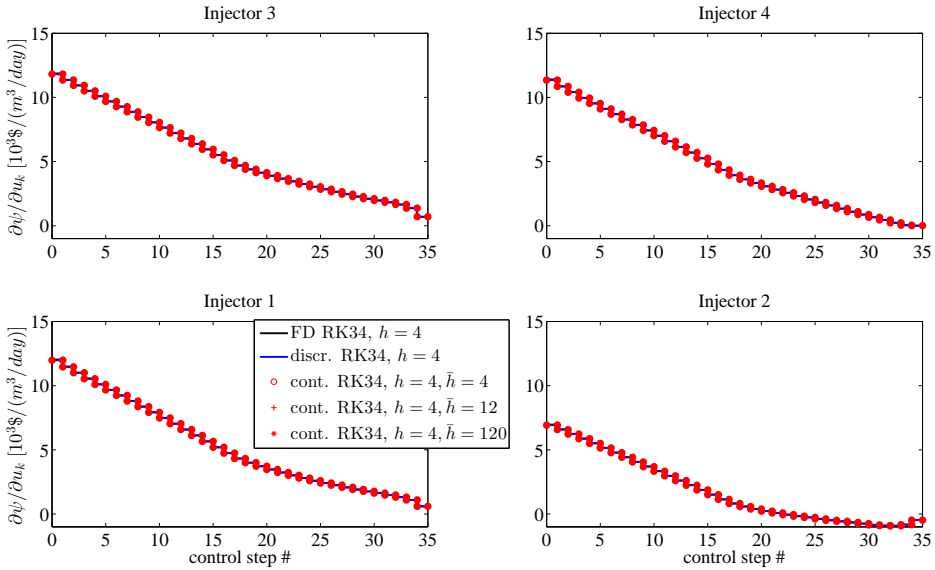
4.4.2 Summary

We propose the use of high order continuous and discrete adjoint methods in a gradient based algorithm for oil reservoir production optimization. The resulting algorithm is tested for a production optimization problem of an oil reservoir with a slightly compressible two phase flow. For all cases considered, the dynamic optimization increases the net present value of the field and gives increased oil production.

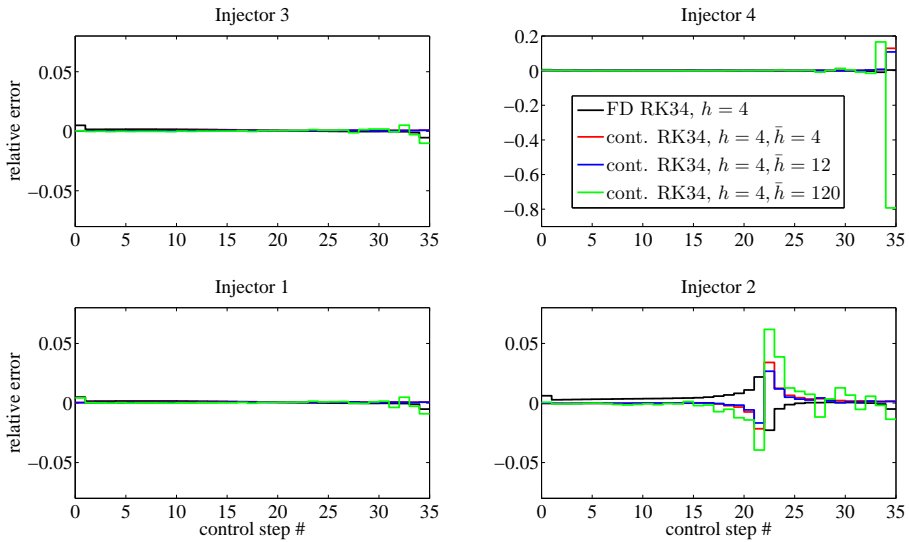
Computational experiments demonstrate that the accuracy of the sensitivities obtained

by the adjoint methods are comparable to the accuracy obtained by the finite difference method. Using the ESDIRK method, the continuous adjoint method is able to use a time grid different from the time grid used for forward integration. Therefore, it can compute these sensitivities much faster than the discrete adjoint method and the finite-difference method. The discrete adjoint method produces the gradients of the numerical schemes and this an advantage when the gradient is used in a numerical optimization algorithm. Computational experiments show that when the time steps are controlled in a certain range, the continuous adjoint method produces gradients sufficiently accurate for the optimization algorithm and somewhat faster than the discrete adjoint method.

4.4 Case Study I: Production Optimization for a Conventional Oil Field 49

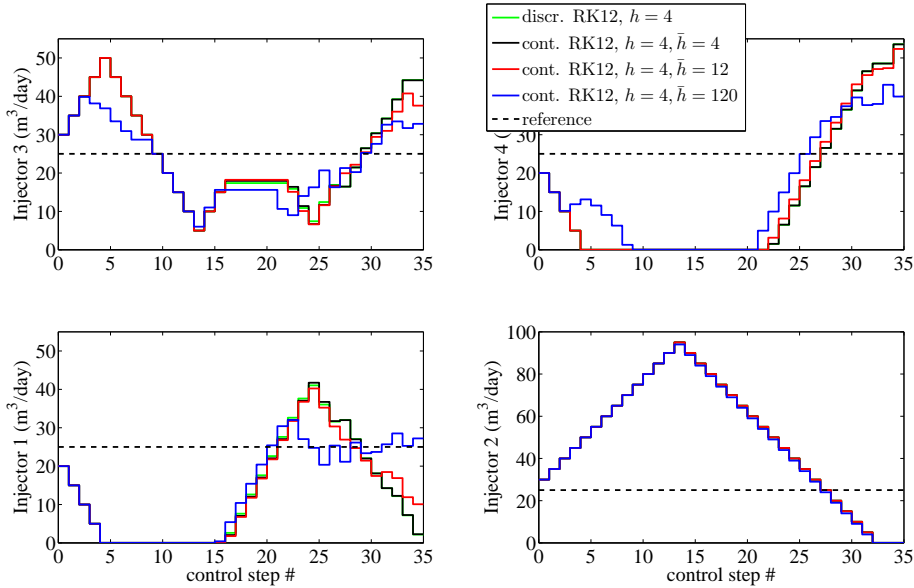


(1) Gradient of the cost function, $\frac{\partial \psi}{\partial u_k}$, with respect to the control vector. FD: Central Finite Difference, RK34: ESDIRK34, cont.: continuous adjoint method, discr.: discrete adjoint method., h : forward step size in days, \bar{h} : adjoint step size in days.

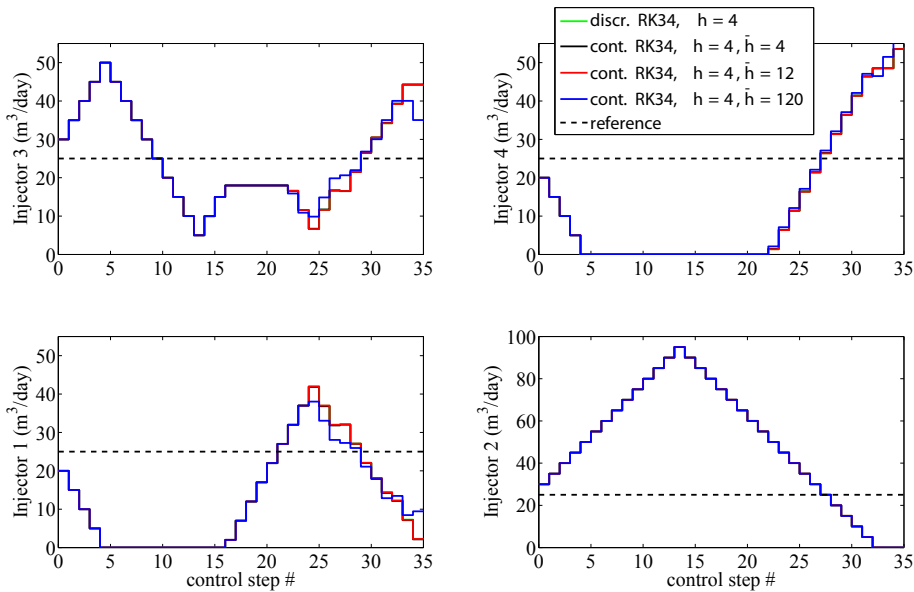


(2) Relative error of the gradients, $\frac{\partial \psi}{\partial u_k}$, computed by the continuous adjoint method and the central finite difference method with respect to the gradient computed by the discrete adjoint method using a forward step size of $h = 4$ days.

Figure 4.3

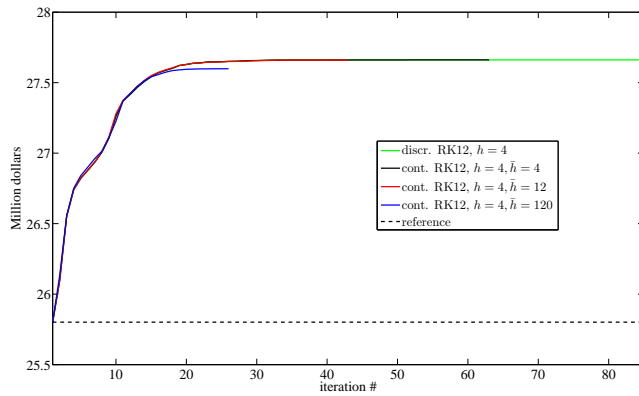


(1) ESDIRK1(2).

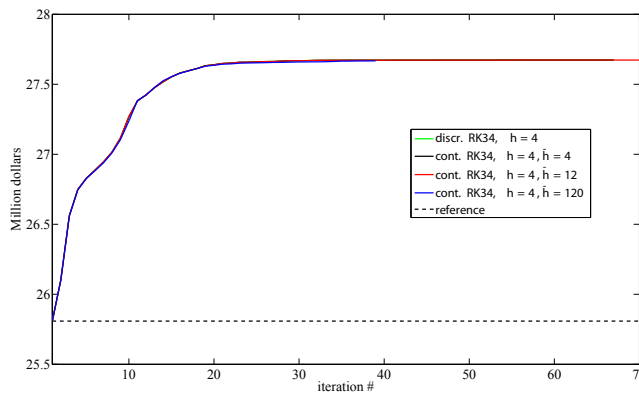


(2) ESDIRK3(4)

Figure 4.4: Optimal water injection rates using different adjoint methods based on ESDIRK1(2) and ESDIRK3(4). discr.: discrete adjoint method., cont.: continuous adjoint method, h : forward step size in days, \bar{h} : adjoint step size in days.



(1) NPVs using ESDIRK12



(2) NPVs using ESDIRK34

Figure 4.5: NPVs convergence using different methods. discr.: discrete adjoint method., cont.: continuous adjoint method, RK12: ESDIRK12, RK34: ESDIRK34, h : forward step size in days, \bar{h} : adjoint step size in days.

CHAPTER 5

Production Optimization under Uncertainty

This chapter is based on [56, 104].

In this chapter, we focus on the formulation of the optimization problem in the NMPC for CLRM under parameter uncertainty. In RO of an oil reservoir, the water injection and production borehole pressures (bhp) are computed such that the expected net present value (NPV) of an ensemble of realizations of the permeability field is maximized. A main problem with the RO is that the risk management enters only indirectly into the solution. Compared to a certainty equivalent optimization, the risk is reduced because we model the uncertainty with an ensemble of realizations of the reservoir model. To mitigate the risk, we propose a mean-variance (MV) bi-criterion objective function for an ensemble of reservoir models and demonstrate that the RO is a special extreme case in this objective function. The key to mitigate the risk for the oil production optimization problem is to optimize a bi-criterion objective function including both the expected NPV (mean of NPV) and the risk (variance of NPV) for the ensemble of possible reservoir models. With the inclusion of the risk directly in the objective function, we are able to compute the solution that gives the best return-risk balance. To illustrate the performance of the RO and the MV strategies under geological uncertainty, we present two case studies.

In the first case study, we compare both the open-loop and the closed loop performances

of the CE and the RO strategies. The CE optimization is based on a single realization of the permeability field. It uses the mean of the ensemble as its permeability field. In open-loop we also suggest a modified RO strategy that improve RO by adding a reactive control. In closed-loop we make use of the ensemble Kalman filter (EnKF) for model updating through data assimilation (history-matching) and of the moving horizon principle for data assimilation and implementation of the computed control input. This is the first time in the literature that the RO optimization has been investigated in closed-loop. Surprisingly, for the case studied, the closed-loop certainty equivalent strategy yields a higher NPV than the closed-loop RO strategy. The uncertainty reduction of the permeability field estimate due to data assimilation explains the good performance of the closed-loop certainty equivalent optimization strategy. Consequently, in closed-loop, the increased computational effort of the RO strategy compared to the certainty equivalent strategy is not justified for the particular case studied in this paper.

In the second case study, we investigate and compare the performance of the MV optimization to a certainty equivalent optimization, a reactive control strategy, and RO. In the study of different optimization formulations, we leave out data assimilation (history matching) as well as the effect of feedback from a moving horizon implementation and consider only the predictions and computations of the manipulated variables in the open-loop optimization of NMPC. This can be regarded as an optimal control study. The reason for this is twofold. First, in the initial development of a field, no production data would be available and the production optimization would be an open-loop optimal control problem. Secondly, the ability of different optimization strategies to mitigate the significant uncertainties present in reservoir models is better understood if investigated in isolation. With this case study, we demonstrate that a return-risk bi-criterion objective function is a valuable tool for the profit-risk tradeoff. This result trigger the question of how the closed-loop CE strategy would compare with the closed-loop MV strategy.

Both case studies presented in this chapter use the incompressible reservoir model (2.10)-(2.11) implemented in the MRST simulator.

5.1 Optimal Control Problem

Production optimization aims at maximizing the net present value (NPV) or oil recovery, for the life time of the oil reservoir. The stage cost, Φ , in the objective function for

a NPV maximization can be expressed as

$$\Phi(x(t), u(t)) = \frac{-1}{\left(1 + \frac{d}{365}\right)^{\tau(t)}} \left[\sum_{i \in \mathcal{P}} \left(r_o q_{o,i}(u(t), x(t)) - r_{wp} q_{w,i}(u(t), x(t)) \right) + \sum_{l \in \mathcal{I}} r_{wi} q_l(u(t), x(t)) \right] \quad (5.1)$$

r_o , r_{wp} , and r_{wi} represent the oil price, the water separation cost, and the water injection cost, respectively. $q_{w,i}$ and $q_{o,i}$ are the volumetric water and oil flow rate at producer i ; q_l is the volumetric well injection rate at injector l ; d is the annual interest rate and $\tau(t)$ is the integer number of days at time t . The discount factor $\left(1 + \frac{d}{365}\right)^{-\tau(t)}$ accounts for a daily compounded value of the capital. Note that from the well model (2.15), it follows that the flow rates q are negative for the producer wells and positive for the injector wells. Hence, the negative sign in front of the square bracket in the stage cost ψ . Note that in the special case when the discount factor is zero ($d = 0$) and the water injection and separation costs are zero as well, the NPV is equivalent to the quantity of produced oil.

The optimizer maximizes the net present value by manipulating the well bhp. With reference to the time discretization introduced in Section 2.2.1, the manipulated variables at time period $k \in \mathcal{N}$ are $u_k = \{\{p_{i,k}^{bhp}\}_{i \in \mathcal{I}}, \{p_{i,k}^{bhp}\}_{i \in \mathcal{P}}\}$ with \mathcal{I} being the set of injectors and \mathcal{P} being the set of producers. For $i \in \mathcal{I}$, $p_{i,k}^{bhp}$ is the bhp (bar) in time period $k \in \mathcal{N}$ at injector i . For $i \in \mathcal{P}$, $p_{i,k}^{bhp}$ is the bhp (bar) at producer i in time period $k \in \mathcal{N}$.

5.1.1 Control Constraints

The bhp are constrained by well and reservoir conditions. To maintain the two phase situation, we require the pressure to be above the bubble point pressure (290 bar). To avoid fracturing the rock, the pressure must be below the fracture pressure of the rock (350 bar). To maintain flow from the injectors to the producers, the injection pressure is maintained above 310 bar and the producer pressures are kept below 310 bar. With these bounds, we did not experience that the flow was reversed. Without these pressure bounds, state constraints must be included to avoid flow reversion.

5.1.2 Certainty-Equivalent, Robust, and Mean-Variance Optimization

In reservoir models, geological uncertainty is generally profound because of the noisy and sparse nature of seismic data, core samples, and borehole logs. The consequence of a large number of uncertain model parameters (θ) is the broad range of possible models that may satisfy the seismic and core-sample data. Obviously, the optimal controls, $\{u_k\}_{k=0}^{N-1} = \{u_k(x_0, \theta)\}_{k=0}^{N-1}$, computed as the solution of the finite dimensional optimization problem (2.27) with the objective function (2.26) depend on the values of the uncertain parameters, θ . In practice, the initial states, x_0 , will also be uncertain, but in this paper we assume that all uncertainty is contained within θ . When θ is deterministic, the objective function $\psi = \psi(\{u_k\}_{k=0}^{N-1}; x_0, \theta)$ is deterministic and the optimization problem (2.27) is well defined. In contrast, when θ is stochastic $\psi = \psi(\{u_k\}_{k=0}^{N-1}; x_0, \theta)$ is stochastic and the optimization problem (2.27) is not well defined. To define the optimization problem (2.27) for the stochastic case, a deterministic objective function for (2.27) must be constructed. The Certainty Equivalent (CE) optimization obtains a deterministic objective function by using the expected value of the uncertain parameters

$$\psi_{CE} = \psi(\{u_k\}_{k=0}^{N-1}; x_0, E_\theta[\theta]) \quad (5.2)$$

The MV optimization strategy is obtained by using the bi-criterion function

$$\psi_{MV} = \lambda E_\theta[\psi] - (1 - \lambda)V_\theta[\psi] \quad \lambda \in [0, 1] \quad (5.3)$$

as the objective function in (2.27). The term $E_\theta[\psi]$ is related to maximizing return while the term $V_\theta[\psi]$ is related to minimizing risk.

[58] introduces Robust Optimization (RO) for production optimization to reduce the effect of geological uncertainties compared to the CE optimization. The RO objective is

$$\psi_{RO} = E_\theta[\psi] \quad (5.4)$$

The RO objective, ψ_{RO} , is a special case of the MV objective, ψ_{MV} , i.e. $\psi_{RO} = \psi_{MV}$ for $\lambda = 1$.

We use a Monte-Carlo approach for computation of the expected value of the parameters, $E_\theta[\theta]$. The expected value of the return, $E_\theta[\psi]$, and the variance of the return, $V_\theta[\psi]$, are also computed by the Monte-Carlo approach. A sample is a set of realizations of the stochastic variables, θ :

$$\Theta_d = \left\{ \theta^1, \theta^2, \dots, \theta^{n_d} \right\} = \left\{ \theta^i \right\}_{i=1}^{n_d} \quad (5.5)$$

This sample is also called an ensemble and is generated by the Monte-Carlo method. The objective function values, ψ^i , corresponding to this ensemble are

$$\psi^i = \psi(\{u_k\}_{k=0}^{N-1}; x_0, \theta^i) \quad i = 1, \dots, n_d \quad (5.6)$$

The sample estimators of the means and the variance are

$$\hat{\theta} = \frac{1}{n_d} \sum_{i=1}^{n_d} \theta^i \quad (5.7a)$$

$$\hat{\psi} = \frac{1}{n_d} \sum_{i=1}^{n_d} \psi^i \quad (5.7b)$$

$$\sigma^2 = \frac{1}{n_d - 1} \sum_{i=1}^{n_d} (\psi^i - \hat{\psi})^2 \quad (5.7c)$$

$\hat{\theta}$ is an estimator for $E_\theta[\theta]$ and $\hat{\psi}$ is an estimator for $E_\theta[\psi]$. σ^2 is an unbiased estimate of $V_\theta[\psi]$ and therefore, σ is an unbiased estimator of the standard deviation $\sigma_\theta[\psi] = \sqrt{V_\theta[\psi]}$.

The CE objective function, ψ_{CE} , is computed using the sample estimator $\hat{\theta} \approx E_\theta[\theta]$, i.e.

$$\psi_{CE} = \psi(\{u_k\}_{k=0}^{N-1}, x_0, \hat{\theta}) \quad (5.8)$$

Similarly, the MV objective function, ψ_{MV} , is computed using the sample estimators $\hat{\psi} \approx E_\theta[\psi]$ and $\sigma^2 \approx V_\theta[\psi]$, i.e.

$$\psi_{MV} = \lambda \hat{\psi} - (1 - \lambda) \sigma^2 \quad \lambda \in [0, 1] \quad (5.9)$$

ψ_{MV} is computed by computation of ψ^i for each parameter, $i = 1, \dots, n_d$, and subsequent computation of the sample estimators, $\hat{\psi}$ and σ^2 . The gradient based optimizer used in this paper needs the objective, ψ_{MV} , and the gradients, $\nabla_{u_k} \psi_{MV}$ for $k \in \mathcal{N}$. Appendix A.5 provides an explicit derivation of these gradients. The computation of the objectives and the gradients, $\psi^i \left\{ \nabla_{u_k} \psi_{MV} \right\}_{k=0}^{N-1}$, can be conducted in parallel for $i = 1, 2, \dots, n_d$. The RO objective based on the sample estimator, $\hat{\psi} \approx E_\theta[\psi]$, is

$$\psi_{RO} = \hat{\psi} \quad (5.10)$$

The computational effort in computing ψ_{MV} is similar to the computational effort in computing ψ_{RO} . Therefore, no computational penalty is adopted by using the MV approach rather than the RO approach. The CE optimization needs one function and gradient evaluation in each iteration, while the MV optimization needs n_d function and gradient evaluations in each iteration. However, these n_d function and gradient evaluations may be conducted in parallel.

5.2 Key Performance Indicators

In this section, we present the key performance indicators (KPIs) used to evaluate the optimal control strategies. The KPIs are divided into economic KPIs and production

related KPIs.

5.2.1 Profit, Risk and Market Solution

Given a control sequence, $\{u_k\}_{k=0}^{N-1}$, computed by some strategy, the NPV may be computed for each realization of the ensemble, $\psi^i = \psi(\{u_k\}_{k=0}^{N-1}; x_0, \theta^i)$ for $i = 1, \dots, n_d$. This gives a set of NPVs, $\{\psi^i\}_{i=1}^{n_d}$. By itself, these NPVs and their distribution is of interest. Economic KPIs such as NPV mean, NPV standard deviation, ratio of NPV mean to NPV standard deviation, and the minimum and maximum NPV in the finite set are used to summarize and evaluate the performance of a given control strategy, $\{u_k\}_{k=0}^{N-1}$. Given $\{\psi^i\}_{i=1}^{n_d}$, the expected mean NPV may be approximated using (5.7b), $E_\theta[\psi] \approx \hat{\psi}$. Similarly, the standard deviation of the mean may be approximated using (5.7c), $\sigma_\theta[\psi] \approx \sigma$. The ratio of return and risk is called the Sharpe ratio and is defined as [105]

$$S_h = \frac{E_\theta[\psi]}{\sigma_\theta[\psi]} \approx \frac{\hat{\psi}}{\sigma} \quad (5.11)$$

The ensemble, $\{\psi^i\}_{i=1}^{n_d}$, is finite. Therefore, the minimum and maximum NPV may be computed by

$$\underline{\psi} = \min \{\psi^i\}_{i=1}^{n_d} \quad (5.12a)$$

$$\bar{\psi} = \max \{\psi^i\}_{i=1}^{n_d} \quad (5.12b)$$

We interpret $\underline{\psi}$, $\bar{\psi}$ as the worst case NPV and the best case NPV, respectively.

The economic KPIs, $\left\{ \hat{\psi}, \sigma, S_h, \underline{\psi}, \bar{\psi} \right\}$, provide a set of values that may be used to quickly evaluate and compare different control strategies, $\{u_k\}_{k=0}^{N-1}$, in terms of return and risk. Subsequently, selected solutions, $\{u_k\}_{k=0}^{N-1}$, may be evaluated in detail by inspection of the distribution of $\{\psi^i\}_{i=1}^{n_d}$ and by inspection of the solution trajectories, $\{u_k\}_{k=0}^{N-1}$. The idea in the mean-variance model, i.e. MV, is to compute the optimal solution for different values of the return-risk trade-off parameter, $\lambda \in [0, 1]$ [59, 60].

As part of the mean-variance optimization, the NPV of each realization of the ensemble is computed for various values of λ in the mean-variance objective function (5.9). This gives $\{\psi^i(\lambda)\}_{i=1}^{n_d}$ and $\{u_k(\lambda)\}_{k=0}^{N-1}$ for a range of values of the mean-variance trade-off parameter, $\lambda \in [0, 1]$. For each value of λ , the set of NPVs and (5.7b) are used to approximate the expected NPV as function of λ , $E_\theta[\psi(\lambda)] \approx \hat{\psi}(\lambda)$. Similarly, the set of NPVs and (5.7c) are used to approximate the standard deviation of the NPV as function of λ , $\sigma_\theta[\psi(\lambda)] \approx \sigma(\lambda)$. The expected NPV, $E_\theta[\psi(\lambda)]$, and the risk $\sigma_\theta[\psi(\lambda)]$, may be plotted and tabulated as a function of λ . This gives some overview of the behaviour of key economic performance indicators such as expected profit and risk as

a function of λ . Also a phase plot of risk versus return, $\left\{ \sigma_\theta[\psi(\lambda)], E_\theta[\psi(\lambda)] \right\}$ for $\lambda \in [0, 1]$, illustrates the risk-return relationship of the mean-variance model. Further, from this phase plot, we can compute the efficient frontier defined as the set of solutions with the highest expected return for a defined level of risk. The efficient frontier gives a curve for the maximal return as function of risk. The efficient frontier in itself does not provide a unique solution but only efficient pairs of return and risk; the preferred solution depends on the risk preferences of the decision maker. One way to choose a solution among the efficient risk-return pairs is to choose the solution that maximizes the Sharpe ratio (5.11) [105]. The solution that maximizes the Sharpe ratio is called the market solution.

5.2.2 Cumulative Productions Indicators

Other indicators that we use are the expected cumulative oil and water productions and the production efficiency. We approximate the cumulative oil production (5.13a) and water injection (5.13b) at final time t_b by using the right rectangle (implicit Euler) integration method

$$Q_o = Q_o(t_b) = \sum_{k=0}^{N-1} \left(\sum_{i \in \mathcal{O}} q_{o,i}(x_{k+1}, u_k) \right) \Delta t_k \quad (5.13a)$$

$$Q_{w,inj} = Q_w(t_b) = \sum_{k=0}^{N-1} \left(\sum_{i \in \mathcal{I}} q_i(x_{k+1}, u_k) \right) \Delta t_k \quad (5.13b)$$

and then we compute the expected values of the cumulative productions (5.13a)-(5.13b) as the sample averages

$$E_\theta[Q_o] = \frac{1}{n_d} \sum_{i=1}^{n_d} Q_o^i \quad (5.14a)$$

$$E_\theta[Q_{w,inj}] = \frac{1}{n_d} \sum_{i=1}^{n_d} Q_{w,inj}^i \quad (5.14b)$$

Superscript i refers to the quantity computed using realization i .

The production efficiency

$$\xi = \frac{E_\theta[Q_o]}{E_\theta[Q_{w,inj}]} \quad (5.15)$$

is defined as the volumetric ratio of the produced oil and the injected water.

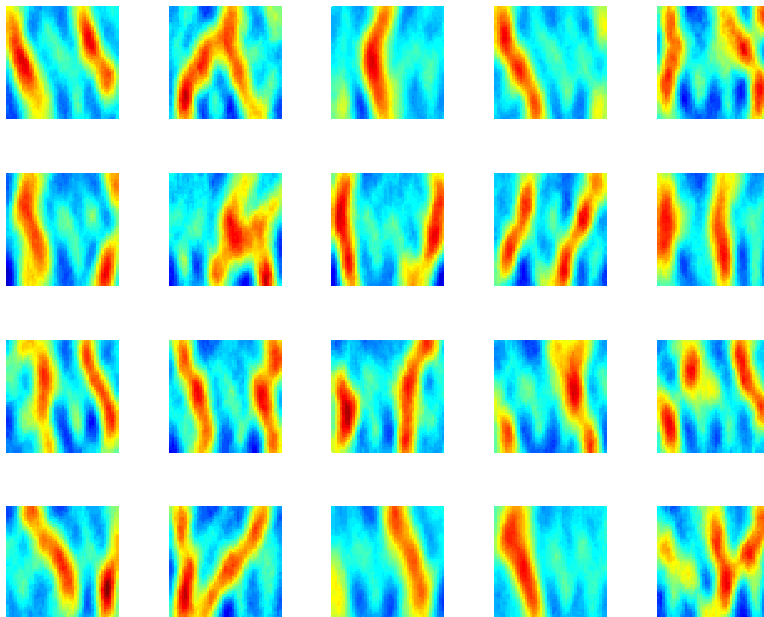


Figure 5.1: Excerpt from the ensemble of 100 permeability realizations. The realizations are quite heterogeneous, values are in the range 6 – 2734 mD.

5.2.3 Uncertain Parameters

In our study, the permeability field is the uncertain parameter. We generate 100 permeability field realizations of a 2D reservoir in a fluvial depositional environment with a known vertical main-flow direction. Fig. 5.1 illustrates such an ensemble of permeability fields. To generate the permeability fields, we first create a set of 100 binary (black and white) training images by using the sequential Monte Carlo algorithm 'SNESIM' [106]. Then a Kernel PCA [107] procedure is used to preserve the channel structures and to smooth the original binary images. The realizations obtained by this procedure are quite heterogeneous. The values of the permeability are in the range 6 – 2734 mD.

5.2.4 Optimizer

For the case studies described in this chapter we use two commercial optimization software packages to solve (2.27): Knitro [84] and Matlab's `fmincon` function [85]. Knitro as well as `fmincon` allow us to use an interior point or an active-set method. The initial guesses are constant bhp trajectories. We use up to 10 different initial guesses when

running the optimizations and we find similar qualitative results with both softwares. The interior point algorithms and the active set algorithms give similar solutions. However, when using Knitro as well as `fmincon`, we select an interior point method since we experience lowest computation times with this method. Further, a local optimal solution is reported if the KKT conditions are satisfied to within a relative and absolute tolerance of 10^{-6} . The current best but non-optimal iterate is also returned in cases when the optimization algorithm uses more than 100 iterations (200 in case study III). Similarly, the current best, but non-optimal, iterate is also returned in the case of a relative cost function or step size change less than 10^{-8} . Furthermore, in our simulations we noted that normalizing the cost function improved the convergence.

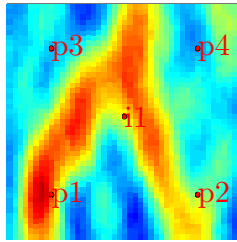


Figure 5.2: Configuration of injection wells and producer wells for Case Study II.

5.3 Case Study II: Robust Optimization Performances

We consider a conventional horizontal oil field that can be modeled as a two phase flow in a porous medium (2.10)-(2.11). The reservoir size is $450 \text{ m} \times 450 \text{ m} \times 10 \text{ m}$. By spatial discretization this reservoir is divided into $45 \times 45 \times 1$ grid blocks. The permeability field is uncertain. We assume that the ensemble in Fig. 5.1 represents the range of possible geological uncertainties. The configuration of injection wells and producers is illustrated in Fig. 5.2. As indicated in Fig. 5.2, the four producers are located in the corners of the field, while the single injector is located in the center of the field.

The reservoir's petrophysical parameters are listed in Table 5.1. The initial reservoir pressure is 300 bar everywhere in the reservoir. The initial water saturation is 0.1 everywhere in the reservoir. This implies that initially, the reservoir has a uniform oil saturation of 0.9. The manipulated variables are the bhp of the five wells (four producers, one injector) over the life of the reservoir. In this study, we consider a zero discount factor d in the cost function (5.1). This means that we maximize NPV at the final time without caring about the shorter horizon [21].

The case study is divided into an open-loop optimization part and a closed-loop optimization part. In open-loop optimization, we compute the control strategy without using measurement feedback to update the parameters, i.e. the ensemble in Fig. 5.1 is fixed in time. In closed-loop optimization, we use production measurements and the EnKF to estimate the permeability field parameters. To simulate the reservoir and create production data, the first realization of the permeability field, $\theta_{0|0}^1$, in Fig. 5.1 is used. This permeability field represents the true permeability field of the reservoir.

In reality, we never know the true model when performing data assimilation with EnKF. We can only implicitly assume that we can generate a reasonable approximation of the true reservoir. Since we focus on the optimizer formulation and separate the effects

Table 5.1: Parameters for the two phase model, the discounted state cost function (5.1), and the measurement noise.

Symbol	Description	Value	Unit
ϕ	Porosity	0.2	-
c_r	Rock compressibility	0	Pa ⁻¹
ρ_o	Oil density (300 bar)	700	kg/m ³
ρ_w	Water density (300 bar)	1000	kg/m ³
μ_o	Dynamic oil viscosity	$3 \cdot 10^{-3}$	Pa · s
μ_w	Dynamic water viscosity	$0.3 \cdot 10^{-3}$	Pa · s
S_{or}	Residual oil saturation	0.1	-
S_{ow}	Connate water saturation	0.1	-
n_o	Corey exponent for oil	2	-
n_w	Corey exponent for water	2	-
P_{init}	Initial reservoir pressure	300	bar
S_{init}	Initial water saturation	0.1	-
r_o	Oil price	120	USD/bbl
r_{wp}	Water production cost	20	USD/bbl
r_{wi}	Water injection cost	10	USD/bbl
d	Discount factor	0	-
R	Meas. noise cov. matrix	Diag($5 \cdot 10^{-3}$, $5 \cdot 10^{-3}$, $5 \cdot 10^{-3}$, $5 \cdot 10^{-3}$, 30)	

of the quality in data assimilation from the quality of CE, RO and reactive strategies as much as possible, we assume that the true reservoir is contained in the ensemble of initial guesses.

5.3.1 Open-Loop Optimization

We consider a prediction horizon of $t_N = 4 \cdot 365 = 1460$ days divided in $N = 60$ control periods (i.e. a control period $T_s \approx 24$ days). We control the reservoir using five different strategies that we call: the reactive strategy, the nominal strategy (NO), the certainty equivalent strategy, the robust optimization strategy (RO), and the modified robust optimization strategy (modified RO).

The reactive strategy develops the field at the maximum production rate (setting the producers at the lowest allowed value of 290 bar and the injector at the maximum allowed value of 350 bar) and subsequently shut-in each production well when it is no longer economical. From the values in Table 5.1, we observe that a producer well becomes uneconomical when the fractional flow f_w is above the value $120/(120 + 20) = 0.857$. The nominal strategy is based on a single realization. For each realization in the ensemble we compute the optimal control trajectory. Then we apply each of these

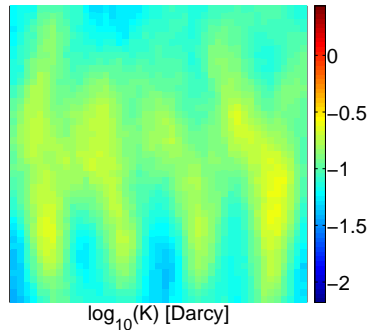


Figure 5.3: Permeability mean $E_\theta[\theta]$ of the ensemble given in Fig. 5.1

100 optimal control trajectories to each of the ensemble members obtaining 100 NPV values for each control trajectory. The certainty equivalent strategy is based on solving problem (2.27) using the certainty equivalent cost function ψ_{CE} (5.8). It uses the mean of the ensemble as its permeability field. Fig. 5.3 illustrates the mean of the permeability field ensemble given in Fig. 5.1. The RO strategy is based on solving problem (2.27) using the robust cost function ψ_{ro} (5.10). The modified robust optimization is the RO strategy with an added reactive strategy, i.e. we solve problem (2.27) using (5.10) but we shut in a producer well when it is non economical. This means that when we solve the flow equations (2.10)-(2.11), the number of active producer wells can change. This in turn means that once a well is shut-in, its later contribution to the NPV and its gradient will be zero. We could say that for each realization we manipulate producer wells bhps as long as they are profitable. Further, this strategy stops the production of a reservoir when all wells are non-economical. To our knowledge, there exist no extension of robust optimization to include a reactive control. However, the idea of adding reactive control has been used to improve the NPV of a single reservoir model. In [108] they consider production optimization in the absence of uncertainty by including a watercut constraint on the well completions. This results in increased NPV and a faster convergence of the optimizer.

Simulations reveal that for the present case, the RO strategy yields an higher expected NPV $E_\theta[\psi]$ and a lower standard deviation of the NPV (see Table 5.5) compared to the certainty equivalent strategy. However, both the RO and the certainty equivalent strategies are worse than the reactive strategy because of a much lower expected NPV $E_\theta[\psi]$ with a much higher NPV standard deviation. The modified RO strategy has a NPV standard deviation comparable to the reactive strategy, but a higher expected NPV $E_\theta[\psi]$. It is important to stress that the results concerning the merits of the different strategies are particular to this case study and not universal. [58] presents a case in which the RO strategy provides higher expected NPV and lower NPV standard deviation than the reactive strategy. In making a comparison with [58], there are a number

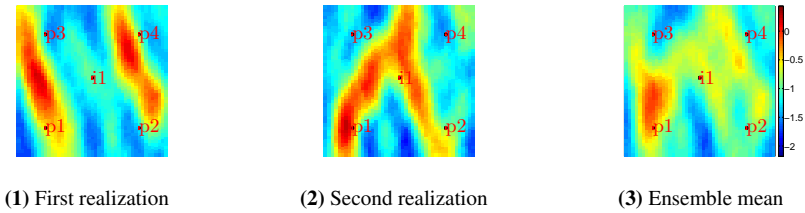


Figure 5.4: $\log_{10} K$ [D] of the first two realizations of the ensemble in Fig.5.1 and their ensemble mean $\hat{\theta}_{0|0}$.

of things we should stress. First of all, in [58] they control directly the liquid rates of 12 wells with no direct control on the bhp values. In our test case we control the bhp values of only 5 wells with no direct control on the liquid rates. In [58], all the realizations give positive NPV for all the control strategies. Further, they find that the reactive strategy is the worst to use. In our test case, the NO strategy is the worst to use, and it gives a substantial negative NPV contribution. Hence, it seems like the test case in [58] favors optimal control strategies. In our case, however, the heterogeneities in the ensemble realizations make it hard for optimal control strategies to improve on a reactive strategy. To summarize, the problems treated in [58] and in this case study have quite different characteristics. Hence, different preferences with respect to open-loop strategies is not necessarily surprising. The results in our case study indicates the value of feedback. The reactive strategy as well as the modified robust strategy both use a simple form of feedback. The nominal strategy, the certainty equivalent strategy, and the robust optimization strategy are pure open-loop strategies that do not use feedback.

To illustrate the results in a tutorial way, we split the discussion of the open-loop optimization into a two ensemble case and a hundred ensemble case. In the two ensemble case, we present the results of open-loop optimization using an ensemble of two realizations. Fig. 5.4 illustrates the two realizations of the uncertain permeability field for this case. In the case with hundred ensemble members, we use the entire ensemble in Fig. 5.1 to represent the uncertain permeability field.

5.3.1.1 Case - Ensemble with Two Members

In this subsection, we describe the performance of the RO strategy for the case with an ensemble consisting of the two permeability field realizations illustrated in Fig. 5.4. We compare the results of the RO control strategy with the results of the reactive, the modified RO and the optimal control strategies. By the optimal control strategies for the two realizations in Fig. 5.4, we mean the optimal control strategies, $\{u_k\}_{k=0}^{N-1}$, that are computed by solving the optimization problem (2.27) using the true permeability

fields. These are

$$\begin{aligned}\psi &= \psi(\{u_k\}_{k=0}^{N-1}; \bar{x}_0, \theta^1) = \psi^1 \\ \psi &= \psi(\{u_k\}_{k=0}^{N-1}; \bar{x}_0, \theta^2) = \psi^2\end{aligned}$$

The NPVs computed using these optimal control strategies act as an upper bound for the NPVs computed using the other control strategies. In selecting the two realizations to use, we first compute optimal control trajectories for the realizations in the ensemble of Fig. 5.1. Then we select two realizations with large differences in the optimal production strategies.

Fig. 5.5(1), Fig. 5.5(2) and Fig. 5.5(3) show the terms ψ^1 , ψ^2 and $E_\theta[\psi] \approx \hat{\psi}$ (5.7b) for the reactive strategy, the RO strategy, and the modified RO strategy, respectively. As expected, the NPVs computed using the optimal control strategies give the highest values for ψ^1 and ψ^2 . Compared to the reactive strategy, the RO strategy gives a lower NPV, ψ^1 , for realization 1, and a higher NPV, ψ^2 , for realization 2. As illustrated in Fig. 5.5(3), this results in a lower NPV mean, $E_\theta[\psi]$, for the RO strategy compared to the reactive strategy. The modified RO control strategy gives the highest NPVs for all the realizations.

Furthermore, it is interesting to observe the difference in production times for the different strategies. For the RO strategy, the production continue for the entire time horizon (1460 days) considered. In the reactive strategy, the production lasts 949 days in the first realization (ψ^2) and 1119 days in the second realization (ψ^2). So there is an important difference in the field developing time of the two realizations. In the modified RO strategy, the production lasts 1289 days in the first realization and 1240 days in the second realization. We note that with the modified RO strategy, the production time is longer than the production time of the reactive strategy.

Fig. 5.6 shows the control trajectories of the RO, the modified RO and the optimal strategies. We note that because of the heterogeneity between the realizations, the resulting optimal control trajectory of one realization can be very different and conflicting with the optimal control trajectory for the other realization. To find a common optimal control that takes all these differences into account can be difficult if not impossible. Especially if we do not allow for changes in the configuration of active wells. E.g. producer number 4 is producing at its minimum (310 bar) in the solution for ensemble 1 and at its maximum (290 bar) in the solution for ensemble 2. The RO and modified RO solutions for the producer number 4 stay in between the two optimal trajectories.

In conclusion, the two-ensemble case demonstrates that the optimizer produces the maximal profit for the optimal cases. Therefore, the optimizer works well and the lower profit of the RO strategy is not the result of lack of convergence in the optimizer, but rather the result of heterogeneous permeability fields giving conflicting control trajectories.

5.3.1.2 Case - Ensemble with Hundred Members

In this subsection, we describe the results for the case in which we do open-loop optimization using the entire ensemble of 100 realizations in Fig 5.1. Fig. 5.3 illustrates the mean permeability field for the ensemble of permeability fields in Fig. 5.1. Fig. 5.7 shows the profit evolution in the case of an ensemble consisting of 100 permeability fields for the certainty equivalent strategy, the reactive strategy, the RO strategy, and the modified RO strategy. Table 5.5 reports the corresponding key performance indicators (expected NPV $E_\theta[\psi]$ and standard deviation of the NPV). As in the two ensemble case, the reactive strategy yields both a larger expected NPV and a smaller standard deviation for the NPV compared to the certainty equivalent and the RO strategies. The reasons for the inferior performance of the RO strategy should be searched in the conflicting controls required for the different realizations. Fig. 5.8(1) shows that the RO strategy cannot avoid that some ψ^i gives a negative contribution to the expected NPV $E_\theta[\psi]$. In contrast, as illustrated in Fig.5.8(2), the modified RO strategy does not produce realizations with negative profit. Furthermore, each realization of the modified RO strategy seems to increase the profit compared to the RO strategy. The reactive strategy performs better than both the RO and certainty equivalent strategies because it can shut in a well when it is no longer profitable to operate the well. The modified RO strategy inherits the ability of the reactive strategy to shut in unprofitable wells. This is in essence a simple feedback mechanism. Fig. 5.9 and Fig. 5.10 show the saturation profiles of the first two realizations for the open-loop strategies. We note that the reactive strategy and the modified strategy inject a higher water quantity and displace the oil more uniformly compared to the RO and the certainty equivalent strategies.

Fig. 5.11 shows the control trajectories of the RO, the modified RO and the certainty equivalent strategies. Compared to the trajectories in Fig. 5.6, for the two ensemble case, it seems that the RO and certainty equivalent strategies include some averaging (smoothing) in the resulting control trajectories that limits their effectiveness. The result is a control trajectory that produces less oil than the modified RO strategy that can shut in uneconomical producer wells.

As indicated by Fig. 5.6, the RO control trajectories may be the average of conflicting control trajectories and therefore inefficient for the uncertain system.

Fig. 5.12 shows the cumulative distribution function for the different control strategies, i.e. the probability to get a NPV $\leq x$. These curves are similar to the ones reported in [58] with the difference that the RO and the certainty equivalent strategies have a positive probability of giving negative NPVs. Fig. 5.12 confirms that the modified RO strategy is superior to the other open-loop strategies.

Table 5.2: Key indicators for the open loop optimized cases. Improvements are relative to the nominal case.

	NO 10 ⁶ USD	Reactive 10 ⁶ USD, %	Certainty equivalent 10 ⁶ USD, %	RO 10 ⁶ USD, %	RO modified 10 ⁶ USD, %
$E_{\theta}[\psi]$	33.84	56.47, +66.9	42.72, +26.2	44.11, +30.3	58.18, +71.9
Std. dev.	26.35	6.05	18.27	13.19	6.25

5.3.2 Closed-Loop optimization

The closed-loop optimization strategies are implemented using the moving horizon principle. In this method, each time new measurements from the real or simulated reservoir are available, the EnKF uses these measurements to update the estimates of the permeability field, and an open-loop optimization problem is solved using the updated permeability field. Only the first part of the resulting optimal control trajectory is implemented. As new measurements become available, the procedure is repeated. The sampling time for the system is $T_s = 146$ days, i.e. the data assimilation and optimization is performed every 146 days. The open-loop optimization uses a prediction and control horizon of $4 \cdot 365 = 1460$ days that is divided into $N = 60$ periods (the same as for the open-loop optimization strategies). With this parametrization, the control steps for the first six periods are implemented to the system, and then we receive new measurements to do new data assimilation and optimization computations for a shifted time window. In this case study, we consider 35 of these steps such that the total production horizon is $146 \cdot 35 = 5110$ days.

We compare three closed-loop optimization strategies: A reactive strategy, a certainty equivalent strategy, and a RO strategy. We did not implement a modified RO strategy because that would be complicated by the need to manage situations with a variable number of active wells and measurements for different ensemble realizations. Further, it would require a strategy to replace ensemble realizations when all the producing wells are shut-in.

Fig. 5.13 shows the NPV, $\psi(\{u_k\}_{k=0}^{N-1}; x_0, \theta_{0|0}^1)$, for the reactive strategy, the closed-loop RO strategy, the closed-loop certainty equivalent strategy, the optimal control strategy, and the open-loop strategies introduced in the previous section. The optimal control strategy is obtained solving the optimization problem (2.27) using the true permeability field (the first realization of the permeability field in Fig. 5.1). The NPV computed by the optimal control strategy represents the best possible operation of the reservoir. Table 5.3 reports key performance indicators (expected NPV and improvements compared to the reactive strategy) for the closed-loop strategies at different levels of measurement noise. Fig. 5.13 and Table 5.3 show that for all investigated cases, both the

closed-loop certainty equivalent strategy and the closed-loop RO strategy yield significantly higher NPV than the reactive strategy. As is also evident from Fig. 5.13 and Table 5.3, the closed-loop certainty equivalent strategy yields higher NPV than the closed-loop RO strategy. Furthermore, the NPV of the closed-loop certainty equivalent strategy is very close to the NPV of the optimal strategy. Consequently, the closed-loop certainty equivalent strategy is preferable over the closed-loop RO strategy as it yields higher NPV and requires significantly less computational effort. This observation is also confirmed when using the second realization in Fig. 5.1 as the permeability field. From Fig. 5.13 we note also that the modified RO is the best open-loop strategy and that the closed-loop strategies CE and RO provide better results compared to the modified RO starting from the assimilation steps 13 ($t \approx 1898$ days) and 16 ($t \approx 2336$ days), respectively. Fig. 5.14 shows the cumulative water injection and the cumulative oil production for different strategies. The slope of the curves is the reservoir injection/production rate. In general, we note that the closed-loop strategies inject at a lower rate compared to the open-loop strategies. This happens since we use a zero discount factor, i.e. we focus on long term behaviour. Moreover, there are no direct bounds on the liquid rates. We note that the open-loop strategies, so as the optimal strategy, have an upward concavity. This means that the water injection rate increases with time. These strategies increase the injection at the final time to exploit the high oil-to-water price ratio. The closed-loop strategies, instead, have a downward concavity. At the beginning (first 300 days) the closed-loop strategies inject at a similar pace as their open-loop counterparts (same slope in the initial part of the curves). However, as the data assimilation proceed, and a better estimate of the true field is given, the closed-loop strategies try to inject/produce as much as the optimal strategy (black curves in figure). This explains the change in concavity of the closed-loop strategies, i.e. why the closed-loop strategies reduce the water injection rate with time. Fig. 5.15 illustrates the saturation profiles of the true field for the closed-loop strategies. We note that they have similar field sweep at the final time. Fig. 5.16 shows the corresponding control trajectories of the different closed-loop control strategies. It is evident that the control trajectories of the optimal control strategy are very different from the control trajectories for the closed-loop certainty equivalent and the closed-loop RO strategies.

Fig. 5.17 illustrates the RMSE (2.45) and the ensemble spread (2.44) of the EnKF when applied together with the certainty equivalent strategy. The RMSE indicates whether the permeability parameter estimate of the EnKF converges toward the true permeability parameters. The ensemble spread indicates the uncertainty in the estimated permeability parameters. The RMSE and the ensemble spread sequences are computed for different levels of measurement noise, i.e. different values of R in (2.29b). Fig. 5.17(2) indicates that decreasing levels of measurements noise, R , decrease the ensemble spread (2.44). This decrease does not always results in a lower RMSE (2.45) value. However, as is evident from Fig. 5.17(1), in most of the cases, lower measurement noise levels reduce the RMSE. In this case study there is no ensemble collapse. In fact, Fig. 5.19 shows that the ensemble realizations have different distances at the last assimilation time. This distances is an index of the heterogeneity in the ensemble of

Table 5.3: Key indicators for the closed loop optimized cases. Improvements are relative to the reactive case.

Meas. noise	Reactive	Certainty equivalent		RO		Optimal	
	10 ⁶ USD	10 ⁶ USD, %		10 ⁶ USD, %		10 ⁶ USD, %	
$5 \cdot R$	51.24	59.13,	+15.4	58.34,	+13.9	60.41,	+17.3
R	51.24	59.79,	+16.7	59.09,	+15.3	60.41,	+17.3
$5^{-1} \cdot R$	51.24	59.84,	+16.8	59.52,	+16.2	60.41,	+17.3
$5^{-2} \cdot R$	51.24	59.95,	+17.0	59.56,	+16.2	60.41,	+17.3

realizations.

In the EnKF, at each data assimilation step, we update the estimated permeability field for each ensemble member. Fig. 5.18 illustrates the time evolution of the mean, $\hat{\theta}_{k|k-1}$, of these estimated permeability field ensembles for the closed-loop certainty equivalent optimization strategy. Fig. 5.18 indicates that the estimated mean permeability field captures the main features of the true permeability field. We start out with a mean permeability field having four channel structures and converge towards the correct two channel structure.

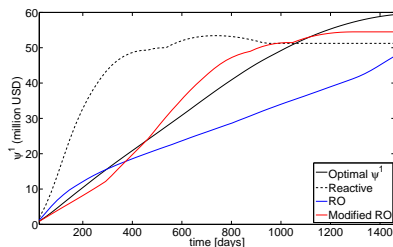
5.3.3 Summary

In this section, we demonstrate the open-loop and the closed-loop performance of the certainty equivalent strategy and the RO strategy. For the open-loop case we present a modified RO strategy that performs significantly better than the other open-loop strategies. In the closed-loop situation for the case studied, we arrive at the surprising conclusion that the certainty equivalent strategy is slightly better than the RO strategy.

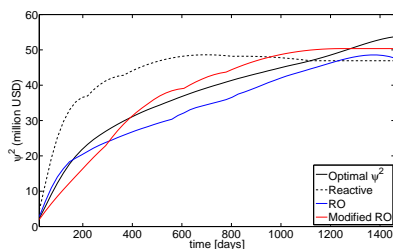
For the case presented, the open-loop RO strategy yields 3% higher expected NPV and 28% lower NPV standard deviation than the open-loop certainty equivalent strategy. Yet, the reactive strategy performed even better than the open-loop RO strategy. Simulations indicate that the inferior performance of the open-loop RO strategy compared to the reactive strategy is due to the inability of the RO strategy to efficiently encompass ensembles with very different and conflicting optimal control trajectories. We propose a modified RO strategy that allow shut in of uneconomical wells. The modified RO strategy performs significantly better than the other open-loop strategies and the reactive strategy. The modified RO optimization strategy yields an expected NPV that is 36% higher than the expected NPV of the open-loop certainty equivalent strategy and 3% higher than the expected NPV for the reactive strategy. The NPV standard deviation of the modified RO strategy is similar to the NPV standard deviation of

the reactive strategy. These observations are non-trivial, as previous literature suggests that the open-loop RO strategy performs better than the reactive strategy [58]. The improved economic performance of the open-loop modified RO strategy justifies the computational effort used in determining the trajectories for this strategy.

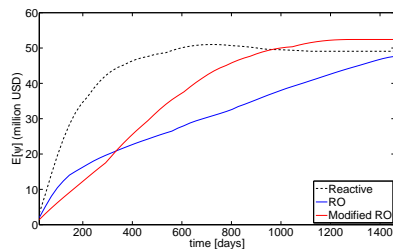
The simulations for the closed-loop strategies, reveal that the RO strategy and the certainty equivalent strategy yields significantly higher NPV than the reactive strategy. Surprisingly, the closed-loop certainty equivalent strategy yields a higher NPV than the closed-loop RO strategy for the case studied. The uncertainty reduction of the permeability field estimate due to data assimilation explains the good performance of the closed-loop certainty equivalent optimization strategy. Consequently, in closed-loop, the increased computational effort of the RO strategy compared to the certainty equivalent strategy is not justified for the particular case studied in this section.



(1) First realization



(2) Second realization



(3) Combined NPV

Figure 5.5: Profit evolutions for open-loop optimization of the two ensemble case. The optimal trajectories computed using the true permeability fields give the highest possible profit. The profit of the RO strategy is below the profit of the reactive strategy for the first permeability realization and slightly above the second permeability realization. On average the RO strategy gives less profit than the reactive strategy. For all cases, the modified RO strategy produces a higher profit than the reactive strategy.

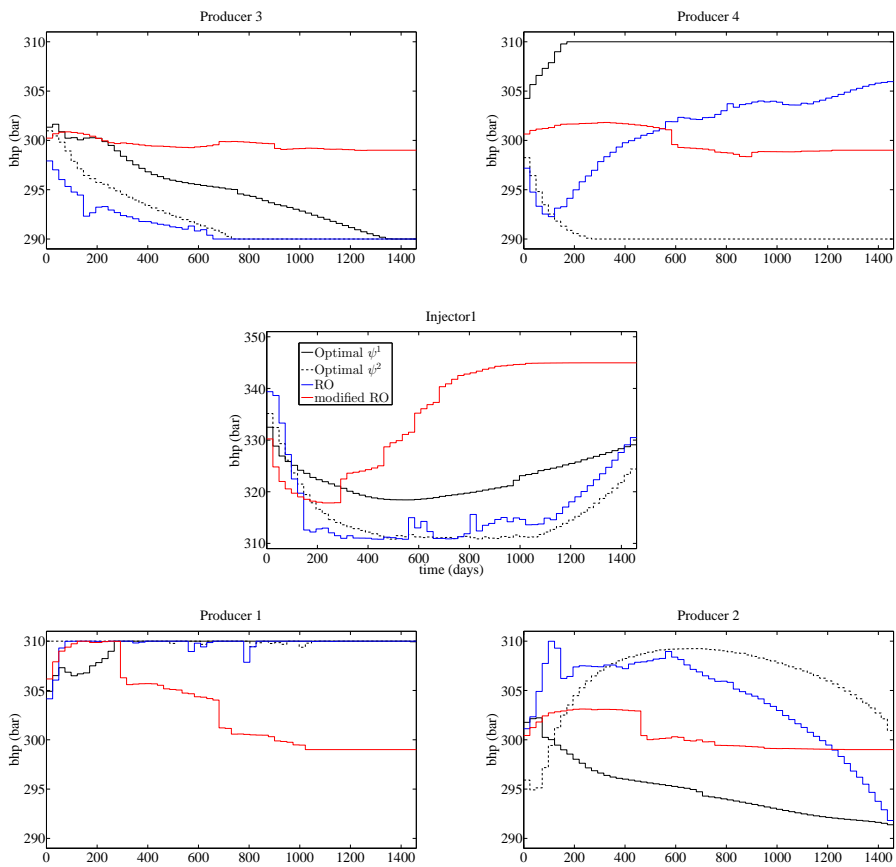


Figure 5.6: Control trajectories for open-loop optimization of the two ensemble case. The control trajectories for the considered optimization strategies are very different.

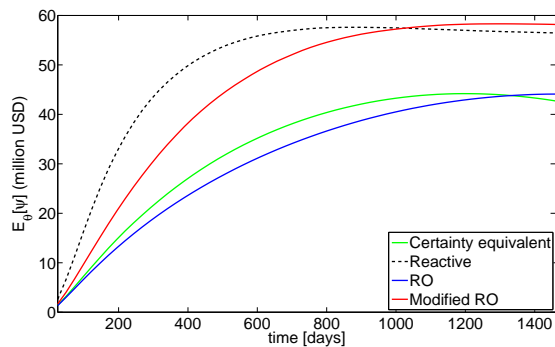


Figure 5.7: Profit evolution for open-loop optimization in the hundred ensemble case.

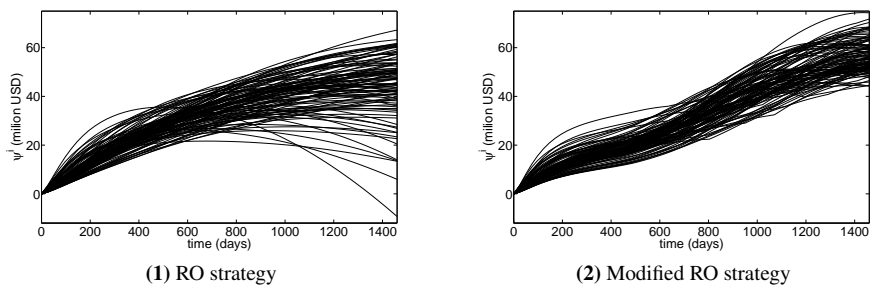


Figure 5.8: Profit evolution of the open-loop RO strategy and the open-loop modified RO-strategy for each realization of the permeability field. Some scenarios in the RO strategy give negative profits while the modified RO strategy avoids that by shutting in uneconomical producer wells.

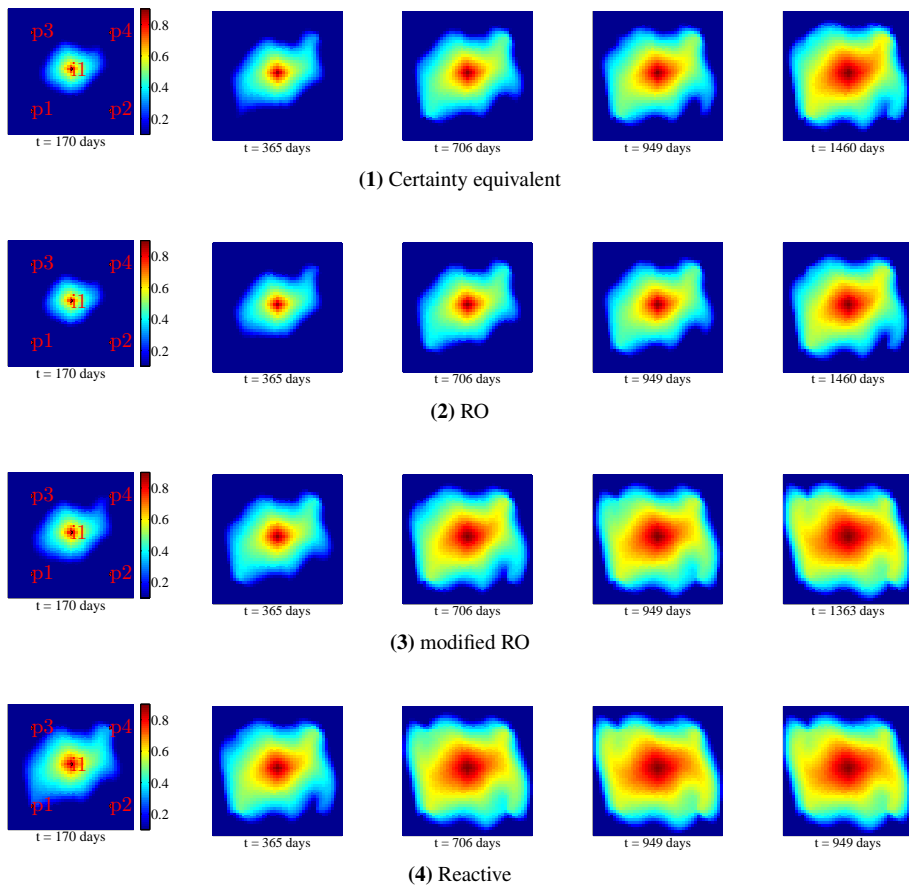


Figure 5.9: Saturation profiles of the first realization for the open-loop optimization strategies in the hundred ensemble case.

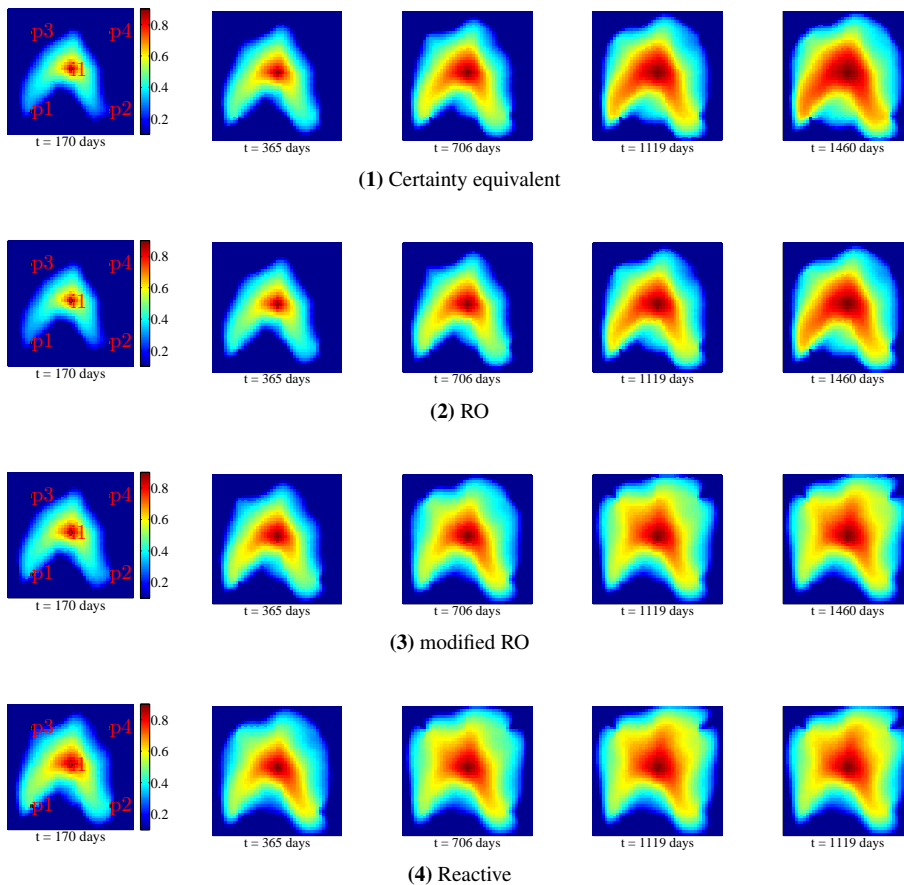


Figure 5.10: Saturation profiles of the second realization for the open-loop optimization strategies in the hundred ensemble case.

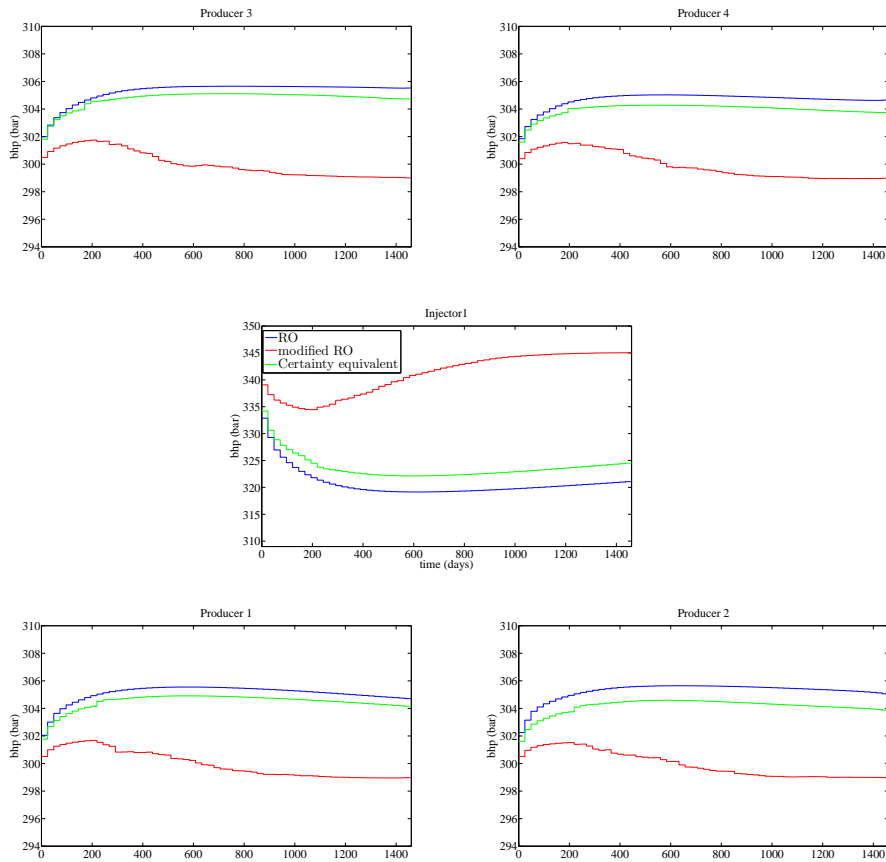


Figure 5.11: Control trajectories for open-loop optimization in the hundred ensemble case.

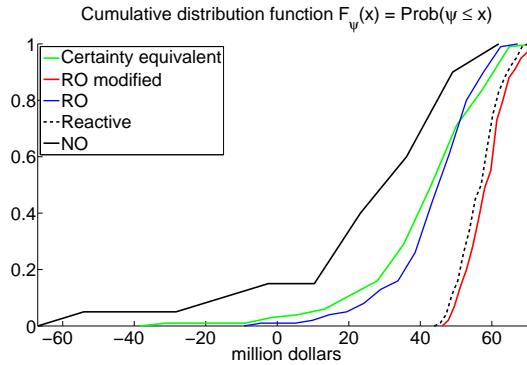


Figure 5.12: Cumulative distribution function for the open-loop optimization strategies. The cumulative distribution functions are for the ensemble with hundred members.

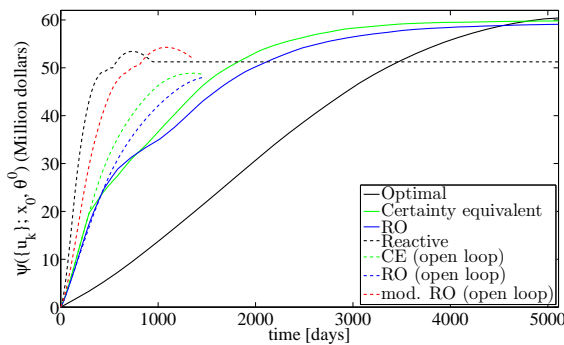
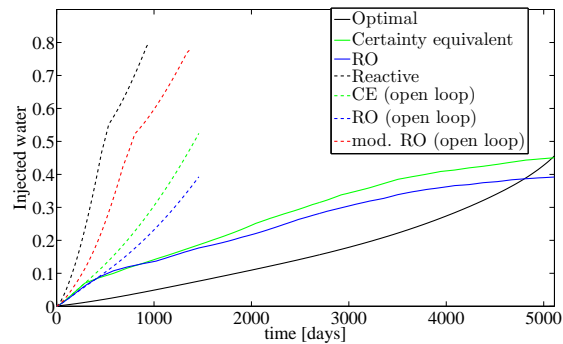
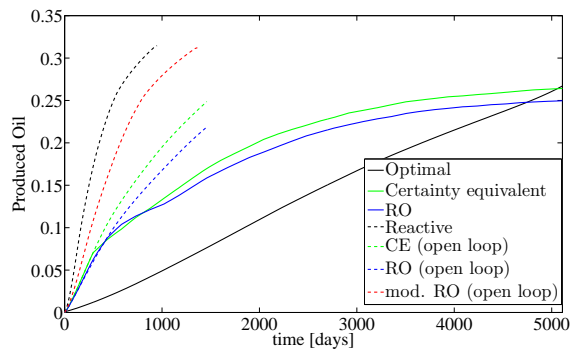


Figure 5.13: Profit evolution for the closed-loop optimization strategies. The profit evolution of the true model controlled by different strategies based on the ensemble in Fig. 5.1. Both the RO and the certainty equivalent strategies give a higher NPV than the the reactive strategy. The optimal control strategy represents the best possible solution. By using the RO strategy and the certainty equivalent strategy we get profits close to the maximum possible profit.



(1) Cumulative water injection



(2) Cumulative oil production

Figure 5.14: Closed-loop. Water injected and produced oil trajectories for different optimization strategies. The values are normalized with respect to the pore volume.

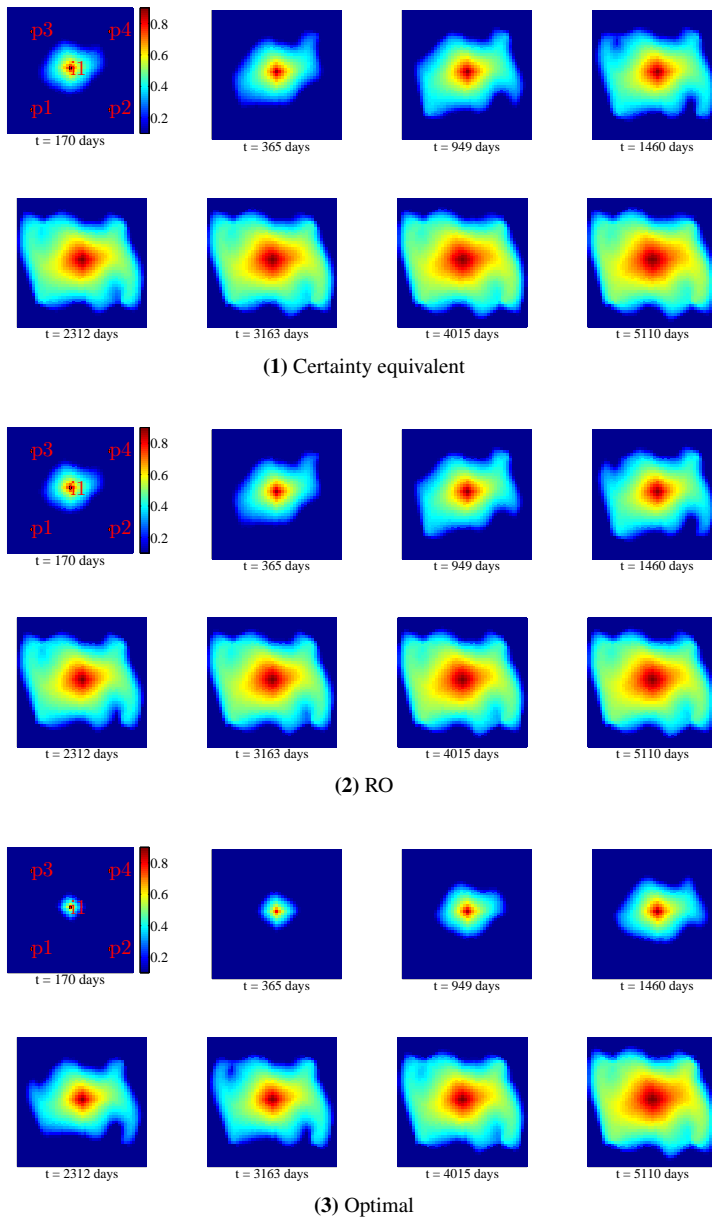


Figure 5.15: Saturation profiles of the true field for the closed-loop optimization strategies.

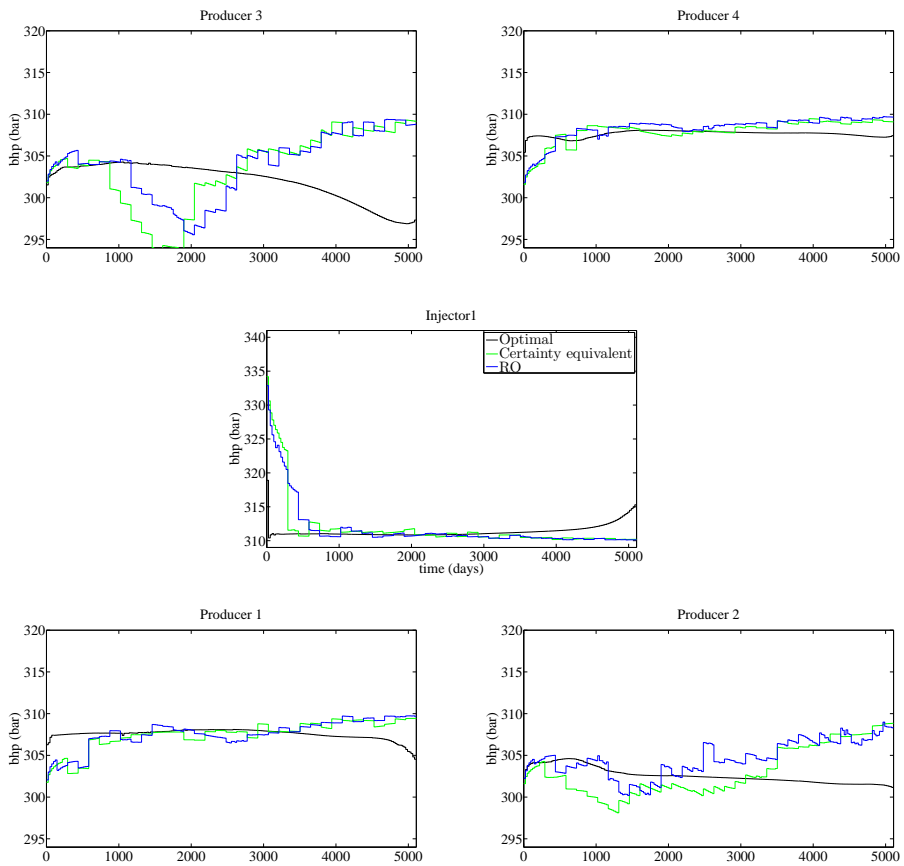
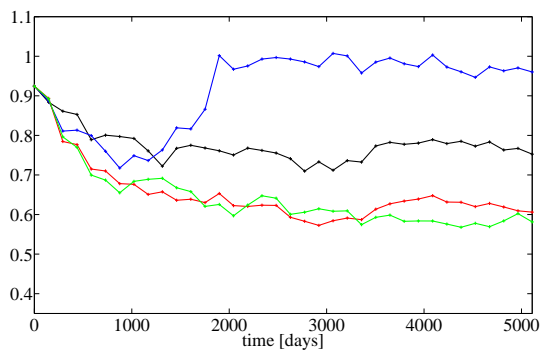
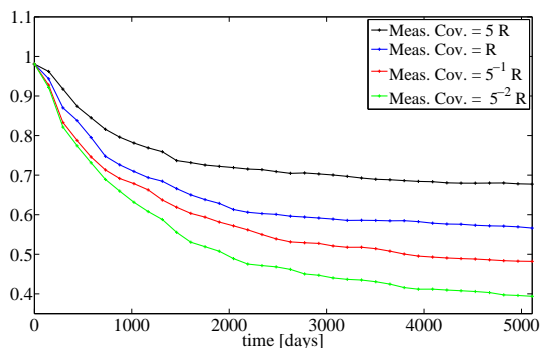


Figure 5.16: Control trajectories for the closed-loop optimization strategies.



(1) RMSE



(2) Ensemble spread

Figure 5.17: Convergence measures for the EnKF with various levels of measurement noise for the closed-loop certainty equivalent strategy. (1) shows that the EnKF does not converge to the true parameters. However, the estimate captures enough features to be useful. (2) illustrates that the parameter uncertainty decreases as more production data is assimilated in the estimates.

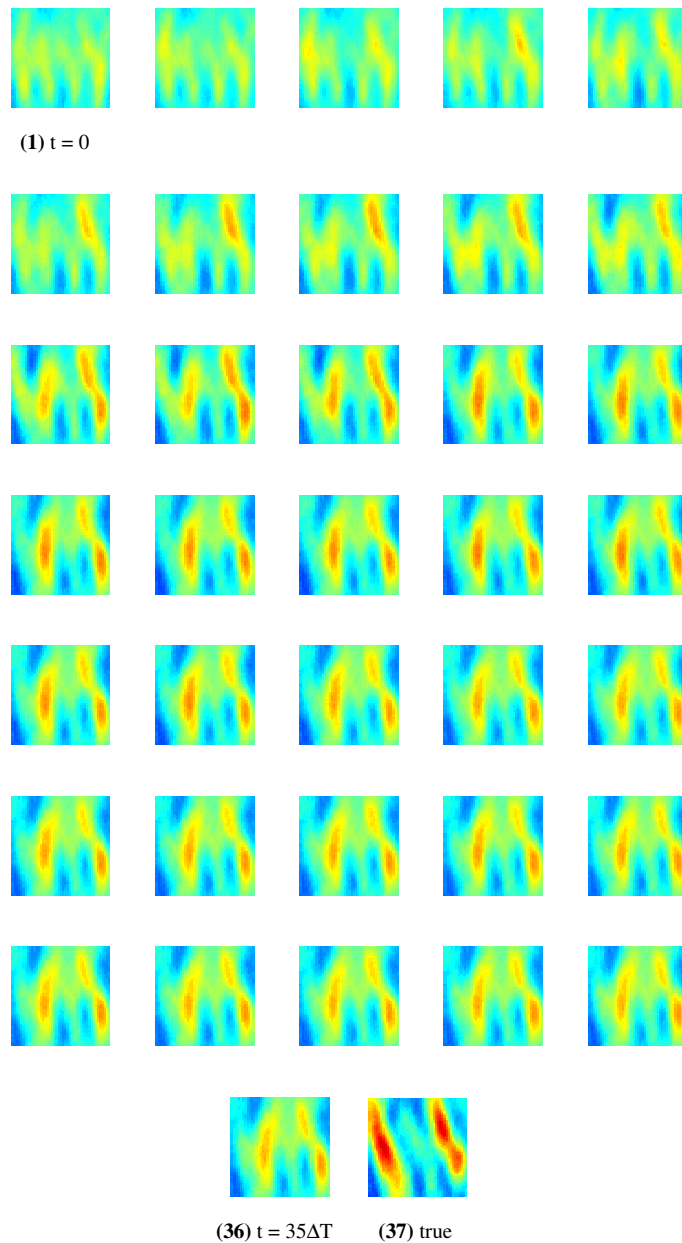


Figure 5.18: Estimates of the mean permeability field as function of time for the closed-loop certainty equivalent strategy. The initial estimate is a four channel structure. The estimates, $\hat{\theta}_{k|k-1}$, converge towards the true two-channel structure as more measurements are assimilated.

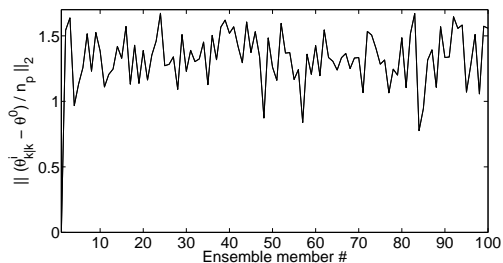
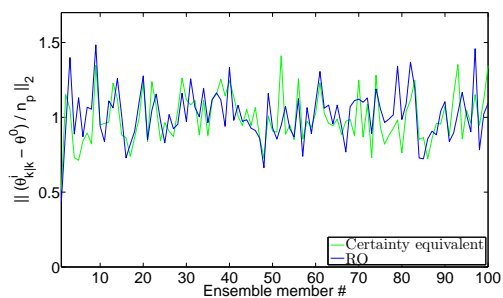
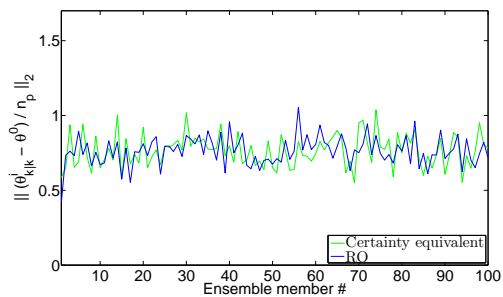
(1) $t=0$ (2) $t=5110$ days, Meas. noise = 5 R(3) $t=5110$ days, Meas. noise = R/5

Figure 5.19: Closed-loop. Distance of the ensemble realizations of the permeability field respect to the true permeability field for (1) the initial ensemble, (2) the final ensemble with a measurement noise of 5 R and (3) the final ensemble with a measurement noise of R/5. We note that also in the case with the lowest measurement noise, the ensemble is not collapsing.

5.4 Case study III: Mean-Variance Optimization

The mean-variance optimization strategy is studied for two test cases. The same reservoir permeability fields and petro-physical parameters are used for the two test cases. Fig. 5.1 illustrates the ensemble of permeability fields used to represent the uncertain reservoir. Fig. 5.3 illustrates the mean permeability field of the ensemble of permeability fields. As illustrated by Fig. 5.20 and reported in Table 5.4, the differences between the two test cases are the well configurations and the economical parameters. Test Case I contains more injector wells than Test Case II. Furthermore, compared to Test Case II, the water injection costs and the water separation costs are higher in Test Case I. This implies that a reactive strategy that injects water at a maximal rate is penalized in Test Case I with high water injection and water separation costs. Consequently, Test Case I is used to illustrate a complicated well configuration benefitting from intelligent coordination of wells and penalizing conventional reactive strategies. Test Case II is simpler and the value of feedback becomes more important than predictive coordination of the wells. This means that in Test Case II, a feedback based reactive strategy will be able to do better than a model based open loop strategy. Combined, the two test cases illustrate that the shape and geometry of the efficient frontier is case dependent, that the value of feedback in a reactive strategy compared to an open-loop optimization strategy is dependent on the well configuration, and that the mean-variance objective formulation is an efficient way to trade off risk and return.

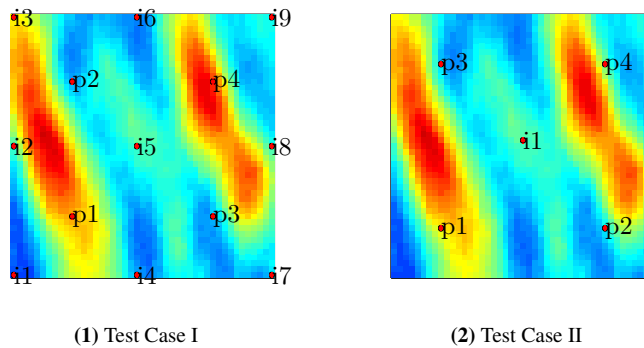


Figure 5.20: The well configuration for Test Case I and II. The permeability field in this plot is the permeability field in the upper left corner of Fig. 5.1. Producer wells are indicated by the letter p, and injector wells are indicated by the letter i. In addition to the injector and producer wells in Test Case II, Test Case I has a number of injector wells on the boundary of the field.

Table 5.4: Petro-physical and economical parameters for the two phase model and the discounted state cost function used in the case studies. TC I = Test Case I. TC II = Test Case II.

	Description	Value	Unit
ϕ	Porosity	0.2	-
c_r	Rock compressibility	0	Pa^{-1}
ρ_o	Oil density (300 bar)	700	kg/m^3
ρ_w	Water density (300 bar)	1000	kg/m^3
μ_o	Dynamic oil viscosity	$3 \cdot 10^{-3}$	$\text{Pa} \cdot \text{s}$
μ_w	Dynamic water viscosity	$0.3 \cdot 10^{-3}$	$\text{Pa} \cdot \text{s}$
S_{or}	Residual oil saturation	0.1	-
S_{ow}	Connate water saturation	0.1	-
n_o	Corey exponent for oil	2	-
n_w	Corey exponent for water	2	-
P_{init}	Initial reservoir pressure	300	bar
S_{init}	Initial water saturation	0.1	-
r_o	Oil price	120	USD/bbl
r_{wp}	Water separation cost (TC I)	25	USD/bbl
r_{wp}	Water separation cost (TC II)	20	USD/bbl
r_{wi}	Water injection cost (TC I)	15	USD/bbl
r_{wi}	Water injection cost (TC II)	10	USD/bbl
d	Discount factor	0	

5.4.1 Description of the Test Cases

We consider a conventional horizontal oil field that can be modeled as two phase flow in a porous medium [3]. The reservoir size is $450 \text{ m} \times 450 \text{ m} \times 10 \text{ m}$. By spatial discretization this reservoir is divided into $45 \times 45 \times 1$ grid blocks. The permeability field is uncertain, $\theta = \ln K$. We assume that the ensemble in Fig. 5.1 represents the range of possible geological uncertainties.

Table 5.4 lists the reservoir's petro-physical and economical parameters. The initial reservoir pressure is 300 bar everywhere in the reservoir. The initial water saturation is 0.1 everywhere in the reservoir. This implies that initially, the reservoir has a uniform oil saturation of 0.9. The manipulated variables are the bhps over the life of the reservoir. In this study, we consider a zero discount factor, d , in the cost function (5.1). This means that we maximize NPV at the final time without short term production considerations [21].

In both test cases, we consider a prediction horizon of $t_N = 4 \cdot 365 = 1460$ days divided

in $N = 60$ control periods (i.e. the control period is $T_s \approx 24$ days). We control the reservoir using three strategies: a reactive strategy, a CE strategy, and a MV strategy. The RO strategy is considered a special MV strategy with $\lambda = 1$. In the reactive strategy, we develop the field at the maximum production rate by setting the producers at the lowest allowed bhp value (290 bar) and the injectors at the maximum allowed bhp value (350 bar). When a production well is no longer economical it is shut in. A production well is uneconomical when the value of the produced oil is less than the separation cost of the produced water. The CE strategy is based on solving problem (2.27) using the CE cost function ψ_{CE} (5.8). It uses the mean (Fig. 5.3) of the ensemble (Fig. 5.1) as its permeability field. The MV strategy is based on solving problem (2.27) using the cost function ψ_{MV} (5.9) for different values of the parameter λ .

5.4.2 Test Case I

Fig. 5.20(1) illustrates the well configuration for Test Case I. Test Case I has 9 injection wells and 4 producer wells. Table 5.4 contains the petro-physical as well as the economic parameters. From the oil price and the water separation cost for Test Case I, it is apparent that a producer well becomes uneconomical when the fractional flow, f_w , exceeds $r_o/(r_o + r_{wp}) = 120/(120 + 25) = 0.828$.

Fig. 5.21 shows the optimal bhp trajectories for the the producer wells, while Fig. 5.22 shows the optimal bhp trajectories for the injector wells. These trajectories are computed using the reactive, the MV, the RO, and the CE optimization strategy. $\lambda = 0.59$ gives the market solution for this case, and this value of λ is used in the MV strategy. Compared to the RO and the market MV strategy, the CE trajectories do not contain sudden large changes in the bhp. This is due to the fact that the mean permeability field used by the CE strategy does not have sharp edges. It is also apparent that the bhp trajectories of the RO strategy has larger sudden changes than the trajectories of the market MV strategy. For some realizations of the permeability field, the RO trajectories would perform very well because they utilize the sharp channel structure in the permeability field. However, sudden large changes in the manipulated variables is an indication of solutions that are sensitive to process noise and model uncertainties. As sensitivity to noise is related to high risk, the trajectories of the bore hole pressures indicate that the RO strategy is more risky than the market MV strategy. This observation is confirmed in Fig. 5.23.

Fig. 5.23 illustrates the profit, ψ^i , for each realization of the permeability field using the reactive strategy as well as the CE, the RO, and the market MV optimal control strategies. The average profit over the realizations is a measure of the expected return, while the fluctuations are a measure of risk. For each control strategy, the bigger the fluctuations in profit the bigger the related risk. It is evident that the CE strategy has the lowest expected return and the biggest risk. The CE strategy also has the lowest worst

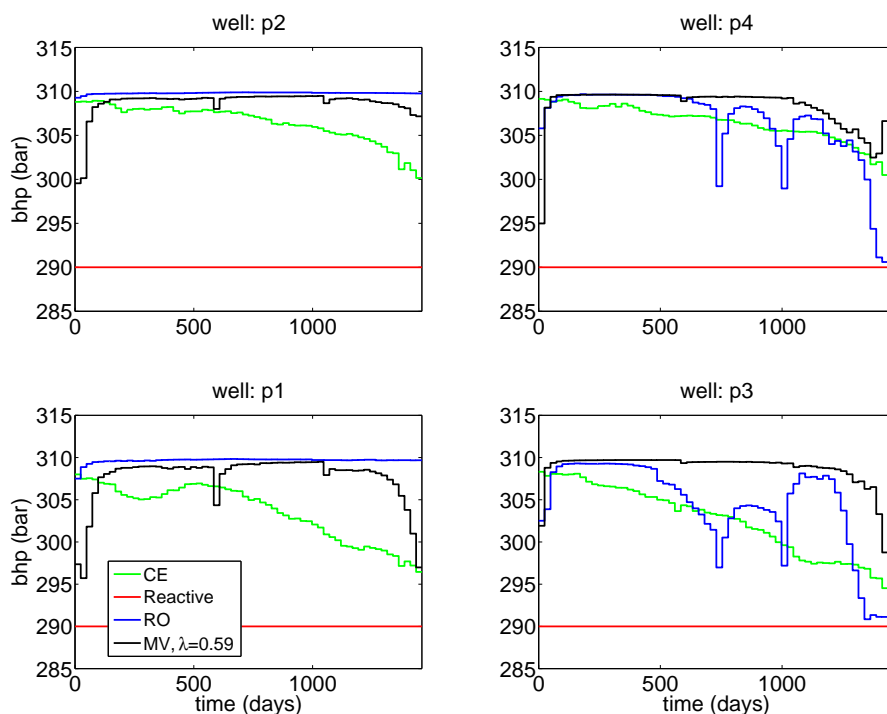


Figure 5.21: Test Case I. Trajectories of the bhp at producer wells using different optimization strategies. In the reactive strategy, the producer wells are shut in when production becomes uneconomical. The shut in time is different for each realization and is not indicated in the plot.

case return. The reactive strategy has a mean return that is higher than the mean return of the CE strategy but lower than the mean returns of the RO and the MV strategies. The risk for the reactive strategy is lower than the risk for the CE strategy but higher than the risks for the RO and the MV strategies. Comparing the market MV and the RO strategies, the RO strategy has a slightly higher mean profit than the market MV strategy but at the price of a significantly higher risk.

Table 5.5 reports key performance indicators for each control strategy. The economical key performance indicators are the expected NPV, the standard deviation NPV, the Sharpe ratio, and the minimum and maximum NPV for the ensemble. The production related key performance indicators are the mean oil production, the mean water injection, and the production efficiency (5.15) for the ensemble. The mean oil production and the mean water injection are scaled by the pore volume of the reservoir. Interestingly, the MV market strategy ($\lambda = 0.59$) has the highest minimum ensemble

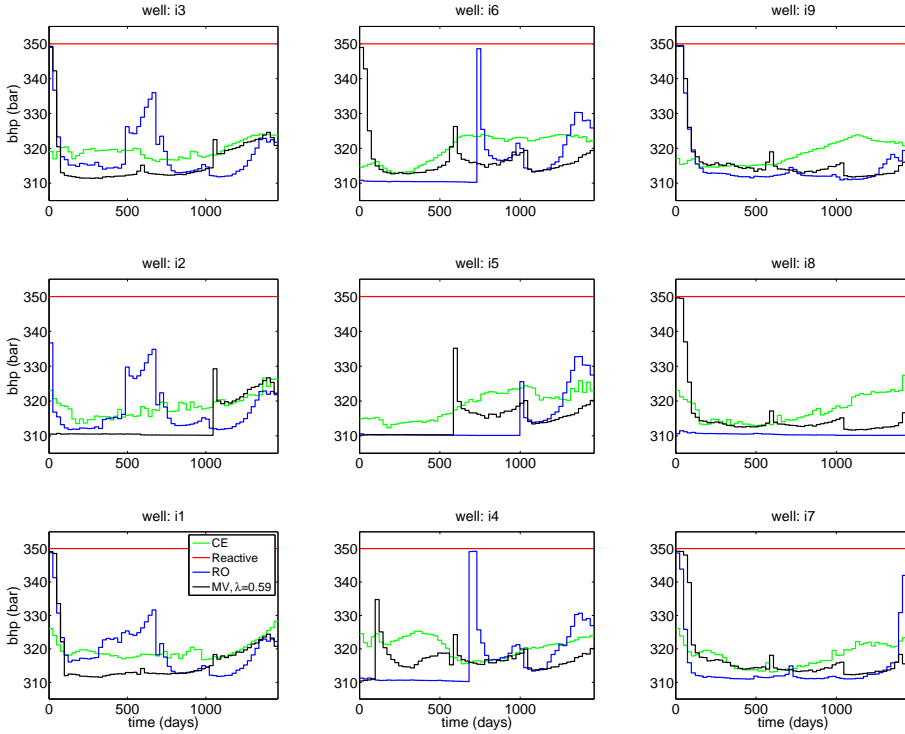


Figure 5.22: Test Case I. Trajectories of bhp for injector wells using different optimization strategies.

Table 5.5: Key performance indicators for Test Case I. The economic KPIs are the expected profit, the standard deviation of the profit, the Sharpe ratio, and the minimum and maximum profit for the ensemble. The reported production related KPIs are the expected oil production, the expected water injection, and the production efficiency, ξ . The productions are normalized by the pore volume. All improvements are relative to the reactive strategy.

Strategy	ψ		σ		S_h	$\underline{\psi}$		$\bar{\psi}$		$E_{\theta}[Q_o]$		$E_{\theta}[Q_{w,inj}]$		ξ
	10 ⁶ USD, %		10 ⁶ USD, %	10 ⁶ USD, %	%	%	%	%						
Reactive	39.04,	/	9.01,	/	4.34	17.62,	/	60.47,	/	0.39,	/	1.04,	/	37.8
CE	28.57,	-26.8	18.93,	+110.2	1.51	-23.86,	-235.4	60.25,	-0.40	0.32,	-18.4	0.88,	-15.3	36.4
MV														
$\lambda = 1$ (RO)	50.40,	+29.1	8.17,	-9.3	6.17	28.11,	+67.2	69.90,	+15.6	0.26,	-34.0	0.44,	-57.4	58.5
$\lambda = 0.75$	48.00,	+25.0	6.13,	-32.0	7.83	34.68,	+96.8	64.52,	+6.7	0.24,	-38.9	0.39,	-62.5	61.6
$\lambda = 0.59$	47.09,	+20.6	4.89,	-45.7	9.63	35.44,	+101	57.747,	-4.5	0.23,	-40.9	0.38,	-63.6	61.5
$\lambda = 0.5$	45.58,	+16.7	5.15,	-42.8	8.85	33.13,	+88.0	57.84,	-4.3	0.23,	-41.0	0.39,	-62.4	59.3
$\lambda = 0.25$	45.09,	+15.5	4.76,	-47.1	9.47	32.39,	+83.8	56.3,	-6.9	0.22,	-42.5	0.37,	-64.0	60.3
$\lambda = 0.125$	44.00,	+12.7	4.61,	-48.8	9.54	31.73,	+80.1	54.67,	-9.6	0.22,	-44.1	0.36,	-65.1	60.5
$\lambda = 0$	41.57,	+6.5	5.02,	-44.2	8.28	29.47,	+67.2	52.40,	-13.3	0.21,	-45.6	0.36,	-64.9	58.6

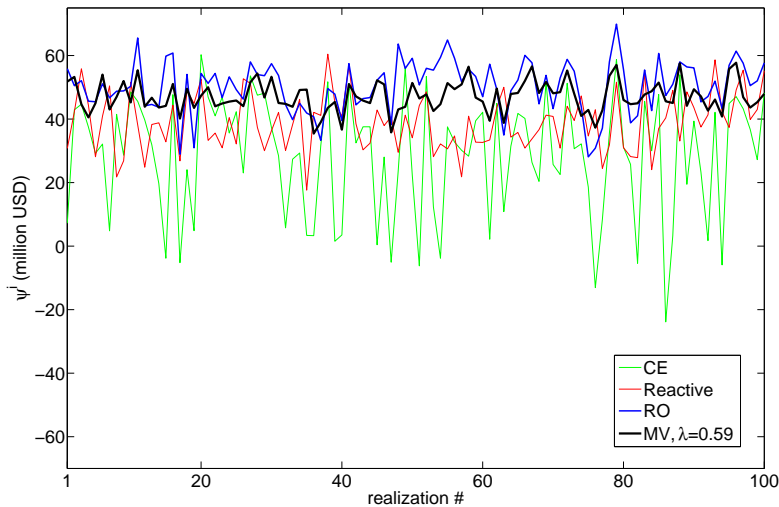
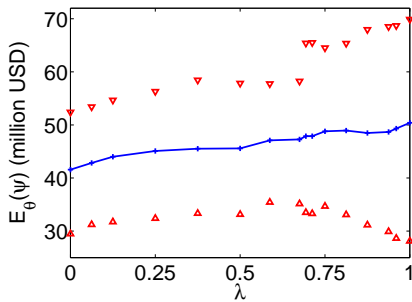
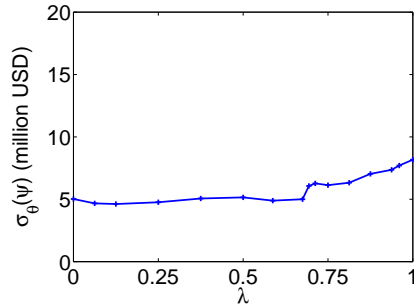


Figure 5.23: Test Case I. The net present value (NPV) of the optimal solution for each realization of the ensemble. The optimal solution is computed using a CE objective, a RO objective, and a MV objective with a mean-variance trade-off corresponding to the market solution ($\lambda = 0.59$). We also show the NPVs for the reactive strategy.

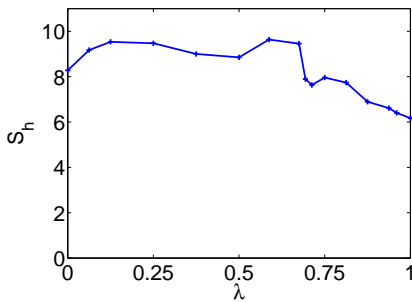
NPV value, i.e. in this case the market solution has a better worst case profit compared to all other control strategies including the MV strategies with lower standard deviation. Compared to the CE strategy and the reactive strategy, all MV control trajectories give higher expected NPV and lower NPV standard deviation. In that sense the MV solutions are said to dominate the CE solution and the solution given by the reactive strategy. The RO solution has the highest maximum NPV and also the highest expected NPV. However, among the MV solutions, it is also the solution with the lowest minimum NPV. This implies that the RO solution is very risky and this is confirmed by its high NPV standard deviation. Among the MV solutions, the RO solution has the highest NPV standard deviation. Fig. 5.24 summarizes the economic key performance indicators of the MV solutions. Fig. 5.24(1) shows the expected NPV as well as the worst and best NPV for the ensemble as function of the mean-variance trade-off parameter, λ . It is easily observed that the market MV solution, coincidentally, is also the max-min solution, i.e. the solution yielding the highest worst case NPV. Similarly, the high risk of the RO solution is evident. Fig. 5.24(2) illustrates the standard deviation of the NPV as function the mean-variance trade-off parameter, λ . The standard deviation of the NPV is a measure of risk. The risk is a non-monotonous function of the mean-variance trade-off parameter, λ . Measured by NPV standard deviation, the minimum



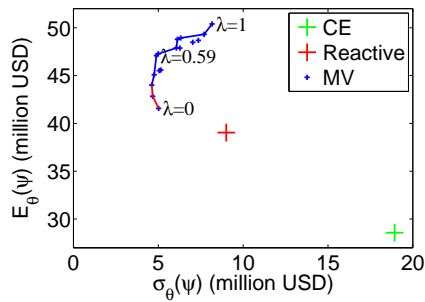
(1) Expected profit, max profit, and min profit.



(2) Risk measured as the standard deviation of profit.



(3) The Sharpe ratio.



(4) A risk-return plot. The expected NPV vs standard deviation of NPV.

Figure 5.24: Mean-variance relations for Test Case I. Profit (1), risk (2), and Sharpe Ratio (3) for different mean-variance trade-offs, λ . (4) is a phase plot of expected profit vs risk measured as the standard deviation of profit. The blue curve is the efficient frontier. The red curve is the inefficient frontier. Also the CE solution and the reactive solution are indicated.

risk solution is obtained for $\lambda = 0.125$. However, this solution is inferior to the market MV solution, as the market MV solution has a higher worst case NPV, a higher mean NPV, and a higher best case NPV (see Fig. 5.24(1)). Fig. 5.24(3) plots the Sharpe ratio as function of the mean-variance trade-off parameter, λ . This plot indicates that the maximal Sharpe ratio, i.e. the market solution, is obtained for $\lambda = 0.59$. The Sharpe ratio is not a concave function of λ in this case. Another local maximum with almost the same Sharpe ratio as the global maximum is obtained for $\lambda = 0.125$, i.e. for the minimum risk solution. As we noted previously, this solution is inferior to the market solution. Also note that the RO solution has the lowest Sharpe ratio. Fig. 5.24(4) illustrates the risk-return relations for the different MV strategies as well as the CE, the RO (MV with $\lambda = 1$), and the reactive strategy. This figure clearly illustrates the superiority

Table 5.6: Key Performance Indicators for Test Case II. The economic KPIs are the expected profit, the standard deviation of the profit, the Sharpe ratio, and the minimum and maximum profit for the ensemble. The reported production related KPIs are the expected oil production, the expected water injection, and the production efficiency, ξ . The productions are normalized by the pore volume. All improvements are relative to the reactive strategy.

Strategy	ψ		σ		S_h	$\underline{\psi}$		$\bar{\psi}$		$E_\theta[Q_o]$		$E_\theta[Q_{w,inj}]$		ξ
	10 ⁶ USD, %		10 ⁶ USD, %			10 ⁶ USD, %		10 ⁶ USD, %		%		%		
Reactive	56.47,	/	6.05,	/	9.33	43.92,	/	70.104,	/	0.35,	/	0.86,	/	39.5
CE	42.72,	-24.35	18.27,	+202.0	2.34	-38.40,	-187.4	72.21,	+3.01	0.26,	-26.0	0.64,	-27.4	40.3
MV														
$\lambda = 1$ (RO)	44.11,	-21.9	13.19,	+118.0	3.34	9.28,	-78.9	67.14,	-4.2	0.23,	-34.9	0.47,	-45.8	47.5
$\lambda = 0.75$	42.52,	-24.7	8.58,	+41.8	4.96	17.93,	-59.2	59.16,	+15.6	0.19,	-44.9	0.33,	-61.9	57.2
$\lambda = 0.5$	39.62,	-29.8	6.39,	+5.6	6.20	21.24,	-51.6	51.82,	-26.1	0.17,	-52.0	0.26,	-70.6	64.6
$\lambda = 0.25$	35.97,	-36.3	4.81,	-20.5	7.48	22.46,	-48.9	46.45,	-33.7	0.15,	-58.0	0.21,	-76.3	70.0
$\lambda = 0.125$	32.64,	-42.2	4.32,	-28.7	7.56	21.29,	-51.5	42.46,	-39.4	0.13,	-62.5	0.18,	-79.6	72.7
$\lambda = 0$	26.23,	-53.5	3.99,	-34.0	6.57	17.37,	-60.5	36.38,	-48.1	0.10,	-71.2	0.12,	-86.1	81.9

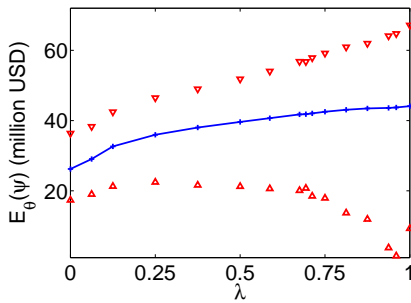
of the market MV strategy over the reactive strategy and the CE strategy. It also shows the reduced risk of the market MV strategy compared to the RO strategy at the cost of slightly reduced mean profit. The risk-return curve for the MV optimization strategies has two arcs. The efficient frontier arc is the blue curve in Fig. 5.24(4); the red curve is the inefficient frontier. In the efficient frontier, an increased risk is associated with an increased mean return. The MV strategy contains some risk-return points that are feasible but not on the efficient frontier, i.e. points that for a given risk level does not produce the maximal expected return.

For Test Case I, the production related key performance indicators in Table 5.5 demonstrate that the reactive strategy produces much more oil compared to the other control strategies. However, it also injects and produces much more water, i.e. $E_\theta[Q_o] = 0.39$ pore volume and $E_\theta[Q_{w,inj}] = 1.04$ pore volume. From a pure production point of view, the most efficient MV solution does not coincide with the market solution nor with the RO solution. It occurs for $\lambda = 0.75$ and has a production efficiency of $\xi = 61.6\%$, i.e. 61.6 barrels of oil is produced for 100 barrels of injected water.

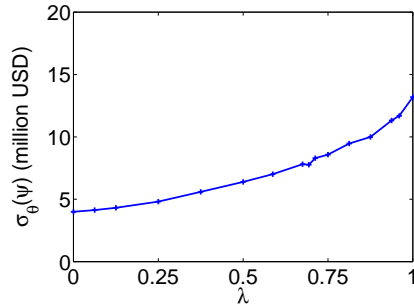
5.4.3 Test Case II

Test Case II has the well configuration indicated in Fig. 5.20(2). The petro-physical and economical parameters reported in Table 5.4 are used for the simulations. This implies that a producer well becomes non-economical when the fractional water flow, f_w , exceeds $r_o/(r_o + r_{wp}) = 120/(120 + 20) = 0.857$. Compared to Test Case I, Test Case II has fewer injection wells and the water separation cost is lower.

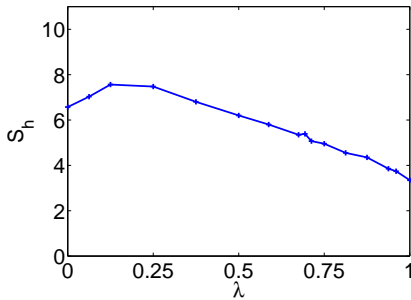
Fig. 5.25 and Table 5.6 report the economic key performance indicators for Test Case



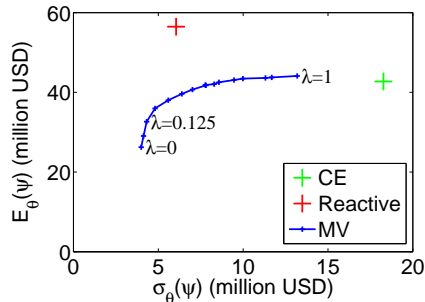
(1) Expected profit, max profit, and min profit.



(2) Risk measured as the standard deviation of profit.



(3) The Sharpe ratio.



(4) A risk-return plot. The expected NPV vs standard deviation of NPV.

Figure 5.25: Mean-variance relations for Test Case II. Profit (1), risk (2), and Sharpe Ratio (3) for different mean-variance trade-offs, λ . (4) is a phase plot of expected profit vs risk measured as the standard deviation of profit. The blue curve is the efficient frontier. Also the CE and reactive strategy are indicated.

II. They summarize and provide an overview of the performance of different control strategies for Test Case II. The Sharpe ratio curve in Fig. 5.25(3) indicates that the market MV solution is obtained for $\lambda = 0.125$. As illustrated by the efficient frontier in the risk-return plot in Fig. 5.25(4), the RO solution and the CE solution both have higher expected return as well as significantly higher risk (NPV standard deviation) than the MV market solution. Comparing with the sketch in Fig. 1.2, the efficient frontier illustrated in Fig. 5.25(4) is a textbook example of the relation between risk and return. At the price of a low reduction in the expected return, the MV market solution decreases the risk significantly compared to the RO solution and CE solution. Also the worst case NPV is much higher for the MV market solution than the corresponding values for the RO solution and the CE solution. For the CE solution, the worst case

NPV is even negative.

Test Case II has been included to demonstrate the value of information and feedback. While the optimization based strategies studied in this paper are open-loop strategies that do not use feedback, the reactive strategy is a feedback controller. As reported in Fig. 5.25(4) and Table 5.6, the reactive strategy has both a higher expected NPV and a lower risk (NPV standard deviation) than the RO solution as well as the CE solution. Consequently, the reactive solution is superior to the open-loop CE and RO strategies. Furthermore, the worst case NPV of the reactive strategy is higher than worst case NPVs of the CE solution and the RO solution. The worst case NPV of the reactive strategy is even better than the mean NPV of the CE strategy. Fig. 5.25(4) illustrates that the reactive strategy has a significantly higher return than the MV market solution. However, the reactive strategy also has a higher risk measured by the NPV standard deviation. Nevertheless, the reactive strategy is still superior to the MV market solution as the worst case NPV of the reactive strategy is larger than the best case NPV of the market MV solution. This illustrates that even though a control strategy may have a larger standard deviation than another control strategy, it may still be superior as all its possible profits are larger than the profits of the other control strategy.

Interestingly and perhaps surprising, Fig. 5.25(1) as well as Table 5.6 indicates that the Market MV solution is in some sense inferior to the MV solution obtained for $\lambda = 0.25$. The MV solution for $\lambda = 0.25$ has a worst case NPV, a mean NPV, and a best case NPV, that are all higher than the corresponding values for the market solution. Even though the market solution has lower risk in terms of standard deviation of the NPV, this becomes in some sense irrelevant as both the mean NPV and the worst case NPV of the MV solution with $\lambda = 0.25$ are higher than the corresponding values of the market solution. A more detailed comparison of the two MV strategies would require the distribution of the NPVs for the two strategies and not only the just discussed statistics.

In addition to economic key performance indicators, Table 5.6 also reports key performance indicators related to production. The reactive strategy has the highest oil recovery but also the highest water injection such that the production efficiency, ξ , is the lowest of all strategies. The most efficient solution measured by the production efficiency, ξ , would be the minimum variance solution obtained for $\lambda = 0$. This solution would have a production efficiency of $\xi = 81.9\%$. In economic terms, this solution would still be inferior to the reactive strategy.

5.4.4 Summary

Using two test cases, we have demonstrated production optimization of an uncertain oil reservoir by open-loop optimal control using a mean-variance objective function. We have compared optimal control using a mean-variance objective function to open-loop

optimal control with a CE objective function and an RO objective function, respectively. For uncertain reservoirs, the market solution of the mean-variance objective provides better and more well-behaved bhp trajectories with less risk (standard deviation) of the NPV. This reduced risk typically comes at the price of reduced profit. The simulations reveal that for the reservoirs in this paper, the reduction in expected NPV is modest compared to the risk reduction. Risk mitigation by the mean-variance objective can be regarded as a regularization of the RO objective and has the same regularizing effect on the solution, i.e. the bhp trajectories, as the effect of e.g. a Tikhonov regularizer in least squares problems [109].

The analysis, evaluation and discussion of control performance in uncertain oil reservoirs is facilitated by Fig. 5.24 and Fig. 5.25. In practice a dash board of risk return relations similar to Fig. 5.24 and Fig. 5.25 will be very valuable for reservoir management and risk mitigation. A closed-loop reservoir management system, should compute MV optimal control solutions for $\lambda \in [0, 1]$. This would give the expected NPV, the NPV standard deviation, the Sharpe ratio, and the efficient frontier in a risk-return diagram. The range of possible NPVs are subsequently computed by simulating each of the optimal control solutions for each of the permeability fields in the ensemble. Reservoir engineers and managers could then analyze the diagrams as well as selected bhp trajectories. Based on this analysis, they should select a mean-variance trade-off parameter, λ . This could be the market solution, but it could also be another value. A set of optimal injector and producer well bhp trajectories corresponds to the selected value of λ . The bhp values in the first control period are implemented in the reservoir. Test Case II demonstrated the importance of feedback. To incorporate measurements obtained one control period later, a history matching procedure should be used to update the ensemble of permeability fields. Based on this updated ensemble of permeability fields, the mean-variance open-loop optimal control computations are repeated and the first part of the selected optimal bhps are implemented [56].

In the analysis and discussion of the performance of different control strategies, worst case analysis is beneficial and informative. In this study, we analyzed worst case performance by simulation using a bhp trajectory obtained by open-loop MV optimization; i.e. as part of solving the mean-variance optimal control problem, we computed the NPV, ψ^i , for each member of the ensemble, and the set $\{\psi^i\}_{i=1}^{n_d}$ was used to determine $\underline{\psi} = \min \{\psi^i\}_{i=1}^{n_d}$ and $\bar{\psi} = \max \{\psi^i\}_{i=1}^{n_d}$. In a future study, it would be interesting to compare the MV solution to a max-min solution, i.e. to compute the optimal control trajectories by solution of

$$\max_{\{u_k\}_{k=0}^{N-1}} \min_{i \in \{1, 2, \dots, n_d\}} \psi = \psi(\{u_k\}_{k=0}^{N-1}; x_0, \theta^i) \quad (5.16a)$$

$$s.t. \quad c(\{u_k\}_{k=0}^{N-1}) \leq 0 \quad (5.16b)$$

Subsequently, key performance indicators such as the mean, the standard deviation, and the Sharpe ratio may be computed. These key performance indicators can be used to evaluate and compare the max-min solution to the mean-variance solutions.

CHAPTER 6

Concluding Remarks and Recommendations for Further Work

In this section, we offer some concluding remarks, possible extensions, and directions for future research.

In this thesis we have looked at the application of Nonlinear Model Predictive Control to the oil production optimization problem. Specifically, we focused on three active research areas in the oil industry:

1. *Efficient High Order Forward and Adjoint gradients computation by ESDIRK methods*

In Chapter 4 we propose the use of high order continuous and discrete adjoints, based on ESDIRK methods, in a gradient based algorithm for oil reservoir production optimization. The resulting algorithm is tested for a production optimization problem of an oil reservoir with a slightly compressible two phase flow. For all cases considered, the dynamic optimization increases the net present value of the field and gives increased oil production. Computational experiments demonstrate that the accuracy of the sensitivities obtained by the adjoint methods are comparable to the accuracy obtained by the finite difference method. Using the

ESDIRK method, the continuous adjoint method is able to use a time grid different from the time grid used for forward integration. Therefore, it can compute these sensitivities much faster than the discrete adjoint method and the finitedifference method. Computational experiments show that when the time steps are controlled in a certain range, the continuous adjoint method produces gradients sufficiently accurate for the optimization algorithm and somewhat faster than the discrete adjoint method.

Future work in this area should investigate the use of a variable step-size in the forward integration. For basic simulation tasks, our software is equipped with a PI stepsize controller, while the forward integration reported in this thesis is based on a fixed step size. In this work we didn't report preliminary results of using the adaptive step size controller as it is not clear yet how to set the controller tolerances during the adjoint integration. Simulations suggests that relatively smaller step-sizes should be taken at the end of the horizon when integrating backward with the continuous adjoint.

2. *Study of Open-loop and Closed-loop Robust Optimization Strategies*

In Chapter 5, we demonstrate the open-loop and the closed-loop performance of the certainty equivalent strategy and the RO strategy. For the open-loop case we present a modified RO strategy that performs significantly better than the other open-loop strategies. In the closed-loop situation for the case studied, we arrive at the surprising conclusion that the certainty equivalent strategy is slightly better than the RO strategy.

For the case presented, the open-loop RO strategy yields 3% higher expected NPV and 28% lower NPV standard deviation than the open-loop certainty equivalent strategy. Yet, the reactive strategy performed even better than the open-loop RO strategy. Simulations indicate that the inferior performance of the open-loop RO strategy compared to the reactive strategy is due to the inability of the RO strategy to efficiently encompass ensembles with very different and conflicting optimal control trajectories. We propose a modified RO strategy that allow shut in of uneconomical wells. The modified RO strategy performs significantly better than the other open-loop strategies and the reactive strategy. The modified RO optimization strategy yields an expected NPV that is 36% higher than the expected NPV of the open-loop certainty equivalent strategy and 3% higher than the expected NPV for the reactive strategy. The NPV standard deviation of the modified RO strategy is similar to the NPV standard deviation of the reactive strategy. These observations are non-trivial, as previous literature suggests that the open-loop RO strategy performs better than the reactive strategy [58]. The improved economic performance of the open-loop modified RO strategy justifies the computational effort used in determining the trajectories for this strategy.

The simulations for the closed-loop strategies, reveal that the RO strategy and the certainty equivalent strategy yields significantly higher NPV than the reac-

tive strategy. Surprisingly, the closed-loop certainty equivalent strategy yields a higher NPV than the closed-loop RO strategy for the case studied. The uncertainty reduction of the permeability field estimate due to data assimilation explains the good performance of the closed-loop certainty equivalent optimization strategy. Consequently, in closed-loop, the increased computational effort of the RO strategy compared to the certainty equivalent strategy is not justified for the particular case studied in Section 5.3.

Future work in this area should include a test of the strategies discussed in Section 5.3 for a more complex scenario (many wells, 3D grid, state/output constraints, spurious correlations), and we plan to work on the "Brugge field" [46]. In open-loop simulations, we expect that the modified RO strategy will improve the RO strategy as seen here. This result is in some way anticipated in [108], where, despite they do not consider uncertainty in the reservoir parameters, they get an increased NPV on the "Brugge field" by adding a reactive control to an optimal control strategy. In closed-loop simulations, we expect to obtain similar results for the RO and the CE strategies provided the data assimilation converges properly, as in the case showed in Section 5.3.

3. *Return-risk Mitigation in Production Optimization*

In Chapter 5, we describe a mean-variance approach to risk mitigation in production optimization by open-loop optimal control. The mean-variance approach to risk mitigation is well known in finance and design optimization, but have to our knowledge not been used previously for production optimization of oil reservoirs. By simulation, we demonstrate a computationally tractable method for mean-variance optimal control calculations of a reservoir model consisting of an ensemble of permeability fields. Compared to the RO strategy and the CE strategy, the MV strategy based on the market value of the mean-variance trade-off parameter, λ , is able to reduce risk significantly. This comes at the price of slightly reduced mean profits. In Test Case II we indicated the importance of feedback. Therefore, future studies should investigate the mean-variance optimal control strategy in a moving horizon closed-loop fashion. Implemented in closed-loop using the moving horizon principle, the optimal control problem for production optimization of an oil reservoir is an example of an Economic Non-linear Model Predictive Controller (Economic NMPC). Therefore, we believe that the mean-variance objective function introduced in this paper will be of interest to not only production optimization for closed-loop reservoir management but also for Economic NMPC in general. Further, a modified MV strategy that can shut in uneconomical wells (similar to the modified RO in [56]) should be investigated. Finally, we should take in consideration modifications to the MV cost function (5.9). For example, we should investigate the results of directly maximizing the Sharpe ratio (5.11) in (2.27) or investigate what happens if we consider the dimensional correct standard deviation σ instead of the dimensional incorrect variance σ^2 in (5.9).

Future work should include also other important tasks, as:

- In this thesis, we used a direct sparse LU solver to solve the flow equations. Future work should use efficient large-scale iterative solvers as implemented in the Stanford General Purpose Reservoir Simulator [110].
- Implementations of the algorithms as efficient C++/MPI code are needed to solve more realistic scenarios (the algorithms described in this thesis have been implemented in Matlab).
- Integrations of the implemented algorithms in a unique software for CLRM
- Test the algorithms discussed in this thesis for more complex scenarios to generalize the results presented in this thesis
- Comparisons with state-of-the-art commercial simulators as a validation of the developed software.
- Lastly, to fully exploit the potential of high order schemes, we should combine the high order time integration scheme ESDIRK with a high order spatial integration scheme. In [111] they solve a two-phase flow by combining a higher order discontinuous Galerkin method with a high order explicit RK method. The method proposed shows very promising results in both quality of the results and computational efficiency.

APPENDIX **A**

Useful Results

A.1 ESDIRK Coefficients

The coefficients for ESDIRK12, ESDIRK23 and ESDIRK34 used in chapters 3 and 4 are found in Table A.1, A.2 and A.3 respectively.

Table A.1: Coefficients for ESDIRK12

Coefficient	Value
s	2
c_1	0
c_2	1
a_{21}	0
γ	1
b_1	0
b_2	1
d_1	$-\frac{1}{2}$
d_2	$\frac{1}{2}$
q	2
$\bar{b}_{i,k}$	$\begin{pmatrix} 0 & -1/2 \\ 0 & 1/2 \end{pmatrix}$

Table A.2: Coefficients for ESDIRK23

Coefficient	Value
s	3
c_1	0
c_2	0.585786437626905
c_3	1
a_{21}	0.292893218813452
γ	0.292893218813452
a_{31}	0.353553390593274
a_{32}	0.353553390593274
b_1	0.353553390593274
b_2	0.353553390593274
b_3	0.292893218813452
d_1	0.13807118745769
d_2	-0.333333333333333
d_3	0.195262145875635
q	3
$\bar{b}_{i,k}$	$\begin{pmatrix} 1 & -1.35355339059327 & 0.569035593728849 \\ 0 & 2.06066017177982 & -1.37377344785321 \\ 0 & -0.707106781186547 & 0.804737854124365 \end{pmatrix}$

Table A.3: Coefficients for ESDIRK34

Coefficient	Value
s	4
c_1	0
c_2	0.871733043016918
c_3	0.468238744851844
c_4	1
a_{21}	0.435866521508459
γ	0.435866521508459
a_{31}	0.140737774724706
a_{32}	-0.108365551381321
a_{41}	0.102399400619911
a_{42}	-0.376878452255556
a_{43}	0.838612530127186
a_{44}	γ
b_1	a_{41}
b_2	a_{42}
b_3	a_{43}
b_4	a_{44}
d_1	-0.054625497240414
d_2	-0.494208893625995
d_3	0.221934499735065
d_4	0.326899891131344
q	3
$\bar{b}_{i,k}$	$\begin{pmatrix} 0.92277773077164 & -1.53835725968353 & 0.71797892953181 \\ -0.69864686211777 & 0.26665836746888 & 0.05511004239334 \\ 0.31374150452444 & 1.88835458133266 & -1.36348355572992 \\ 0.46212762682169 & -0.61665568911801 & 0.59039458380477 \end{pmatrix}$

A.2 Proof of Proposition 1.

The idea in the proof stems from [66]. Define

$$G(x, \dot{x}, u) = \frac{d}{dt} g(x(t)) - f(x(t), u(t)) = \frac{\partial g}{\partial \dot{x}} \dot{x}(t) - f(x(t), u(t)) = 0 \quad (\text{A.1})$$

and introducing the adjoint variable, $\lambda(t)$, to define the augmented objective function as

$$J_A = J + \int_{t_a}^{t_b} \lambda^T(t) G(x, \dot{x}, u) dt \quad (\text{A.2a})$$

(A.1) implies that the derivative of the augmented objective function, J_A , can be expressed as

$$\begin{aligned} \frac{dJ_A}{du_k} &= \frac{dJ}{du_k} = \left. \frac{\partial \hat{\Phi}}{\partial x} \frac{\partial x}{\partial u_k} \right|_{t_b} + \int_{t_a}^{t_b} \left(\frac{\partial \Phi}{\partial u} \frac{\partial u(t)}{\partial u_k} + \frac{\partial \Phi}{\partial x} \frac{\partial x(t)}{\partial u_k} \right) dt \\ &+ \int_{t_a}^{t_b} \lambda^T(t) \left(\frac{\partial G}{\partial u} \frac{\partial u(t)}{\partial u_k} + \frac{\partial G}{\partial x} \frac{\partial x(t)}{\partial u_k} + \frac{\partial G}{\partial \dot{x}} \frac{\partial \dot{x}}{\partial u_k} \right) dt \end{aligned} \quad (\text{A.3})$$

where

$$\frac{\partial u(t)}{\partial u_k} = \begin{cases} I & t_k \leq t < t_{k+1} \\ 0 & \text{otherwise} \end{cases} \quad (\text{A.4})$$

Integrating by part

$$\int_{t_a}^{t_b} \lambda^T(t) \frac{\partial G}{\partial \dot{x}} \frac{\partial \dot{x}}{\partial u_k} dt = \left[\lambda^T \frac{\partial G}{\partial \dot{x}} \frac{\partial x(t)}{\partial u_k} \right] \Big|_{t_a}^{t_b} - \int_{t_a}^{t_b} \frac{d}{dt} \left(\lambda^T \frac{\partial G}{\partial \dot{x}} \right) \frac{\partial x}{\partial u_k} dt \quad (\text{A.5})$$

and using $\frac{\partial x}{\partial u_k}(t_a) = 0$ in our case, we can rearrange equation (A.3) as

$$\begin{aligned} \frac{dJ}{du_k} &= \int_{t_k}^{t_{k+1}} \left(\frac{\partial \Phi}{\partial u} + \lambda^T \frac{\partial G}{\partial u} \right) dt + \int_{t_k}^{t_{k+1}} \left(\frac{\partial \Phi}{\partial x} + \lambda^T \frac{\partial G}{\partial x} - \frac{d}{dt} \left(\lambda^T \frac{\partial G}{\partial \dot{x}} \right) \right) \frac{\partial x}{\partial u_k} dt \\ &+ \left[\left(\frac{\partial \hat{\Phi}}{\partial x} + \lambda^T \frac{\partial G}{\partial \dot{x}} \right) \frac{\partial x}{\partial u_k} \right] \Big|_{t_b} \end{aligned} \quad (\text{A.6})$$

This expression gives the derivative dJ/du_k for any value (not just the optimal one) of $\lambda(t)$. We choose $\lambda(t)$ such that it satisfies

$$\frac{\partial \Phi}{\partial x} + \lambda^T \frac{\partial G}{\partial x} - \frac{d}{dt} \left(\lambda^T \frac{\partial G}{\partial \dot{x}} \right) = 0 \quad (\text{A.7a})$$

$$\left[\frac{\partial \hat{\Phi}}{\partial x} + \lambda^T \frac{\partial G}{\partial \dot{x}} \right] \Big|_{t_b} = 0 \quad (\text{A.7b})$$

and gives a simple expression for evaluation of dJ/du_k

$$\frac{\partial \Psi}{\partial u_k} = \frac{dJ}{du_k} = \int_{t_k}^{t_{k+1}} \left(\frac{\partial \Phi}{\partial u} - \lambda^T \frac{\partial f}{\partial u} \right) dt \quad (\text{A.8})$$

(A.1) implies

$$\frac{\partial G}{\partial x} = \frac{d}{dt} \left(\frac{\partial g}{\partial x} \right) - \frac{\partial f}{\partial x} \quad (\text{A.9a})$$

$$\frac{\partial G}{\partial \dot{x}} = \frac{\partial g}{\partial \dot{x}} \quad (\text{A.9b})$$

such that (A.7) can be rearranged to

$$\frac{d\lambda^T}{dt} \frac{\partial g}{\partial x} + \lambda^T \frac{\partial f}{\partial x} - \frac{\partial \Phi}{\partial x} = 0 \quad (\text{A.10a})$$

$$\frac{\partial \hat{\Phi}}{\partial x}(x(t_b)) + \lambda^T(t_b) \frac{\partial g}{\partial x}(x(t_b)) = 0 \quad (\text{A.10b})$$

Similarly we derive the expression for dJ/dx_0

$$\begin{aligned} \frac{dJ_A}{dx_0} = \frac{dJ}{dx_0} &= \frac{\partial \hat{\Phi}}{\partial x} \frac{\partial x}{\partial x_0} \Big|_{t_b} + \int_{t_a}^{t_b} \left(\frac{\partial \Phi}{\partial x} \frac{\partial x(t)}{\partial x_0} \right) dt \\ &+ \int_{t_a}^{t_b} \lambda^T(t) \left(\frac{\partial G}{\partial x} \frac{\partial x(t)}{\partial x_0} + \frac{\partial G}{\partial \dot{x}} \frac{\partial \dot{x}}{\partial x_0} \right) dt \end{aligned} \quad (\text{A.11})$$

Integrating by part

$$\int_{t_a}^{t_b} \lambda^T(t) \frac{\partial G}{\partial \dot{x}} \frac{\partial \dot{x}}{\partial x_0} dt = \left[\lambda^T \frac{\partial G}{\partial \dot{x}} \frac{\partial x(t)}{\partial x_0} \right] \Big|_{t_a}^{t_b} - \int_{t_a}^{t_b} \frac{d}{dt} \left(\lambda^T \frac{\partial G}{\partial \dot{x}} \right) \frac{\partial x}{\partial x_0} dt \quad (\text{A.12})$$

and using $\frac{\partial x}{\partial x_0}(t_a) = I$ in our case, we can rearrange equation (A.11) as

$$\frac{dJ}{dx_0} = \int_{t_k}^{t_{k+1}} \left(\frac{\partial \Phi}{\partial x} + \lambda^T \frac{\partial G}{\partial x} - \frac{d}{dt} \left(\lambda^T \frac{\partial G}{\partial \dot{x}} \right) \right) \frac{\partial x}{\partial x_0} dt + \left[\left(\frac{\partial \hat{\Phi}}{\partial x} + \lambda^T \frac{\partial G}{\partial \dot{x}} \right) \frac{\partial x}{\partial x_0} \right] \Big|_{t_b} - \lambda^T(t_a) \frac{\partial G}{\partial \dot{x}}(t_a) \quad (\text{A.13})$$

finally using $\lambda(t)$ computed in (A.7) we have

$$\frac{dJ}{dx_0} = -\lambda^T(t_a) \frac{\partial g}{\partial x}(t_a) \quad (\text{A.14})$$

A.3 Proof of Proposition 4.

We follow the same adjoint formalism as in [112, 113]. This is different, but equivalent to the more common one based on the Lagrange formalism [12, 65, 114] which make use of the augmented objective function $J_a = J - \lambda \bar{R}$. Adjoint formalism have a wider scope because adjoint variables are defined not only when optimal conditions are satisfied. When optimal conditions are satisfied, the adjoint variables coincide with Lagrange multipliers.

Starting from the discretized dynamical model in residual form (4.35)

$$\bar{R}(x_0, \bar{x}, \bar{u}) = 0 \quad (\text{A.15})$$

we use the implicit function theorem to find the sensitivities of the dependent variables with respect to the independent ones

$$\frac{\partial \bar{x}}{\partial \bar{u}} = -\frac{\partial \bar{R}^{-1}}{\partial \bar{x}} \frac{\partial \bar{R}}{\partial \bar{u}} \quad (\text{A.16a})$$

$$\frac{\partial \bar{x}}{\partial x_0} = -\frac{\partial \bar{R}^{-1}}{\partial \bar{x}} \frac{\partial \bar{R}}{\partial x_0}. \quad (\text{A.16b})$$

The total derivatives of the cost function in (4.35) are given by

$$\frac{dJ}{d\bar{u}}(x_0, \bar{x}, \bar{u}) = \frac{\partial J}{\partial \bar{u}} + \frac{\partial J}{\partial \bar{x}} \frac{\partial \bar{x}}{\partial \bar{u}} = \frac{\partial J}{\partial \bar{u}} - \frac{\partial J}{\partial \bar{x}} \frac{\partial \bar{R}^{-1}}{\partial \bar{x}} \frac{\partial \bar{R}}{\partial \bar{u}} \quad (\text{A.17a})$$

$$\frac{dJ}{dx_0}(x_0, \bar{x}, \bar{u}) = \frac{\partial J}{\partial x_0} + \frac{\partial J}{\partial \bar{x}} \frac{\partial \bar{x}}{\partial x_0} = \frac{\partial J}{\partial x_0} - \frac{\partial J}{\partial \bar{x}} \frac{\partial \bar{R}^{-1}}{\partial \bar{x}} \frac{\partial \bar{R}}{\partial x_0}. \quad (\text{A.17b})$$

Introducing the adjoint variables λ as solution of

$$\lambda^T \frac{\partial \bar{R}}{\partial \bar{x}} = -\frac{\partial J}{\partial \bar{x}} \quad (\text{A.18})$$

we can rewrite (A.17) as

$$\frac{\partial \psi}{\partial \bar{u}} = \frac{dJ}{d\bar{u}} = \frac{\partial J}{\partial \bar{u}} + \lambda^T \frac{\partial \bar{R}}{\partial \bar{u}} \quad (\text{A.19a})$$

$$\frac{\partial \psi}{\partial x_0} = \frac{dJ}{dx_0} = \frac{\partial J}{\partial x_0} + \lambda^T \frac{\partial \bar{R}}{\partial x_0}. \quad (\text{A.19b})$$

A.4 Derivatives $\frac{\partial R_{j,i}}{\partial X_{j,l}}$.

$$\begin{aligned}\frac{\partial R_{j,i}}{\partial X_{j,l}} &= \left(\frac{\partial g}{\partial x}(X_{j,l}) - h_j \gamma \frac{\partial f}{\partial x}(X_{j,l}, \tilde{u}_j) \right) \delta_{li} - \frac{\partial \phi_{j,i}}{\partial X_{j,l}} \\ \frac{\partial \phi_{j,i}}{\partial X_{j,l}} &= (1 - \delta_{li}) \left(\frac{\partial g}{\partial x}(X_{j,1}) \delta_{l1} + h_j a_{il} \frac{\partial f}{\partial x}(X_{j,l}, \tilde{u}_j) \right)\end{aligned}\quad (\text{A.20})$$

where δ_{li} is the Kronecker function.

$$\begin{aligned}\frac{\partial R_{j,i}}{\partial \tilde{u}_j} &= -\frac{\partial \phi_{j,i}}{\partial \tilde{u}_j} - h_j \gamma \frac{\partial f}{\partial u}(X_{j,i}, \tilde{u}_j) \\ \frac{\partial \phi_{j,i}}{\partial \tilde{u}_j} &= h_j \sum_{l=1}^{i-1} a_{il} \frac{\partial f}{\partial u}(X_{j,l}, \tilde{u}_j)\end{aligned}\quad (\text{A.21})$$

$$\frac{\partial J}{\partial u_k} = \sum_{j:u(\tilde{r}_j)=u_k} h_j \sum_{l=1}^s b_l \frac{\partial \Phi}{\partial u}(X_{j,l}, u_k) \quad (\text{A.22})$$

$$\frac{\partial J}{\partial x_0} = h_0 b_1 \frac{\partial \Phi}{\partial x_0}(X_{0,1}, u_0) \quad (\text{A.23})$$

$$\frac{\partial J}{\partial X_{j,i}} = h_j b_i \frac{\partial \Phi}{\partial x}(X_{j,i}, \tilde{u}_j) \quad i \in \{2, \dots, s-1\}, j \in \{0, \dots, \bar{N}-1\} \quad (\text{A.24})$$

$$\frac{\partial J}{\partial X_{j,s}} = h_j b_s \frac{\partial \Phi}{\partial x}(X_{j,s}, \tilde{u}_j) + h_{j+1} b_1 \frac{\partial \Phi}{\partial x}(X_{j+1,1}, \tilde{u}_{j+1}) \quad j \in \{0, \dots, \bar{N}-2\} \quad (\text{A.25})$$

$$\frac{\partial J}{\partial X_{\bar{N}-1,s}} = \frac{\partial \hat{\Phi}}{\partial X_{\bar{N}-1,s}}(\partial X_{\bar{N}-1,s}) + h_{\bar{N}-1} b_s \frac{\partial \Phi}{\partial X_{\bar{N}-1,s}}(\partial X_{\bar{N}-1,s}, u_N) \quad (\text{A.26})$$

A.5 Computation of the MV Objective and its Gradients

The mean-variance objective function for an ensemble is defined as

$$\psi_{MV} = \lambda \hat{\psi} - (1 - \lambda) \sigma^2 \quad (\text{A.27})$$

with the mean and variances computed by

$$\hat{\psi} = \frac{1}{n_d} \sum_{i=1}^{n_d} \psi^i \quad (\text{A.28a})$$

$$\sigma^2 = \frac{1}{n_d - 1} \sum_{i=1}^{n_d} (\psi^i - \hat{\psi})^2 \quad (\text{A.28b})$$

The gradient, $\nabla_{u_k} \psi_{MV}$ for $k \in \mathcal{N}$, is computed as

$$\nabla_{u_k} \psi_{MV} = \lambda \nabla_{u_k} \hat{\psi} - (1 - \lambda) \nabla_{u_k} \sigma^2 \quad k \in \mathcal{N} \quad (\text{A.29})$$

with the gradient of the mean, $\nabla_{u_k} \hat{\psi}$, computed as

$$\nabla_{u_k} \hat{\psi} = \frac{1}{n_d} \sum_{k=1}^{n_d} \nabla_{u_k} \psi^i \quad (\text{A.30})$$

The gradient of the variance, $\nabla_{u_k} \sigma^2$, is

$$\begin{aligned} \nabla_{u_k} \sigma^2 &= \frac{1}{n_d - 1} \sum_{i=1}^{n_d} \left[\nabla_{u_k} (\psi^i - \hat{\psi})^2 \right] \\ &= \frac{2}{n_d - 1} \sum_{i=1}^{n_d} \left[(\psi^i - \hat{\psi}) \nabla_{u_k} (\psi^i - \hat{\psi}) \right] \\ &= \frac{2}{n_d - 1} \sum_{i=1}^{n_d} \left[(\psi^i - \hat{\psi}) (\nabla_{u_k} \psi^i - \nabla_{u_k} \hat{\psi}) \right] \end{aligned} \quad (\text{A.31})$$

$\nabla_{u_k} \sigma^2$ can be computed by (A.31). To compute $\nabla_{u_k} \sigma^2$ more efficiently we express $\nabla_{u_k} \sigma^2$ as

$$\nabla_{u_k} \sigma^2 = \frac{2}{n_d - 1} \left(\sum_{i=1}^{n_d} \left[(\psi^i - \hat{\psi}) \nabla_{u_k} \psi^i \right] - \sum_{i=1}^{n_d} \left[(\psi^i - \hat{\psi}) \nabla_{u_k} \hat{\psi} \right] \right) \quad (\text{A.32})$$

and note that

$$\begin{aligned} \sum_{i=1}^{n_d} ((\psi^i - \hat{\psi}) \nabla_{u_k} \hat{\psi}) &= \left(\sum_{i=1}^{n_d} (\psi^i - \hat{\psi}) \right) \nabla_{u_k} \hat{\psi} \\ &= \underbrace{\left(\sum_{i=1}^{n_d} \psi^i - n_d \hat{\psi} \right)}_{=0} \nabla_{u_k} \hat{\psi} = 0 \end{aligned}$$

Consequently, the gradient of the variance can be computed efficiently by

$$\nabla_{u_k} \sigma^2 = \frac{2}{n_d - 1} \sum_{i=1}^{n_d} (\psi^i - \hat{\psi}) \nabla_{u_k} \psi^i \quad (\text{A.33})$$

APPENDIX B

Paper I

Solution of Constrained Optimal Control Problems using Multiple Shooting and ESDIRK Methods

Authors:

Andrea Capolei and John Bagterp Jørgensen

Published in:

Proceedings of the 2012 American Control Conference. Fairmont Queen Elizabeth, Montréal, Canada. June 27-June 29, 2012.

Solution of Constrained Optimal Control Problems using Multiple Shooting and ESDIRK Methods

Andrea Capolei and John Bagterp Jørgensen

Abstract—In this paper, we describe a novel numerical algorithm for solution of constrained optimal control problems of the Bolza type for stiff and/or unstable systems. The numerical algorithm combines explicit singly diagonally implicit Runge-Kutta (ESDIRK) integration methods with a multiple shooting algorithm. As we consider stiff systems, *implicit* solvers with sensitivity computation capabilities for initial value problems must be used in the multiple shooting algorithm. Traditionally, multi-step methods based on the BDF algorithm have been used for such problems. The main novel contribution of this paper is the use of ESDIRK integration methods for solution of the initial value problems and the corresponding sensitivity equations arising in the multiple shooting algorithm. Compared to BDF-methods, ESDIRK-methods are advantageous in multiple shooting algorithms in which restarts and frequent discontinuities on each shooting interval are present. The ESDIRK methods are implemented using an inexact Newton method that reuses the factorization of the iteration matrix for the integration as well as the sensitivity computation. Numerical experiments are provided to demonstrate the algorithm.

I. INTRODUCTION

Single-shooting (control vector parametrization) [1], multiple-shooting [2]–[4], and full discretization (the simultaneous method or collocation) algorithms [5] are the most common direct methods for numerical solution of constrained optimal control problems. These algorithms are widely used for solution of constrained optimal control problems as they arise in Nonlinear Model Predictive Control (NMPC) [6], [7].

The multiple-shooting algorithm has become a popular choice in NMPC applications as it has stability properties comparable to the full discretization method and can use state-of-the-art ODE/DAE solvers. For non-stiff systems, explicit Runge-Kutta solvers with sensitivity computation capabilities are used within the multiple-shooting algorithm [4]. For stiff systems, multi-step BDF based methods with sensitivity computation capabilities are typically used [8]–[11]. A one-step extrapolation method based on linearly implicit Euler discretization [12] as well as an explicit singly diagonally implicit Runge-Kutta (ESDIRK) [13], [14] method have subsequently been suggested for integration and sensitivity computation of stiff systems. Both these methods are one-step methods and advantageous in single- as well as multiple-shooting applications. Such applications have frequent discontinuities due to the control parametrization. Compared to multi-step methods, one-step methods have the

advantage that they do not suffer from re-start computation overhead at discontinuities.

In this paper, we describe a numerical algorithm for solution of constrained optimal control problems using multiple shooting and ESDIRK methods with sensitivity capabilities. ESDIRK methods are special implicit Runge-Kutta methods that are computationally efficient and often constructed such that they have an embedded error estimator and are both A- and L-stable, i.e. implying that they can be used for stiff systems, and are stiffly accurate [15]–[17]. ESDIRK methods have been reported to outperform multi-step methods such as BDF for problems in which medium- to high-accuracy solutions are required [17]–[19]. [20] develops ESDIRK methods of order 1-3 with embedded error estimators, i.e. ESDIRK1(2), ESDIRK2(3) and ESDIRK3(4), that are A- and L-stable as well as stiffly accurate. [13], [14] implement the ESDIRK3(4) with approximate computation of the sensitivities for ODEs and index-1 DAEs. [21] propose a novel representation of systems of differential equations

$$\frac{d}{dt}g(x(t)) = f(x(t), u(t)) \quad x(t_0) = x_0 \quad (1)$$

that are useful in describing systems arising in reservoir simulation. [21] also investigates simulation, step-size control, and adjoint-based single-shooting optimal control of such large-scale systems (1) using ESDIRK1(2), ESDIRK2(3), and ESDIRK3(4).

The main novel contribution of this paper is exact numerical computation of the sensitivities in differential equations (1) based on ESDIRK1(2), ESDIRK2(3) and ESDIRK3(4). The sensitivities are computed using the staggered corrector approach [8], [13] and an efficient inexact Newton algorithm that reuses the factorization of the iteration matrix. The solution of the differential equation (1) and its sensitivities are used within a multiple-shooting algorithm for constrained optimal control. To facilitate use of the integrator within an optimization algorithm the implemented ESDIRK methods employ the internal numerical differentiation principle [22].

The paper is organized as follows. Section II defines the constrained optimal control problem, the multiple-shooting discretization, and the resulting discrete-time nonlinear program. The ESDIRK algorithm for solution of the differential equation systems and computation of the associated sensitivities is described in Section III. Section IV provides examples to demonstrate the algorithm. Conclusions and ideas for future work are presented in Section V.

A. Capolei and J.B. Jørgensen are with the Department of Informatics and Mathematical Modeling, Technical University of Denmark, DK-2800 Kgs. Lyngby, Denmark. E-mail: {acap, jbj}@imm.dtu.dk

II. OPTIMAL CONTROL PROBLEM

We consider constrained optimal control problems in the Bolza form

$$\min_{x(t), u(t)} J = \hat{\Phi}(x(t_b)) + \int_{t_a}^{t_b} \Phi(x(t), u(t)) dt \quad (2a)$$

subject to

$$x(t_a) = x_0 \quad (2b)$$

$$\frac{d}{dt}g(x(t)) = f(x(t), u(t)), \quad t \in [t_a, t_b], \quad (2c)$$

$$c(u(t)) \geq 0 \quad (2d)$$

$x(t) \in \mathbb{R}^{n_x}$ is the state vector and $u(t) \in \mathbb{R}^{n_u}$ is the control vector. The time interval $I = [t_a, t_b]$ as well as the initial state, x_0 , are assumed to be fixed. (2c) represents the dynamic model and includes systems described by index-1 differential algebraic equations (DAE). (2d) represents bounds on the input values and their variation in time. Path constraints

$$\eta(x(t), u(t)) \geq 0 \quad (3)$$

may render the optimization problem infeasible. Therefore, we include these constraints as soft constraints using the following smooth approximation

$$\chi_i(x(t), u(t)) = \frac{1}{2} \left(\sqrt{\eta_i(x(t), u(t))^2 + \beta_i^2} - \eta_i(x(t), u(t)) \right) \quad (4)$$

to the exact penalty function $\max(0, -\eta_i(x(t)))$ for $i \in \{1, \dots, n_\eta\}$ [23]. With this approximation of the path constraints, the resulting stage cost, $\Phi(x(t), u(t))$, used in (2a) consist of the inherent stage cost, $\hat{\Phi}(x(t), u(t))$, and terms penalizing violation of the path constraints (3)

$$\Phi(x, u) = \hat{\Phi}(x, u) + \|\chi(x, u)\|_{1, Q_1} + \frac{1}{2} \|\chi(x, u)\|_{2, Q_2}^2 \quad (5)$$

A. Discretization

1) *Control Parametrization*: Let T_s denote the sample time such that an equidistant mesh can be defined as

$$t_a = t_0 < \dots < t_S < \dots < t_N = t_b \quad (6)$$

with $t_j = t_a + jT_s$ for $j = 0, 1, \dots, N$. We use a piecewise constant representation of the control function on this equidistant mesh, i.e. we approximate the control vector on every subinterval $[t_j, t_{j+1}]$ by the zero-order-hold parametrization

$$u(t) = u_j, \quad u_j \in \mathbb{R}^{n_u}, \quad t_j \leq t < t_{j+1}, \quad j = 0, \dots, N-1 \quad (7)$$

2) *State Discretization*: The key idea in solving the Initial Value Problem (2c) using multiple shooting is to divide the time interval $[t_a, t_b]$ into W subintervals $[t_{kS}, t_{(k+1)S}]$ called shooting windows. S denote the number of control vectors in each shooting window and k is an index of shooting-windows. $\mathbf{u}_k = [u_{kS}; u_{(k+1)S}; \dots; u_{(k+1)S-1}]$ represents

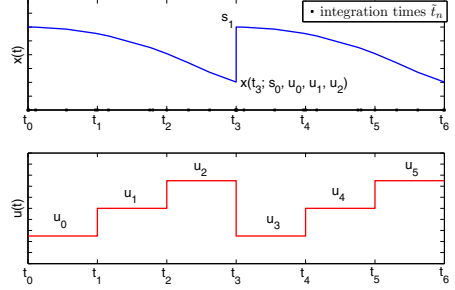


Fig. 1. An example of state and control discretization. Here we have $W = 2$ shooting windows, $N = 6$ control vectors and $S = 3$ control vectors for each shooting window. Also $n_x = n_u = 1$.

the control vectors in a shooting window. Accordingly, the multiple-shooting algorithm solves independent IVPs

$$\begin{aligned} \frac{d}{dt}g(x(t)) &= f(x(t), u(t)), \quad t \in I_k = [t_{kS}, t_{(k+1)S}] \\ x(t_{kS}) &= s_k, \quad k = 0, \dots, W-1 \end{aligned} \quad (8)$$

for each shooting window and determines the vectors s_k and \mathbf{u}_k in such a way that the function x pieced together by these IVP solutions,

$$x(t) := x_k(t; s_k, \mathbf{u}_k) \quad \text{for } t \in [t_{kS}, t_{(k+1)S}[\quad (9)$$

$k \in \{0, \dots, W-1\}$ is continuous and hence represents the solution of the differential equation (2c) in the interval $[t_a, t_b]$.

Define the augmented parameter vector $y \in \mathbb{R}^n$ with $n = Nn_u + (W-1)n_x$ by

$$y = [\mathbf{u}_0; s_1; \mathbf{u}_1; \dots; s_{W-1}; \mathbf{u}_{W-1}] \quad (10)$$

such that the continuity equations can be expressed as

$$G(y) = \begin{bmatrix} x_0(t_S, x_0, \mathbf{u}_0) - s_1 \\ x_1(t_{2S}, s_1, \mathbf{u}_1) - s_2 \\ \vdots \\ x_{W-2}(t_{(W-1)S}, s_{W-2}, \mathbf{u}_{W-2}) - s_{W-1} \end{bmatrix} = 0 \quad (11)$$

where $x_k(t, s_k, \mathbf{u}_k)$ denotes the solution of the IVP (8) in I_k . Similarly, the multiple-shooting discretization yields the following objective function, $J = F(y)$:

$$\begin{aligned} F(y) &= \hat{\Phi}(x_{W-1}(t_N, s_{W-1}, \mathbf{u}_{W-1})) \\ &+ \sum_{k=0}^{W-1} F_k(s_k, \mathbf{u}_k) \end{aligned} \quad (12a)$$

$$F_k(s_k, \mathbf{u}_k) = \int_{t_{kS}}^{t_{(k+1)S}} \Phi(t, x_k(t, s_k, \mathbf{u}_k), u(t)) dt \quad (12b)$$

3) *Input Constraints*: The input constraints (2d) include bound constraints $u_{\min} \leq u_k \leq u_{\max}$. In the discrete problem using the zero-order-hold parametrization, we also include rate of movement constraints in the form $\Delta u_{\min} \leq \Delta u_k \leq \Delta u_{\max}$ with $\Delta u_k = u_k - u_{k-1}$. These input constraints and rate of movement constraints may be represented by the function

$$H(y) \geq 0 \quad (13)$$

B. NLP Problem

Using the zero-order-hold parametrization, the multiple-shooting discretization, and the additions described in Section II-A, the constrained optimal control problem (2) can be approximated by the finite dimensional constrained optimization problem

$$\min_y F(y) \quad (14a)$$

$$\text{s.t. } G(y) = 0 \quad (14b)$$

$$H(y) \geq 0 \quad (14c)$$

We solve (14) using a quasi-Newton implementation of Powell's Sequential Quadratic Programming (SQP) method [24]. F is separable and the constraints, G and H , are linearly coupled. Consequently, the associated Lagrangian becomes partially separable. This property implies that the Hessian of the Lagrangian is block structured and is exploited in the BFGS approximation [2]. A full space sparse quadratic program exploiting this structure is solved at each iteration.

III. ESDIRK METHODS

In this section, we describe our implementation of the ESDIRK method for solution of the initial value problem (8) and for computation of the associated sensitivities. The sensitivities are needed when gradient based optimization algorithms are used for the solution of (14).

Let \tilde{t}_n denote the the integration times chosen by the step size controller in the integrator (see Fig. 1). Since each integration step, h_n , is always smaller than or equal to the sample time, T_s , the number of integration steps is always larger or equal to the number of control steps, N .

A. Solution of the IVP by ESDIRK Methods

The numerical solution of the IVP (8) by an s -stage, stiffly accurate, Runge-Kutta ESDIRK method with an embedded error estimator, may in each integration step $[\tilde{t}_n, \tilde{t}_{n+1}]$ be denoted [20]

$$T_1 = \tilde{t}_n, \quad T_i = \tilde{t}_n + c_i h_n \quad (15a)$$

$$X_1 = x_n \quad (15b)$$

$$\phi_i(\{X_j\}_{j=1}^{i-1}, u) = g(X_1) + h_n \sum_{j=1}^{i-1} a_{ij} f(X_j, u) \quad (15c)$$

$$g(X_i) = \phi_i(\{X_j\}_{j=1}^{i-1}, u) + h_n \gamma f(X_i, u) \quad (15d)$$

$$x_{n+1} = X_s \quad (15e)$$

$$e_{n+1} = h_n \sum_{j=1}^s d_i f(X_j, u) \quad (15f)$$

with $i = 2, \dots, s$. X_i denotes the numerical solution at time T_i for $i \in \{1, \dots, s\}$. x_{n+1} is the numerical solution at time $\tilde{t}_{n+1} = \tilde{t}_n + h_n$. e_{n+1} is the estimated error of the numerical solution, i.e. $\|e_{n+1}\| \approx \|g(x_{n+1}) - g(x(\tilde{t}_{n+1}))\|$.

The main computational effort in the ESDIRK method is solution of the implicit equations (15d) using a Newton based method. (15d) is solved by sequential solution of

$$R_i(X_i) := [g(X_i) - h_n \gamma f(X_i, u)] - \phi_i(\{X_j\}_{j=1}^{i-1}, u) = 0 \quad (16)$$

for $i = 2, \dots, s$. (16) is solved using an inexact Newton method. Each iteration in the inexact Newton method for solution of (16) may be denoted

$$M \Delta X_i^{[l]} = -R_i(X_i^{[l]}) \quad (17a)$$

$$X_i^{[l+1]} = X_i^{[l]} + \Delta X_i^{[l]} \quad (17b)$$

The iteration matrix, M , is an approximation

$$M \approx J(X_i^{[l]}) \quad (18)$$

to the Jacobian of the residual function

$$J_i(X_i) = \frac{\partial R_i}{\partial X_i}(X_i) = \frac{\partial g}{\partial x}(X_i) - h_n \gamma \frac{\partial f}{\partial x}(X_i, u) \quad (19)$$

The iteration matrix, M , and its LU factorization is updated adaptively by monitoring the convergence rate of the inexact Newton iterations.

Convergence of the inexact Newton iteration is measured by

$$\|R_i(X_i^{[l]})\| = \max_{j=1, \dots, n_x} \frac{|(R_i(X_i^{[l]}))_j|}{\max\{\text{atol}_j, \text{rtol}_j g_j(X_i^{[l]})\}} < \tau \quad (20)$$

where atol is the absolute tolerance and rtol is the relative tolerance. Steps are accepted if this measure of the residual is smaller than $\tau \approx 0.1$ [25]. In case of divergence or slow convergence, the iterations are terminated, the step size, h_n , is decreased and the Jacobian of the iteration matrix is re-evaluated and factorized [25].

B. Sensitivity Equations

The state sensitivity of (8) is defined as

$$S_{s_k}(t) = \frac{\partial}{\partial s_k} x_k(t; s_k, \mathbf{u}_k) \quad (21)$$

and satisfies

$$S_{s_k}(t_{kS}) = I \quad (22a)$$

$$\frac{\partial}{\partial t} \left(\frac{\partial g}{\partial x}(x(t)) S_{s_k}(t) \right) = \frac{\partial f}{\partial x}(x(t), u(t)) S_{s_k}(t) \quad (22b)$$

in the interval I_k with $k \in \{1, \dots, W-1\}$.

Similarly, the input sensitivity of (8) is defined as

$$S_{u_j}(t) = \frac{\partial}{\partial u_j} x_k(t; s_k, \mathbf{u}_k) \quad (23)$$

for $j \in \{kS, \dots, (k+1)S-1\}$ and $k = 0, 1, \dots, N-1$. $S_{u_j}(t)$ satisfies

$$S_{u_j}(t_j) = 0 \quad (24a)$$

$$\begin{aligned} \frac{\partial}{\partial t} \left(\frac{\partial g}{\partial x}(x(t)) S_{u_j}(t) \right) &= \frac{\partial f}{\partial x}(x(t), u(t)) S_{u_j}(t) \\ &+ \frac{\partial f}{\partial u}(x(t), u(t)) \frac{\partial u}{\partial u_j}(t) \end{aligned} \quad (24b)$$

in the interval $t_j \leq t \leq t_{(k+1)S}$ for $j \in \{kS, kS+1, \dots, (k+1)S-1\}$ and

$$\frac{\partial u}{\partial u_j}(t) = \begin{cases} I & t_j \leq t < t_{j+1} \\ 0 & \text{otherwise} \end{cases} \quad (25)$$

(22) and (24) may be derived from (8) by taking the derivatives with respect to s_k and u_j , by use of the chain rule and the Schwartz theorem.

C. Discrete Sensitivity equations

The ESDIRK method is used in a staggered-corrector fashion to integrate the sensitivity equations (22) and (24) at the quadrature points also used for integration of the initial value problem (8).

The state sensitivities are computed using the ESDIRK method by solution of

$$\bar{S}_{s_k,1} = S_{s_k,n} \quad (26a)$$

$$\Theta_{x,i} = \frac{\partial g}{\partial x}(X_1) \bar{S}_{s_k,1} + h_n \sum_{j=1}^{i-1} a_{ij} \frac{\partial f}{\partial x}(X_j, u) \bar{S}_{s_k,j} \quad (26b)$$

$$\frac{\partial g}{\partial x}(X_i) \bar{S}_{s_k,i} = \Theta_{x,i} + h_n \gamma \frac{\partial f}{\partial x}(X_i, u) \bar{S}_{s_k,i} \quad (26c)$$

$$S_{s_k,n+1} = \bar{S}_{s_k,s} \quad (26d)$$

for $i = 2, \dots, s$. The computationally expensive step in these computations is solution of the linear system of equations (26c)

$$R_{x,i}(\bar{S}_{s_k,i}) = J(X_i) \bar{S}_{s_k,i} - \Theta_{x,i} = 0 \quad (27)$$

with $J(X_i)$ defined by (19).

Similarly, the parameter sensitivities are computed using the ESDIRK method by solution of

$$\bar{S}_{u_j,1} = S_{u_j,n} \quad (28a)$$

$$\begin{aligned} \Theta_{u_j,i} &= \frac{\partial g}{\partial x}(X_1) \bar{S}_{u_j,1} \\ &+ h_n \sum_{l=1}^{i-1} a_{il} \left(\frac{\partial f}{\partial x}(X_l, u) \bar{S}_{u_j,l} + \frac{\partial f}{\partial u}(X_l, u) \frac{\partial u}{\partial u_j}(T_l) \right) \\ &+ h_n \gamma \frac{\partial f}{\partial u}(X_i, u) \frac{\partial u}{\partial u_j}(T_i) \end{aligned} \quad (28b)$$

$$\frac{\partial g}{\partial x}(X_i) \bar{S}_{u_j,i} = \Theta_{u_j,i} + h_n \gamma \frac{\partial f}{\partial x}(X_i, u) \bar{S}_{u_j,i} \quad (28c)$$

$$S_{u_j,n+1} = \bar{S}_{u_j,s} \quad (28d)$$

for $i = 2, \dots, s$. The computationally expensive step in these computations is the solution of the linear system of equations (28c)

$$R_{u_j,i}(\bar{S}_{u_j,i}) = J(X_i) \bar{S}_{u_j,i} - \Theta_{u_j,i} = 0 \quad (29)$$

with $J(X_i)$ defined by (19).

The linear system of equations (27) and (29) may be solved in identical ways. Therefore, we only discuss the solution of the state sensitivity equation (27) in the following. It is implied that the parameter sensitivity equation (29) is solved in a similar way.

(27) is solved using an inexact Newton method that employs that the LU-factors of an approximation, M , of the Jacobian matrix, $J(X_i)$, are already available. The steps in this inexact Newton procedure may be denoted

$$M \Delta \bar{S}_{s_k,i}^{[l]} = -R_{x,i}(\bar{S}_{s_k,i}^{[l]}) \quad (30a)$$

$$\bar{S}_{s_k,i}^{[l+1]} = \bar{S}_{s_k,i}^{[l]} + \Delta \bar{S}_{s_k,i}^{[l]} \quad (30b)$$

where M is the already factorized matrix (18). These factors are used in the solution of (30a).

Convergence of the inexact Newton iteration is measured by

$$\|R_{x,i}(\bar{S}_{s_k,i}^{[l]})\| < \tau \quad (31)$$

using the norm defined by (20) columnwise. The tolerances specified for the differential equations (8) may be different from the tolerances specified for the sensitivity equations.

D. Convergence- and Error-Control

The ESDIRK method computes the sensitivities using a staggered-corrector approach [8]; the method solves for the state equations and only when they have converged it solves the sensitivity equations. The method is implemented such that it satisfies the internal-numerical-differentiation principle [22]. Satisfaction of this principle is achieved by converging the discrete-time sensitivity equations (26) and (28) and keeping the same step size as used in the state equations. Consequently, no error estimation is needed in the sensitivity computations.

The step size controller for the state equations (15) is based on the error estimator embedded in the ESDIRK method. We use a predictive step size controller [25]. The convergence in the inexact Newton iterations is monitored by observing the ratio

$$\alpha_{l+1} = \frac{\|R_i^{l+1}\|}{\|R_i^l\|} \quad (32)$$

with R_i^l being the relevant residual at iteration l and $\|\cdot\|$ being the norm defined by (20). In case of divergence ($\alpha_{l+1} > 1$) the step size is reduced and the computations at the current step are repeated.

The initial guesses of the solution to the residual equations are obtained using an explicit Euler step from either the previous converged solution or the first stage value.

IV. EXAMPLES

In this section, we illustrate the ESDIRK-based multiple-shooting algorithm for constrained optimal control problems (2). The algorithms have been implemented in Matlab. We demonstrate the algorithm using two examples. The first example is a continuous stirred tank reactor with an exothermic

reaction [13]. This system is stiff and operated around an unstable equilibrium. The second example is the quadruple tank process [26]. We compare the computational performance of ESDIRK1(2), ESDIRK2(3), and ESDIRK3(4) using an absolute and relative tolerance of 10^{-5} .

A. Continuous Stirred Tank Reactor (CSTR)

In a CSTR, a reactant A at temperature T_f is fed to a stirred vessel with a cooling/heating jacket. The dynamic of the constant volume CSTR is described by [13]

$$\dot{x}_1(t) = \frac{q}{V}(c_{A,f} - x_1(t)) - k_0 e^{\frac{-E}{R x_2(t)}} x_1(t) \quad (33a)$$

$$\begin{aligned} \dot{x}_2(t) = \frac{q}{V}(T_f - x_2(t)) + \frac{(-\Delta H)}{\rho C_p} k_0 e^{\frac{-E}{R x_2(t)}} x_1(t) \\ + \frac{UA}{V \rho C_p}(u(t) - x_2(t)) \end{aligned} \quad (33b)$$

The system is to be operated around the unstable equilibrium $x_s = [0.5; 350]$, $u_s = 300$ by manipulation of the jacket fluid temperature, $u(t)$. The jacket fluid temperature is determined by solution of (2) using the cost-to-go and stage costs

$$\hat{\Phi}(x(t_b)) = \frac{1}{2}(x(t_b) - x_s)' P(x(t_b) - x_s) \quad (34a)$$

$$\begin{aligned} \Phi(x(t), u(t)) = \left[(x(t) - x_s)' Q(x(t) - x_s) \right. \\ \left. + (u(t) - u_s)' R(u(t) - u_s) \right] \end{aligned} \quad (34b)$$

with $Q = [0, 0; 0, 2]$, $R = 4$, $P = [99165, 2104; 2104, 73]$, and $t_b = 10$. The control and prediction horizon is $N = 40$ and the sample time is $T_s = 0.25$.

Fig. 2 shows the computed optimal solution trajectories and Table I reports the computational statistics for ESDIRK1(2), ESDIRK2(3), and ESDIRK3(4). The major part of the computational time is spend solving the initial value problems and their sensitivities. All ESDIRK methods have approximately the same number of SQP iterations, KKT-factorizations in the QP-solver, and line-searches (call to ESDIRK). Nevertheless, ESDIRK3(4) uses only a quarter of the computational time of ESDIRK1(2). This difference is due to the fact the higher order of ESDIRK3(4) allows it to take longer step sizes than ESDIRK1(2).

B. Quadruple Tank Process

The quadruple tank process has been suggested as a control benchmark problem and is modeled by the equations [26]

$$\dot{x}_1(t) = -\frac{a_1}{A_1} \sqrt{2gx_1} + \frac{a_3}{A_1} \sqrt{2gx_3} + \frac{\gamma_1 k_1}{A_1} u_1(t) \quad (35a)$$

$$\dot{x}_2(t) = -\frac{a_2}{A_2} \sqrt{2gx_2} + \frac{a_4}{A_2} \sqrt{2gx_4} + \frac{\gamma_2 k_2}{A_2} u_2(t) \quad (35b)$$

$$\dot{x}_3(t) = -\frac{a_3}{A_3} \sqrt{2gx_3} + \frac{(1-\gamma_2)k_2}{A_3} u_2(t) \quad (35c)$$

$$\dot{x}_4(t) = -\frac{a_4}{A_4} \sqrt{2gx_4} + \frac{(1-\gamma_1)k_1}{A_4} u_1(t) \quad (35d)$$

A_i and a_i represent the cross section area of the tanks and holes respectively. γ_i describes the distribution of water

TABLE I

COMPUTATIONAL STATISTICS FOR THE CSTR SYSTEM AND THE QUADRUPLE TANK PROCESS. THE ABSOLUTE AND RELATIVE TOLERANCES ARE 10^{-5} . SQP: NUMBER OF ITERATIONS IN THE SQP-ALGORITHM. QP: NUMBER OF KKT-MATRIX FACTORIZATIONS IN THE INTERIOR-POINT QP-SOLVER. LS: NUMBER OF LINE SEARCHES AND CALL TO THE ESDIRK ALGORITHM. TIME: RELATIVE TIME TO SOLVE THE PROBLEM.

	ESDIRK	SQP	QP	LS	time
CSTR	1(2)	25	119	35	1
	2(3)	21	101	29	0.26
	3(4)	22	106	30	0.25
Quadruple Tank Process	1(2)	340	44	26	1
	2(3)	331	43	26	0.23
	3(4)	312	44	26	0.19

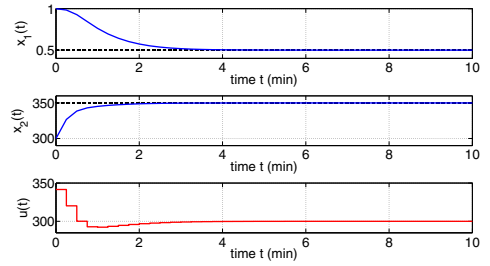


Fig. 2. Optimal state trajectories and manipulated variables for the CSTR process operated around an unstable equilibrium. The initial states are $x(0) = [1.0; 300]$ and the initial jacket fluid temperature is $u(0^-) = 350$.

flows. u_i is the flow rate from the pumps and x_i are the water level heights in the four tanks. Table II contains the model parameters used in this study.

The aim of the control is to manipulate the flow rates $u(t)$ such that the system is brought to the steady state (x_{s1}, u_{s1}) . Therefore, the cost-to-go and stage costs of (2) are formulated as

$$\hat{\Phi}(x(t_b)) = \frac{0.1}{2}(x(t_b) - x_{s1})'(x(t_b) - x_{s1}) \quad (36a)$$

$$\begin{aligned} \Phi(x(t), u(t)) = \left[(x(t) - x_{s1})'(x(t) - x_{s1}) \right. \\ \left. + (u(t) - u_{s1})'(u(t) - u_{s1}) \right] \end{aligned} \quad (36b)$$

with $t_b = 700$, $x_{s1} = [15; 20; 4.235; 7.635]$, and $u_{s1} = [4.04; 3.279]$. The sampling time is chosen as $T_s = 700/40$ and we use a control and prediction horizon of $N = 40$. The constraints are $0 \leq u(t) \leq 20$, $-5.0 \leq \Delta u_k \leq 5.0$, and $x_3 \leq 9.0$.

TABLE II

MODEL PARAMETERS FOR THE QUADRUPLE-TANK PROCESS

a_1, a_3	$7.1 \cdot 10^{-2} \text{ cm}^2$	A_2, A_4	$3.2 \cdot 10 \text{ cm}^2$	γ_1	0.45
a_2, a_4	$5.7 \cdot 10^{-2} \text{ cm}^2$	k_1	$3.14 \frac{\text{cm}^3}{\text{V} \cdot \text{s}}$	γ_2	0.4
A_1, A_3	$2.8 \cdot 10 \text{ cm}^2$	k_2	$3.29 \frac{\text{cm}^3}{\text{V} \cdot \text{s}}$	g	$981 \frac{\text{cm}}{\text{s}^2}$

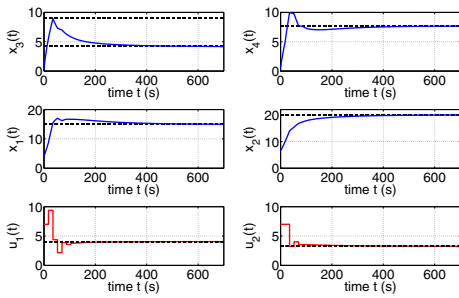


Fig. 3. Optimal trajectories and manipulated variables for the quadruple tank process. The initial conditions are $x(0) = [4.103; 6.608; 0.394; 0.557]$ and the initial manipulated variables are $u(0^-) = [2; 2]$.

The computed solution is illustrated in Fig. 3. It should be noted that the soft output constraint, $x_3(t) \leq 9.0$, is satisfied. Also the computational statistics in Table I confirms the observations for the CSTR case study; for this tolerance level ESDIRK3(4) is the fastest of the three algorithms. This is due to its ability to take longer steps.

V. CONCLUSIONS AND FUTURE WORK

In this paper we address the solution of unstable and stiff constrained optimal control problems. We present an algorithm that combines multiple shooting with ESDIRK integration methods. The ESDIRK implementation is based on an efficient and accurate inexact Newton method to compute the sensitivities that are required in the optimization process.

The numerical examples demonstrated the convergence of the algorithm to meaningful solutions. They also demonstrated that ESDIRK3(4) is the fastest of the three algorithms when medium to high accuracy of the solution is required.

The algorithm described in this paper has been implemented in Matlab. Future work will include implementation of the algorithms as efficient C++ code and comparison with multiple-shooting algorithms based on SUNDIALS [9]. In addition, future work will address coordination of the accuracy of the ESDIRK solution method with the required precision of the optimization algorithm.

REFERENCES

- [1] M. Schlegel, K. Stockmann, T. Binder, and W. Marquardt, "Dynamic optimization using adaptive control vector parameterization," *Computers and Chemical Engineering*, vol. 29, pp. 1731–1751, 2005.
- [2] H. G. Bock and K. J. Plitt, "A multiple shooting algorithm for direct solution of optimal control problems," in *In Proceedings 9th IFAC World Congress Budapest*. Pergamon Press, 1984, pp. 243–247.
- [3] D. B. Leineweber, I. Bauer, H. G. Bock, and J. P. Schlöder, "An efficient multiple shooting based reduced SQP strategy for large-scale dynamic process optimization. part 1: theoretical aspects," *Computers and Chemical Engineering*, vol. 27, pp. 157–166, 2003.
- [4] B. Houska, H. J. Ferreau, and M. Diehl, "ACADO toolkit - an open-source framework for automatic control and dynamic optimization," *Optim. Control Appl. Meth.*, vol. 32, pp. 298–312, 2011.
- [5] L. T. Biegler, "Solution of dynamic optimization problems by successive quadratic programming and orthogonal collocation," *Computers and Chemical Engineering*, vol. 8, pp. 243–248, 1984.
- [6] M. Diehl, H. J. Ferreau, and N. Haverbeke, "Efficient numerical methods for nonlinear MPC and moving horizon estimation," in *Nonlinear Model Predictive Control. Towards New Challenging Applications*, ser. Lecture Notes in Control and Information Sciences, L. Magni, D. M. Raimondo, and F. Allgöwer, Eds. Springer, 2009, vol. 384, pp. 391–417.
- [7] V. M. Zavala and L. T. Biegler, "Nonlinear programming strategies for state estimation and model predictive control," in *Nonlinear Model Predictive Control. Towards New Challenging Applications*, ser. Lecture Notes in Control and Information Sciences, L. Magni, D. M. Raimondo, and F. Allgöwer, Eds. Springer, 2009, vol. 384.
- [8] W. F. Feehery, J. E. Tolsma, and P. I. Barton, "Efficient sensitivity analysis of large-scale differential-algebraic systems," *Applied Numerical Mathematics*, vol. 25, pp. 41–54, 1997.
- [9] A. C. Hindmarsh, P. N. Brown, K. E. Grant, S. L. Lee, R. Serban, D. E. Shumaker, and C. S. Woodward, "SUNDIALS: Suite of nonlinear and differential/algebraic equation solvers," *ACM Transactions on Mathematical Software*, vol. 31, pp. 363–396, 2005.
- [10] L. Petzold, S. Li, Y. Cao, and R. Serban, "Sensitivity analysis of differential-algebraic equations and partial differential equations," *Computers and Chemical Engineering*, vol. 30, pp. 1553–1559, 2006.
- [11] R. Serban and A. C. Hindmarsh, "CVODES, the sensitivity-enabled ODE solver in SUNDIALS," in *Proceedings of the IDETC/CIE*, Long Beach, California, USA, September 24–28 2005, pp. 1–13.
- [12] M. Schlegel, W. Marquardt, R. Ehrig, and U. Nowak, "Sensitivity analysis of linearly-implicit differential-algebraic systems by one-step extrapolation," *Applied Numerical Mathematics*, vol. 48(1), p. 83102., 2004.
- [13] M. R. Kristensen, J. B. Jørgensen, P. G. Thomsen, and S. B. Jørgensen, "AnESDIRK method with sensitivity analysis capabilities," *Computers and Chemical Engineering*, vol. 28(12), pp. 2695–2707, 2004.
- [14] M. R. Kristensen, J. B. Jørgensen, P. G. Thomsen, M. L. Michelsen, and S. B. Jørgensen, "Sensitivity analysis in index-1 differential algebraic equations by ESDIRK methods," in *16th IFAC World Congress*, Prague, 2005.
- [15] R. Alexander, "Diagonally implicit runge-kutta methods for stiff O.D.E's," *SIAM Journal on Numerical Analysis*, vol. 14, pp. 1006–1021, 1977.
- [16] A. Kværnø, "Singly diagonally implicit runge-kutta methods with an explicit first stage," *BIT Numerical Mathematics*, vol. 44, n. 3, pp. 489–502, 2004.
- [17] M. R. Kristensen, M. G. Gerritsen, P. G. Thomsen, M. L. Michelsen, and E. H. Stenby, "Efficient integration of stiff kinetics with phase change detection for reactive reservoir processes," *Transport in Porous Media*, vol. 69, no. 3, pp. 383–409, 2007.
- [18] M. H. Carpenter, S. A. Viken, and E. J. Nielsen, "The efficiency of high order temporal schemes," *41st Aerospace Sciences Meeting and Exhibit*, 2003.
- [19] M. Tabesh and D. W. Zingg, "Efficient implicit time-marching methods using a newton-krylov algorithm," *47th AIAA Aerospace Sciences Meeting Including The New Horizons Forum and Aerospace Exposition*, 2009.
- [20] J. B. Jørgensen, Kristensen, M. R., Thomsen, and P. G., "A family of esdirk integration methods," *SIAM Journal on Scientific Computing*, 2008, manuscript.
- [21] C. Völkler, J. B. Jørgensen, and E. H. Stenby, "Oil reservoir production optimization using optimal control," in *50th IEEE Conference on Decision and Control and European Control Conference*, Orlando, Florida, December 12–15 2011.
- [22] H. G. Bock, "Numerical treatment of inverse problems in chemical reaction kinetics," *Modelling of Chemical Reaction Systems*. (Ebert, K.H. Deufhard, P., Jäger, W. Eds) Springer Series in Chemical Physics, vol. 18, 1981.
- [23] K. F. Bloss, L. T. Biegler, and W. E. Schiesser, "Dynamic process optimization through adjoint formulations and constraint aggregation," *Ind. Eng. Chem. Res.*, 1999, vol. 38 (2), p. 421432, 1999.
- [24] M. J. D. Powell, "A fast algorithm for nonlinearly constrained optimization calculations," *Numerical Analysis (Lecture Notes in Mathematics)*, vol. Volume 630, pp. 144–157, 1978.
- [25] K. Gustafsson, "Control of error convergence in ode solvers," Ph.D. dissertation, Department of automatic control, Lund Institute of Technology, 1992.
- [26] K. H. Johansson, "The quadruple-tank process: a multivariable laboratory process with an adjustable zero," *IEEE Transactions on Control Systems Technology*, vol. 8, issue: 3, pp. 456–465, 2000.

APPENDIX C

Paper II

Oil Reservoir Production Optimization using Single Shooting and ESDIRK Methods

Authors:

Andrea Capolei, Carsten Völcker, Jan Frydendall and John Bagterp Jørgensen

Published in:

Proceedings of the 2012 IFAC Workshop on Automatic Control in Offshore Oil and Gas Production, Norwegian University of Science and Technology, Trondheim, Norway. May 31 - June 1, 2012.

Oil Reservoir Production Optimization using Single Shooting and ESDIRK Methods^{*}

Andrea Capolei^{*} Carsten Völcker^{*} Jan Frydendall^{*}
John Bagterp Jørgensen^{*}

^{*} *Department of Informatics and Mathematical Modeling & Center for Energy Resources Engineering, Technical University of Denmark, DK-2800 Kgs. Lyngby, Denmark.
(e-mail: {acap,cv,jf,jb}@imm.dtu.dk).*

Abstract: Conventional recovery techniques enable recovery of 10–50% of the oil in an oil field. Advances in smart well technology and enhanced oil recovery techniques enable significant larger recovery. To realize this potential, feedback model-based optimal control technologies are needed to manipulate the injections and oil production such that flow is uniform in a given geological structure. Even in the case of conventional water flooding, feedback based optimal control technologies may enable higher oil recovery than with conventional operational strategies. The optimal control problems that must be solved are large-scale problems and require specialized numerical algorithms. In this paper, we combine a single shooting optimization algorithm based on sequential quadratic programming (SQP) with explicit singly diagonally implicit Runge-Kutta (ESDIRK) integration methods and a continuous adjoint method for sensitivity computation. We demonstrate the procedure on a water flooding example with conventional injectors and producers.

Keywords: Optimal Control, Optimization, Numerical Methods, Oil Reservoir

1. INTRODUCTION

The growing demand for oil and the decreasing number of newly discovered significant oil fields require more efficient management of the existing oil fields. Oil fields are developed in two or three phases. In the primary phase, the reservoir pressure is large enough to make the oil flow to the production wells. In the secondary phase, water must be injected to maintain pressure and move the oil towards the producers. In some cases, a tertiary phase known as enhanced oil recovery is considered. Enhanced oil recovery includes technologies such as in situ combustion, surfactant flooding, polymer flooding, and steam flooding (Thomas, 2008). After the secondary phase, typically the oil recovery is somewhere between 10% and 50% (Chen, 2007; Jansen, 2011).

Optimal control technology and Nonlinear Model Predictive Control have been suggested for improving the oil recovery of the secondary phase (Jansen et al., 2008). In such applications, the controller adjusts the water injection rates and the bottom hole well pressures to maximize oil recovery or a financial measure such as net present value. In the oil industry, this control concept is also known as closed-loop reservoir management (Jansen et al., 2009). The controller in closed-loop reservoir management consists of a state estimator for history matching and an optimizer that solves a constrained optimal control

^{*} This research project is financially supported by the Danish Research Council for Technology and Production Sciences. FTP Grant no. 274-06-0284

problem for the production optimization. The main difference of the closed-loop reservoir management system from a traditional Nonlinear Model Predictive Controller (Binder et al., 2001) is the large state dimension (10^6 is not unusual) of an oil reservoir model. The size of the problem dictates that the ensemble Kalman filter is used for state estimation (history matching) and that single shooting optimization algorithms compute gradient based on adjoints (Jansen, 2011; Jørgensen, 2007; Sarma et al., 2005; Suwartadi et al., 2011; Völcker et al., 2011).

In this paper, we propose a high order temporal integration method (Explicit Singly Diagonally Implicit Runge-Kutta, ESDIRK) for forward computation of the initial value problem and for backward solution of the associated continuous-time adjoint. Conventional practice by commercial reservoir simulators is limited to the use of first order temporal implicit or semi-implicit integrators for the initial value problem and the adjoints. Völcker et al. (2010a,b, 2009) introduce high order ESDIRK methods in two phase reservoir simulation. The high order scheme allows larger steps and therefore faster solution of the reservoir model equations. To compute the gradient of the objective function in a single shooting optimization method, Völcker et al. (2011) propose a method based on adjoints for the discretized equations. Cao et al. (2002) and Jansen (2011) provide an overview of gradient computation using the adjoint. Brouwer and Jansen (2004) and Sarma et al. (2005) explain and demonstrate gradient computation by the adjoint equations based on the implicit Euler discretization. Kourounis et al. (2010) suggest the

continuous-time high order adjoint equations for gradient computation in production optimization. Nadarajah and Jameson (2007) compare gradients computed by discrete and continuous adjoints for problems arising in aerodynamics. They conclude that the gradients computed from continuous adjoints is accurate enough to be used in optimization algorithms. Since computation of gradients based on continuous time adjoints is faster than gradients based on discrete adjoints, this conclusion implies that the gradient computations can be accelerated by using the continuous time adjoint equations.

The novel contribution in this paper is an extension of the adjoint based optimization method suggested by Völcker et al. (2011) to include gradient computation based on the continuous-time adjoint equation. Using a conventional oil field as case study, we demonstrate the new single-shooting optimization algorithm based on ESDIRK integration of the initial value problem and ESDIRK integration of the continuous-time adjoint equation. The case study illustrates the potential of optimal control for production optimization of water flooded oil reservoirs by maximizing the net present value. We do a parameter study to illustrate the sensitivity of the optimal solution to the discount factor.

The paper is organized as follows. Section 2 states the general constrained optimal control problem using a novel representation of the system dynamics. The ESDIRK algorithm for solution of the differential equation systems is described in Section 3, while Section 4 presents the continuous adjoint method. Section 5 describes the numerical case study and discusses the sensitivity of the optimal solution to the discount factor in the net present value. Conclusions are presented in Section 6.

2. OPTIMAL CONTROL PROBLEM

In this section, we present the continuous-time constrained optimal control problem and its transcription by the single shooting method to a finite dimensional constrained optimization problem. First we present the continuous-time optimal control problem. Then we parameterize the control function using piecewise constant basis functions, and finally we convert the problem into a constrained optimization problem using the single shooting method.

Consider the continuous-time constrained optimal control problem in the Bolza form

$$\min_{x(t), u(t)} J = \hat{\Phi}(x(t_b)) + \int_{t_a}^{t_b} \Phi(x(t), u(t)) dt \quad (1a)$$

subject to

$$x(t_a) = x_0 \quad (1b)$$

$$\frac{d}{dt}g(x(t)) = f(x(t), u(t)), \quad t \in [t_a, t_b], \quad (1c)$$

$$u(t) \in \mathcal{U}(t) \quad (1d)$$

$x(t) \in \mathbb{R}^{n_x}$ is the state vector and $u(t) \in \mathbb{R}^{n_u}$ is the control vector. The time interval $I = [t_a, t_b]$ as well as the initial state, x_0 , are assumed to be fixed. (1c) represents the dynamic model and includes systems described by index-1 differential algebraic equations (DAE). (1d) represents constraints on the input values, e.g. $u_{\min} \leq u(t) \leq u_{\max}$, $c(u(t)) \geq 0$, and some constraints related to rate of movement that are dependent on the input parametrization.

Path constraints

$$\eta(x(t), u(t)) \geq 0 \quad (2)$$

may render the optimization problem infeasible. For this reason and due to computational efficiency considerations when computing the sensitivities by the adjoint method (Capolei and Jørgensen, 2012; Jørgensen, 2007), we include these constraints as soft constraints using the following smooth approximation

$$\chi_i(x(t), u(t)) = \frac{1}{2} \left(\sqrt{\eta_i(x(t), u(t))^2 + \beta_i^2} - \eta_i(x(t), u(t)) \right) \quad (3)$$

to the exact penalty function $\max(0, -\eta_i(x(t)))$ for $i \in \{1, \dots, n_\eta\}$. With this approximation of the path constraints, the resulting stage cost, $\Phi(x(t), u(t))$, used in (1a) consist of the inherent stage cost, $\tilde{\Phi}(x(t), u(t))$, and terms penalizing violation of the path constraints (2)

$$\Phi(x, u) = \tilde{\Phi}(x, u) + \|\chi(x, u)\|_{1, Q_1} + \frac{1}{2} \|\chi(x, u)\|_{2, Q_2}^2 \quad (4)$$

2.1 Discretization

Control Parametrization Let T_s denote the sample time such that an equidistant mesh can be defined as

$$t_a = t_0 < \dots < t_s < \dots < t_N = t_b \quad (5)$$

with $t_j = t_a + jT_s$ for $j = 0, 1, \dots, N$. We use a piecewise constant representation of the control function on this equidistant mesh, i.e. we approximate the control vector on every subinterval $[t_j, t_{j+1}]$ by the zero-order-hold parametrization

$$u(t) = u_j, \quad u_j \in \mathbb{R}^{n_u}, \quad t_j \leq t < t_{j+1}, \quad j = 0, \dots, N-1 \quad (6)$$

Input Constraints The input constraints (1d) include bound constraints $u_{\min} \leq u_k \leq u_{\max}$. In the discrete problem using the zero-order-hold parametrization, we also include rate of movement constraints in the form $\Delta u_{\min} \leq \Delta u_k \leq \Delta u_{\max}$ with $\Delta u_k = u_k - u_{k-1}$.

2.2 Single Shooting Optimization

For the single shooting approach (control vector parametrization), we introduce the function

$$\psi(\{u_k\}_{k=0}^{N-1}, x_0) = \left\{ \begin{array}{l} J = \int_{t_a}^{t_b} \Phi(x(t), u(t)) dt + \hat{\Phi}(x(t_b)) : \\ x(t_0) = x_0, \\ \frac{d}{dt}g(x(t)) = f(x(t), u(t)), \quad t_a \leq t \leq t_b, \\ u(t) = u_k, \quad t_k \leq t < t_{k+1}, \quad k = 0, 1, \dots, N-1 \end{array} \right\} \quad (7)$$

such that (1) can be approximated with the finite dimensional constrained optimization problem

$$\min_{\{u_k\}_{k=0}^{N-1}} \psi = \psi(\{u_k\}_{k=0}^{N-1}, x_0) \quad (8a)$$

$$s.t. \quad u_{\min} \leq u_k \leq u_{\max} \quad k \in \mathcal{N} \quad (8b)$$

$$\Delta u_{\min} \leq \Delta u_k \leq \Delta u_{\max} \quad k \in \mathcal{N} \quad (8c)$$

$$c_k(u_k) \geq 0 \quad k \in \mathcal{N} \quad (8d)$$

with $\mathcal{N} = \{0, 1, \dots, N-1\}$.

3. ESDIRK METHODS

In this section, we describe our implementation of the ESDIRK method for the computation of $\psi(\{u_k\}_{k=0}^{N-1}, x_0)$ in (7). Computation of $\psi(\{u_k\}_{k=0}^{N-1}, x_0)$ consists of two major operations: 1) For each integration step we first compute the model states $x(t)$ solving the initial value problem (1c), 2) and then we compute, using the same quadrature points, the value of the Lagrange term

$$\bar{\psi}(t) := \int_{t_a}^t \Phi(x(t), u(t)) dt \quad t_a \leq t \leq t_b. \quad (9)$$

in the cost function (1a). Let \tilde{t}_n denote the integration times chosen by the step size controller in the integrator. Each integration step size, h_n , is chosen such that it is smaller than or equal to the sample time, T_s . Therefore, one sample interval contains many integration steps. The numerical solution of the IVP (1c) by an s -stage, stiffly accurate, Runge-Kutta ESDIRK method with an embedded error estimator, may in each integration step $[\tilde{t}_n, \tilde{t}_{n+1}]$ be denoted (Capolei and Jørgensen, 2012; Völcker et al., 2010a)

$$T_1 = \tilde{t}_n, \quad T_i = \tilde{t}_n + c_i h_n \quad (10a)$$

$$X_1 = x_n \quad (10b)$$

$$\phi_i(\{X_j\}_{j=1}^{i-1}, u) = g(X_1) + h_n \sum_{j=1}^{i-1} a_{ij} f(X_j, u) \quad (10c)$$

$$g(X_i) = \phi_i(\{X_j\}_{j=1}^{i-1}, u) + h_n \gamma f(X_i, u) \quad (10d)$$

$$x_{n+1} = X_s \quad (10e)$$

$$e_{n+1} = h_n \sum_{j=1}^s d_i f(X_j, u) \quad (10f)$$

with $i = 2, \dots, s$. X_i denotes the numerical solution at time T_i for $i \in \{1, \dots, s\}$. x_{n+1} is the numerical solution at time $\tilde{t}_{n+1} = \tilde{t}_n + h_n$. e_{n+1} is the estimated error of the numerical solution, i.e. $\|e_{n+1}\| \approx \|g(x_{n+1}) - g(x(\tilde{t}_{n+1}))\|$.

Subsequent to solution of (10), we compute the numerical solution of the cost function (9)

$$\bar{\psi}(\tilde{t}_{n+1}) = \bar{\psi}(\tilde{t}_n) + h_n \sum_{i=1}^s b_i \Phi(X_i, u) \quad (11)$$

When $\tilde{t}_{n+1} = t_b$, we add the Mayer term of (1a) such that

$$\psi(\{u_k\}_{k=0}^{N-1}, x_0) = \psi(t_b) = \bar{\psi}(t_b) + \hat{\Phi}(x(t_b)) \quad (12)$$

The main computational effort in the ESDIRK method is solution of the implicit equations (10d) using a Newton based method. (10d) is solved by sequential solution of

$$R_i(X_i) := [g(X_i) - h_n \gamma f(X_i, u)] - \phi_i(\{X_j\}_{j=1}^{i-1}, u) = 0 \quad (13)$$

for $i = 2, \dots, s$. (13) is solved using an inexact Newton method. Each iteration in the inexact Newton method for solution of (13) may be denoted

$$M \Delta X_i^{[l]} = -R_i(X_i^{[l]}) \quad (14a)$$

$$X_i^{[l+1]} = X_i^{[l]} + \Delta X_i^{[l]} \quad (14b)$$

The iteration matrix, M , is an approximation

$$M \approx J(X_i^{[l]}) \quad (15)$$

to the Jacobian of the residual function

$$J_i(X_i) = \frac{\partial R_i}{\partial X_i}(X_i) = \frac{\partial g}{\partial x}(X_i) - h_n \gamma \frac{\partial f}{\partial x}(X_i, u) \quad (16)$$

The iteration matrix, M , and its LU factorization is updated adaptively by monitoring the convergence rate of the inexact Newton iterations. Convergence of the inexact Newton iteration is measured by

$$\|R_i(X_i^{[l]})\| = \max_{j \in \{1, \dots, n_x\}} \frac{|(R_i(X_i^{[l]}))_j|}{\max\{\text{atol}_j, \text{rtol}_j g_j(X_i^{[l]})\}} < \tau \quad (17)$$

where atol is the absolute tolerance and rtol is the relative tolerance. Steps are accepted if this measure of the residual is smaller than $\tau \approx 0.1$. In case of divergence or slow convergence, the iterations are terminated, the step size, h_n , is decreased and the Jacobian of the iteration matrix is re-evaluated and factorized. As explained in e.g. Völcker et al. (2010b) and Capolei and Jørgensen (2012), the step size controller adjust the temporal step sizes such that the error estimate satisfies a norm similar to the norm used in (17).

4. CONTINUOUS ADJOINT METHOD

Gradient based methods such as sequential quadratic programming (SQP) methods for solution of (8) require the gradient of the objective function (7) with respect to the control vector parameters, i.e. $\partial\psi/\partial u_k$ for $k = 0, 1, \dots, N-1$. In this section, we describe a continuous-time adjoint based method for computation of these gradients.

Proposition 1. (Gradients based on Continuous Adjoint). Consider the function $\psi = \psi(\{u_k\}_{k=0}^{N-1}; x_0)$ defined by (7).

The gradients, $\partial\psi/\partial u_k$, may be computed as

$$\frac{\partial\psi}{\partial u_k} = \int_{t_k}^{t_{k+1}} \left(\frac{\partial\Phi}{\partial u} - \lambda^T \frac{\partial f}{\partial u} \right) dt \quad k = 0, 1, \dots, N-1 \quad (18)$$

in which $x(t)$ is computed by solution of (1b)-(1c) and $\lambda(t)$ is computed by solution of the adjoint equations

$$\frac{d\lambda^T}{dt} \frac{\partial g}{\partial x} + \lambda^T \frac{\partial f}{\partial x} - \frac{\partial\Phi}{\partial x} = 0 \quad (19a)$$

$$\frac{\partial\hat{\Phi}}{\partial x}(x(t_b)) + \lambda^T(t_b) \frac{\partial g}{\partial x}(x(t_b)) = 0 \quad (19b)$$

Remark 2. (Computation using ESDIRK). $x(t)$ is computed using the ESDIRK method applied to (1b)-(1c) and integration forwards. This solution is stored. The same ESDIRK method is applied for computation of $\lambda(t)$ by solving (19) integrating backwards in time.

Remark 3. (Gradients Computed by Continuous Adjoint). The gradients computed using the continuous adjoints are not the exact gradients, $\partial\psi/\partial u_k$, when the involved differential equations and integrals are computed by discretization using the ESDIRK method. However, they can be made sufficiently precise for the optimizer such that they do not affect the convergence (Nadaraajah and Jameson, 2007). The advantage of the continuous adjoint equations (19) is that they can be solved faster than the adjoint equations for the discretized system (10)-(12).

5. PRODUCTION OPTIMIZATION FOR A CONVENTIONAL OIL FIELD

In this section, we apply our algorithm for constrained optimal control problems to production optimization in a

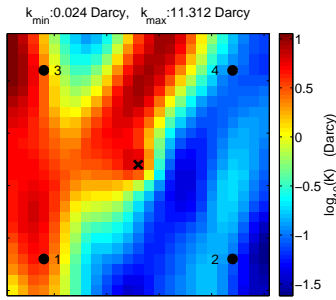


Fig. 1. The permeability field and the location of wells. A circle indicates the location of an injector and a cross indicates the location of a producer.

Table 1. Parameters for the two phase model and the discounted state cost function (20).

Symbol	Description	Value	Unit
ϕ	Porosity	0.2	-
c_r	Rock compressibility	0	Pa ⁻¹
ρ_o	Oil density (400 atm)	800	kg/m ³
ρ_w	Water density (400 atm)	1000	kg/m ³
c_o	Oil compressibility	10 ⁻⁵	1/atm
c_w	Water compressibility	10 ⁻⁵	1/atm
μ_o	Dynamic oil viscosity	2 · 10 ⁻³	Pa · s
μ_w	Dynamic water viscosity	1 · 10 ⁻³	Pa · s
S_{or}	Residual oil saturation	0.1	-
S_{ow}	Connate water saturation	0.1	-
n_o	Corey exponent for oil	1.5	-
n_w	Corey exponent for water	1.4	-
P_{init}	Initial reservoir pressure	400	atm
S_{mit}	Initial water saturation	0.1	-
r_o	Oil price	100	USD/m ³
r_w	Water production cost	20	USD/m ³

conventional horizontal oil field that can be modeled as two phase flow in a porous medium (Chen, 2007; Völcker et al., 2009). The reservoir size is 450 m × 450 m × 10 m. By spatial discretization this reservoir is divided into 25 × 25 × 1 grid blocks. The configuration of injection wells and producers as well as the permeability field is illustrated in Fig. 1. As indicated in Fig. 1, the four injectors are located in the corners of the field, while the single producer is located in the center of the field. The specification of the two phase oil model consists of the injector ($i \in \mathcal{I}$) and the producer ($i \in \mathcal{P}$) location, the permeability parameters indicated in Fig. 1, and the parameters listed in Table 1. The initial reservoir pressure is 400 atm everywhere in the reservoir. The initial water saturation is 0.1 everywhere in the reservoir. This implies that initially the reservoir has a uniform oil saturation of 0.9.

The inherent discounted stage cost function (see (4))

$$\begin{aligned} \tilde{\Phi}(t) &= \tilde{\Phi}(x(t), u(t)) \\ &= -\frac{1}{(1+b)^{t/365}} \sum_{j \in \mathcal{P}} (r_o(1-f_w) - f_w r_w) q_j(t) \end{aligned} \quad (20)$$

accounts for the value of the oil produced minus the processing cost of the produced water. In this cost function, we have neglected the processing cost of injected water as well as the effect of pressure on injecting water. b is the discount factor. The fractional flow of water, $f_w = \lambda_w / (\lambda_w + \lambda_o)$, indicates the relative flow of water. $\lambda_w = \rho_w k k_{rw} / \mu_w$

and $\lambda_o = \rho_o k k_{ro} / \mu_o$ are the water and oil mobilities, respectively. In the problems considered, we do not have any cost-to-go terms, i.e. $\hat{\Phi}(t_b) = 0$. Neither do we have any path constraints (2). Therefore, maximizing the net present value of the oil field corresponds to minimization of

$$J(t_b) = -\text{NPV}(t_b) = \int_{t_a}^{t_b} \Phi(x(t), u(t)) dt \quad (21)$$

with $\Phi(x(t), u(t)) = \tilde{\Phi}(x(t), u(t))$. The optimizer maximizes the net present value by manipulating the injection of water at the injectors and by manipulation of the total fluid production (oil and water) at the producers. Hence, the manipulated variable at time period $k \in \mathcal{N}$ is $u_k = \{\{q_{w,i,k}\}_{i \in \mathcal{I}}, \{q_{i,k}\}_{i \in \mathcal{P}}\}$ with \mathcal{I} being the set of injectors and \mathcal{P} being the set of producers. For $i \in \mathcal{I}$, $q_{w,i,k}$ is the injection rate (m³/day) of water in time period $k \in \mathcal{N}$ at injector i . For $i \in \mathcal{P}$, $q_{i,k}$ is the total flow rate (m³/day) at producer i in time period $k \in \mathcal{N}$. Therefore, at producer $i \in \mathcal{P}$, the water flow rate is $q_{w,i,k} = f_w q_{i,k}$ and the oil flow rate is $q_{o,i,k} = (1 - f_w) q_{i,k}$.

The bound constraints (8b) appear in the production optimization problem because the water injected at injectors and the production at the producers must both be positive and because each production facility has a maximum flow capacity. In the considered problem we have

$$|q_{i,k} - q_{i,k-1}| \leq 5 \quad i \in \mathcal{I} \cup \mathcal{P}, k \in \mathcal{N} \quad (22a)$$

$$0 \leq q_{i,k} \leq q_{\max} \quad i \in \mathcal{P}, k \in \mathcal{N} \quad (22b)$$

The maximum flow capacity, q_{\max} , is the same for all injectors and producers in this case study. The rate of change for all injectors and producers are $|q_{i,k} - q_{i,k-1}| \leq 5$ for $i \in \mathcal{I} \cup \mathcal{P}$ and $k \in \mathcal{N}$. Since the injection of oil is zero, $q_{o,i,k} = 0$ for $i \in \mathcal{I}$, we get $|q_{w,i,k} - q_{w,i,k-1}| \leq 5$ for $i \in \mathcal{I}$ and $k \in \mathcal{N}$. This leads to the rate of movement constraints (8c). In addition we use a voidage replacement constraint (Brouwer and Jansen, 2004; Jansen, 2011)

$$\sum_{i \in \mathcal{I}} q_{i,k} = \sum_{i \in \mathcal{I}} q_{w,i,k} = \sum_{i \in \mathcal{P}} q_{i,k} \quad k \in \mathcal{N} \quad (23)$$

and enforce a constant total injection, $\sum_{i \in \mathcal{I}} q_{w,i,k} = q_{\max}$ for $k \in \mathcal{N}$. This translates into constraints of the type (8d). By the total injection constraint, the optimization problem reduces to a problem of redistributing the flows among the injectors.

The prediction and control horizon is $t_b = 4270$ days and the sampling period is $T_s = 35$. Hence the prediction and control horizon corresponds to $N = 122$ periods. With a total injection at each time period of $q_{\max} = 100$ m³/day, these specifications corresponds to injection of 1.05 pore volume during operation of the reservoir. The prediction horizon is optimal in the reference case for a total injection of 100 m³/day.

The optimal water injection rates computed by solution of the constrained optimal control problem (1) for different discount factors, b , are illustrated in Fig. 2. In addition, a base case with constant and equal water injection rates is illustrated. It is evident that the optimal injection rates are very sensitive to the discount factor, b . The corresponding cumulative oil and water production are plotted in Fig. 3. Independent of the discount factor value, the optimized strategies produce more oil than the base case. For the high discount factor case, $b = 0.12$, less oil is recovered than in

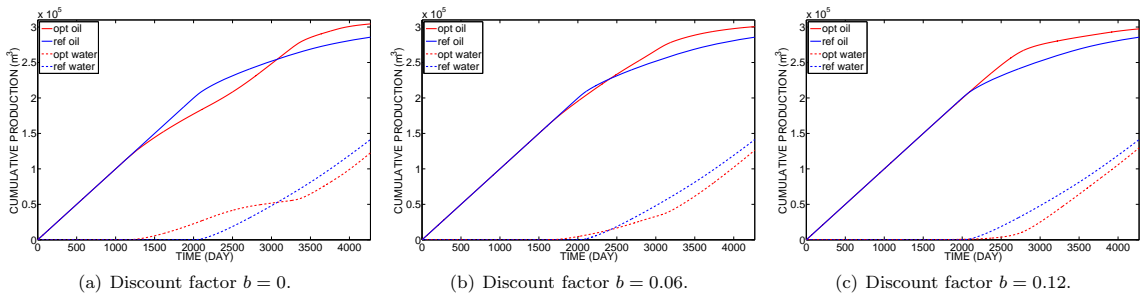


Fig. 3. Cumulative oil and water productions for different discount factors, b .

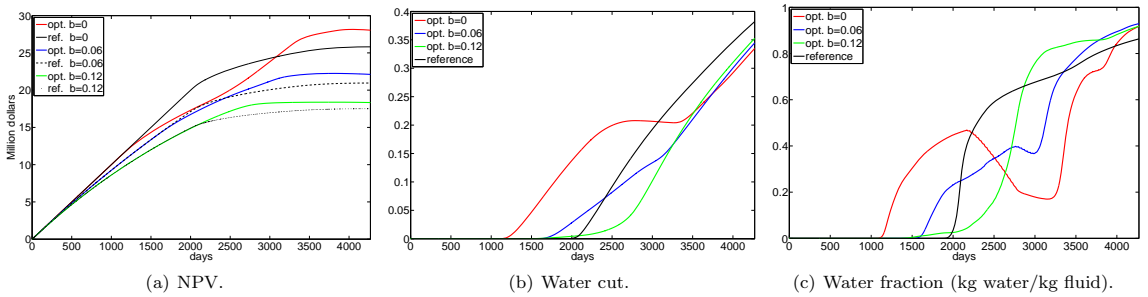


Fig. 4. The net present value (NPV), water cut (accumulated water production per produced fluid), and the water fraction as function of time for the scenarios considered.

Table 2. Key indicators for the optimized cases. Improvements are compared to the base case.

b	NPV 10^6 USD	Δ NPV %	Cum. Oil 10^5 m^3	Δ Oil %	Cum. water 10^5 m^3	Δ Water %	Oil Rec. factor %	Δ Oil Rec. factor %-point
0	28.0	+8.7	3.05	+6.5	0.122	-13.2	83.7	+5.2
0.06	22.1	+5.6	3.01	+5.2	0.126	-10.5	82.6	+4.1
0.12	18.3	+4.8	2.98	+4.1	0.129	-8.2	81.7	+3.2

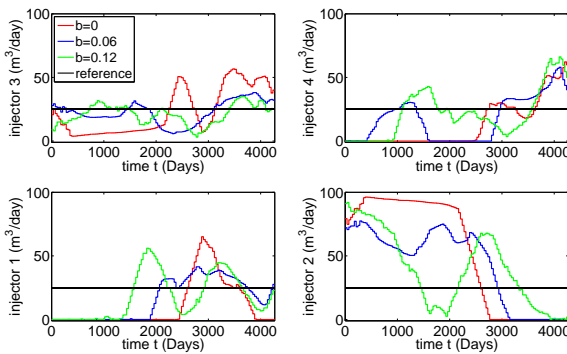


Fig. 2. Optimal water injection rates for different discount factors, b .

the low discount factor case, $b = 0$. However, the produced oil is always above the reference case when $b = 0.12$. This is not the case for $b = 0$ and $b = 0.06$. Fig. 4 illustrates the net present value, the water cut and the water fraction for the base case scenarios as well as the optimized scenarios. The plot of NPV demonstrates that when $b = 0$, the NPV is lower than the base case NPV at some time during the production. At the end of the production the optimized

NPV is largest. In order to recover the maximum amount of oil less oil must be produced at some times. This is also confirmed by the water fraction curves. The results are summarized in Table 2. Table 2 shows that most oil is recovered in the case without discount ($b = 0$), while least oil is recovered when the discount factor is high ($b = 0.12$).

Fig. 5 illustrates the evolution of the oil saturation for the optimized case ($b = 0$) and the base case. The figures show that initially, less oil is produced from the upper left corner in the optimal case compared to the base case. This gives a better sweep of the oil field and results ultimately in higher oil recovery.

6. CONCLUSIONS

In this paper, we solve constrained optimal control problems using a single shooting method based on a quasi-Newton implementation of Powell's sequential quadratic programming (SQP) algorithm. The system of differential equations are formulated in a novel way to ensure mass conservation and the resulting initial value problem (1c) is solved with tailored ESDIRK integration methods. We also introduce a high order continuous adjoint system for efficient computation of the gradients. The algorithm is implemented in Matlab.

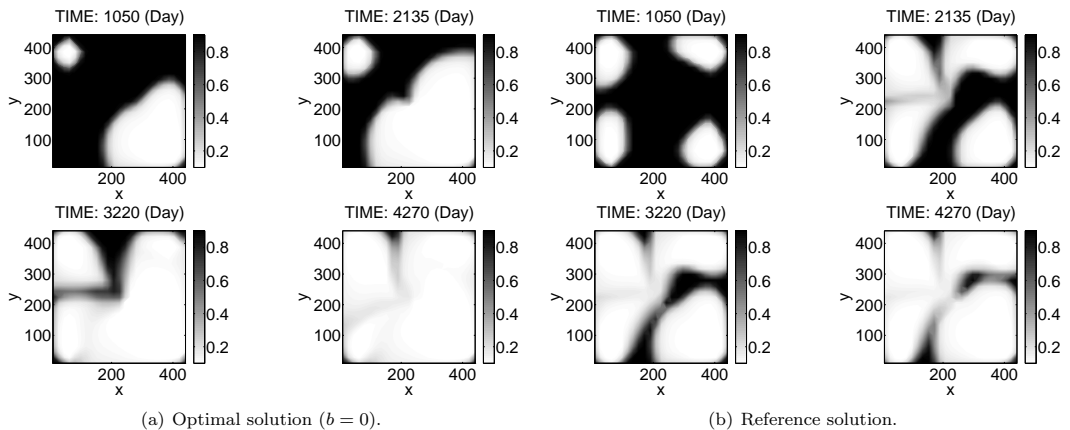


Fig. 5. Oil saturations at different times for the optimal solution and the reference solution.

The resulting algorithm is tested on a production optimization problem for an oil reservoir with two phase flow. For all cases considered, the dynamic optimization increase the net present value of the oil field and give increased oil production. However, the optimal injection rates are very sensitive to the discount factor.

REFERENCES

- Binder, T., Blank, L., Bock, H.G., Burlisch, R., Dahmen, W., Diehl, M., Kronseeder, T., Marquardt, W., Schlöder, J.P., and von Stryk, O. (2001). Introduction to model based optimization of chemical processes on moving horizons. In M. Grötschel, S. Krumke, and J. Rambau (eds.), *Online Optimization of Large Scale Systems*. Springer.
- Brouwer, D.R. and Jansen, J.D. (2004). Dynamic optimization of waterflooding with smart wells using optimal control theory. *SPE Journal*, 9(4), 391–402.
- Cao, Y., Li, S., Petzold, L., and Serban, R. (2002). Adjoint sensitivity analysis for differential-algebraic equations: The adjoint DAE system and its numerical solution. *SIAM Journal on Scientific Computing*, 24(3), 1076–1089.
- Capolei, A. and Jørgensen, J.B. (2012). Solution of constrained optimal control problems using multiple shooting and ESDIRK methods. In *2012 American Control Conference*. Accepted.
- Chen, Z. (2007). *Reservoir Simulation. Mathematical Techniques in Oil Recovery*. SIAM, Philadelphia, USA.
- Jansen, J.D., Douma, S.D., Brouwer, D.R., Van den Hof, P.M.J., Bosgra, O.H., and Heemink, A.W. (2009). Closed-loop reservoir management. In *2009 SPE Reservoir Simulation Symposium*, SPE 119098. The Woodlands, Texas, USA.
- Jansen, J.D., Bosgra, O.H., and Van den Hof, P.M.J. (2008). Model-based control of multiphase flow in subsurface oil reservoirs. *Journal of Process Control*, 18, 846–855.
- Jansen, J. (2011). Adjoint-based optimization of multiphase flow through porous media - A review. *Computers & Fluids*, 46, 40–51.
- Jørgensen, J.B. (2007). Adjoint sensitivity results for predictive control, state- and parameter-estimation with nonlinear models. In *Proceedings of the European Control Conference 2007*, 3649–3656. Kos, Greece.
- Kourounis, D., Voskov, D., and Aziz, K. (2010). Adjoint methods for multicomponent flow simulation. In *12th European Conference on the Mathematics of Oil Recovery*. Oxford, UK.
- Nadarajah, S.K. and Jameson, A. (2007). Optimum shape design for unsteady flows with time-accurate continuous and discrete adjoint methods. *AIAA Journal*, 45(7), 1478–1491.
- Sarma, P., Aziz, K., and Durlofsky, L.J. (2005). Implementation of adjoint solution for optimal control of smart wells. In *SPE Reservoir Simulation Symposium, 31 January-2 February 2005, The Woodlands, Texas*.
- Suwartadi, E., Krogstad, S., and Foss, B. (2011). Nonlinear output constraints handling for production optimization of oil reservoirs. *Computational Geosciences*. doi: 10.1007/s10596-011-9253-3. Accepted.
- Thomas, S. (2008). Enhanced oil recovery - an overview. *Oil & Gas Science and Technology*, 63, 9–19.
- Völcker, C., Jørgensen, J.B., Thomsen, P.G., and Stenby, E.H. (2010a). Explicit singly diagonally implicit Runge-Kutta methods and adaptive stepsize control for reservoir simulation. In *ECMOR XII - 12th European Conference on the Mathematics of Oil Recovery*. Oxford, UK.
- Völcker, C., Jørgensen, J.B., Thomsen, P.G., and Stenby, E.H. (2010b). Adaptive stepsize control in implicit Runge-Kutta methods for reservoir simulation. In M. Kothare, M. Tade, A.V. Wouwer, and I. Smets (eds.), *Proceedings of the 9th International Symposium on Dynamics and Control of Process Systems (DYCOPS 2010)*, 509–514. Leuven, Belgium.
- Völcker, C., Jørgensen, J.B., and Stenby, E.H. (2011). Oil reservoir production optimization using optimal control. In *50th IEEE Conference on Decision and Control and European Control Conference*. Orlando, Florida. Accepted.
- Völcker, C., Jørgensen, J.B., Thomsen, P.G., and Stenby, E.H. (2009). Simulation of subsurface two-phase flow in an oil reservoir. In *Proceedings of the European Control Conference 2009*, 1221–1226. Budapest, Hungary.

APPENDIX D

Paper III

High Order Adjoint Derivatives using ESDIRK Methods for Oil Reservoir Production Optimization

Authors:

Andrea Capolei, Erling Halfdan Stenby and John Bagterp Jørgensen

Published in:

Proceedings of the 13th European Conference on the Mathematics of Oil Recovery (ECMOR XIII) Biarritz, France 10-13 September 2012.

A42

High Order Adjoint Derivatives using ESDIRK Methods for Oil Reservoir Production Optimization

A. Capolei* (DTU), E.H. Stenby (DTU) & J.B. Jørgensen (DTU)

SUMMARY

In production optimization, computation of the gradients is the computationally expensive step. We improve the computational efficiency of such algorithms by improving the gradient computation using high-order ESDIRK (Explicit Singly Diagonally Implicit Runge-Kutta) temporal integration methods and continuous adjoints. The high order integration scheme allows larger time steps and therefore faster solution times. We compare gradient computation by the continuous adjoint method to the discrete adjoint method and the finite-difference method. The methods are implemented for a two phase flow reservoir simulator. Computational experiments demonstrate that the accuracy of the sensitivities obtained by the adjoint methods are comparable to the accuracy obtained by the finite difference method. The continuous adjoint method is able to use a different time grid than the forward integration. Therefore, it can compute these sensitivities much faster than the discrete adjoint method and the finite-difference method. On the other hand, the discrete adjoint method produces the gradients of the numerical schemes, which is beneficial for the numerical optimization algorithm. Computational experiments show that when the time steps are controlled in a certain range, the continuous adjoint method produces gradients sufficiently accurate for the optimization algorithm and somewhat faster than the discrete adjoint method.

Introduction

The growing demand for oil and the decreasing number of newly discovered significant oil fields require more efficient management of the existing oil fields. Oil fields are developed in two or three phases. In the primary phase, the reservoir pressure is large enough to make the oil flow to the production wells. In the secondary phase, water must be injected to maintain pressure and move the oil towards the producers. In some cases, a tertiary phase known as enhanced oil recovery is considered. Enhanced oil recovery includes technologies such as in situ combustion, surfactant flooding, polymer flooding, and steam flooding (Thomas, 2008). After the secondary phase, typically the oil recovery is somewhere between 10% and 50% (Chen, 2007; Jansen, 2011).

Optimal control technology and Nonlinear Model Predictive Control have been suggested for improving the oil recovery of the secondary phase (Jansen et al., 2008). In such applications, the controller adjusts the water injection rates and the bottom hole well pressures to maximize oil recovery or a financial measure such as net present value. In the oil industry, this control concept is also known as closed-loop reservoir management (Jansen et al., 2009). The controller in closed-loop reservoir management consists of a state estimator for history matching and an optimizer that solves a constrained optimal control problem for the production optimization. The main difference of the closed-loop reservoir management system from a traditional Nonlinear Model Predictive Controller (Binder et al., 2001) is the large state dimension (10^6 is not unusual) of an oil reservoir model. The size of the problem dictates that the ensemble Kalman filter is used for state estimation (history matching) and that single shooting optimization algorithms compute gradient based on adjoints (Jansen, 2011; Sarma et al., 2005; Jørgensen, 2007; Capolei et al., 2012; Suwartadi et al., 2011; Völcker et al., 2011).

In this paper, we propose a high order temporal integration method (Explicit Singly Diagonally Implicit Runge-Kutta, ESDIRK) for forward computation of the initial value problem and for backward solution of the associated continuous-time and discrete-time adjoints. Conventional practice by commercial reservoir simulators is limited to the use of first order temporal implicit or semi-implicit integrators for the initial value problem and the adjoints. Völcker et al. (2009, 2010, 2011) introduce high order ESDIRK methods in two phase reservoir simulation and production optimization based on the discrete adjoints. The high order scheme allows larger steps and therefore faster solution of the reservoir model equations. To compute the gradient of the objective function in a single shooting optimization method, Hager (1999) introduces the discrete adjoint of a generic Runge-kutta method to solve an optimal control problem governed by ODEs. Sandu (2006) shows that such discrete adjoint has the same order and linear stability as the forward integrator. He also points out that the calculation of gradients by reverse automatic differentiation leads to the discrete adjoint approach. Jansen (2011) provide an overview of gradient computation using the discrete adjoint. Brouwer and Jansen (2004) and Sarma et al. (2005) explain and demonstrate gradient computation by the adjoint equations based on the implicit Euler discretization. Cao et al. (2002) describes the continuous adjoint method and studies the stability of the continuous adjoint system. Kourounis et al. (2010) suggest the continuous-time high order adjoint equations for gradient computation in production optimization. Capolei et al. (2012) apply high order continuous-time adjoint based on ESDIRK to a conventional oil field case study. Nadarajah and Jameson (2007) compare gradients computed by discrete and continuous adjoints for problems arising in aerodynamics. They conclude that the gradients computed from continuous adjoints is accurate enough to be used in optimization algorithms. Since computation of gradients based on continuous time adjoints is faster than gradients based on discrete adjoints, this conclusion implies that the gradient computations can be accelerated by using the continuous time adjoint equations.

The novel contribution in this paper is an extension of the adjoint based optimization method suggested by Capolei et al. (2012) to include gradient computation based on a high order discrete adjoint. Further discrete and continuous adjoints are compared in performance using a conventional oil field as case study. Computational experiments demonstrate that the accuracy of the sensitivities obtained by the

adjoint methods are comparable to the accuracy obtained by the finite difference method. Using the ES-DIRK method, the continuous adjoint method is able to use a different time grid respect to the forward integration. So it can compute the sensitivities much faster than the discrete adjoint method and the finite-difference method. On the other hand the discrete adjoint method produces the gradients of the numerical schemes and this causes the optimizer to converge faster. Computational experiments show that when the time steps are controlled in a certain range, the continuous adjoint method produces gradients sufficiently accurate for the optimization algorithm and somewhat faster than the discrete adjoint method.

The Optimal Control Problem

In this section, we present the continuous-time constrained optimal control problem and its transcription by the single shooting method to a finite dimensional constrained optimization problem. First we present the continuous-time optimal control problem. Then we parametrize the control function using piecewise constant basis functions, and finally we convert the problem into a constrained optimization problem using the single shooting method.

Consider the continuous-time constrained optimal control problem in the Bolza form

$$\min_{x(t), u(t)} J = \hat{\Phi}(x(t_b)) + \int_{t_a}^{t_b} \Phi(x(t), u(t)) dt \quad (1a)$$

subject to

$$x(t_a) = x_0 \quad (1b)$$

$$\frac{d}{dt}g(x(t)) = f(x(t), u(t)), \quad t \in [t_a, t_b], \quad (1c)$$

$$u(t) \in \mathcal{U}(t) \quad (1d)$$

$x(t) \in \mathbb{R}^{n_x}$ is the state vector and $u(t) \in \mathbb{R}^{n_u}$ is the control vector. The time interval $I = [t_a, t_b]$ as well as the initial state, x_0 , are assumed to be fixed. (1c) represents the dynamic model and includes systems described by index-1 differential algebraic equations (DAE). (1d) represents constraints on the input values, e.g. $u_{\min} \leq u(t) \leq u_{\max}$, $c(u(t)) \geq 0$, and some constraints related to the rate of movement that are dependent on the input parametrization.

Path constraints

$$\eta(x(t), u(t)) \geq 0 \quad (2)$$

may render the optimization problem infeasible. For this reason and due to computational efficiency considerations when computing the sensitivities by the adjoint method (Capolei and Jørgensen, 2012; Jørgensen, 2007), we include these constraints as soft constraints using the following smooth approximation

$$\chi_i(x(t), u(t)) = \frac{1}{2} \left(\sqrt{\eta_i(x(t), u(t))^2 + \beta_i^2} - \eta_i(x(t), u(t)) \right) \quad (3)$$

to the exact penalty function $\max(0, -\eta_i(x(t)))$ for $i \in \{1, \dots, n_\eta\}$. With this approximation of the path constraints, the resulting stage cost, $\Phi(x(t), u(t))$, used in (1a) consist of the inherent stage cost, $\tilde{\Phi}(x(t), u(t))$, and terms penalizing violation of the path constraints (2)

$$\Phi(x, u) = \tilde{\Phi}(x, u) + \|\chi(x, u)\|_{1, \mathcal{Q}_1} + \frac{1}{2} \|\chi(x, u)\|_{2, \mathcal{Q}_2}^2 \quad (4)$$

Control Parametrization

Let T_s denote the sample time such that an equidistant mesh can be defined as

$$t_a = t_0 < \dots < t_S < \dots < t_N = t_b \quad (5)$$

with $t_j = t_a + jT_s$ for $j = 0, 1, \dots, N$. We use a piecewise constant representation of the control function on this equidistant mesh, i.e. we approximate the control vector for every subinterval $[t_j, t_{j+1}]$ by the zero-order-hold parametrization

$$u(t) = u_j, u_j \in \mathbb{R}^{n_u}, t_j \leq t < t_{j+1}, j \in 0, \dots, N-1 \quad (6)$$

Input Constraints

The input constraints (1d) include bound constraints $u_{\min} \leq u_k \leq u_{\max}$. In the discrete problem using the zero-order-hold parametrization, we also include rate of movement constraints in the form $\Delta u_{\min} \leq \Delta u_k \leq \Delta u_{\max}$ with $\Delta u_k = u_k - u_{k-1}$.

Single Shooting Optimization

For the single shooting approach (control vector parametrization), we introduce the function

$$\begin{aligned} \psi(\{u_k\}_{k=0}^{N-1}, x_0) = & \left\{ J = \int_{t_a}^{t_b} \Phi(x(t), u(t)) dt + \hat{\Phi}(x(t_b)) : \quad x(t_0) = x_0, \right. \\ & \left. \frac{d}{dt} g(x(t)) = f(x(t), u(t)), t_a \leq t \leq t_b, \quad u(t) = u_k, t_k \leq t < t_{k+1}, k = 0, 1, \dots, N-1 \right\} \end{aligned} \quad (7)$$

such that (1) can be approximated with the finite dimensional constrained optimization problem

$$\min_{\{u_k\}_{k=0}^{N-1}} \quad \psi = \psi(\{u_k\}_{k=0}^{N-1}, x_0) \quad (8a)$$

$$s.t. \quad u_{\min} \leq u_k \leq u_{\max} \quad k \in \mathcal{N} \quad (8b)$$

$$\Delta u_{\min} \leq \Delta u_k \leq \Delta u_{\max} \quad k \in \mathcal{N} \quad (8c)$$

$$c_k(u_k) \geq 0 \quad k \in \mathcal{N} \quad (8d)$$

with $\mathcal{N} = \{0, 1, \dots, N-1\}$. We solve (8) using a quasi-Newton implementation of Powell's Sequential Quadratic Programming (SQP) method (Capolei and Jørgensen, 2012).

ESDIRK Methods

In this section, we describe our implementation of the ESDIRK method for the computation of $\psi(\{u_k\}_{k=0}^{N-1}, x_0)$ in (7). Computation of $\psi(\{u_k\}_{k=0}^{N-1}, x_0)$ consists of two major operations: 1) For each integration step we first compute the model states $x(t)$ solving the initial value problem (1c), 2) and then we compute, using the same quadrature points, the value of the Lagrange term

$$\tilde{\psi}(t) := \int_{t_a}^t \Phi(x(t), u(t)) dt \quad t_a \leq t \leq t_b. \quad (9)$$

in the cost function (1a). Let \tilde{t}_n denote the integration times chosen by the step size controller in the integrator. Each integration step size, h_n , is chosen such that it is smaller than or equal to the sample time, T_s . Therefore, one sample interval contains many integration steps. We consider ESDIRK methods with s stages that are designed to be stiffly accurate and with an embedded error estimator. The numerical solution of the IVP (1c) by such ESDIRK method may in each integration step $[\tilde{t}_n, \tilde{t}_{n+1}]$ be denoted

(Capolei and Jørgensen, 2012; Völcker et al., 2010)

$$T_1 = \tilde{t}_n, \quad T_i = \tilde{t}_n + c_i h_n \quad (10a)$$

$$X_1 = x_n \quad (10b)$$

$$\phi_i(\{X_j\}_{j=1}^{i-1}, u) = g(X_1) + h_n \sum_{j=1}^{i-1} a_{ij} f(X_j, u) \quad (10c)$$

$$g(X_i) = \phi_i(\{X_j\}_{j=1}^{i-1}, u) + h_n \gamma f(X_i, u) \quad (10d)$$

$$x_{n+1} = X_s \quad (10e)$$

$$e_{n+1} = h_n \sum_{j=1}^s d_j f(X_j, u) \quad (10f)$$

with $i = 2, \dots, s$. X_i denotes the numerical solution at time T_i for $i \in \{1, \dots, s\}$. x_{n+1} is the numerical solution at time $\tilde{t}_{n+1} = \tilde{t}_n + h_n$. e_{n+1} is the estimated error of the numerical solution, i.e. $\|e_{n+1}\| \approx \|g(x_{n+1}) - g(x(\tilde{t}_{n+1}))\|$.

Subsequent to solution of (10), we compute the numerical solution of the cost function (9)

$$\bar{\psi}(\tilde{t}_{n+1}) = \bar{\psi}(\tilde{t}_n) + h_n \sum_{i=1}^s b_i \Phi(X_i, u) \quad (11)$$

When $\tilde{t}_{n+1} = t_b$, we add the Mayer term of (1a) such that

$$\Psi(\{u_k\}_{k=0}^{N-1}, x_0) = \psi(t_b) + \hat{\Phi}(x(t_b)) \quad (12)$$

The main computational effort in the ESDIRK method is solution of the implicit equations (10d) using a Newton based method. (10d) is solved by sequential solution of

$$R_i(X_i) := [g(X_i) - h_n \gamma f(X_i, u)] - \phi_i(\{X_j\}_{j=1}^{i-1}, u) = 0 \quad (13)$$

for $i = 2, \dots, s$. (13) is solved using an inexact Newton method. Each iteration in the inexact Newton method for solution of (13) may be denoted

$$M \Delta X_i^{[l]} = -R_i(X_i^{[l]}) \quad (14a)$$

$$X_i^{[l+1]} = X_i^{[l]} + \Delta X_i^{[l]} \quad (14b)$$

The iteration matrix, M , is an approximation

$$M \approx \mathbf{J}(X_i^{[l]}) \quad (15)$$

to the Jacobian of the residual function

$$\mathbf{J}_i(X_i) = \frac{\partial R_i}{\partial X_i}(X_i) = \frac{\partial g}{\partial x}(X_i) - h_n \gamma \frac{\partial f}{\partial x}(X_i, u) \quad (16)$$

The iteration matrix, M , and its LU factorization is updated adaptively by monitoring the convergence rate of the inexact Newton iterations. Convergence of the inexact Newton iteration is measured by

$$\|R_i(X_i^{[l]})\| = \max_{j \in \{1, \dots, n_x\}} \frac{|(R_i(X_i^{[l]}))_j|}{\max\{\text{atol}_j, \text{rtol}_j g_j(X_i^{[l]})\}} < \tau \quad (17)$$

where atol is the absolute tolerance and rtol is the relative tolerance. Steps are accepted if this measure of the residual is smaller than $\tau \approx 10^{-2}$. In case of divergence or slow convergence, the iterations are terminated, the step size, h_n , is decreased, and the Jacobian of the iteration matrix is re-evaluated and factorized. As explained in e.g. Völcker et al. (2010) and Capolei and Jørgensen (2012), the controller adjusts the temporal step sizes such that the error estimate satisfies a norm similar to the norm used in (17).

Continuous Adjoint Method

Gradient based methods such as Sequential Quadratic Programming (SQP) methods for solution of (8) require the gradient of the objective function (7) with respect to the control vector parameters, i.e. $\partial\psi/\partial u_k$ for $k = 0, 1, \dots, N-1$. In this section, we describe a continuous-time adjoint based method for computation of these gradients.

Proposition 1 (Gradients based on Continuous Adjoints). *Consider the function $\psi = \psi(\{u_k\}_{k=0}^{N-1}; x_0)$ defined by (7).*

The gradients, $\partial\psi/\partial u_k$ and $\partial\psi/\partial x_0$, may be computed as

$$\begin{aligned} \frac{\partial\psi}{\partial u_k} &= \int_{t_k}^{t_{k+1}} \left(\frac{\partial\Phi}{\partial u} - \lambda^T \frac{\partial f}{\partial u} \right) dt \quad k = 0, 1, \dots, N-1 \\ \frac{\partial\psi}{\partial x_0} &= -\lambda^T(t_a) \frac{\partial g}{\partial x}(t_a) \end{aligned} \quad (18)$$

in which $x(t)$ is computed by solution of (1b)-(1c) and $\lambda(t)$ is computed by solution of the adjoint equations

$$\frac{d\lambda^T}{dt} \frac{\partial g}{\partial x} + \lambda^T \frac{\partial f}{\partial x} - \frac{\partial\Phi}{\partial x} = 0 \quad (19a)$$

$$\frac{\partial\hat{\Phi}}{\partial x}(x(t_b)) + \lambda^T(t_b) \frac{\partial g}{\partial x}(x(t_b)) = 0 \quad (19b)$$

Proof. See the Appendix . □

Remark 2 (Computation using ESDIRK). $x(t)$ is computed using the ESDIRK method applied to (1b)-(1c) and integrating forwards. This gives an approximations $x_n \approx x(t_n)$. This solution is stored. The same ESDIRK method is applied for computation of $\lambda(t)$ by solving (19) integrating backwards in time.

Remark 3 (Gradients Computed by Continuous Adjoints). The gradients computed using the continuous adjoints are not the exact gradients, $\partial\psi/\partial u_k$, when the involved differential equations and integrals are computed by discretization using the ESDIRK method. However, they can be made sufficiently precise for the optimizer such that they do not affect the convergence (Nadarajah and Jameson, 2007). The advantage of the continuous adjoint equations (19) is that they can be solved faster than the adjoint equations for the discretized system (10)-(12).

Solving the Adjoint Equations

Usually, integration software is written to integrate forward in time. Our ESDIRK methods are also implemented in that way. To integrate the linear equations (19), we introduce the change of variables

$$t = t_b + t_a - \bar{t} \quad (20)$$

$$\bar{\lambda}(\bar{t}) = \lambda(t_b + t_a - \bar{t}) \quad (21)$$

such that (19) becomes

$$A(\bar{t}) \frac{d\bar{\lambda}}{d\bar{t}} - B(\bar{t})\bar{\lambda} + C(\bar{t}) = 0 \quad (22a)$$

$$D(t_a) + A(t_a)\bar{\lambda}(t_a) = 0 \quad (22b)$$

where

$$A(\bar{t}) = \nabla_x g(x(t_b + t_a - \bar{t})) \quad (23)$$

$$B(\bar{t}) = \nabla_x f(x(t_b + t_a - \bar{t}), u(t_b + t_a - \bar{t})) \quad (24)$$

$$C(\bar{t}) = \nabla_x \Phi(x(t_b + t_a - \bar{t}), u(t_b + t_a - \bar{t})) \quad (25)$$

$$D(\bar{t}) = \nabla_x \hat{\Phi}(x(t_b + t_a - \bar{t})) \quad (26)$$

We integrate this system (22) forward in $\bar{t} \in [t_a, t_b]$.

The solution of system (22) by an s -stage, stiffly accurate, Runge-Kutta ESDIRK method may in each integration step $[\bar{t}_{n-1}, \bar{t}_n]$ be denoted (Brenan et al., 1996)

$$A(\bar{t}_{n-1})\dot{Y}_1 - B(\bar{t}_{n-1})\bar{\lambda}_{n-1} + C(\bar{t}_{n-1}) = 0 \quad (27a)$$

$$[A(\bar{t}_{n-1} + c_i\bar{h}_{n-1}) - \bar{h}_{n-1}\gamma B(\bar{t}_{n-1} + c_i\bar{h}_{n-1})]\dot{Y}_i = B(\bar{t}_{n-1} + c_i\bar{h}_{n-1})[\bar{\lambda}_{n-1} + \bar{h}_{n-1}\sum_{j=1}^{i-1} a_{ij}\dot{Y}_j] + \\ - C(\bar{t}_{n-1} + c_i\bar{h}_{n-1}) \quad (27b)$$

with $i = 2, \dots, s$, where

$$\dot{Y}_i \approx \frac{d\bar{\lambda}}{d\bar{t}}(\bar{t}_{n-1} + c_i\bar{h}_{n-1}) \quad (28)$$

$$Y_i = \bar{\lambda}_{n-1} + \bar{h}_{n-1}\sum_{j=1}^s a_{ij}\dot{Y}_j \approx \bar{\lambda}(\bar{t}_{n-1} + c_i\bar{h}_{n-1}) \quad (29)$$

$$\bar{\lambda}_n = \bar{\lambda}_{n-1} + \bar{h}_{n-1}\sum_{j=1}^s b_j\dot{Y}_j \approx \bar{\lambda}(\bar{t}_n) \quad (30)$$

The main computational effort in solving the adjoint equations using the ESDIRK method is solving the linear equations (27).

Continuous Extension

When we solve the system (22) using the ESDIRK solver, we need a numerical approximation of the state vector $x(t)$ in temporal points \bar{T}_i that in general are not the same as the quadrature points T_i of the forward integration in (10). To compute this approximation we use a continuous extension. The numerical approximation to $x(\bar{t}_n + h_n\theta)$ for $\theta \in [0, 1]$ is given by (Jørgensen et al., 2008)

$$x(\bar{t}_n + h_n\theta) = x_n + h_n\sum_{i=1}^s \bar{b}_i(\theta)\bar{f}(X_i, u) \quad (31a)$$

X_i are the stage values of solving the system (10) in $t \in [\bar{t}_n, \bar{t}_{n+1}]$ and

$$\bar{f}(X_i, u) = \frac{\partial g}{\partial x}(X_i)^{-1} f(X_i, u). \quad (32)$$

$\bar{b}_i(\theta)$ is a matrix function given in Jørgensen et al. (2008). Further the continuous extension used is of the same order as the forward integration method.

Discrete Adjoint Method

In this section, we describe a discrete adjoint based method to compute the gradients of the cost function with respect to the control vector parameters, $\partial\psi/\partial u_k$ for $k = 0, 1, \dots, N-1$. In the following, we use \bar{N} to indicate the total number of (forward) integration steps.

Let $X_{j,i}$ denote the i -th stage values in the integration step $[\bar{t}_j, \bar{t}_{j+1}]$, such that we have

$$X_{0,1} \equiv x_0, \quad t = \bar{t}_0 \\ X_{j,i}, \quad t \in [\bar{t}_j, \bar{t}_{j+1}] \\ X_{j+1,1} \equiv X_{j,s}, \quad t = \bar{t}_{j+1} \quad \forall j \in \{0, \dots, \bar{N}-2\} \\ X_{\bar{N}-1,s}, \quad t = t_b = \bar{t}_{\bar{N}}. \quad (33)$$

With this notation, the ESDIRK discretization of (7) is

$$\psi(\{u_k\}_{k=0}^{N-1}, x_0) = \left\{ J = \hat{\Phi}(X_{\bar{N}-1,s}) + \sum_{j=0}^{\bar{N}-1} \sum_{i=1}^s h_j b_i \Phi(X_{j,i}, \bar{u}_j) : \right. \\ \left. R_{j,i}(\{X_{j,l}\}_{l=1}^i, \bar{u}_j) = 0 \quad j \in \{0, \dots, \bar{N}-1\}, i \in \{2, \dots, s\} \right\} \quad (34)$$

where $\bar{u}_j \equiv u(\tilde{t}_j) = u_k$ for some $k \in \{0, \dots, N-1\}$ and

$$\begin{aligned} R_{j,i} &= g(X_{j,i}) - \phi_{j,i}(\{X_{j,l}\}_{l=1}^{i-1}, \bar{u}_j) - h_j \gamma f(X_{j,i}, \bar{u}_j) \\ \phi_{j,i}(X_{j,1}, \dots, X_{j,i-1}, \bar{u}_j) &= g(X_{j,1}) + h_j \sum_{l=1}^{i-1} a_{il} f(X_{j,l}, \bar{u}_j). \end{aligned} \quad (35)$$

Introduce the vectors $z \in \mathbb{R}^{(\bar{N} \cdot (s-1)) \cdot n_x}$, $\bar{R} \in \mathbb{R}^{(\bar{N} \cdot (s-1)) \cdot n_x}$, and $y \in \mathbb{R}^{N \cdot n_u}$ by

$$z = \begin{bmatrix} X_{0,2} \\ \vdots \\ X_{0,s} \\ X_{1,2} \\ \vdots \\ X_{N-2,s} \\ X_{N-1,2} \\ \vdots \\ X_{N-1,s} \end{bmatrix}, \quad y = \begin{bmatrix} u_0 \\ u_1 \\ \vdots \\ u_{N-1} \end{bmatrix}, \quad \bar{R} = \begin{bmatrix} R_{0,2} \\ \vdots \\ R_{0,s} \\ R_{1,2} \\ \vdots \\ R_{N-2,s} \\ R_{N-1,2} \\ \vdots \\ R_{N-1,s} \end{bmatrix}, \quad (36)$$

Then we can rewrite the problem (8) in the compact form

$$\min_y \quad \psi(x_0, y) = \left\{ J(x_0, z, y) : \bar{R}(x_0, z, y) = 0 \right\} \quad (37a)$$

$$s.t. \quad y \in \mathcal{U} \quad (37b)$$

$\bar{R}(x_0, z, y) = 0$ is the discretized dynamical model (1b-1c) in residual form. The relation $\bar{R}(x_0, z, y) = 0$ and the vectors x_0 and y determine the state vector z .

This leads to the following proposition for computation of the discrete adjoints.

Proposition 4 (Gradients based on Discrete Adjoint). *Consider the function $\psi = \psi(\{u_k\}_{k=0}^{N-1}; x_0)$ defined in (37).*

The gradients, $\partial \psi / \partial y$, $\partial \psi / \partial x_0$, may be computed as

$$\begin{aligned} \frac{\partial \psi}{\partial y} &= \frac{\partial J}{\partial y} + \lambda^T \frac{\partial \bar{R}}{\partial y} \\ \frac{\partial \psi}{\partial x_0} &= \frac{\partial J}{\partial x_0} + \lambda^T \frac{\partial \bar{R}}{\partial x_0} \end{aligned} \quad (38)$$

in which z is computed by solution of (35) and λ is computed by solution of the discrete adjoint equations

$$\lambda^T \frac{\partial \bar{R}}{\partial z} = - \frac{\partial J}{\partial z} \quad (39a)$$

Proof. See Appendix . □

Solving the Discrete System

Due to the special block structure of $\frac{\partial \bar{R}}{\partial z}$, the solution of the discrete adjoint equations (39) is computed backward. Define the vector λ as

$$\lambda = \begin{bmatrix} \lambda_{0,2} \\ \vdots \\ \lambda_{0,s} \\ \lambda_{1,2} \\ \vdots \\ \lambda_{\bar{N}-2,s} \\ \lambda_{\bar{N}-1,2} \\ \vdots \\ \lambda_{\bar{N}-1,s} \end{bmatrix} \quad (40)$$

We compute λ by computing its subvectors in the reverse order, i.e. $\lambda_{\bar{N}-1,s}, \dots, \lambda_{\bar{N}-1,2}, \dots, \lambda_{0,2}, \lambda_{0,0}$. The last subvector, $\lambda_{\bar{N}-1,s}$, is computed by

$$\lambda_{\bar{N}-1,s}^T \cdot \frac{\partial R_{\bar{N}-1,s}}{\partial X_{\bar{N}-1,s}} = -\frac{\partial J}{\partial X_{\bar{N}-1,s}} \quad (41)$$

which is equivalent to the expression

$$\lambda_{\bar{N}-1,s}^T \cdot \left(\frac{\partial g}{\partial x}(X_{\bar{N}-1,s}) - h_{\bar{N}-1} \gamma \frac{\partial f}{\partial x}(X_{\bar{N}-1,s}, u_N) \right) = - \left(\frac{\partial \hat{\Phi}}{\partial x}(X_{\bar{N}-1,s}) + h_{\bar{N}-1} b_s \frac{\partial \Phi}{\partial x}(X_{\bar{N}-1,s}, u_N) \right) \quad (42)$$

Subsequently, the remaining subvectors, $\lambda_{k,j}$ and $\lambda_{k-1,s}$, are computed by marching backwards

$$\lambda_{k,s-j}^T \cdot \frac{\partial R_{k,s-j}}{\partial X_{k,s-j}} = -\frac{\partial J}{\partial X_{k,s-j}} - \sum_{i=1}^j \lambda_{k,s-j+i}^T \cdot \frac{\partial R_{k,s-j+i}}{\partial X_{k,s-j}} \quad (43a)$$

$$\lambda_{k-1,s}^T \cdot \frac{\partial R_{k-1,s}}{\partial X_{k-1,s}} = -\frac{\partial J}{\partial X_{k-1,s}} - \sum_{i=1}^{s-1} \lambda_{k,i+1}^T \cdot \frac{\partial R_{k,i+1}}{\partial X_{k-1,s}} \quad (43b)$$

for $k \in \{\bar{N}-1, \dots, 1\}$, $j \in \{1, \dots, s-2\}$. Finally we solve (43a) for $k=0, j \in \{1, \dots, s-2\}$ to find $\lambda_{0,s-1}, \dots, \lambda_{0,2}$. Note that in case that $s=2$ (as in ESDIRK12), we don't solve the equation (43a). With this notation (38) becomes

$$\begin{aligned} \frac{\partial \psi}{\partial u_k} &= \sum_{j:u(\tilde{t}_j) \equiv u_k} \left(h_j \sum_{l=1}^s b_l \frac{\partial \Phi}{\partial u}(X_{j,l}, u_k) + \sum_{i=2}^s \lambda_{j,i}^T \frac{\partial R_{j,i}}{\partial u}(\{X_{j,r}\}_{r=1}^i, u_k) \right) \\ \frac{\partial \psi}{\partial x_0} &= h_0 b_1 \frac{\partial \Phi}{\partial x_0}(x_0, u_0) + \lambda_{0,2}^T \frac{\partial g}{\partial x_0}(x_0) \end{aligned} \quad (44)$$

The derivatives, $\frac{\partial R_{j,i}}{\partial X_{j,l}}$, are provided in the appendix.

Production Optimization for a Conventional Oil Field

In this section, we apply our algorithm for constrained optimal control problems to production optimization in a conventional horizontal oil field that can be modeled as a slightly compressible two phase flow in a porous medium (Völcker et al., 2009; Chen, 2007). This test case is taken from (Capolei et al., 2012). The reservoir size is $450 \text{ m} \times 450 \text{ m} \times 10 \text{ m}$. By spatial discretization this reservoir is divided into $25 \times 25 \times 1$ grid blocks. The configuration of injection wells and producers as well as the permeability

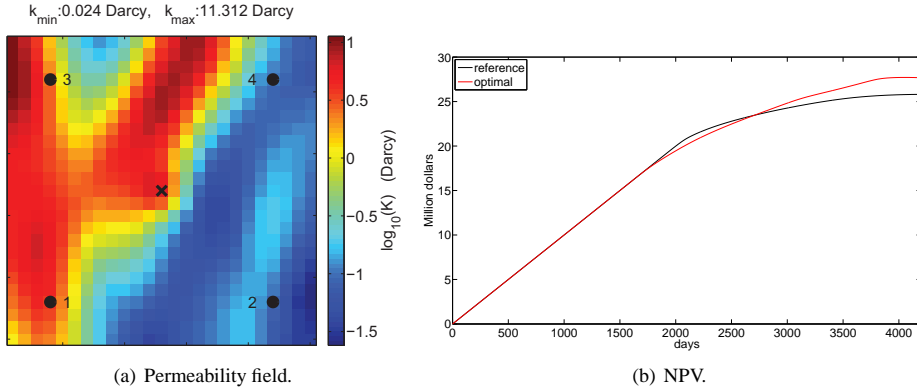


Figure 1 Left: Permeability field with the location of the wells. A circle indicates the location of an injector and a cross indicates the location of a producer. **Right:** The net present value (NPV) computed using ESDIRK3(4) and the discrete adjoint.

field is illustrated in Fig. 1(a). As indicated in Fig. 1(a), the four injectors are located in the corners of the field, while the single producer is located in the center of the field.

The specification of the two phase oil model consists of the injector ($i \in \mathcal{I}$) and the producer ($i \in \mathcal{P}$) location, the permeability parameters indicated in Fig. 1(a), and the parameters listed in Table 1. The initial reservoir pressure is 400 atm everywhere in the reservoir. The initial water saturation is 0.1 everywhere in the reservoir. This implies that initially the reservoir has a uniform oil saturation of 0.9.

The inherent discounted stage cost function (see (4))

$$\tilde{\Phi}(t) = \tilde{\Phi}(x(t), u(t)) = -\frac{1}{(1+b)^{t/365}} \sum_{j \in \mathcal{P}} (r_o(1-f_w) - f_w r_w) q_j(t) \quad (45)$$

accounts for the value of the oil produced minus the processing cost of the produced water. In this cost function, we have neglected the processing cost of injected water as well as the effect of pressure on injecting water. b is the discount factor. The fractional flow of water, $f_w = \lambda_w / (\lambda_w + \lambda_o)$, indicates the relative flow of water. $\lambda_w = \rho_w k k_{rw} / \mu_w$ and $\lambda_o = \rho_o k k_{ro} / \mu_o$ are the water and oil mobilities, respectively. In the problems considered, we do not have any cost-to-go terms, i.e. $\hat{\Phi}(t_b) = 0$. Neither do we have any path constraints (2). Therefore, maximizing the net present value of the oil field corresponds to minimization of

$$J(t_b) = -\text{NPV}(t_b) = \int_{t_a}^{t_b} \Phi(x(t), u(t)) dt \quad (46)$$

with $\Phi(x(t), u(t)) = \tilde{\Phi}(x(t), u(t))$. The optimizer maximizes the net present value by manipulating the injection of water at the injectors and by manipulation of the total fluid production (oil and water) at the producers. Hence, the manipulated variable at time period $k \in \mathcal{N}$ is $u_k = \{\{q_{w,i,k}\}_{i \in \mathcal{I}}, \{q_{i,k}\}_{i \in \mathcal{P}}\}$ with \mathcal{I} being the set of injectors and \mathcal{P} being the set of producers. For $i \in \mathcal{I}$, $q_{w,i,k}$ is the injection rate (m^3/day) of water in time period $k \in \mathcal{N}$ at injector i . For $i \in \mathcal{P}$, $q_{i,k}$ is the total flow rate (m^3/day) at producer i in time period $k \in \mathcal{N}$. Therefore, at producer $i \in \mathcal{P}$, the water flow rate is $q_{w,i,k} = f_w q_{i,k}$ and the oil flow rate is $q_{o,i,k} = (1-f_w)q_{i,k}$.

The bound constraints (8b) appear in the production optimization problem because the water injected at injectors and the production at the producers must both be positive and because each production facility

Table 1 Parameters for the two phase model and the discounted state cost function (45).

Symbol	Description	Value	Unit
ϕ	Porosity	0.2	-
c_r	Rock compressibility	0	Pa^{-1}
ρ_o	Oil density (400 atm)	800	kg/m^3
ρ_w	Water density (400 atm)	1000	kg/m^3
c_o	Oil compressibility	10^{-5}	$1/\text{atm}$
c_w	Water compressibility	10^{-5}	$1/\text{atm}$
μ_o	Dynamic oil viscosity	$2 \cdot 10^{-3}$	$\text{Pa} \cdot \text{s}$
μ_w	Dynamic water viscosity	$1 \cdot 10^{-3}$	$\text{Pa} \cdot \text{s}$
S_{or}	Residual oil saturation	0.1	-
S_{ow}	Connate water saturation	0.1	-
n_o	Corey exponent for oil	1.5	-
n_w	Corey exponent for water	1.4	-
P_{init}	Initial reservoir pressure	400	atm
S_{init}	Initial water saturation	0.1	-
r_o	Oil price	100	USD/m^3
r_w	Water production cost	20	USD/m^3

has a maximum flow capacity. In the considered problem we have

$$|q_{i,k} - q_{i,k-1}| \leq 5 \quad i \in \mathcal{I} \cup \mathcal{P}, k \in \mathcal{N} \quad (47a)$$

$$0 \leq q_{i,k} \leq q_{\max} \quad i \in \mathcal{P}, k \in \mathcal{N} \quad (47b)$$

The maximum flow capacity, q_{\max} , is the same for all injectors and producers in this case study. The rate of change for all injectors and producers are $|q_{i,k} - q_{i,k-1}| \leq 5$ for $i \in \mathcal{I} \cup \mathcal{P}$ and $k \in \mathcal{N}$. Since the injection of oil is zero, $q_{o,i,k} = 0$ for $i \in \mathcal{I}$, we get $|q_{w,i,k} - q_{w,i,k-1}| \leq 5$ for $i \in \mathcal{I}$ and $k \in \mathcal{N}$. This leads to the rate of movement constraints (8c). In addition we use a voidage replacement constraint (Brouwer and Jansen, 2004; Jansen, 2011)

$$\sum_{i \in \mathcal{I}} q_{i,k} = \sum_{i \in \mathcal{I}} q_{w,i,k} = \sum_{i \in \mathcal{P}} q_{i,k} \quad k \in \mathcal{N} \quad (48)$$

and enforce a constant total injection, $\sum_{i \in \mathcal{I}} q_{w,i,k} = q_{\max}$ for $k \in \mathcal{N}$. This translates into constraints of the type (8d). By the total injection constraint, the optimization problem reduces to a problem of redistributing the flows among the injectors.

The prediction and control horizon is $t_b = 4200$ days and the sampling period is $T_s = 120$. Hence the prediction and control horizon corresponds to $N = 35$ periods. With a total injection at each time period of $q_{\max} = 100 \text{ m}^3/\text{day}$, these specifications corresponds to injection of 1.05 pore volume during operation of the reservoir. A reference case with a constant injection of $25 \text{ m}^3/\text{day}$ from each injector is considered. A prediction horizon of 4270 days is optimal in the reference case for a total injection of $100 \text{ m}^3/\text{day}$. We consider the case of no discount, i.e. $b = 0$.

Fig. 1(b) illustrates the net present value for the base case scenarios as well as the optimized scenarios. The plot of NPV demonstrates that the NPV is lower than the base case NPV at some time during the production. At the end of the production, the optimized NPV increases with 7.2% compared to the reference case.

Results

The ESDIRK methods that we refer to in this paper are ESDIRK1(2), ESDIRK2(3) and ESDIRK3(4). They are first, second, and third order accurate methods, respectively. Their embedded error estimator is

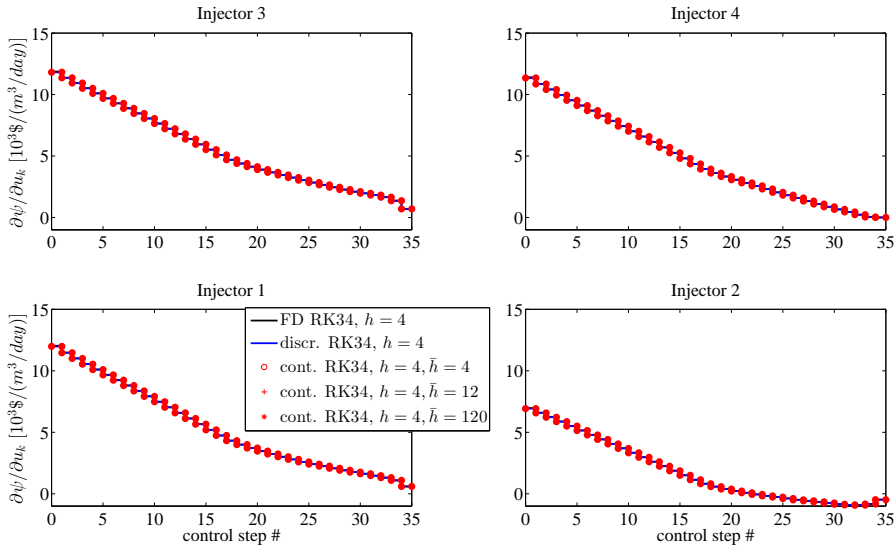


Figure 2 Gradient of the cost function $\frac{\partial \psi}{\partial u_k}$ respect to the control vector. FD: Central Finite Difference, RK34: ESDIRK34, cont.: continuous adjoint method, discr.: discrete adjoint method., h : forward step size in days, \bar{h} : adjoint step size in days

one order higher than the order of the advancing method. ESDIRK1(2) is the implicit Euler integration scheme with an embedded error estimator of order two.

Firstly, we test the gradient computation using the continuous adjoint, the discrete adjoint and the central finite differences. These methods produce gradients of comparable numerical values. We compare the gradients computed by the continuous adjoint method and the finite difference method to adjoints computed by the discrete adjoint method. We do this by computing the relative error with respect to the gradient computed by the discrete adjoint method. Finally, a table with the computational statistics of ESDIRK3(4) is provided. It reveals that for increasing stepsizes \bar{h} of the adjoint integration, the continuous adjoint method is significantly faster than the discrete adjoint method (which is based on a fixed forward integration step h).

Secondly, we report the optimization results of the test case introduced in the previous section. We report a table with the computational statistics. We find that there is a benefit in using the continuous adjoint method because the optimization algorithm requires less time and the value of the net present values is comparable with the one obtained by using the discrete adjoint. Finally, the optimal trajectories are compared.

In all the examples in this work, we use a fixed stepsize, $h = 4$ days, for the forward integration. We tried also smaller stepsizes $h = 0.5, 1, 2$ days finding similar qualitative results. Using a bigger stepsize, e.g. $h = 5$ days, was not possible because of a failure in the convergence of the equation solver (10). We solve (10) using absolute and relative tolerances in (17) equal to 10^{-8} . The perturbation used for the central finite difference method is $\delta u = 10^{-4}$.

Gradient Computation

Fig. 2 shows the gradients, $\frac{\partial \psi}{\partial u_k}$, computed using the different methods. The different gradients are comparable and by visual inspection we see no difference. Fig. 3 reports the relative error of computing the gradient $\frac{\partial \psi}{\partial u_k}$ using the finite difference and the continuous adjoint methods with respect to the gradients computed by the discrete adjoint method. In general, the error increases as the adjoint stepsize \bar{h}

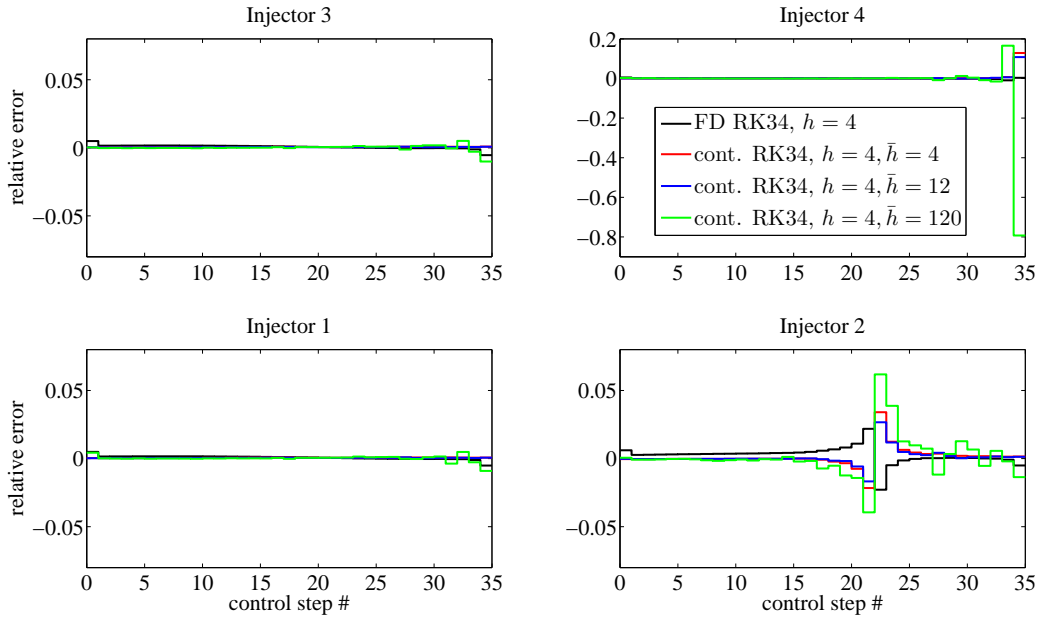


Figure 3 Relative error of the gradients, $\frac{\partial \psi}{\partial u_k}$, computed by the continuous adjoint method and the central finite difference method with respect to the gradient computed by the discrete adjoint method using a forward step size of $h = 4$ days. FD: Central Finite Difference, RK34: ESDIRK34, cont.: continuous adjoint method, h : forward step size, \bar{h} : adjoint step size

increases; this is particular noticeable for the last control step. Different injectors have different relative errors. Injector 4 has the largest relative error, i.e. 80%. This error occurs in the last control step. Large differences in the last control step was also noted in Kourounis et al. (2010). They computed the continuous adjoint based on the implicit Euler method.

Table 2 reports computational statistics for gradient computations using ESDIRK3(4). We note that using the continuous adjoint, the time, T_{adj} , spend for gradient computation is inversely proportional to the continuous adjoint step-size, \bar{h} . Using the same step size, $h = \bar{h}$, the continuous adjoint method uses more computation time, t_{adj} , than the discrete adjoint method. This is due to the increased time spend in computing the continuous extension.

Using the others ESDIRK methods, 1(2)-3(4), we get similar tables. However there is an issue in our implementation. Using the continuous ESDIRK1(2) adjoint method, we don't need to solve both linear systems in (27) in each step. It is enough to solve only (27b) as we don't need \dot{Y}_1 to compute $Y_2 = \bar{\lambda}_n$ for ESDIRK1(2). This gives a penalty in using the continuous adjoint with ESDIRK1(2). In a future implementation, we will tailor the method for ESDIRK1(2) such that we avoid this penalty.

Optimization Results

We use the following stopping criteria for our SQP algorithm. An optimal solution is reported if the KKT conditions are satisfied to within a relative and absolute tolerance of 10^{-6} . The current best but non-optimal iterate is also returned in case of failure in the line search procedure, i.e. if the line search uses more than 20 iterations. Finally, the current best but non-optimal iterate is also returned in case of a

Table 2 Computational statistics for the gradient computation. h : forward integration step size. \bar{h} : continuous adjoint stepsize. t_{adj} : time to compute the gradient with the adjoint method scaled with respect to the forward integration time. T_{adj} : time to compute the gradient with the continuous adjoint method scaled with respect to the time to compute the gradient with the adjoint method using $\bar{h} = 4$.

	ESDIRK	h [day]	\bar{h} [day]	t_{adj}	T_{adj}
discrete adjoint	3(4)	4	–	1.37	–
continuous adjoint	3(4)	4	4	1.70	1
	3(4)	4	12	0.58	0.33
	3(4)	4	120	0.06	0.03

relative change in the cost function less than 10^{-10} or if the number of SQP iterations exceeds 100. For the current case, we have never experienced that the SQP algorithm uses more than 100 iterations.

Table 3 reports computational statistics for the optimization process. We note that the NPVs computed using ESDIRK3(4) are bigger than the ones computed using ESDIRK1(2). Also the NPVs computed by the discrete adjoints are bigger than the ones computed using the continuous adjoint (with the same ESDIRK scheme). For both ESDIRK1(2)-3(4), we note that using the continuous adjoint with the biggest stepsize $\bar{h} = 20$ days, the computation time $T/T_{discr,RK12}$ is reduced by a factor of about three. Furthermore, we note that using the continuous adjoint based on ESDIRK3(4) with $\bar{h} = 20$, the computation time is halved when compared to using the ESDIRK1(2) method with the discrete adjoint gradient computation. This is indicated by $T/T_{discr,RK12}$ in Table 3.

Fig. 4 and Fig. 5 report the optimal water injection rates using the different adjoint methods based on ESDIRK1(2) and ESDIRK3(4), respectively. We note that when $h = \bar{h} = 4$, the trajectories agree for all times and visually we see no differences. Increasing \bar{h} produces a change in the solution and this change is more marked in the last control steps. This is in agreement with the results of Fig. 3. We note that the solutions computed using continuous adjoints are closer to the solution computed by discrete adjoints for ESDIRK3(4) than for ESDIRK1(2).

Fig. 6(a) and Fig. 6(b) report the NPVs as function of the SQP iteration number. We note that in general the different methods converge to similar numerical values. As reported in Table 3, they converge with a different rate (i.e. they use a different number of iterations). Increasing the step size, \bar{h} , the NPV decreases and this decrease is greater using ESDIRK1(2) compared to ESDIRK3(4).

Conclusions

We propose the use of high order continuous and discrete adjoint methods in a gradient based algorithm for oil reservoir production optimization. The resulting algorithm is tested for a production optimization problem of an oil reservoir with a slightly compressible two phase flow. For all cases considered, the dynamic optimization increases the net present value of the field and gives increased oil production. Computational experiments demonstrate that the accuracy of the sensitivities obtained by the adjoint methods are comparable to the accuracy obtained by the finite difference method. Using the ESDIRK method, the continuous adjoint method is able to use a time grid different from the time grid used for forward integration. Therefore, it can compute these sensitivities much faster than the discrete adjoint method and the finite-difference method. The discrete adjoint method produces the gradients of the numerical schemes and this is an advantage when the gradient is used in a numerical optimization algorithm. Computational experiments show that when the time steps are controlled in a certain range, the continuous adjoint method produces gradients sufficiently accurate for the optimization algorithm and

Table 3 Computational statistics for the optimization process. h : forward integration stepsize. \bar{h} : continuous adjoint stepsize. SQP: Number of iterations in the SQP-algorithm. QP: Number of KKT-matrix factorizations in the interior-point QP-solver. LS: Number of line searches and call to the ESDIRK algorithm. $T/T_{discr,RK12}$: time to compute the optimal solution scaled to the time to compute the optimal solution using the ESDIRK1(2) discrete gradient. $T/T_{discr,RK34}$: time to compute the optimal solution scaled to the time to compute the optimal solution using the ESDIRK3(4) discrete gradient.

ESDIRK	Adjoint	$h[day]$	$\bar{h}[day]$	SQP	QP	LS	$T/T_{discr,RK12}$	$T/T_{discr,RK34}$	NPV [\\$]
1(2)	discr.	4	–	84	1248	111	1	–	27.661.373
	cont.	4	4	62	894	129	0.94	–	27.661.351
	cont.	4	12	42	552	74	0.50	–	27.659.895
	cont.	4	120	25	272	45	0.27	–	27.598.463
3(4)	discr.	4	–	66	938	92	1.42	1	27.672.877
	cont.	4	4	66	945	134	1.85	1.30	27.672.870
	cont.	4	12	69	998	106	1.32	0.93	27.672.875
	cont.	4	120	38	507	58	0.57	0.40	27.667.576

somewhat faster than the discrete adjoint method.

Future work should investigate the use of a variable step-size in the forward integration. For basic simulation tasks, our software is equipped with a PI stepsize controller, while the forward integration reported in this paper is based on a fixed step size. In this work we didn't report preliminary results of using the adaptive step size controller as it is not clear yet how to set the controller tolerances during the adjoint integration. Fig. 3 suggests that relatively smaller step-sizes should be taken at the end of the horizon when integrating backward with the continuous adjoint.

The algorithm described in this paper has been implemented in Matlab. Future work will include implementations of the algorithms as efficient C++ code and comparison with other simulators.

Acknowledgements

This research project is financially supported by the Danish Research Council for Technology and Production Sciences. FTP Grant no. 274-06-0284

References

- Binder, T. et al. [2001] Introduction to model based optimization of chemical processes on moving horizons. In: Grötschel, M., Krumke, S. and Rambau, J. (Eds.) *Online Optimization of Large Scale Systems*. Springer.
- Brenan, K.E., Campbell, S.L. and Petzold, L.R. [1996] *Numerical Solution of Initial-Value Problems in Differential-Algebraic Equations*. Siam.
- Brouwer, D.R. and Jansen, J.D. [2004] Dynamic optimization of waterflooding with smart wells using optimal control theory. *SPE Journal*, **9**(4), 391–402.
- Cao, Y., Li, S., Petzold, L. and Serban, R. [2002] Adjoint sensitivity analysis for differential-algebraic equations: The adjoint DAE system and its numerical solution. *SIAM Journal on Scientific Computing*, **24**(3), 1076–1089.
- Capolei, A., Völcker, C., Frydendall, J. and Jørgensen, J.B. [2012] Oil reservoir production optimization using single shooting and esdirk methods. *IFAC Workshop*, Trondheim, Norway.
- Capolei, A. and Jørgensen, J.B. [2012] Solution of constrained optimal control problems using multiple shooting and ESDIRK methods. *2012 American Control Conference*.
- Chen, Z. [2007] *Reservoir Simulation. Mathematical Techniques in Oil Recovery*. SIAM, Philadelphia, USA.
- Hager, W.W. [1999] Runge-kutta methods in optimal control and the transformed adjoint system. *Numerische Mathematik*, **87**, 247–282.
- Jansen, J.D., Douma, S.D., Brouwer, D.R., Van den Hof, P.M.J., Bosgra, O.H. and Heemink, A.W. [2009] Closed-loop reservoir management. *2009 SPE Reservoir Simulation Symposium*, SPE 119098, The Woodlands, Texas, USA.
- Jansen, J.D., Bosgra, O.H. and Van den Hof, P.M.J. [2008] Model-based control of multiphase flow in subsurface oil reservoirs. *Journal of Process Control*, **18**, 846–855.
- Jansen, J. [2011] Adjoint-based optimization of multi-phase flow through porous media - A review. *Computers &*

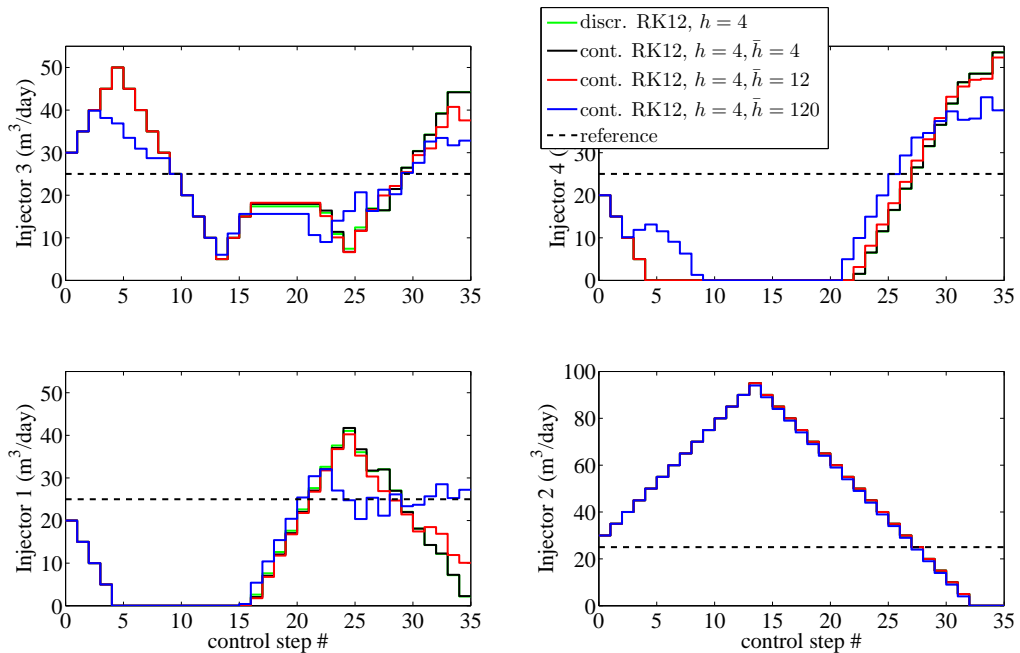


Figure 4 Optimal water injection rates using different adjoint methods based on ESDIRK1(2). *discr.:* discrete adjoint method., *cont.:* continuous adjoint method, *h:* forward step size in days, \bar{h} : adjoint step size in days.

Fluids, **46**, 40–51.

- Jørgensen, J.B., Kristensen, R., M., Thomsen and G., P. [2008] A family of esdirk integration methods. *Submitted to SIAM Journal on Scientific Computing*.
- Jørgensen, J.B. [2007] Adjoint sensitivity results for predictive control, state- and parameter-estimation with nonlinear models. *Proceedings of the European Control Conference 2007*, Kos, Greece, 3649–3656.
- Kourounis, D., Voskov, D. and Aziz, K. [2010] Adjoint methods for multicomponent flow simulation. *12th European Conference on the Mathematics of Oil Recovery*, Oxford, UK.
- Kraaijevanger, J., Egberts, P., Valstar, J. and Buurman, H. [2007] Optimal waterflood design using the adjoint method. *SPE Reservoir Simulation Symposium*, Society of Petroleum Engineers, Houston, Texas, U.S.A.
- Nadarajah, S.K. and Jameson, A. [2007] Optimum shape design for unsteady flows with time-accurate continuous and discrete adjoint methods. *AIAA Journal*, **45**(7), 1478–1491.
- Oliver, D.S., Reynolds, A.C. and Liu, N. [2008] *Inverse Theory for Petroleum Reservoir Characterization and History Matching*. Cambridge University Press.
- Sandu, A. [2006] On the properties of Runge-Kutta discrete adjoints. *International Conference for Computational Science*, Springer-Verlag Berlin Heidelberg, 550–557.
- Sarma, P., Aziz, K. and Durlafsky, L.J. [2005] Implementation of adjoint solution for optimal control of smart wells. *SPE Reservoir Simulation Symposium, 31 January-2 February 2005, The Woodlands, Texas*.
- Suwartadi, E., Krogstad, S. and Foss, B. [2011] Nonlinear output constraints handling for production optimization of oil reservoirs. *Computational Geosciences*, doi:10.1007/s10596-011-9253-3, accepted.
- Thomas, S. [2008] Enhanced oil recovery - an overview. *Oil & Gas Science and Technology*, **63**, 9–19.
- Völcker, C., Jørgensen, J.B., Thomsen, P.G. and Stenby, E.H. [2010] Explicit singly diagonally implicit Runge-Kutta methods and adaptive stepsize control for reservoir simulation. *ECMOR XII - 12th European Conference on the Mathematics of Oil Recovery*, Oxford, UK.
- Völcker, C., Jørgensen, J.B. and Stenby, E.H. [2011] Oil reservoir production optimization using optimal control. *50th IEEE Conference on Decision and Control and European Control Conference*, Orlando, Florida, 7937–7943, doi:http://dx.doi.org/10.1109/CDC.2011.6161271, accepted.
- Völcker, C., Jørgensen, J.B., Thomsen, P.G. and Stenby, E.H. [2009] Simulation of subsurface two-phase flow in an oil reservoir. *Proceedings of the European Control Conference 2009*, Budapest, Hungary, 1221–1226.

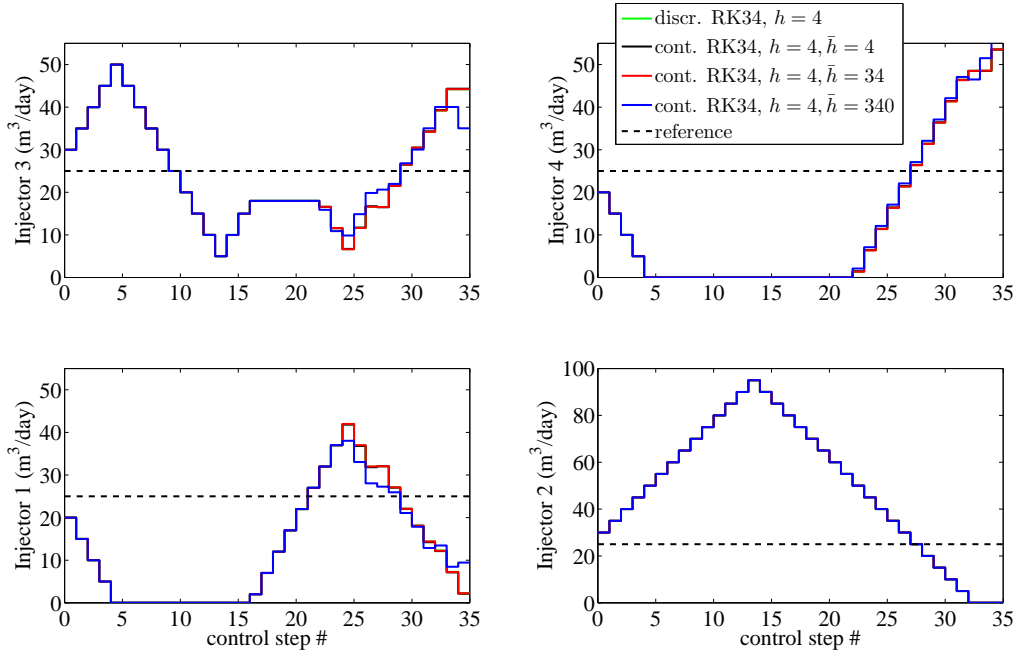


Figure 5 Optimal water injection rates using different adjoint methods based on ESDIRK3(4). *discr.*: discrete adjoint method., *cont.*: continuous adjoint method, h : forward step size in days, \bar{h} : adjoint step size in days.

Proof of Proposition 1.

The idea in the proof stems from Cao et al. (2002). Define

$$G(x, \dot{x}, u) = \frac{d}{dt}g(x(t)) - f(x(t), u(t)) = \frac{\partial g}{\partial x}\dot{x}(t) - f(x(t), u(t)) = 0 \quad (49)$$

and introducing the adjoint variable, $\lambda(t)$, to define the augmented objective function as

$$J_A = J + \int_{t_a}^{t_b} \lambda^T(t) G(x, \dot{x}, u) dt \quad (50a)$$

(49) implies that the derivative of the augmented objective function, J_A , can be expressed as

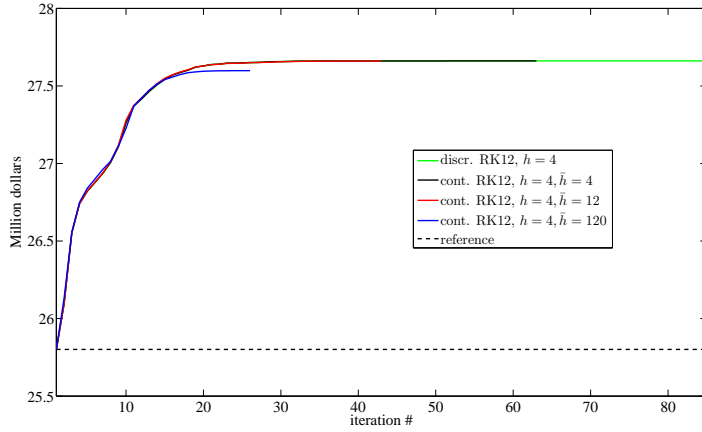
$$\begin{aligned} \frac{dJ_A}{du_k} &= \frac{dJ}{du_k} = \frac{\partial \Phi}{\partial x} \frac{\partial x}{\partial u_k} \Big|_{t_b} + \int_{t_a}^{t_b} \left(\frac{\partial \Phi}{\partial u} \frac{\partial u(t)}{\partial u_k} + \frac{\partial \Phi}{\partial x} \frac{\partial x(t)}{\partial u_k} \right) dt \\ &+ \int_{t_a}^{t_b} \lambda^T(t) \left(\frac{\partial G}{\partial u} \frac{\partial u(t)}{\partial u_k} + \frac{\partial G}{\partial x} \frac{\partial x(t)}{\partial u_k} + \frac{\partial G}{\partial \dot{x}} \frac{\partial \dot{x}}{\partial u_k} \right) dt \end{aligned} \quad (51)$$

where

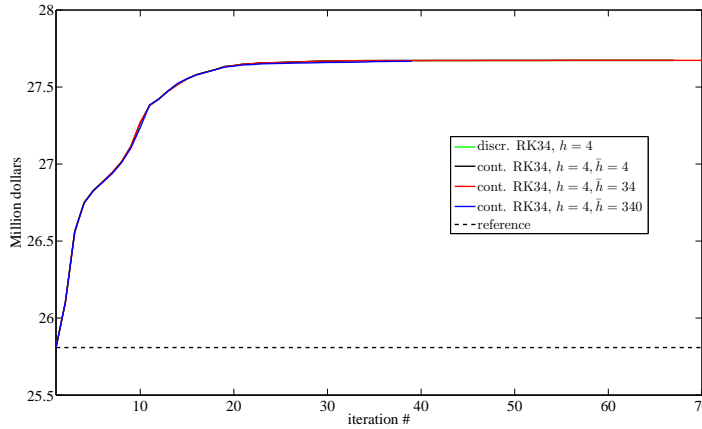
$$\frac{\partial u(t)}{\partial u_k} = \begin{cases} I & t_k \leq t < t_{k+1} \\ 0 & \text{otherwise} \end{cases} \quad (52)$$

Integrating by part

$$\int_{t_a}^{t_b} \lambda^T(t) \frac{\partial G}{\partial \dot{x}} \frac{\partial \dot{x}}{\partial u_k} dt = \left[\lambda^T \frac{\partial G}{\partial x} \frac{\partial x(t)}{\partial u_k} \right] \Big|_{t_a}^{t_b} - \int_{t_a}^{t_b} \frac{d}{dt} \left(\lambda^T \frac{\partial G}{\partial x} \right) \frac{\partial x}{\partial u_k} dt \quad (53)$$



(a) NPVs using ESDIRK12



(b) NPVs using ESDIRK34

Figure 6 NPVs convergence using different methods. *discr.*: discrete adjoint method., *cont.*: continuous adjoint method, *RK12*: ESDIRK12, *RK34*: ESDIRK34, *h*: forward step size in days, \bar{h} : adjoint step size in days.

and using $\frac{\partial x}{\partial u_k}(t_a) = 0$ in our case, we can rearrange equation (51) as

$$\begin{aligned} \frac{dJ}{du_k} &= \int_{t_k}^{t_{k+1}} \left(\frac{\partial \Phi}{\partial u} + \lambda^T \frac{\partial G}{\partial u} \right) dt + \int_{t_k}^{t_{k+1}} \left(\frac{\partial \Phi}{\partial x} + \lambda^T \frac{\partial G}{\partial x} - \frac{d}{dt} \left(\lambda^T \frac{\partial G}{\partial \dot{x}} \right) \right) \frac{\partial x}{\partial u_k} dt \\ &+ \left[\left(\frac{\partial \hat{\Phi}}{\partial x} + \lambda^T \frac{\partial G}{\partial \dot{x}} \right) \frac{\partial x}{\partial u_k} \right] \Big|_{t_b} \end{aligned} \quad (54)$$

This expression gives the derivative dJ/du_k for any value (not just the optimal one) of $\lambda(t)$. We choose $\lambda(t)$ such that it satisfies

$$\frac{\partial \Phi}{\partial x} + \lambda^T \frac{\partial G}{\partial x} - \frac{d}{dt} \left(\lambda^T \frac{\partial G}{\partial \dot{x}} \right) = 0 \quad (55a)$$

$$\left[\frac{\partial \hat{\Phi}}{\partial x} + \lambda^T \frac{\partial G}{\partial \dot{x}} \right] \Big|_{t_b} = 0 \quad (55b)$$

and gives a simple expression for evaluation of dJ/du_k

$$\frac{\partial \psi}{\partial u_k} = \frac{dJ}{du_k} = \int_{t_k}^{t_{k+1}} \left(\frac{\partial \Phi}{\partial u} - \lambda^T \frac{\partial f}{\partial u} \right) dt \quad (56)$$

(49) implies

$$\frac{\partial G}{\partial x} = \frac{d}{dt} \left(\frac{\partial g}{\partial x} \right) - \frac{\partial f}{\partial x} \quad (57a)$$

$$\frac{\partial G}{\partial \dot{x}} = \frac{\partial g}{\partial \dot{x}} \quad (57b)$$

such that (55) can be rearranged to

$$\frac{d\lambda^T}{dt} \frac{\partial g}{\partial x} + \lambda^T \frac{\partial f}{\partial x} - \frac{\partial \Phi}{\partial x} = 0 \quad (58a)$$

$$\frac{\partial \hat{\Phi}}{\partial x}(x(t_b)) + \lambda^T(t_b) \frac{\partial g}{\partial x}(x(t_b)) = 0 \quad (58b)$$

Similarly we derive the expression for dJ/dx_0

$$\begin{aligned} \frac{dJ_A}{dx_0} = \frac{dJ}{dx_0} &= \frac{\partial \hat{\Phi}}{\partial x} \frac{\partial x}{\partial x_0} \Big|_{t_b} + \int_{t_a}^{t_b} \left(\frac{\partial \Phi}{\partial x} \frac{\partial x(t)}{\partial x_0} \right) dt \\ &+ \int_{t_a}^{t_b} \lambda^T(t) \left(\frac{\partial G}{\partial x} \frac{\partial x(t)}{\partial x_0} + \frac{\partial G}{\partial \dot{x}} \frac{\partial \dot{x}}{\partial x_0} \right) dt \end{aligned} \quad (59)$$

Integrating by part

$$\int_{t_a}^{t_b} \lambda^T(t) \frac{\partial G}{\partial \dot{x}} \frac{\partial \dot{x}}{\partial x_0} dt = \left[\lambda^T \frac{\partial G}{\partial \dot{x}} \frac{\partial x(t)}{\partial x_0} \right] \Big|_{t_a}^{t_b} - \int_{t_a}^{t_b} \frac{d}{dt} \left(\lambda^T \frac{\partial G}{\partial \dot{x}} \right) \frac{\partial x}{\partial x_0} dt \quad (60)$$

and using $\frac{\partial \dot{x}}{\partial x_0}(t_a) = I$ in our case, we can rearrange equation (59) as

$$\frac{dJ}{dx_0} = \int_{t_k}^{t_{k+1}} \left(\frac{\partial \Phi}{\partial x} + \lambda^T \frac{\partial G}{\partial x} - \frac{d}{dt} \left(\lambda^T \frac{\partial G}{\partial \dot{x}} \right) \right) \frac{\partial x}{\partial x_0} dt + \left[\left(\frac{\partial \hat{\Phi}}{\partial x} + \lambda^T \frac{\partial G}{\partial \dot{x}} \right) \frac{\partial x}{\partial x_0} \right] \Big|_{t_b} - \lambda^T(t_a) \frac{\partial G}{\partial \dot{x}}(t_a) \quad (61)$$

finally using $\lambda(t)$ computed in (55) we have

$$\frac{dJ}{dx_0} = -\lambda^T(t_a) \frac{\partial g}{\partial x}(t_a) \quad (62)$$

Proof of Proposition 4.

We follow the same adjoint formalism as in (Kraaijevanger et al., 2007; Oliver et al., 2008). This is different, but equivalent to the more common one based on the Lagrange formalism (Brouwer and Jansen, 2004; Sarma et al., 2005; Jørgensen, 2007) which make use of the augmented objective function $J_a = J - \lambda \bar{R}$. Adjoint formalism have a wider scope because adjoint variables are defined not only when optimal conditions are satisfied. When optimal conditions are satisfied, the adjoint variables coincide with Lagrange multipliers.

Starting from the discretized dynamical model in residual form (37)

$$\bar{R}(x_0, z, y) = 0 \quad (63)$$

we use the implicit function theorem to find the sensitivities of the dependent variables with respect to the independent ones

$$\frac{\partial z}{\partial y} = -\frac{\partial \bar{R}^{-1}}{\partial z} \frac{\partial \bar{R}}{\partial y} \quad (64a)$$

$$\frac{\partial z}{\partial x_0} = -\frac{\partial \bar{R}^{-1}}{\partial z} \frac{\partial \bar{R}}{\partial x_0}. \quad (64b)$$

The total derivatives of the cost function in (37) are given by

$$\frac{dJ}{dy}(x_0, z, y) = \frac{\partial J}{\partial y} + \frac{\partial J}{\partial z} \frac{\partial z}{\partial y} = \frac{\partial J}{\partial y} - \frac{\partial J}{\partial z} \frac{\partial \bar{R}^{-1}}{\partial z} \frac{\partial \bar{R}}{\partial y} \quad (65a)$$

$$\frac{dJ}{dx_0}(x_0, z, y) = \frac{\partial J}{\partial x_0} + \frac{\partial J}{\partial z} \frac{\partial z}{\partial x_0} = \frac{\partial J}{\partial x_0} - \frac{\partial J}{\partial z} \frac{\partial \bar{R}^{-1}}{\partial z} \frac{\partial \bar{R}}{\partial x_0}. \quad (65b)$$

Introducing the adjoint variables λ as solution of

$$\lambda^T \frac{\partial \bar{R}}{\partial z} = -\frac{\partial J}{\partial z} \quad (66)$$

we can rewrite (65) as

$$\frac{\partial \psi}{\partial y} = \frac{dJ}{dy} = \frac{\partial J}{\partial y} + \lambda^T \frac{\partial \bar{R}}{\partial y} \quad (67a)$$

$$\frac{\partial \psi}{\partial x_0} = \frac{dJ}{dx_0} = \frac{\partial J}{\partial x_0} + \lambda^T \frac{\partial \bar{R}}{\partial x_0}. \quad (67b)$$

Derivatives $\frac{\partial R_{j,i}}{\partial X_{j,l}}$.

$$\begin{aligned} \frac{\partial R_{j,i}}{\partial X_{j,l}} &= \left(\frac{\partial g}{\partial x}(X_{j,l}) - h_j \gamma \frac{\partial f}{\partial x}(X_{j,l}, \bar{u}_j) \right) \delta_{li} - \frac{\partial \phi_{j,i}}{\partial X_{j,l}} \\ \frac{\partial \phi_{j,i}}{\partial X_{j,l}} &= (1 - \delta_{li}) \left(\frac{\partial g}{\partial x}(X_{j,l}) \delta_{li} + h_j a_{il} \frac{\partial f}{\partial x}(X_{j,l}, \bar{u}_j) \right) \end{aligned} \quad (68)$$

where δ_{il} is the Kronecker function.

$$\begin{aligned} \frac{\partial R_{j,i}}{\partial \bar{u}_j} &= -\frac{\partial \phi_{j,i}}{\partial \bar{u}_j} - h_j \gamma \frac{\partial f}{\partial u}(X_{j,l}, \bar{u}_j) \\ \frac{\partial \phi_{j,i}}{\partial \bar{u}_j} &= h_j \sum_{l=1}^{i-1} a_{il} \frac{\partial f}{\partial u}(X_{j,l}, \bar{u}_j) \end{aligned} \quad (69)$$

$$\frac{\partial J}{\partial u_k} = \sum_{j: u(\bar{t}_j) \equiv u_k} h_j \sum_{l=1}^s b_l \frac{\partial \Phi}{\partial u}(X_{j,l}, u_k) \quad (70)$$

$$\frac{\partial J}{\partial x_0} = h_0 b_1 \frac{\partial \Phi}{\partial x_0}(X_{0,1}, u_0) \quad (71)$$

$$\frac{\partial J}{\partial X_{j,i}} = h_j b_i \frac{\partial \Phi}{\partial x}(X_{j,i}, \bar{u}_j) \quad i \in \{2, \dots, s-1\}, j \in \{0, \dots, \bar{N}-1\} \quad (72)$$

$$\frac{\partial J}{\partial X_{j,s}} = h_j b_s \frac{\partial \Phi}{\partial x}(X_{j,s}, \bar{u}_j) + h_{j+1} b_1 \frac{\partial \Phi}{\partial x}(X_{j+1,1}, \bar{u}_{j+1}) \quad j \in \{0, \dots, \bar{N}-2\} \quad (73)$$

$$\frac{\partial J}{\partial X_{\bar{N}-1,s}} = \frac{\partial \hat{\Phi}}{\partial X_{\bar{N}-1,s}}(\partial X_{\bar{N}-1,s}) + h_{\bar{N}-1} b_s \frac{\partial \Phi}{\partial X_{\bar{N}-1,s}}(\partial X_{\bar{N}-1,s}, u_N) \quad (74)$$

APPENDIX **E**

Paper IV

Waterflooding Optimization in Uncertain Geological Scenarios

Authors:

Andrea Capolei, Eka Suwartadi, Bjarne Foss and John Bagterp Jørgensen

Published online in:

Computational Geosciences Journal.

Waterflooding optimization in uncertain geological scenarios

Andrea Capolei · Eka Suwartadi · Bjarne Foss ·
John Bagterp Jørgensen

Received: 21 March 2013 / Accepted: 21 August 2013
© Springer Science+Business Media Dordrecht 2013

Abstract In conventional waterflooding of an oil field, feedback based optimal control technologies may enable higher oil recovery than with a conventional reactive strategy in which producers are closed based on water breakthrough. To compensate for the inherent geological uncertainties in an oil field, robust optimization has been suggested to improve and robustify optimal control strategies. In robust optimization of an oil reservoir, the water injection and production borehole pressures (bhp) are computed such that the predicted net present value (NPV) of an ensemble of permeability field realizations is maximized. In this paper, we both consider an open-loop optimization scenario, with no feedback, and a closed-loop optimization scenario. The closed-loop scenario is implemented in a moving horizon manner and feedback is obtained using an ensemble Kalman filter for estimation of the permeability field from the production data. For open-loop implementations, previous test case studies presented in the literature,

show that a traditional robust optimization strategy (RO) gives a higher expected NPV with lower NPV standard deviation than a conventional reactive strategy. We present and study a test case where the opposite happen: The reactive strategy gives a higher expected NPV with a lower NPV standard deviation than the RO strategy. To improve the RO strategy, we propose a modified robust optimization strategy (modified RO) that can shut in uneconomical producer wells. This strategy inherits the features of both the reactive and the RO strategy. Simulations reveal that the modified RO strategy results in operations with larger returns and less risk than the reactive strategy, the RO strategy, and the certainty equivalent strategy. The returns are measured by the expected NPV and the risk is measured by the standard deviation of the NPV. In closed-loop optimization, we investigate and compare the performance of the RO strategy, the reactive strategy, and the certainty equivalent strategy. The certainty equivalent strategy is based on a single realization of the permeability field. It uses the mean of the ensemble as its permeability field. Simulations reveal that the RO strategy and the certainty equivalent strategy give a higher NPV compared to the reactive strategy. Surprisingly, the RO strategy and the certainty equivalent strategy give similar NPVs. Consequently, the certainty equivalent strategy is preferable in the closed-loop situation as it requires significantly less computational resources than the robust optimization strategy. The similarity of the certainty equivalent and the robust optimization based strategies for the closed-loop situation challenges the intuition of most reservoir engineers. Feedback reduces the uncertainty and this is the reason for the similar performance of the two strategies.

A. Capolei · J. B. Jørgensen (✉)
Department of Applied Mathematics and Computer Science
and Center for Energy Resources Engineering,
Technical University of Denmark (DTU),
2800 Kgs. Lyngby, Denmark
e-mail: jbj@dtu.dk

A. Capolei
e-mail: acap@dtu.dk

E. Suwartadi · B. Foss
Department of Engineering Cybernetics,
Norwegian University of Science and Technology (NTNU),
7491 Trondheim, Norway

E. Suwartadi
e-mail: eka.suwartadi@ieec.org

B. Foss
e-mail: Bjarne.Foss@itk.ntnu.no

Keywords Robust optimization · Ensemble Kalman filter · Oil reservoir · Production optimization · Automatic history matching

1 Introduction

In the oil industry, closed-loop reservoir management (CLRM) has been suggested to maximize oil recovery or a financial measure such as the net present value of a given oil reservoir [1–12]. Fig. 1 illustrates the components in closed-loop reservoir management. The controller consists of model based data assimilation, also known as a parameter and state estimator, and a model based optimizer for maximizing the oil recovery or some predicted financial measure such as the net present value. The inputs to the controller is production measurements, forecasts of the oil price, the interest rate, and the operating unit costs. Based on these inputs the controller computes water injection trajectories as well as borehole pressure trajectories. Only the first part of these trajectories are implemented in the real oil reservoir. As new measurements become available, the process is repeated. The parameters and the states of the model are re-estimated using the data assimilation component. These filtered states and parameters are used in the model based optimization for computation of optimal trajectories for the manipulated variables, and the first part of the trajectories are implemented. This form of control is also known as Nonlinear Model Predictive Control (NMPC) [13–19]. A key difference of NMPC applied to reservoir management and traditional process control applications is the size of the model describing the system. In reservoir management, spatial discretization of the partial differential equation (PDE) system describing the flow results in a system of differential equations that is much larger than

the systems typically encountered in process control applications. The large-scale nature of the closed-loop reservoir management problem requires special numerical techniques for the data assimilation [20] as well as the optimization [21, 22].

In this paper, we study and discuss two closed-loop approaches for real-time production optimization. Both of the two closed-loop approaches consist of three key elements: 1) A gradient based optimization algorithm for computation of the control input, 2) an ensemble Kalman filter (EnKF) for model updating through data assimilation (history-matching), and 3) use of the moving horizon principle for data assimilation and implementation of the computed control input. The first closed-loop approach is a certainty equivalent strategy. In this strategy, the EnKF is used to estimate permeabilities of each member of the ensemble. The average of these permeabilities is used in the optimization. The second closed-loop approach is a strategy based on robust optimization. In this strategy, all members of the ensemble are used to compute the mean net present value for the optimization.

We know from finance that strategies which attempt to increase returns are often accompanied by an increased uncertainty [23]. The robust strategy typically reduces the uncertainty of the expected outcome compared to a non-robust strategy and one would consequently expect a decrease in return [24, 25]. Figure 2 sketches this phenomenon. For the test cases used in the oil industry to test robust optimization strategies, this phenomenon has not been reported [26]. Due to the large-scale nature of an oil reservoir model, we cannot compute the entire distribution of the net present value for the closed-loop system. Accordingly, the ambition in this paper is in a computational tractable way, using a few realizations, to demonstrate the closed-loop performance of the certainty equivalent and the robust optimization strategy.

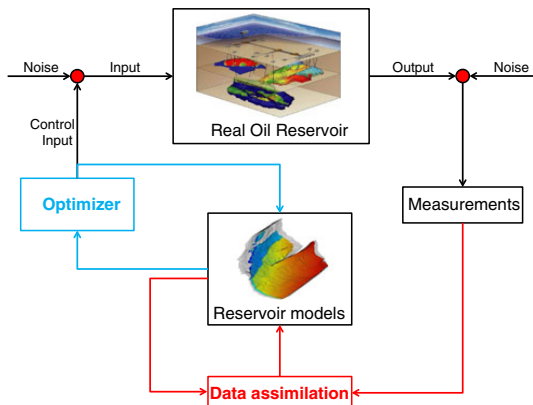


Fig. 1 Closed-loop reservoir management

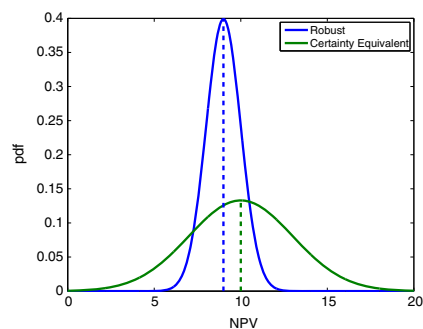


Fig. 2 Conceptual sketch of the distribution of the net present value for two strategies in finance. A robust strategy has lower variance and typically also lower mean value than non-robust strategies such as a certainty equivalent strategy

Data assimilation by the EnKF is a popular method for history matching as well as closed-loop reservoir management [1, 3, 4, 6, 27]. In [28], different data assimilation and optimization methods are tested on the synthetic "Brugge field" to maximize its NPV. The three best results are all obtained by methods using an EnKF for data assimilation. The EnKF method is a Monte Carlo implementation of the Kalman filter [29]. The literature available on the EnKF in petroleum engineering is rather large and mature. Data assimilation using the ensemble Kalman filter has been reviewed by [30–32] and [20, 33, 34] provide overviews of filtering techniques. A review of various issues of the EnKF, including sampling error because of small ensembles, covariance localization (limiting the influence of the observations to the state variables that are located spatially close to them), filter divergence, and model error, is given in [31] and [30]. [35] describes the necessity of introducing a confirming step to ensure consistency of the updated static and dynamic variables with the flow equations, while [30] discusses the reduction of the ensemble size with a resampling scheme. The problem of ensemble collapse is discussed in [36]. [37] considers a way to handle model constraints within the EnKF. [38] investigates an update step that preserves multi-point statistics and not only two point-statistics.

In the model based optimization part of CLRM, a traditional choice is to use methods based on one realization, usually the ensemble mean from the EnKF. To reduce the risk arising from uncertainty in the geological description, [26] proposes to optimize the expectation of net present value over a set of reservoir models using a gradient based method. This procedure is referred to as robust optimization (RO). In open-loop simulations, [26] compares the results of the RO procedure to two alternative approaches: a nominal optimization (NO) and a reactive control approach. They find that RO yields a much smaller variance than the alternatives. Moreover the RO strategy significantly improves the expected NPV over the alternative methods (on average 9.5 % higher than using reactive-control and 5.9 % higher than the average of NO strategies). [27, 39, 40] do closed-loop reservoir management using an EnKF for data assimilation and robust optimization with a gradient-free ensemble based optimization scheme for the model based optimization. [39] reports that an ensemble based optimization results in a NPV improvement of 22 % compared to a reactive strategy. However, they do not compare the closed-loop robust strategy to a closed-loop certainty equivalent strategy.

To our knowledge, there is no closed-loop application of the gradient-based robust optimization strategy as implemented in [26] available in the literature. Furthermore, the CLRM literature misses an open-loop as well as a closed-loop comparison of the performance of an ensemble

based optimization scheme [39] or a gradient-based robust optimization scheme [26] with a certainty equivalent optimization strategy based on the ensemble mean. In this work we partially fill this gap and do CLRM comparing a RO strategy [26] to three alternative approaches: a reactive strategy, a nominal strategy, and a certainty equivalent strategy. By using feedback, the ensemble of permeability fields converge to a point such that the RO strategy becomes equivalent to the certainty equivalent strategy based on the ensemble mean. The RO is more expensive computationally than the certainty equivalent strategy. In this paper, we use a case study to compare the RO strategy in closed-loop to other strategies.

The paper is organized as follows. Section 2 defines the reservoir model. Section 3 states the constrained optimal control problem and describes the robust optimization strategy. The ensemble Kalman filter for data assimilation is described in Section 4. Section 5 describes the numerical case study and conclusions are presented in Section 6.

2 Reservoir model

In this work, we assume that the reservoirs are in the secondary recovery phase where the pressures are above the bubble point pressure of the oil phase. Therefore, two-phase immiscible flow, i.e. flow without mass transfer between the two phases, is a reasonable assumption. We focus on water-flooding cases for two-phase (oil and water) reservoirs. Further, we assume incompressible fluids and rocks, no gravity effects or capillary pressure, no-flow boundaries, constant porosity, and finally isothermal conditions. The state equations in an oil reservoir Ω , with boundary $\partial\Omega$ and outward facing normal vector \mathbf{n} , can be represented by pressure and saturation equations. The pressure equation is described as

$$\begin{aligned} \mathbf{v} &= -\lambda_t \mathbf{K} \nabla p, & \nabla \cdot \mathbf{v} &= q & \text{in } \Omega \\ \mathbf{v} \cdot \mathbf{n} &= 0 & \text{on } \partial\Omega \end{aligned} \tag{1}$$

\mathbf{v} is the Darcy velocity (total velocity), \mathbf{K} is the permeability, p is the pressure, q is the volumetric well rate, and λ_t is the total mobility, which in this setting is the sum of the water and oil mobility functions,

$$\lambda_t = \lambda_w(s) + \lambda_o(s) = k_{rw}(s)/\mu_w + k_{ro}(s)/\mu_o \tag{2}$$

The saturation equation is given by

$$\phi \frac{\partial}{\partial t} S_w + \nabla \cdot (f_w(S_w) \mathbf{v}) = \frac{q_w}{\rho_w} \tag{3}$$

ϕ is the porosity, s is the saturation, $f_w(s)$ is the water fractional flow which is defined as $\frac{\lambda_w}{\lambda_t}$, and q_w is the volumetric water rate at the well. We use the MRST [41] reservoir simulator to solve the pressure and saturation equations,

(1) and (3), sequentially. Wells are implemented using the Peaceman well model [42]

$$q_i = -\lambda_t W I_i \left(p_i - p_i^{BHP} \right) \tag{4}$$

q_i is the flow rate into grid block i , p_i^{BHP} is the wellbore pressure, and $W I_i$ is the Peaceman well-index.

3 Production optimization

Production optimization aims at maximizing a performance index, net present value or oil recovery, for the life time of the oil reservoir. Spatial and temporal discretization of the model equations and the performance index yield a finite dimensional nonlinear constrained optimization problem on a time horizon from 0 to N that can be formulated as

$$\max_{\{x_k\}_{k=0}^N, \{u_k\}_{k=0}^{N-1}} J = \sum_{k=0}^{N-1} J_k(x_k, x_{k+1}, u_k) \tag{5a}$$

subject to

$$x_0 = \bar{x}_0 \tag{5b}$$

$$g_k(x_k, x_{k+1}, u_k; \theta) = 0 \quad k \in \mathcal{N} := \{0, 1, \dots, N - 1\} \tag{5c}$$

$$c \left(\{u_k\}_{k=0}^{N-1} \right) \leq 0 \tag{5d}$$

\bar{x}_0 is the initial states, θ is a parameter vector in an uncertain space Θ (in our case the permeability field), x_k is the state vector, u_k is a piecewise constant control vector, g_k is the discretization of the dynamical model, (1) and (3), and $c \left(\{u_k\}_{k=0}^{N-1} \right)$ are linear bounds on the control vector. In our formulations we do not allow nonlinear state or output constraints, see e.g. [43].

3.1 Objective function

The optimizer maximizes the net present value by manipulating the well bhps. Hence, the manipulated variable at time period $k \in \mathcal{N}$ is $u_k = \left\{ \{p_{i,k}^{bhp}\}_{i \in \mathcal{I}}, \{p_{i,k}^{bhp}\}_{i \in \mathcal{P}} \right\}$ with \mathcal{I} being the set of injectors and \mathcal{P} being the set of producers. For $i \in \mathcal{I}$, $p_{i,k}^{bhp}$ is the bhp (bar) in time period $k \in \mathcal{N}$ at injector i . For $i \in \mathcal{P}$, $p_{i,k}^{bhp}$ is the bhp (bar) at producer i in time period $k \in \mathcal{N}$.

The stage cost, J_k , in the objective function for a net present value (NPV) maximization can be expressed as

$$J_k = - \frac{\Delta t_k}{(1+d)^{\frac{k+1}{\tau}}} \left[\sum_{i \in \mathcal{P}} r_o q_{o,i}^{k+1}(u_k, x_{k+1}) - \sum_{i \in \mathcal{P}} r_{wp} q_{w,i}^{k+1}(u_k, x_{k+1}) + \sum_{l \in \mathcal{I}} r_{wi} q_l^{k+1}(u_k, x_{k+1}) \right] \tag{6}$$

r_o , r_{wp} , and r_{wi} represent the oil price, the water separation cost, and the water injection cost, respectively. The water flow rate (bbl/day) in producer i at time period k is $q_{w,i}^k = f_w q_i^k$ and the oil flow rate is $q_{o,i}^k = (1 - f_w) q_i^k$. q_i^k is the flow rate at producer i as given by (4). The well rates at the injector wells are denoted by q_l (only water is injected). Note that from the well model (4), it follows that the flow rates q are negative for the producer wells and positive for the injector wells. d is the discount factor, Δt_k is the time interval, and N is the number of control steps. Note that in the special case when the discount factor is zero ($d = 0$) and the water injection and separation costs are zero as well, the NPV is equivalent to the quantity of produced oil.

3.2 Control and constraints

We control the bhp of the wells and assume that these control inputs are piecewise constant functions. The bhps are constrained by well and reservoir conditions. To maintain the two phase situation we require the pressure to be above the bubble point pressure (290 bar). To avoid fracturing the rock, the pressure must be below the fracture pressure of the rock (350 bar). To maintain flow from the injectors to the producers, the injection pressure is maintained above 310 bar and the producer pressures are kept below 310 bar. With these bounds we did not experience that the flow was reversed. Without these pressure bounds, however, state constraints, like bounds on flow rates (4), must be applied to avoid flow reversion.

3.3 Single-shooting optimization

We use a single shooting algorithm [11, 44] for solution of (5a). Alternatives are multiple-shooting [45, 46] and collocation methods [47]. Despite the fact that the multiple shooting and the collocation methods offer better convergence properties than the single-shooting method [45–47], their application in production optimization is restricted by the large state dimension of such problems. The use of multiple-shooting is prevented by the need for computation of state sensitivities. The collocation method do not allow for adaptive time stepping and would need to solve huge-scale optimization problems. In

the single shooting optimization algorithm, we define the function

$$\psi = \psi \left(\{u_k\}_{k=0}^{N-1}; \bar{x}_0, \theta \right) = \left\{ J = \sum_{k=0}^{N-1} J_k(x_k, x_{k+1}, u_k) : x_0 = \bar{x}_0, g_k(x_k, x_{k+1}, u_k; \theta) = 0, k \in \mathcal{N} \right\} \quad (7)$$

such that (5a) can be expressed as the optimization problem

$$\max_{\{u_k\}_{k=0}^{N-1}} \psi = \psi \left(\{u_k\}_{k=0}^{N-1}; \bar{x}_0, \theta \right) \quad \text{s.t.} \quad c \left(\{u_k\}_{k=0}^{N-1} \right) \leq 0 \quad (8)$$

Gradient based optimization algorithms for solving (8) require evaluation of $\psi = \psi \left(\{u_k\}_{k=0}^{N-1}; \bar{x}_0, \theta \right)$, $\nabla_{u_k} \psi$ for $k \in \mathcal{N}$, $c \left(\{u_k\}_{k=0}^{N-1} \right)$, and $\nabla_{u_k} c \left(\{u_k\}_{k=0}^{N-1} \right)$ for $k \in \mathcal{N}$. The constraint function is in the cases considered linear bounds such that evaluation of these constraint functions and their gradients is trivial. Given an iterate, $\{u_k\}_{k=0}^{N-1}$, ψ is computed by solving (7) marching forwards. $\nabla_{u_k} \psi$ for $k \in \mathcal{N}$ is computed by the adjoint method [9, 11, 43, 48–51]. In this method, the gradients $\{\nabla_{u_k} \psi\}_{k=0}^{N-1}$ are computed using Algorithm 1 with

$$\nabla_{x_k} g_k = \nabla_{x_k} g_k(x_k, x_{k+1}, u_k; \theta) \quad k \in \mathcal{N} \quad (9a)$$

$$\nabla_{x_{k+1}} g_k = \nabla_{x_{k+1}} g_k(x_k, x_{k+1}, u_k; \theta) \quad k \in \mathcal{N} \quad (9b)$$

$$\nabla_{u_k} g_k = \nabla_{u_k} g_k(x_k, x_{k+1}, u_k; \theta) \quad k \in \mathcal{N} \quad (9c)$$

$$\nabla_{x_k} J_k = \nabla_{x_k} J_k(x_k, x_{k+1}, u_k) \quad k \in \mathcal{N} \setminus \{0\} \quad (9d)$$

$$\nabla_{x_{k+1}} J_k = \nabla_{x_{k+1}} J_k(x_k, x_{k+1}, u_k) \quad k \in \mathcal{N} \quad (9e)$$

$$\nabla_{u_k} J_k = \nabla_{u_k} J_k(x_k, x_{k+1}, u_k) \quad k \in \mathcal{N} \quad (9f)$$

that are computed and stored during the forward solution of (7).

Algorithm 1 Adjoint method for computing $\{\nabla_{u_k} \psi\}_{k=0}^{N-1}$.

```

Solve for  $\lambda_N$  in  $\nabla_{x_N} g_{N-1} \lambda_N = \nabla_{x_N} J_{N-1}$ 
for  $k = N - 1, N - 2, \dots, 1$  do
  Compute  $\nabla_{u_k} \psi = \nabla_{u_k} J_k - \nabla_{u_k} g_k \lambda_{k+1}$ 
  Solve for  $\lambda_k$  in  $\nabla_{x_k} g_{k-1} \lambda_k = \nabla_{x_k} J_{k-1} + \nabla_{x_k} J_k - \nabla_{x_k} g_k \lambda_{k+1}$ 
end for
Compute  $\nabla_{u_0} \psi = \nabla_{u_0} J_0 - \nabla_{u_0} g_0 \lambda_1$ 

```

To solve (8), we use two commercial optimization software packages: Knitro [52] and Matlab’s `fmincon` function [53]. Knitro as well as `fmincon`, allows us to use an interior point or an active-set methods. We use up to 10 different initial guesses when running the optimizations and we find similar qualitative results with both software packages. Further, similar results are found with interior point and active-set methods. When using Knitro as well as `fmincon`, we select an interior point method since we experience the lowest computation times with this method. A local optimal solution is reported if the KKT conditions are satisfied to within a relative and absolute tolerance of 10^{-6} . The current best but non-optimal iterate is also returned in cases when the optimization algorithm uses more than 100 iterations. Similarly, the current best, but non-optimal, iterate is also returned in the case of a relative cost function or step size change less than 10^{-8} . Furthermore, in our simulations we noted that normalizing the cost function improved the convergence.

3.4 Certainty-equivalent and robust optimization

In certainty equivalent optimization, (8) is solved using the expected value for the parameters, $\eta = E[\theta]$, such that the objective used in (8) is

$$\psi_{CE} = \psi \left(\{u_k\}_{k=0}^{N-1}; \bar{x}_0, \eta \right) \quad (10)$$

[26] introduces robust optimization to reduce the effect of geological uncertainties in the field development phase. Robust optimization uses a set of realizations that reflect the range of possible geological structures honoring the statistics of the geological uncertainties. In reservoir models, geological uncertainty is generally profound because of the noisy and sparse nature of seismic data, core samples, and borehole logs. The consequence of a large number of uncertain model parameters (θ) is the broad range of possible models that may satisfy the seismic and core-sample data. Nevertheless, in many cases, a single reservoir model is adopted in which the uncertain parameters, θ , are converted to deterministic parameters η by taking their expected values (i.e. $\eta = E[\theta]$). However, because the NPV is used as our measure of performance, we are more interested in the expected NPV over the uncertainty space, Θ (spanned by the uncertain parameters θ), than the mean of the parameters. The expected NPV over the uncertainty space, Θ , is in general not the same as the NPV computed using the expected values of the uncertain parameters, $\eta = E[\theta]$, as NPV is a nonlinear function of the parameters, θ . Consequently

$$E_{\theta} \left[\psi \left(\{u_k\}_{k=0}^{N-1}; \bar{x}_0, \theta \right) \right] \neq \psi \left(\{u_k\}_{k=0}^{N-1}; \bar{x}_0, E_{\theta}[\theta] \right), \theta \in \Theta \quad (11)$$

Consider a discretization, $\Theta_d = \{\theta_1, \dots, \theta_{n_d}\}$, of the uncertainty space, Θ , such that expected NPV may be approximated by

$$E_{\theta} \left[\psi \left(\{u_k\}_{k=0}^{N-1}; \bar{x}_0, \theta \in \Theta \right) \right] \approx E_{\theta} \left[\psi \left(\{u_k\}_{k=0}^{N-1}; \bar{x}_0, \theta \in \Theta_d \right) \right] \tag{12}$$

This approximation of the expected NPV is a better approximation than the NPV computed using the expected parameters, η . In the special case of equiprobable realizations, the right-hand side of (12) is the arithmetic average

$$E_{\theta} \left[\psi \left(\{u_k\}_{k=0}^{N-1}; \bar{x}_0, \theta \in \Theta_d \right) \right] = \frac{1}{n_d} \sum_{i=1}^{n_d} \psi \left(\{u_k\}_{k=0}^{N-1}; \bar{x}_0, \theta^i \right) \tag{13}$$

The robust optimization method uses the ensemble average as its objective function in (8)

$$\psi_{rob} = \frac{1}{n_d} \sum_{i=1}^{n_d} \psi \left(\{u_k\}_{k=0}^{N-1}; \bar{x}_0, \theta^i \right) = \frac{1}{n_d} \sum_{i=1}^{n_d} \psi^i \tag{14}$$

The corresponding gradients may be computed by

$$\nabla_{u_k} \psi_{rob} = \frac{1}{n_d} \sum_{i=1}^{n_d} \nabla_{u_k} \psi \left(\{u_k\}_{k=0}^{N-1}; \bar{x}_0, \theta^i \right) \quad k \in \mathcal{N} \tag{15}$$

Compared to a certainty-equivalent computation, the computation of the robust cost function (14) and its gradient (15) results in an increased computational effort by a factor n_d . As the addends in these computations are decoupled, they can be computed in parallel.

3.5 Permeability field

In our study, the uncertainty lies in the permeability field. We generate 100 permeability field realizations of a 2D reservoir in a fluvial depositional environment with a known vertical main-flow direction, see Fig. 3. To generate the permeability fields we started by creating a set of 100 binary (black and white) training images by using the sequential Monte Carlo algorithm 'SNESIM' [54]. Then a Kernel PCA [55] procedure is used to preserve the channel structures and smooths the original binary images. The realizations so obtained are quite heterogeneous with permeabilities in the range 6 – 2734 mD.

4 Ensemble Kalman filter

We use the Ensemble Kalman filter (EnKF) for estimating the permeability field based on production data measurements. The EnKF is a Monte Carlo implementation of the

Kalman filter [13, 56–58] using an ensemble of n_d realizations to represent the necessary first and second moments (means and covariances). In this section we describe the EnKF.

Consider the discrete time system

$$\mathbf{x}_{k+1} = F(\mathbf{x}_k, u_k, \theta) \tag{16a}$$

$$\mathbf{y}_k = G(\mathbf{x}_k, u_k) + \mathbf{v}_k \quad \mathbf{v}_k \sim N(0, R) \tag{16b}$$

The dynamic equation (16a) is a representation of the model dynamics (5c) in explicit form. It should be noted that in this representation we do not consider stochastic model errors (process noise) [20]. The uncertain parameters θ are the logarithm of the permeability field, $\theta = \log(K)$. The states are the pressure and water saturation in each grid block, $x = [P; S_w]$. The initial states, x_0 , can also be considered uncertain. However, in this work we fix them to their average value. u_k is the control input which represents the borehole pressures.

The measurements, y , are the fractional flow for each producer well and the water injection rate for each injector well. In the measurement equation (16b), $G(x_k, u_k)$ includes the Peaceman well model (4) as well as the equations relating fractional flow to pressures and water saturations. v_k is measurement noise that we assume is normally distributed.

4.1 Basic Ensemble Kalman filter

(16a) includes the states, x , and the parameters, θ . Therefore, we form the augmented state space model

$$\mathbf{x}_{k+1} = F(\mathbf{x}_k, u_k, \theta_k) \tag{17a}$$

$$\theta_{k+1} = \theta_k \tag{17b}$$

and apply the EnKF to the dynamic equation (17a) and the measurement equation (16b). In the EnKF all means and covariances are represented by samples of the stochastic variables. Therefore, the initial mean and covariance of the augmented states, $[x_k, \theta_k]$, are represented by

$$\{x_{0|0}^i, \theta_{0|0}^i\}_{i=1}^{n_d} = \left\{ x_0, \theta_{0|0}^i \right\}_{i=1}^{n_d} \tag{18}$$

It should be noted that the initial states, x_0 , in our case are assumed to be known exactly. Only the parameters, θ , are uncertain. Index i refers to each of the n_d members of the ensemble, i.e. each realization.

In the following we describe the algorithm for discrete time instant $k = 1, 2, \dots$. In general, at discrete time instant k , both the states and the parameters from the previous instant, $k - 1$, are uncertain. This is denoted

$$\left\{ x_{k-1|k-1}^i, \theta_{k-1|k-1}^i \right\}_{i=1}^{n_d} \quad k = 1, 2, \dots \tag{19}$$

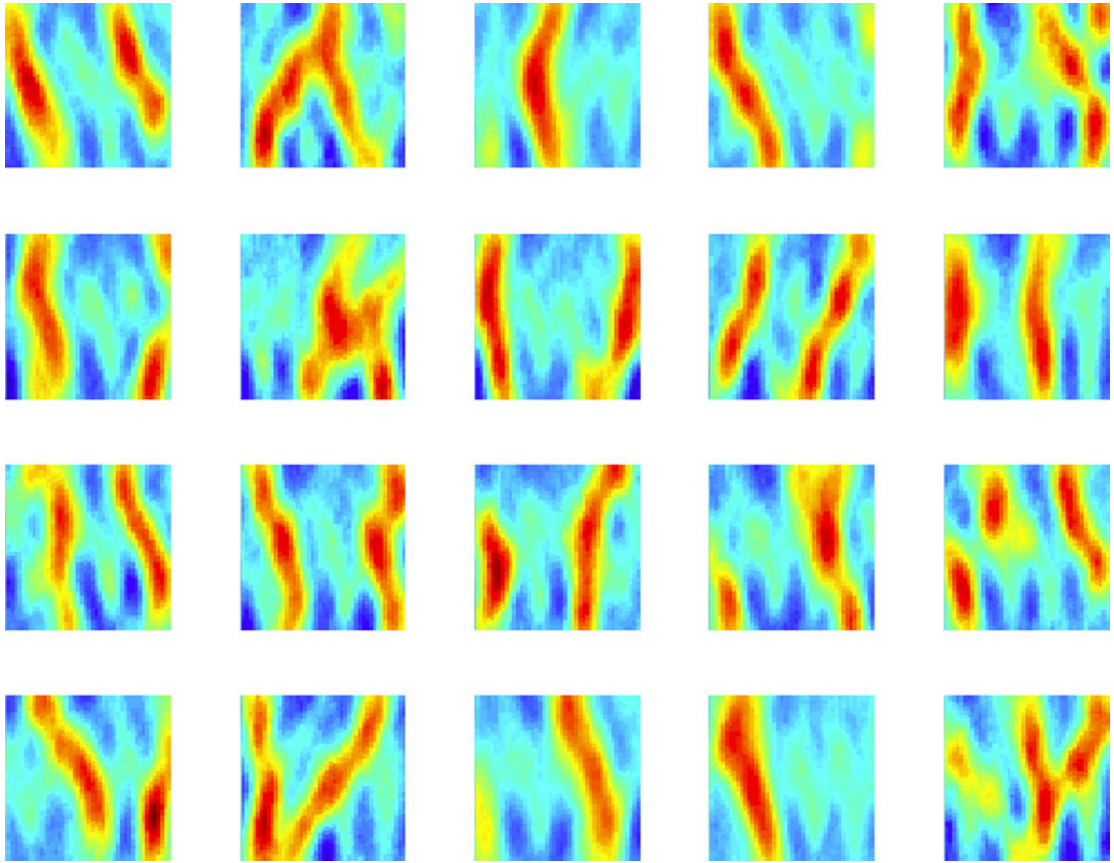


Fig. 3 A selection of realizations from the ensemble of 100 permeability fields. The realizations are quite heterogeneous, values are in the range 6 – 2734 mD

In the EnKF, the one-step prediction step is conducted by passing each ensemble member through the dynamics (17a) such that for $i = 1, 2, \dots, n_d$

$$x_{k|k-1}^i = F \left(x_{k-1|k-1}^i, u_{k-1}, \theta_{k-1|k-1}^i \right), \tag{20a}$$

$$\theta_{k|k-1}^i = \theta_{k-1|k-1}^i, \tag{20b}$$

where the previous input, u_{k-1} , is known. Then the output, $z_{k|k-1}^i$, and the measurement, $y_{k|k-1}^i$, at discrete time k may be computed as

$$z_{k|k-1}^i = G \left(x_{k|k-1}^i, u_{k-1} \right) \quad i = 1, 2, \dots, n_d \tag{21a}$$

$$y_{k|k-1}^i = z_{k|k-1}^i + v_k^i \quad i = 1, 2, \dots, n_d \tag{21b}$$

To obtain the correct covariances of the state estimates in the EnKF, it is important that each ensemble member, $y_{k|k-1}^i$, contain measurement noise, $v_{k|k-1}^i$ [59]. It should also be

noted that u_{k-1} is used in the evaluation of G in (21a). The explanation for the use of u_{k-1} is that we use a zero-order-hold representation of $u(t)$, i.e. $u(t) = u_{k-1}$ for $t_{k-1} \leq t < t_k$, and that we assume the measurement is conducted at time $t_k^- = \lim_{t \rightarrow t_k^-} t$. Then, at time t_k , the EnKF and optimal control computations are conducted infinitely fast such the next decisions, $u(t) = u_k$ for $t_k \leq t < t_{k+1}$, can be implemented at time t_k .

The innovation, e_k^i , for each ensemble member is computed using the actual measurement, y_k , and the predicted measurement

$$\epsilon_k^i = z_{k|k-1}^i - y_k \quad i = 1, 2, \dots, n_d \tag{22a}$$

$$e_k^i = y_k - y_{k|k-1}^i = -\epsilon_k^i - v_k^i \quad i = 1, 2, \dots, n_d \tag{22b}$$

In these equations, y_k is the actual measurement and therefore a deterministic variable. In the EnKF, the realized trajectory of the system and an ensemble of different

Table 1 Parameters for the two phase model, the discounted state cost function (6), and the measurement noise

Symbol	Description	Value	Unit
ϕ	Porosity	0.2	—
c_r	Rock compressibility	0	Pa ⁻¹
ρ_o	Oil density (300 bar)	700	kg/m ³
ρ_w	Water density (300 bar)	1000	kg/m ³
μ_o	Dynamic oil viscosity	$3 \cdot 10^{-3}$	Pa · s
μ_w	Dynamic water viscosity	$0.3 \cdot 10^{-3}$	Pa · s
S_{or}	Residual oil saturation	0.1	—
S_{ow}	Connate water saturation	0.1	—
n_o	Corey exponent for oil	2	—
n_w	Corey exponent for water	2	—
P_{init}	Initial reservoir pressure	300	bar
S_{init}	Initial water saturation	0.1	—
r_o	Oil price	120	USD/bbl
r_{wp}	Water production cost	20	USD/bbl
r_{wi}	Water injection cost	10	USD/bbl
d	Discount factor	0	—
R	Cov. matrix for measurements noises	Diag($5 \cdot 10^{-3}, 5 \cdot 10^{-3}, 5 \cdot 10^{-3}, 5 \cdot 10^{-3}, 30$)	—

state trajectories are considered. In the derivation of the standard Kalman filter [13, 57, 58], it is the other way around. A (infinite) number of system realizations are considered, while the filter is represented by one deterministic trajectory (the mean).

The optimal linear estimator conditioned on the innovations are [57]

$$x_{k|k}^i = x_{k|k-1}^i + K_{x,k} e_k^i \quad i = 1, 2, \dots, n_d \tag{23a}$$

$$\theta_{k|k}^i = \theta_{k|k-1}^i + K_{\theta,k} e_k^i \quad i = 1, 2, \dots, n_d \tag{23b}$$

with the Kalman filter gains computed as

$$K_{x,k} = \langle x_{k|k-1}, e_k \rangle \langle e_k, e_k \rangle^{-1} \tag{24a}$$

$$K_{\theta,k} = \langle \theta_{k|k-1}, e_k \rangle \langle e_k, e_k \rangle^{-1} \tag{24b}$$

using the covariances

$$\langle x_{k|k-1}, e_k \rangle = \langle x_{k|k-1}, \mathbf{e}_k \rangle \tag{25a}$$

$$\langle \theta_{k|k-1}, e_k \rangle = \langle \theta_{k|k-1}, \mathbf{e}_k \rangle \tag{25b}$$

$$\langle e_k, e_k \rangle = \langle \mathbf{e}_k, \mathbf{e}_k \rangle + \langle v_k, v_k \rangle \approx \langle \mathbf{e}_k, \mathbf{e}_k \rangle + R \tag{25c}$$

The Kalman gains may be based on direct computation of the empirical estimates ($\langle x_{k|k-1}, e_k \rangle$, $\langle \theta_{k|k-1}, e_k \rangle$, $\langle e_k, e_k \rangle$) or the relations in (25a). We choose to base the computations

on (25a), the approximate first moments (means) computed as

$$\hat{z}_{k|k-1} = E\{\hat{z}_{k|k-1}\} \approx \frac{1}{n_d} \sum_{i=1}^{n_d} z_{k|k-1}^i$$

$$\hat{\mathbf{e}}_k = E\{\mathbf{e}_k\} \approx \frac{1}{n_d} \sum_{i=1}^{n_d} \mathbf{e}_k^i = \hat{z}_{k|k-1} - y_k$$

$$\hat{x}_{k|k-1} = E\{x_{k|k-1}\} \approx \frac{1}{n_d} \sum_{i=1}^{n_d} x_{k|k-1}^i$$

$$\hat{\theta}_{k|k-1} = E\{\theta_{k|k-1}\} \approx \frac{1}{n_d} \sum_{i=1}^{n_d} \theta_{k|k-1}^i$$

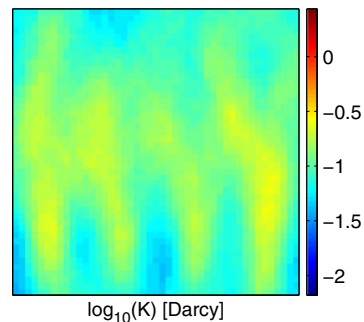


Fig. 4 Permeability mean, $\hat{\theta}_{0|0}$, of the ensemble given in Fig. 3

Table 2 Key indicators for the open-loop optimized cases. Improvements are relative to the nominal case

	NO 10 ⁶ USD	Reactive 10 ⁶ USD, %	Certainty equivalent 10 ⁶ USD, %	RO 10 ⁶ USD, %	RO modified 10 ⁶ USD, %
$E_{\theta}[\psi]$	33.84	56.47, +66.9	42.72, +26.2	44.11, +30.3	58.18, +71.9
Std. dev.	26.35	6.05	18.27	13.19	6.25

and the approximate second moments (covariances) computed by

$$\begin{aligned} \langle x_{k|k-1}, \mathbf{e}_k \rangle &\approx \frac{1}{n_d - 1} \sum_{i=1}^{n_d} (x_{k|k-1}^i - \hat{x}_{k|k-1}) (\mathbf{e}_k^i - \hat{\mathbf{e}}_k)' \\ \langle \theta_{k|k-1}, \mathbf{e}_k \rangle &\approx \frac{1}{n_d - 1} \sum_{i=1}^{n_d} (\theta_{k|k-1}^i - \hat{\theta}_{k|k-1}) (\mathbf{e}_k^i - \hat{\mathbf{e}}_k)' \\ \langle \mathbf{e}_k, \mathbf{e}_k \rangle &\approx \frac{1}{n_d - 1} \sum_{i=1}^{n_d} (\mathbf{e}_k^i - \hat{\mathbf{e}}_k) (\mathbf{e}_k^i - \hat{\mathbf{e}}_k)' \end{aligned}$$

The result of (23a) in this procedure is an ensemble

$$\left\{ x_{k|k}^i, \theta_{k|k}^i \right\}_{i=1}^{n_d} \quad k = 1, 2, \dots \quad (28)$$

representing the states and parameters at time k given measurements up until time k . Using this ensemble, a robust optimization may be performed or various statistics such as the mean may be computed.

(23a) may result in non-physical updates. Therefore, we modify the EnKF such that the ensemble (28) satisfies physical constraints, e.g. that the permeabilities are in certain ranges. To mitigate such effects, we clip the solution according to the constraints

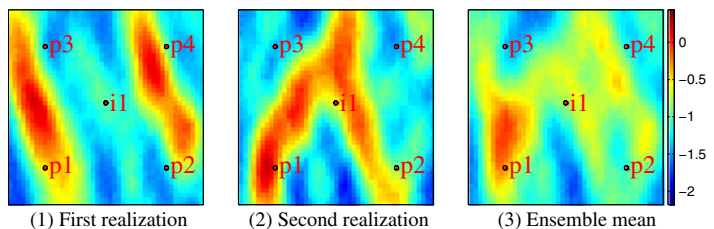
$$\theta_{k|k}^i := \begin{cases} \theta_{\min} & \theta_{k|k}^i < \theta_{\min} \\ \theta_{k|k}^i & \theta_{\min} \leq \theta_{k|k}^i \leq \theta_{\max} \\ \theta_{\max} & \theta_{k|k}^i > \theta_{\max} \end{cases} \quad (29)$$

and compute the filtered states, $\hat{x}_{k|k}^i$, by solving the dynamic model equations

$$\begin{aligned} x_{j+1|k}^i &= F(x_{j|k}^i, u_j, \theta_{k|k}^i), \quad x_{0|k}^i = x_0, \\ j &= 0, 1, \dots, k - 1 \end{aligned} \quad (30)$$

for each ensemble member, $i \in \{1, \dots, n_d\}$, using the clipped parameter estimates computed by (29). In this way,

Fig. 5 $\log_{10} K [D]$ of the first two realizations of the ensemble in Fig.3 and their ensemble mean $\hat{\theta}_{0|0}$



state updates consistent with the model is guaranteed [35]. In particular, this eliminates the possibility of nonphysical states (nonphysical pressures and saturations). The computational load can potentially be reduced by only doing the initial-value simulation when the estimated saturation and pressure changes passes a certain threshold [39]. The modifications (29) and (30) provides the ensemble (28) that is used for the optimal control computations and for the initiation of the EnKF at the next time step. Finally, the choice of the ensemble size n_d in the EnKF is a topic of research itself [60]. It affects the performance of the filter. In reservoir engineering an ensemble's size of 100 is a common choice based on experience [4], [61]. However, this number is problem dependent and in some cases good results can also be obtained using ensembles with fewer members [61].

4.2 Performance metrics

To measure the convergence of the Kalman filter estimates, we consider the mean standard deviation

$$\sigma_k = \sqrt{\frac{1}{n_p} \left(\frac{1}{n_d - 1} \sum_{i=1}^{n_d} \left\| \theta_{k|k}^i - \hat{\theta}_{k|k} \right\|_2^2 \right)} \quad (31)$$

of the parameters in the parameter vector, $\theta_{k|k}$. σ_k measures the ensemble spread. We also consider the root-mean-square-error of the parameter estimates compared to the true parameters, θ^0 :

$$RMSE_k = \frac{\left\| \hat{\theta}_{k|k} - \theta^0 \right\|_2}{\sqrt{n_p}} \quad (32)$$

θ_k can be computed for real as well as synthetic cases, while $RMSE_k$ can only be computed for synthetic cases in which the true parameters, θ^0 , are available.

In the ideal case, the spread (31) should converge to a number related to the measurement noise and the root-mean-square-error (32) should converge to 0. In practice, (32) will not converge to zero due to e.g. factors like model-plant mismatch. Cases with divergence of the root-mean-square-error may indicate that the ensemble is too small to represent the true uncertainty.

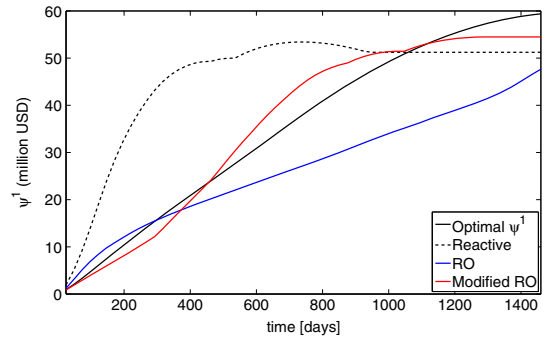
5 Case study

We consider a conventional horizontal oil field that can be modeled as a two phase flow in a porous medium [62–64]. The reservoir size is 450 m × 450 m × 10 m. By spatial discretization this reservoir is divided into 45 × 45 × 1 grid blocks. The permeability field is uncertain. We assume that the ensemble in Fig. 3 represents the range of possible geological uncertainties. The configuration of injection wells and producers is illustrated in Fig. 5(1). As indicated in Fig. 5(1), the four producers are located in the corners of the field, while the single injector is located in the center of the field.

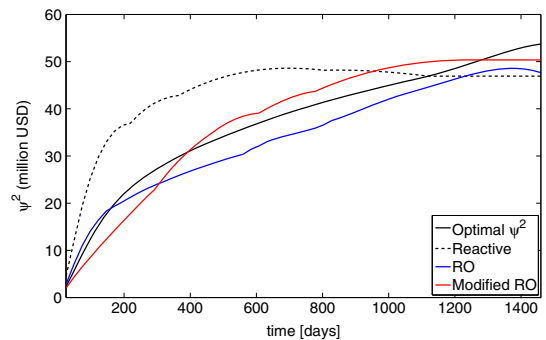
The reservoir’s petrophysical parameters are listed in Table 1. The initial reservoir pressure is 300 bar everywhere in the reservoir. The initial water saturation is 0.1 everywhere in the reservoir. This implies that initially, the reservoir has a uniform oil saturation of 0.9. The manipulated variables are the bhp of the five wells (four producers, one injector) over the life of the reservoir. In this study, we consider a zero discount factor d in the cost function (6). This means that we maximize NPV at the final time, without caring about the shorter horizon [11].

The case study is divided into an open-loop optimization part and a closed-loop optimization part. In open-loop optimization, we compute the control strategy without using measurement feedback to update the parameters, i.e. the ensemble in Fig. 3 is fixed in time. In closed-loop optimization, we use production measurements and the EnKF to estimate the permeability field parameters. To simulate the reservoir and create production data, the first realization of the permeability field, $\theta_{0|0}^1$, in Fig. 3 is used. This permeability field represents the true permeability field of the reservoir.

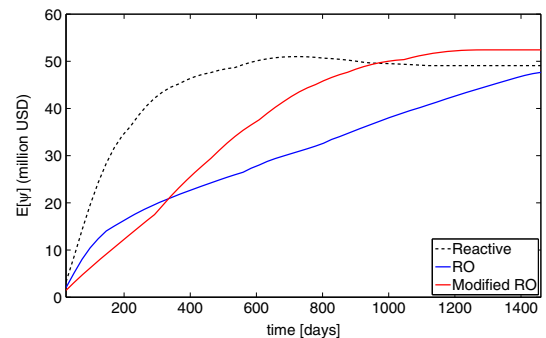
In reality, we never know the true model when performing data assimilation with EnKF. We can only implicitly assume that we can generate a reasonable approximation of the true reservoir. Since we focus on the optimizer formulation and separate the effects of the quality in data assimilation from the quality of CE, RO and reactive strategies as much as possible, we assume that the true reservoir is contained in the ensemble of initial guesses.



(1) First realization



(2) Second realization



(3) Combined NPV

Fig. 6 Profit evolutions for open-loop optimization of the two ensemble case. The optimal trajectories computed using the true permeability fields give the highest possible profit. The profit of the RO strategy is below the profit of the reactive strategy for the first permeability realization and slightly above the second permeability realization. On average the RO strategy gives less profit than the reactive strategy. The modified RO strategy produces for all cases a higher profit than the reactive strategy

5.1 Open-loop optimization

We consider a prediction horizon of $t_N = 4 \cdot 365 = 1460$ days divided in $N = 60$ control periods (i.e. a control

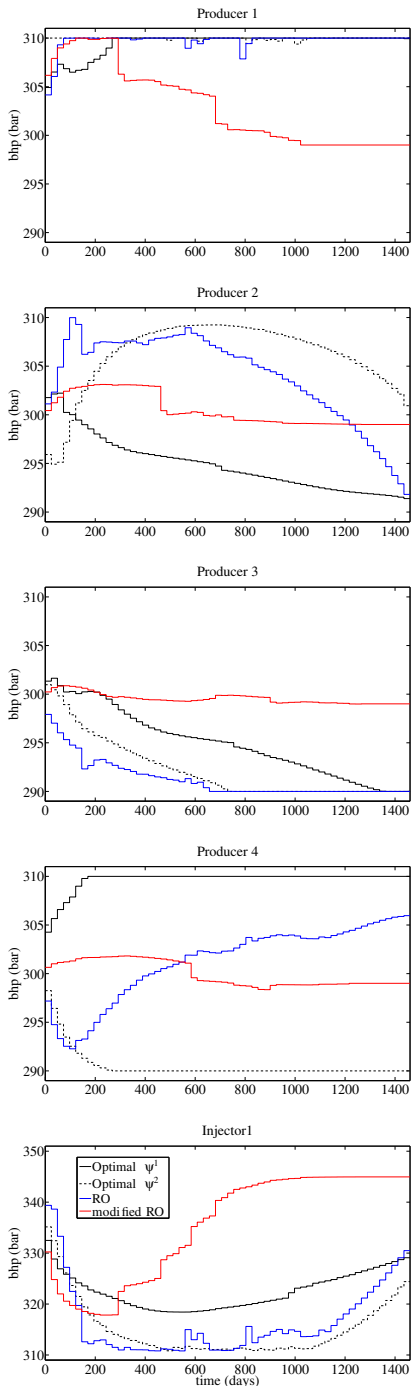


Fig. 7 Control trajectories for open-loop optimization of the two ensemble case. The control trajectories for the considered optimization strategies are very different

period $T_s \approx 24$ days). We control the reservoir using five different strategies that we call: the reactive strategy, the nominal strategy (NO), the certainty equivalent strategy, the robust optimization strategy (RO), and the modified robust optimization strategy (modified RO).

The reactive strategy develops the field at the maximum production rate (setting the producers at the lowest allowed value of 290 bar and the injector at the maximum allowed value of 350 bar) and subsequently shut-in each production well when it is no longer economical. From the values in Table 1, we observe that a producer well becomes uneconomical when the fractional flow f_w is above the value $120/(120 + 20) = 0.857$. The nominal strategy is based on a single realization. For each realization in the ensemble we compute the optimal control trajectory. Then we apply each of these 100 optimal control trajectories to each of the ensemble members obtaining 100 NPV values for each control trajectory. The certainty equivalent strategy is based on solving problem (5a) using the certainty equivalent cost function ψ_{CE} (10). It uses the mean of the ensemble as its permeability field. Figure 4 illustrates the mean of the permeability field ensemble given in Fig. 3. The RO strategy is based on solving problem (5a) using the robust cost function ψ_{rob} (5a) and the robust gradient $\nabla_{u_k} \psi_{rob}$ (15). The modified robust optimization is the RO strategy with an added reactive strategy, i.e. we solve problem (5a) using (14) and (15) but we shut in a producer well when it is non economical. This means that when we solve the flow equations (5c), the number of active producer wells can change. This in turn means that once a well is shut-in, its later contribution to the NPV and its gradient will be zero. We could say that for each realization we manipulate producer wells bbps as long as they are profitable. Further, this strategy stops the production of a reservoir when all wells are non-economical. To our knowledge, there exist no extension of robust optimization that includes reactive control. However, the idea of adding reactive control has been used to improve the NPV of a single reservoir model. In [65] they consider production optimization in the absence of uncertainty by including a watercut constraint on the well completions. This results in increased NPV and a faster convergence of the optimizer.

Simulations reveal that for the present case, the RO strategy yields an higher expected NPV $E_\theta[\psi]$ and a lower standard deviation of the NPV (see Table 2) compared to the certainty equivalent strategy. However, both the RO and the certainty equivalent strategies are worse than the reactive strategy because of a much lower expected NPV $E_\theta[\psi]$ with a much higher NPV standard deviation. The modified RO strategy has a NPV standard deviation comparable to the reactive strategy, but a higher expected NPV $E_\theta[\psi]$. It is important to stress that the results concerning the merits of the different strategies are particular to this case study and

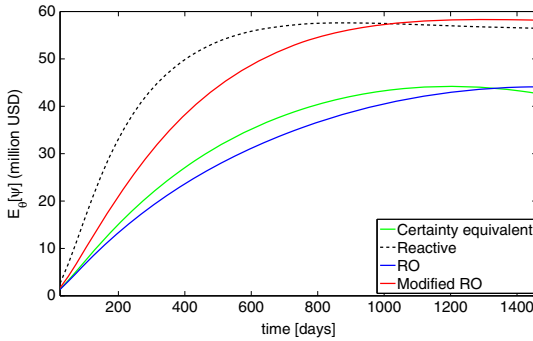


Fig. 8 Profit evolution for open-loop optimization in the hundred ensemble case

not universal. [26] presents a case in which the RO strategy provides higher expected NPV and lower NPV standard deviation than the reactive strategy. In making a comparison with [26], there are a number of things we should stress. First of all, in [26] they are controlling directly the liquid rates of 12 wells with no direct control on the bhp values. In our test case, we control the bhp values of only 5 wells with no direct control on the liquid rates. In [26], all the realizations are giving positive NPV for all the control strategies. Further, they find that the reactive strategy is the worst to use. In our test case, the NO strategy is the worst to use, and it gives a substantial negative NPV contribution. Hence, it seems like the test case in [26] facilitates optimal control strategies. In our case, however, the heterogeneities in the ensemble realizations make it hard for optimal control strategies to improve on a reactive strategy. To summarize, the problems treated in [26] and in this paper have quite different characteristics. Hence, different preferences with respect to open-loop strategies is not necessarily surprising.

The results in our paper indicates the value of feedback. The reactive strategy as well as the modified robust strategy both use a simple form of feedback. The nominal strategy, the certainty equivalent strategy, and the robust optimization strategy are pure open-loop strategies that do not use feedback.

To illustrate the results in a tutorial way, we split the discussion of the open-loop optimization into a two ensemble case and a hundred ensemble case. In the two ensemble case, we present the results of open-loop optimization using an ensemble of two realizations. Figure 5 illustrates the two realizations of the uncertain permeability field for this case. In the case with hundred ensemble members, we use the entire ensemble in Fig. 3 to represent the uncertain permeability field.

5.1.1 Case - ensemble with two members

In this subsection, we describe the performance of the RO strategy for the case with an ensemble consisting of the two permeability field realizations illustrated in Fig. 5. We compare the results of the RO control strategy with the results of the reactive, the modified RO and the optimal control strategies. By the optimal control strategies for the two realizations in Fig. 5, we mean the optimal control strategies, $\{u_k\}_{k=0}^{N-1}$, that are computed by solving the optimization problem (8) using the true permeability fields. These are

$$\psi = \psi \left(\{u_k\}_{k=0}^{N-1}; \bar{x}_0, \theta^1 \right) = \psi^1$$

$$\psi = \psi \left(\{u_k\}_{k=0}^{N-1}; \bar{x}_0, \theta^2 \right) = \psi^2$$

The NPVs computed using these optimal control strategies act as an upper bound for the NPVs computed using the other control strategies. To choose the two realizations to use, we first compute optimal control trajectories for the realizations in the ensemble of Fig. 3. Then we choose two

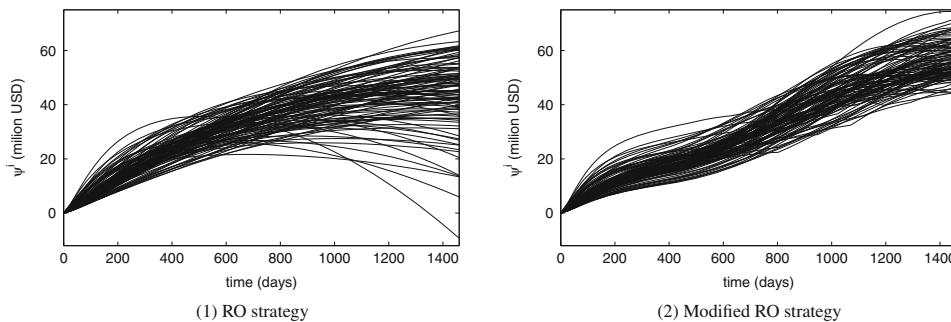


Fig. 9 Profit evolution of the open-loop RO strategy and the open-loop modified RO-strategy for each realization of the permeability field. Some scenarios in the RO strategy gives negative profits while the modified RO strategy avoids that by shutting in uneconomical producer wells

realizations with large differences in the optimal production strategies.

Figures 6(1), 6(2) and 6(3) show the terms ψ^1 , ψ^2 and $E_\theta[\psi]$ (13) for the reactive strategy, the RO strategy, and the modified RO strategy, respectively. As expected, the NPVs computed using the optimal control strategies give the highest values for ψ^1 and ψ^2 . Compared to the reactive strategy, the RO strategy gives a lower NPV, ψ^1 , for realization 1, and a higher NPV, ψ^2 , for realization 2. As illustrated in Fig. 6(3), this results in a lower NPV mean, $E_\theta[\psi]$, for the RO strategy compared to the reactive strategy. The

modified RO control strategy gives the highest NPVs for all the realizations.

Furthermore, it is interesting to observe the difference in production times for the different strategies. For the RO strategy, the production continue for the entire time horizon (1460 days) considered. In the reactive strategy, the production lasts 949 days in the first realization (ψ^2) and 1119 days in the second realization (ψ^2). So there is an important difference in the field developing time of the two realizations. In the modified RO strategy, the production lasts 1289 days in the first realization and 1240 days in the second

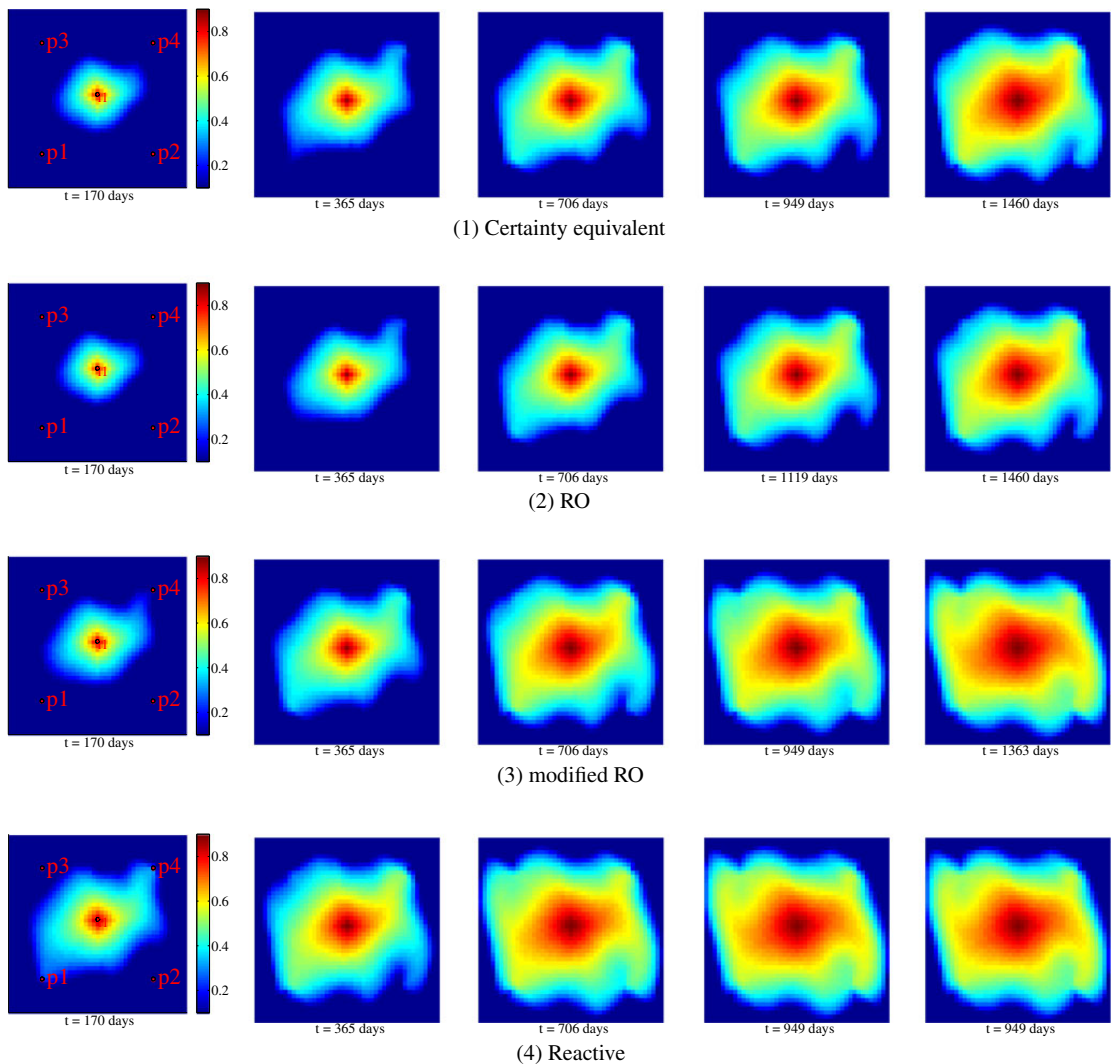


Fig. 10 Saturation profiles of the first realization for the open-loop optimization strategies in the hundred ensemble case

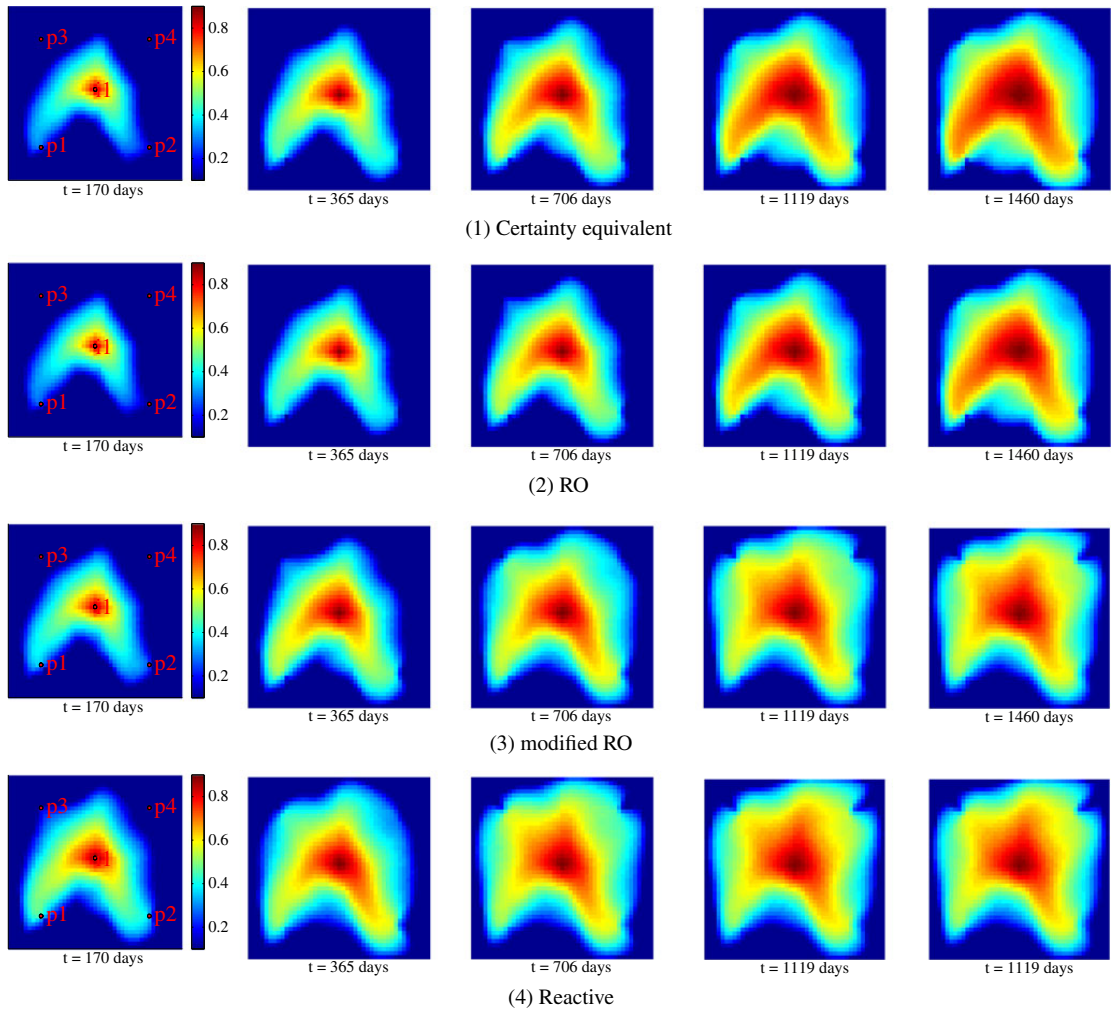


Fig. 11 Saturation profiles of the second realization for the open-loop optimization strategies in the hundred ensemble case

realization. We note that with the modified RO strategy, the production time is longer than the production time of the reactive strategy.

Figure 7 shows the control trajectories of the RO, the modified RO and the optimal strategies. We note that because of the heterogeneity between the realizations, the resulting optimal control trajectory of one realization can be very different and conflicting with the optimal control trajectory for the other realization. To find a common optimal control that takes all these differences into account can be difficult if not impossible. Especially if we don't allow for changes in the configuration of active wells, e.g. producer number 4 is producing at its minimum (310 bar) in the solution for ensemble 1 and at its maximum (290 bar) in the

solution for ensemble 2. The RO and modified RO solutions for the producer number 4 stay in between the two optimal trajectories.

In conclusion, the two-ensemble case demonstrates that the optimizer produces the maximal profit for the optimal cases. Therefore, the optimizer works well and the lower profit of the RO strategy is not the result of lack of convergence in the optimizer, but rather the result of heterogeneous permeability fields giving conflicting control trajectories.

5.1.2 Case - ensemble with hundred members

In this subsection, we describe the results for the case in which we do open-loop optimization using the entire

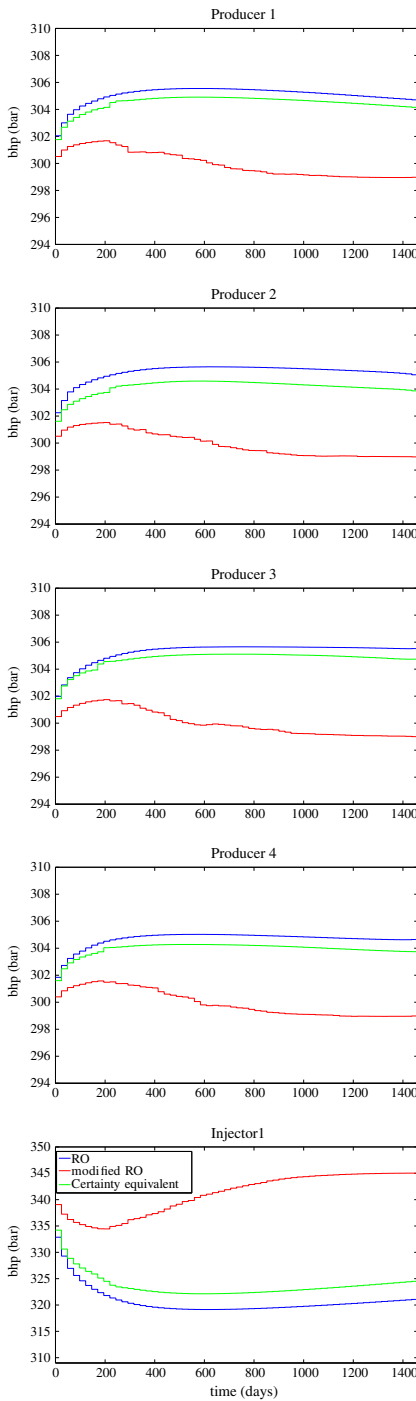


Fig. 12 Control trajectories for open-loop optimization in the hundred ensemble case

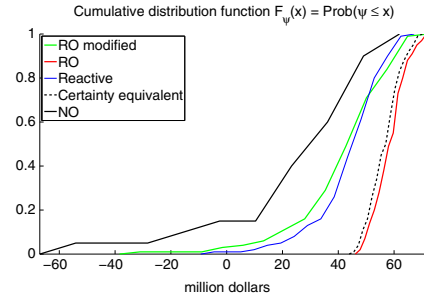


Fig. 13 Cumulative distribution function for the open-loop optimization strategies. The cumulative distribution functions are for the ensemble with hundred members

ensemble of 100 realizations in Fig. 3. Figure 4 illustrates the mean permeability field for the ensemble of permeability fields in Fig. 3. Figure 8 shows the profit evolution in the case of an ensemble consisting of 100 permeability fields for the certainty equivalent strategy, the reactive strategy, the RO strategy, and the the modified RO strategy.

Table 2 reports the corresponding key performance indicators (expected NPV $E_{\theta}[\psi]$ and standard deviation of the NPV). As in the two ensemble case, the reactive strategy yields both a larger expected NPV and a smaller standard deviation for the NPV compared to the certainty equivalent and the the RO strategies. The reasons for the inferior performance of the RO strategy should be searched in the conflicting controls required for the different realizations. Figure 9(1) shows that the RO strategy cannot avoid that some ψ^i gives a negative contribution to the expected NPV

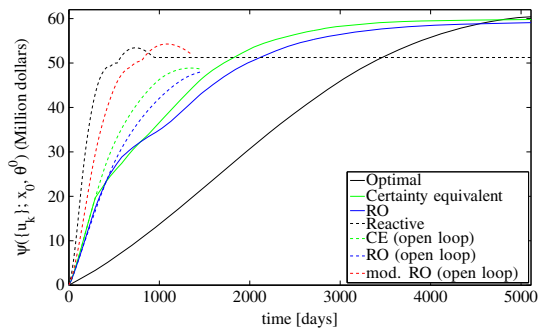


Fig. 14 Profit evolution for the closed-loop optimization strategies. The profit evolution of the true model controlled by different strategies based on the ensemble in Fig. 3. Both the RO and the certainty equivalent strategies give a higher NPV than the the reactive strategy. The optimal control strategy represents the best possible solution. By using the RO strategy and the certainty equivalent strategy we get profits close to the maximum possible profit

Table 3 Key indicators for the closed-loop optimized cases. Improvements are relative to the reactive case

Meas. noise	Reactive	Certainty equivalent		RO		Optimal	
	10 ⁶ USD	10 ⁶ USD, %		10 ⁶ USD, %		10 ⁶ USD, %	
5 · R	51.24	59.13,	+15.4	58.34,	+13.9	60.41,	+17.3
R	51.24	59.79,	+16.7	59.09,	+15.3	60.41,	+17.3
5 ⁻¹ · R	51.24	59.84,	+16.8	59.52,	+16.2	60.41,	+17.3
5 ⁻² · R	51.24	59.95,	+17.0	59.56,	+16.2	60.41,	+17.3

$E_{\theta}[\psi]$. In contrast, as illustrated in Fig. 9(2), the modified RO strategy does not produce realizations with negative profit. Furthermore, each realization of the modified RO strategy seems to increase the profit compared to the RO strategy. The reactive strategy performs better than both the RO and certainty equivalent strategies because it can shut in a well when it is no longer profitable to operate the well. The modified RO strategy inherits the ability of the reactive strategy to shut in unprofitable wells. This is in essence a simple feedback mechanism. Figures 10 and 11 show the saturation profiles of the first two realizations for the open-loop strategies. We note that the reactive strategy and the modified strategy inject a higher water quantity and displace the oil more uniformly compared to the RO and the certainty equivalent strategies.

Figures 12 shows the control trajectories of the RO, the modified RO and the certainty equivalent strategies. Compared to the trajectories in Fig. 7, for the two ensemble case, it seems that the RO and certainty equivalent strategies include some averaging (smoothing) in the resulting control trajectories that limits their effectiveness. The result is a control trajectory that produces less oil than the modified RO strategy that can shut in uneconomical producer wells.

As indicated by Fig. 7, the RO control trajectories may be the average of conflicting control trajectories and therefore inefficient for the uncertain system.

Figure 13 shows the cumulative distribution function for the different control strategies, i.e. the probability to get a NPV $\leq x$. These curves are similar to the ones reported in [26] with the difference that the NO and the certainty equivalent strategies have a positive probability of giving negative NPVs. Figure 13 confirms that the modified RO strategy is superior to the other open-loop strategies.

5.2 Closed-loop optimization

The closed-loop optimization strategies are implemented using the moving horizon principle. In this method, each time new measurements from the real or simulated reservoir are available, the EnKF uses these measurements to update the estimates of the permeability field, and an open-loop optimization problem is solved using the updated permeability field. Only the first part of the resulting optimal control trajectory is implemented. As new measurements become available, the procedure is repeated. The sampling time for the system is $T_s = 146$ days, i.e. the data assimilation and optimization is performed every 146 days. The open-loop optimization uses a prediction and control horizon of $4 \cdot 365 = 1460$ days that is divided into $N = 60$ periods (the same as for the open-loop optimization strategies). With this parametrization, the control steps for the first six periods are implemented to the system, and then

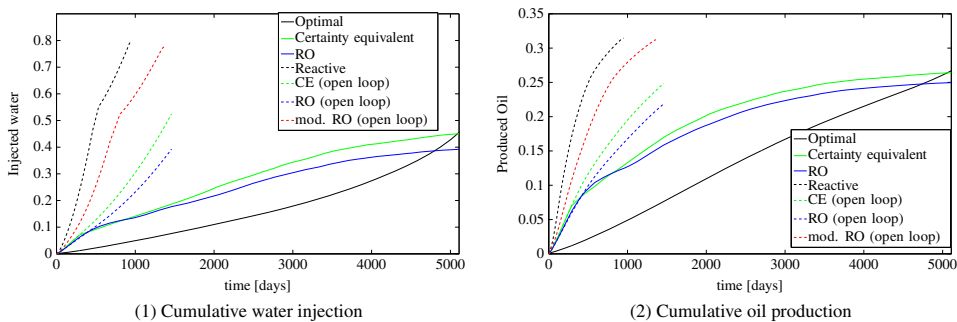
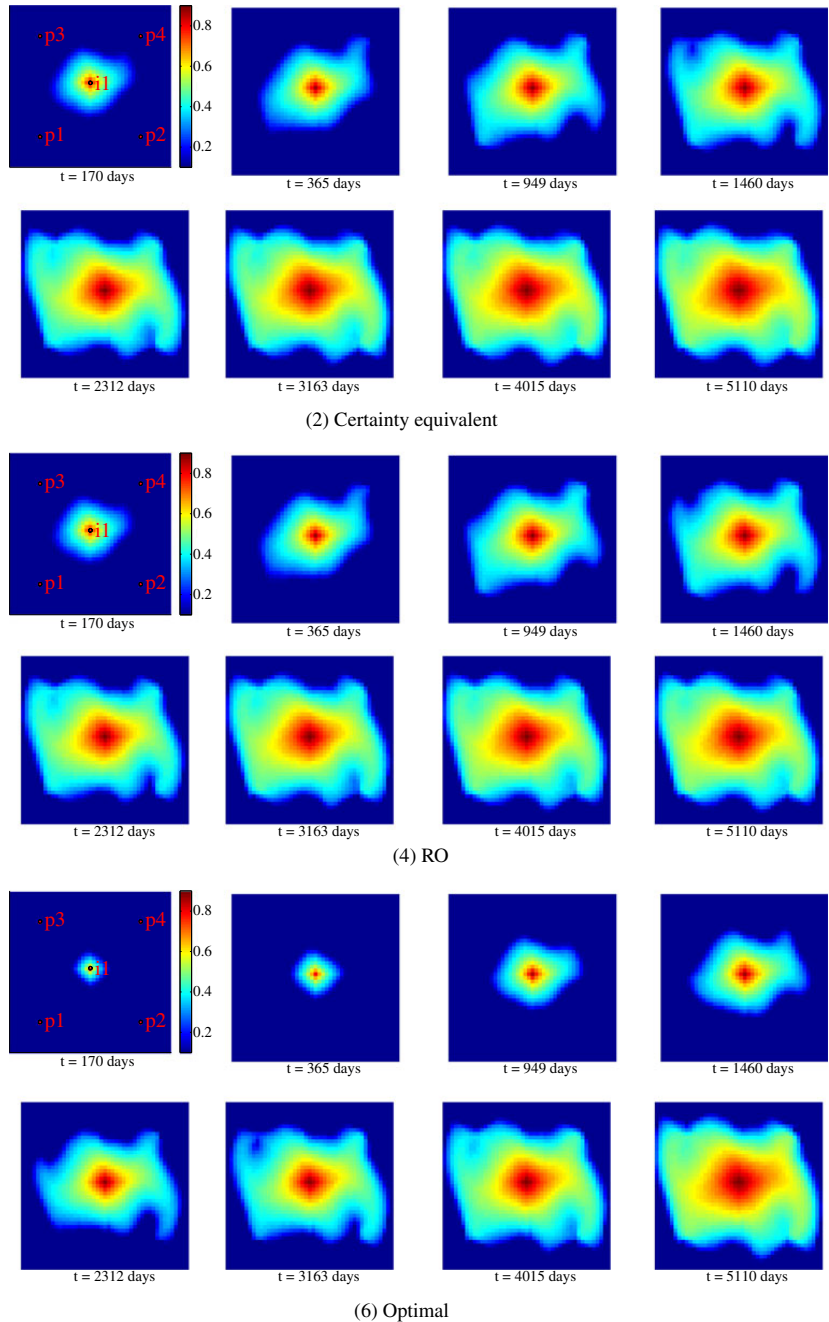


Fig. 15 Closed-loop. Water injected and produced oil trajectories for different optimization strategies. The values are normalized with respect to the pore volume

we receive new measurements to do new data assimilation and optimization computations for a shifted time window. In this paper, we consider 35 of these steps such that the total production horizon is $146 \cdot 35 = 5110$ days.

We compare three closed-loop optimization strategies: A reactive strategy, a certainty equivalent strategy, and a RO strategy. We did not implement a modified RO strategy because that would be complicated by the need to manage

Fig. 16 Saturation profiles of the true field for the closed-loop optimization strategies



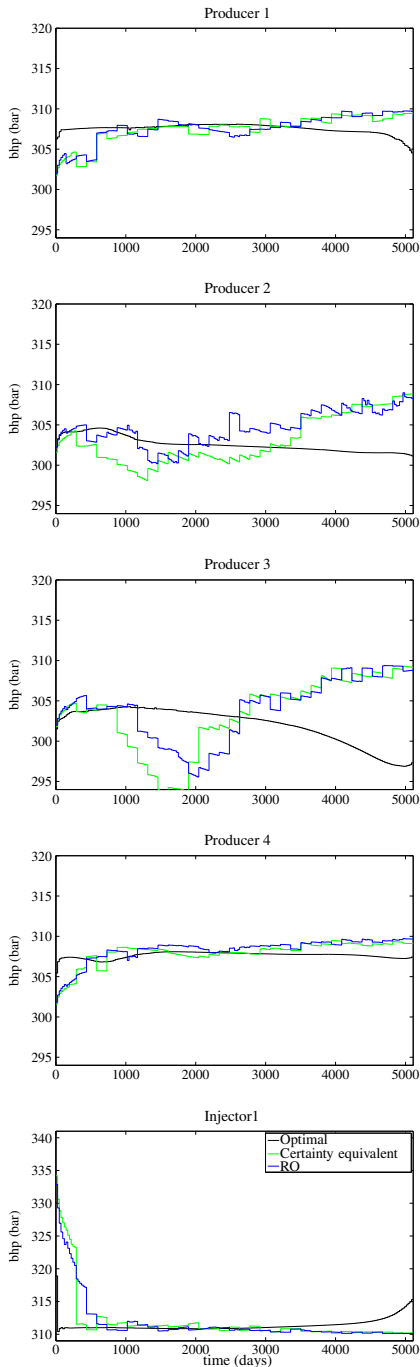


Fig. 17 Control trajectories for the closed-loop optimization strategies

situations with a variable number of active wells and measurements for different ensemble realizations. Further, it would require a strategy to replace ensemble realizations when all the producing wells are shut-in.

Figure 14 shows the NPV $\psi(\{u_k\}_{k=0}^{N-1}; x_0, \theta_{0|0}^1)$ for the reactive strategy, the closed-loop RO strategy, the closed-loop certainty equivalent strategy, the optimal control strategy, and the open-loop strategies introduced in the previous section. The optimal control strategy is obtained solving the optimization problem (7) using the true permeability field (the first realization of the permeability field in Fig. 3). The NPV computed by the optimal control strategy represents the best possible operation of the reservoir. Table 3 reports key indicators (expected NPV and improvements compared to the reactive strategy) for the closed-loop strategies at different levels of measurement noise. Figure 14 and Table 3 shows that for all investigated cases, both the closed-loop certainty equivalent strategy and the closed-loop RO strategy yields significantly higher NPV than the reactive strategy. As is also evident from Fig. 14 and Table 3, the closed-loop certainty equivalent strategy

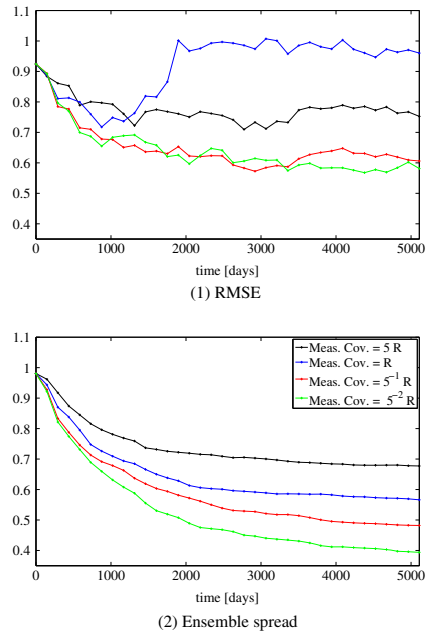
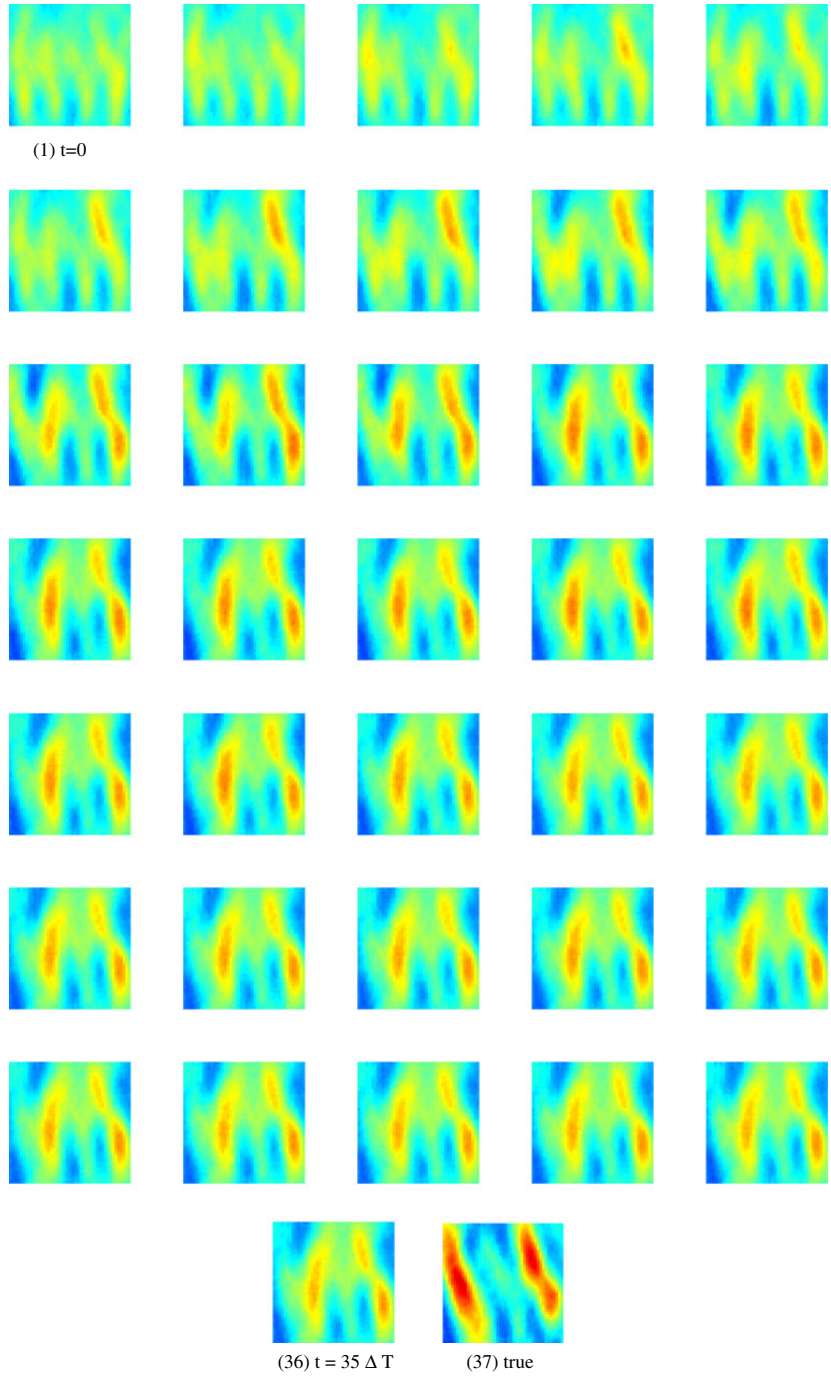


Fig. 18 Convergence measures for the EnKF with various levels of measurement noise for the closed-loop certainty equivalent strategy. (1) shows that the EnKF does not converge to the true parameters. However, the estimate captures enough features to be useful. (2) illustrates that the parameter uncertainty decreases as more production data is assimilated in the estimates

Fig. 19 Estimates of the mean permeability field as function of time for the closed-loop certainty equivalent strategy. The initial estimate is a four channel structure. The estimates, $\hat{\theta}_{k|k-1}$, converge towards the true two-channel structure as more measurements are assimilated



yields higher NPV than the closed-loop RO strategy. Furthermore, the NPV of the closed-loop certainty equivalent strategy is very close to the NPV of the optimal strategy. Consequently, the closed-loop certainty equivalent strategy is preferable over the closed-loop RO strategy as it yields higher NPV and requires significantly less computational effort. This observation is also confirmed when using the second realization in Fig. 3 as the permeability field.

From Fig. 14 we note also that the modified RO is the best open-loop strategy and that the closed-loop strategies CE and RO provide better results compared to the modified RO starting from the assimilation steps 13 ($t \approx 1898$ days) and 16 ($t \approx 2336$ days), respectively. Figure 15 shows the cumulative water injection and the cumulative oil production for different strategies. The slope of the curves is the reservoir injection/production rate. In general, we note that the closed-loop strategies are injecting at a lower rate compared to the open-loop strategies. This happens since we use a zero discount factor, i.e. we focus on long term behaviour. Moreover, there are no direct bounds on the liquid rates. We note that the open-loop strategies, so as the optimal strategy, have an upward concavity. This means that the water injection rate is increasing with time: these strategies increase the injection at the final time to exploit the high oil-to-water price ratio. The closed-loop strategies, instead, have a downward concavity. At the beginning (first 300 days) the closed-loop strategies are injecting at a similar pace as their open-loop counterparts (same slope in the initial part of the curves). However, as the data assimilation proceed, and a better estimate of the true field is given, the closed-loop strategies try to inject/produce as much as the optimal strategy (black curves in figure). This explains the change in concavity of the closed-loop strategies i.e. why the closed-loop strategies reduce the water injection rate with time. Figure 16 illustrates the saturation profiles of the true field for the closed-loop strategies. We note that they have similar field sweep at the final time. Figure 17 shows the corresponding control trajectories of the different closed-loop control strategies. It is evident that the control trajectories of the optimal control strategy are very different from the control trajectories for the closed-loop certainty equivalent and the closed-loop RO strategies.

Figure 18 illustrates the RMSE (32) and the ensemble spread (31) of the EnKF when applied together with the certainty equivalent strategy. The RMSE indicates whether the permeability parameter estimate of the EnKF converges toward the true permeability parameters. The ensemble spread indicates the uncertainty in the estimated permeability parameters. The RMSE and the ensemble spread sequences are computed for different levels of measurement noise, i.e. different values of R in (16b). Figure 18(2) indicates that decreasing levels of measurements noise, R ,

decrease the ensemble spread (31). This decrease does not always result in a lower RMSE (32) value. However, as is evident from Fig. 18(2), in most of the cases, lower measurement noise levels reduce the RMSE. In this case study there is no ensemble collapse. In fact, Fig. 20 shows that the ensemble realizations have different distances at the last assimilation time, this is an index of the variability in the ensemble of realizations.

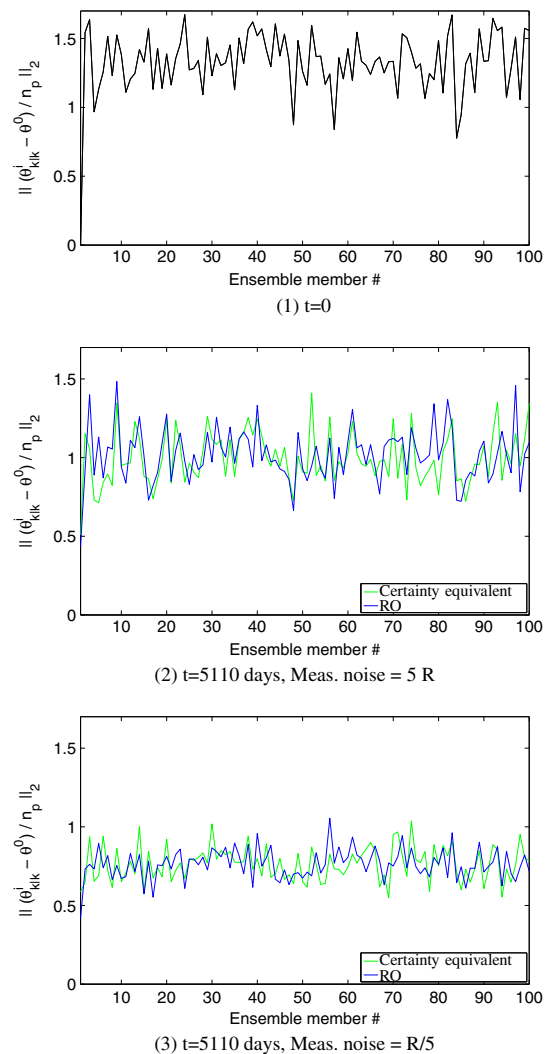


Fig. 20 Closed-loop. Distance of the ensemble realizations of the permeability field respect to the true permeability field for (1) the initial ensemble, (2) the final ensemble with a measurement noise of $5R$ and (3) the final ensemble with a measurement noise of $R/5$. We note that also in the case with the lowest measurement noise, the ensemble is not collapsing

In the EnKF, at each data assimilation step, we update the estimated permeability field for each ensemble member. Figure 19 illustrates the time evolution of the mean, $\hat{\theta}_{k|k-1}$, of these estimated permeability field ensembles for the closed-loop certainty equivalent optimization strategy. Figure 19 indicates that the estimated mean permeability field captures the main features of the true permeability field. We start out with a mean permeability field having four channel structures and converge towards the correct two channel structure. Figure 20 illustrates the associated uncertainty with this permeability estimate.

6 Conclusions

In this paper, we demonstrate the open-loop and the closed-loop performance of the certainty equivalent strategy and the RO strategy. For the open-loop case we present a modified RO strategy that performs significantly better than the other open-loop strategies. In the closed-loop situation for the case studied, we arrive at the surprising conclusion that the certainty equivalent strategy is slightly better than the RO strategy.

For the case presented, the open-loop RO strategy yields 3 % higher expected NPV and 28 % lower NPV standard deviation than the open-loop certainty equivalent strategy. Yet, the reactive strategy performed even better than the open-loop RO strategy. Simulations indicate that the inferior performance of the open-loop RO strategy compared to the reactive strategy is due to the inability of the RO strategy to efficiently encompass ensembles with very different and conflicting optimal control trajectories. We propose a modified RO strategy that allow shut in of uneconomical wells. The modified RO strategy performs significantly better than the other open-loop strategies and the reactive strategy. The modified RO optimization strategy yields an expected NPV that is 36 % higher than the expected NPV of the open-loop certainty equivalent strategy and 3 % higher than the expected NPV for the reactive strategy. The NPV standard deviation of the modified RO strategy is similar to the NPV standard deviation of the reactive strategy. These observations are non-trivial, as previous literature suggests that the open-loop RO strategy performs better than the reactive strategy [26]. The improved economic performance of the open-loop modified RO strategy justifies the computational effort used in determining the trajectories for this strategy.

The simulations for the closed-loop strategies, reveal that the RO strategy and the certainty equivalent strategy yields significantly higher NPV than the reactive strategy. Surprisingly, the closed-loop certainty equivalent strategy yields a higher NPV than the closed-loop RO strategy for the case studied. The uncertainty reduction of the permeability field estimate due to data assimilation

explains the good performance of the closed-loop certainty equivalent optimization strategy. Consequently, in closed-loop, the increased computational effort of the RO strategy compared to the certainty equivalent strategy is not justified for the particular case studied in this paper.

Future work will include a test of the strategies discussed in this paper on a more complex scenario (many wells, 3D grid, state/output constraints, spurious correlations), and we plan to work on the “Brugge field” [28]. In open-loop simulations, we expect that the modified RO strategy will improve the RO strategy as seen here. This result is in some way anticipated in [65], where, despite they do not consider uncertainty in the reservoir parameters, they get an increased NPV for the “Brugge field” by adding a reactive control to an optimal control strategy. In closed-loop simulations, we expect to obtain similar results for the RO and the CE strategies provided the data assimilation converges properly, as in the case showed in this paper. Finally, the optimization strategies presented in this paper and to our knowledge all literature on closed-loop reservoir management deals with optimization of the expected NPV. The approaches only implicitly considers risk and variance of the NPV. Future approaches should more directly include risk and variance of the NPV in the optimization.

Acknowledgments This research project is financially supported by the Danish Research Council for Technology and Production Sciences. FTP Grant no. 274-06-0284 and the Center for Integrated Operations in the Petroleum Industry at NTNU.

References

1. Brouwer, D., Nævdal, G., Jansen, J.: Improved reservoir management through optimal control and continuous model updating. In: SPE Annual Technical Conference and Exhibition, Houston (2004)
2. Brouwer, D.R., Jansen, J.D.: Dynamic optimization of waterflooding with smart wells using optimal control theory. SPE J. **9**, 391–402 (2004)
3. Sarma, P., Durlafsky, L., Aziz, K.: Efficient closed-loop production optimization under uncertainty. In: SPE Europec/EAGE Annual Conference, Madrid (2005)
4. Nævdal, G., Brouwer, D.R., Jansen, J.-D.: Waterflooding using closed-loop control. Comput. Geosci. **10**, 37–60 (2006)
5. Jansen, J.-D., Bosgra, O.H., Van den Hof, P.M.J.: Model-based control of multiphase flow in subsurface oil reservoirs. J. Process Control **18**, 846–855 (2008)
6. Jansen, J.D., et al.: Closed-loop reservoir management. In: 2009 SPE Reservoir Simulation Symposium, SPE 119098 The Woodlands, Texas (2009)
7. Lorentzen, R.J., Shafieirad, A., Nævdal, G.: Closed loop reservoir management using the ensemble Kalman filter and sequential quadratic programming. In: 2009 SPE Reservoir Simulation Symposium, SPE 119101. The Woodlands, Texas (2009)
8. Foss, B., Jensen, J.P.: Performance analysis for closed-loop reservoir management. SPE J. **16**, 183–190 (2011)
9. Capolei, A., Stenby, E.H., Jørgensen, J.B.: High order adjoint derivatives using esdirk methods for oil reservoir production

- optimization. In: ECMOR XIII 13th European Conference on the Mathematics of Oil Recovery (2012)
10. Van den Hof, P.M.J., Jansen, J.D., Heemink, A.: Recent developments in model-based optimization and control of subsurface flow in oil reservoirs. In: Proceedings of the 2012 IFAC Workshop on Automatic Control in Offshore Oil and Gas Production, pp. 189–200, Trondheim (2012)
 11. Capolei, A., Völcker, C., Frydendall, J., Jørgensen, J.B.: Oil reservoir production optimization using single shooting and ESDIRK methods. In: Proceedings of the 2012 IFAC Workshop on Automatic Control in Offshore Oil and Gas Production, pp. 286–291, Trondheim (2012)
 12. Foss, B.: Process control in conventional oil and gas fields - challenges and opportunities. *Control. Eng. Pract.* **20**, 1058–1064 (2012)
 13. Rawlings, J.B., Mayne, D.Q.: *Model predictive control: Theory and design*. Nob Hill Publishing, Madison (2009)
 14. Grüne, L., Pannek, J.: *Nonlinear model predictive control theory and algorithms*. Springer, London (2011)
 15. Grötschel, M., Krumke, S.O., Rambau, J. (eds.): *Online optimization of large scale systems*. Springer, Heidelberg (2001)
 16. Allgöwer, F., Zheng, A. (eds.): *Nonlinear Model Predictive Control*, vol. 26 Progress in Systems and Control Theory. Birkhäuser, Basel (2000)
 17. Findeisen, R., Allgöwer, F., Biegler, L.T. (eds.): *Assessment and future directions of nonlinear model predictive control*. Lecture Notes in Control and Information Sciences, vol. 358, Springer, Heidelberg (2007)
 18. Magni, L., Raimondo, D.M., Allgöwer, F. (eds.): *Nonlinear model predictive control. Towards New Challenging Applications*. Lecture Notes in Control and Information Sciences, vol. 384, Springer, Heidelberg (2009)
 19. Lazar, M., Allgöwer, F. (eds.): *4th IFAC Nonlinear Model Predictive Control Conference (NMPC'12)*. IFAC Noordwijkerhout, NL (2012)
 20. Evensen, G.: *Data Assimilation: The Ensemble Kalman Filter*, 2nd edn. Springer (2009)
 21. Biegler, L.T., Ghattas, O., Heinkenschloss, M., van Bloemen Waanders, B. (eds.): *Large-Scale PDE-Constrained Optimization*. Springer (2003)
 22. Biegler, L.T., Ghattas, O., Heinkenschloss, M., Keyes, D., van Bloemen Waanders, B. (eds.): *Real-Time PDE-Constrained Optimization* SIAM (2007)
 23. Markowitz, H.: Portfolio selection. *J. Finance* **7**, 77–91 (1952)
 24. Terwiesch, P., Ravemark, D., Schenker, B., Rippin, D.W.: Semi-batch process optimization under uncertainty: Theory and experiments. *Comput. Chem. Eng.* **22**, 201–213 (1998)
 25. Srinivasana, B., Bonvina, D., Vissera, E., Palankib, S.: Dynamic optimization of batch processes: II role of measurements in handling uncertainty. *Comp. Chem. Eng.* **27**, 27–44 (2003)
 26. Van Essen, G.M., Zandvliet, M.J., Van den Hof, P.M.J., Bosgra, O.H., Jansen, J.D.: Robust waterflooding optimization of multiple geological scenarios. *SPE J.* **14**, 202–210 (2009)
 27. Chen, C., Wang, Y., Li, G., Reynolds, A.C.: Closed-loop reservoir management on the Brugge test case. *Comput. Geosci.* **14**, 691–703 (2010)
 28. Peters, L., et al.: Results of the Brugge benchmark study for flooding optimization and history matching. *SPE Reserv. Eval. Eng.* **13**, 391–405 (2010)
 29. Evensen, G.: The ensemble Kalman filter: theoretical formulation and practical implementation. *Ocean Dyn.* **53**, 342–367 (2003)
 30. Wen, X.-H., Chen, W.H.: Some practical issues on real-time reservoir model updating using ensemble Kalman filter. *SPE J.* **12**, 156–166 (2007)
 31. Ehrendorfer, M.: A review of issues in ensemble-based Kalman filtering. *Meteorol. Z.* **16**, 795–818 (2007)
 32. Aanonsen, S.I., Nævdal G., Oliver, D.S., Reynolds, A.C., Valls, B.: The ensemble Kalman filter in reservoir engineering—a review. *SPE J.* **14**, 393–412 (2009)
 33. Simon, D.: *Optimal State Estimation Kalman, H_∞, and Nonlinear Approaches*. Wiley, Hoboken (2006)
 34. Rawlings, J.B., Bakshi, B.R.: Particle filtering and moving horizon estimation. *Comput. Chem. Eng.* **30**, 1529–1541 (2006)
 35. Wen, X.-H., Chen, W.H.: Real-time reservoir model updating using ensemble Kalman filter with confirming option. *SPE J.* **11**, 431–442 (2006)
 36. Sarma, P., Chen, W. Preventing ensemble collapse and preserving geostatistical variability across the ensemble with the subspace enfk. In: ECMOR XIII-13th European Conference on the Mathematics of Oil Recovery. Biarritz, France (2012)
 37. Sarma, P., Chen, W.H. Robust and efficient handling of model constraints with the kernel-based ensemble Kalman filter. In: *Reservoir Simulation Symposium*. The Woodlands, Texas (2011)
 38. Sarma, P., Chen, W. Generalization of the ensemble Kalman filter using kernels for nongaussian random fields. In: *SPE Reservoir Simulation Symposium*. The Woodlands, Texas (2009)
 39. Chen, Y., Oliver, D.S., Zhang, D.: Efficient ensemble-based closed-loop production optimization. *SPE J.* **14**, 634–645 (2009)
 40. Chen, Y., Oliver, D.S.: Ensemble-based closed-loop optimization applied to Brugge field. *SPE Reserv. Eval. Eng.* **13**, 56–71 (2010)
 41. Lie, K.A., et al.: Open source matlab implementation of consistent discretisations on complex grids. *Comput. Geosci.* **16**, 297–322 (2012)
 42. Peaceman, D.W.: Interpretation of well-block pressures in numerical reservoir simulation with nonsquare grid blocks and anisotropic permeability. *SPE J.* **23**(3), 531–543 (1983)
 43. Suwartadi, E., Krogstad, S., Foss, B.: Nonlinear output constraints handling for production optimization of oil reservoirs. *Comput. Geosci.* **16**, 499–517 (2012)
 44. Schlegel, M., Stockmann, K., Binder, T., Marquardt, W.: Dynamic optimization using adaptive control vector parameterization. *Comput. Chem. Eng.* **29**, 1731–1751 (2005)
 45. Capolei, A., Jørgensen, J.B. Solution of constrained optimal control problems using multiple shooting and esdirk methods. In: *American Control Conference (ACC)*, 295–300 (2012)
 46. Bock, H.G., Plitt, K.J. A multiple shooting algorithm for direct solution of optimal control problems. In: *Proceedings 9th IFAC World Congress Budapest*, pp. 243–247. Pergamon Press (1984)
 47. Biegler, L.T.: Solution of dynamic optimization problems by successive quadratic programming and orthogonal collocation. *Comput. Chem. Eng.* **8**, 243–248 (1984)
 48. Jansen, J.: Adjoint-based optimization of multi-phase flow through porous media - A review. *Comput. Fluids* **46**, 40–51 (2011)
 49. Sarma, P., Aziz, K., Durlafsky, L.J. Implementation of adjoint solution for optimal control of smart wells. In: *SPE Reservoir Simulation Symposium*, 31 January-2 February 2005, The Woodlands, Texas (2005)
 50. Jørgensen, J.B. Adjoint sensitivity results for predictive control, state- and parameter-estimation with nonlinear models. In: *Proceedings of the European Control Conference 2007*, pp. 3649–3656. Kos, Greece (2007)
 51. Völcker, C., Jørgensen, J.B., Stenby, E.H. Oil reservoir production optimization using optimal control. In: *50th IEEE Conference on Decision and Control and European Control Conference*, 7937–7943 Orlando, Florida (2011)

52. Byrd, R.H., Nocedal, J., Waltz, R.A.: Knitro: An integrated package for nonlinear optimization. In: *Large Scale Nonlinear Optimization*, pp. 35–59 (2006)
53. MATLAB. version 7.13.0.564 (R2011b) (The MathWorks Inc., Natick, Massachusetts, 2011)
54. Liu, Y.: Using the snesim program for multiple-point statistical simulation. *Comput. Geosci.* **32**, 1544–1563 (2006)
55. Schölkopf, B., Smola, A., Müller, K.-R.: Nonlinear component analysis as a kernel eigenvalue problem. *Neural Comput.* **10**, 1299–1319 (1998)
56. Kalman, R.E.: A new approach to linear filtering and predictions problems. *J. Basic Eng.* **82**, 35–45 (1960)
57. Kailath, T., Sayed, A.H., Hassibi, B.: *Linear Estimation*. Prentice Hall (2000)
58. Jazwinski, A.H.: *Stochastic Processes and Filtering Theory*. Academic Press (1970)
59. Burgers, G., van Leeuwen, P.J., Evensen, G.: Analysis scheme in the ensemble Kalman filter. *Mon. Weather Rev.* **126**, 1719–1724 (1998)
60. Wen, X.H., Chen, W.: Real-time reservoir model updating using ensemble Kalman filter. In: *SPE Reservoir Simulation Symposium*. The Woodlands, Texas (2005)
61. Gu, Y., Oliver, D.S.: History matching of the punq-s3 reservoir model using the ensemble Kalman filter. *SPE J.* **10**, 217–224 (2005)
62. Chen, Z. *Reservoir Simulation Mathematical Techniques in Oil Recovery*. SIAM Philadelphia (2007)
63. Aziz, K., Durlafsky, L., Tchelepi, H.: *Notes on petroleum reservoir simulation*. Department of Petroleum Engineering School of Earth Sciences, Stanford University (2005)
64. Völcker, C., Jørgensen, J.B., Thomsen, P.G., Stenby, E.H. Simulation of subsurface two-phase flow in an oil reservoir. In: *Proceedings of the European Control Conference 2009*, pp. 1221–1226. Budapest, Hungary (2009)
65. Dehdari, V., Oliver, D.S.: Sequential quadratic programming for solving constrained production optimization – case study from Brugge field. *SPE J.* **17**, 874–884 (2012)

APPENDIX **F**

Paper V

A Mean-Variance Objective for Robust Production Optimization in Uncertain Geological Scenarios

Authors:

Andrea Capolei, Eka Suwartadi, Bjarne Foss and John Bagterp Jørgensen

Submitted to:

Journal of Petroleum Science and Engineering.

A Mean-Variance Objective for Robust Production Optimization in Uncertain Geological Scenarios

Andrea Capolei^a, Eka Suwartadi^b, Bjarne Foss^b, John Bagterp Jørgensen^{a,*}

^aDepartment of Applied Mathematics and Computer Science & Center for Energy Resources Engineering
Technical University of Denmark, DK-2800 Kgs. Lyngby, Denmark.

^bDepartment of Engineering Cybernetics, Norwegian University of Science and Technology (NTNU), 7491 Trondheim, Norway.

Abstract

In this paper we introduce a mean-variance criterion for production optimization of oil reservoirs and suggest the Sharpe ratio as a systematic procedure to optimally trade-off risk and return. We demonstrate by open-loop simulations of a two-phase synthetic oil field that the mean-variance criterion is able to mitigate the significant inherent geological uncertainties better than the alternative certainty equivalent and robust optimization strategies that have been suggested for production optimization. In production optimization, the optimal water injection profiles and the production borehole pressures are computed by solution of an optimal control problem that maximizes a financial measure such as the Net Present Value (NPV). The NPV is a stochastic variable as the reservoir parameters such as the permeability field is stochastic. In certainty equivalent optimization the mean value of the permeability field is used in the maximization of the NPV of the reservoir over its lifetime. This approach neglects the significant uncertainty in the NPV. Robust optimization maximizes the expected NPV over an ensemble of permeability fields to overcome this shortcoming of certainty equivalent optimization. Robust optimization reduces the risk compared to certainty equivalent optimization because it considers an ensemble of permeability fields instead of just the mean permeability field. This is an indirect mechanism for risk mitigation as the risk does not enter the objective function directly. In the mean-variance bi-criterion objective function risk appears directly, it also considers an ensemble of reservoir models, and has robust optimization as a special extreme case. The mean-variance objective is common for portfolio optimization problems in finance. Markowitz's portfolio optimization problem is the original and simplest example of a mean-variance criterion for mitigating risk. Risk is mitigated in oil production by including both the expected NPV (mean of NPV) and the risk (variance of NPV) for the ensemble of possible reservoir models. With the inclusion of the risk in the objective function, the Sharpe ratio can be used to compute the optimal water injection and production borehole pressure trajectories that give the optimal return-risk ratio. By simulation, we investigate and compare the performance of production optimization by mean-variance optimization, robust optimization, certainty equivalent optimization, and the reactive strategy. The optimization strategies are simulated in open-loop without feedback while the reactive strategy is based on feedback. The simulations demonstrate that certainty equivalent optimization and robust optimization are risky strategies. At the same computational effort as robust optimization, mean-variance optimization is able to reduce risk significantly at the cost of slightly smaller return. In this way, mean-variance optimization is a powerful tool for risk management and uncertainty mitigation in production optimization.

Keywords: Robust Optimization, Risk Management, Oil Production, Optimal Control, Mean-Variance Optimization, Uncertainty Quantification

1. Introduction

In conventional water flooding of an oil field, feedback based optimal control technologies may enable higher oil recovery than with a conventional reactive strategy in which producers are closed based on water breakthrough (Chierici, 1992; Ramirez, 1987).

Optimal control technology and Nonlinear Model Predictive Control (NMPC) have been suggested for improving the oil recovery during the water flooding phase of an oil field (Jansen

et al., 2008). In such applications, the controller adjusts the water injection rates and the bottom hole well pressures to maximize oil recovery or a financial measure such as the NPV. In the oil industry, this control concept is also known as closed-loop reservoir management (CLRM) (Foss, 2012; Jansen et al., 2009). The controller in CLRM consists of a state estimator for history matching (state and parameter estimation) and an optimizer that solves a constrained optimal control problem for the production optimization. Each time new measurements from the real or simulated reservoir are available, the state estimator uses these measurements to update the reservoir's models and the optimizer solves an open loop optimization problem with the updated models (Capolei et al., 2013). Only the first part of the resulting optimal control trajectory is implemented. As new

*Corresponding author

Email addresses: acap@dtu.dk (Andrea Capolei), eka.suwartadi@ieee.org (Eka Suwartadi), Bjarne.Foss@itk.ntnu.no (Bjarne Foss), jbjo@dtu.dk (John Bagterp Jørgensen)

measurements become available, the procedure is repeated. The main difference of the CLRM system from a traditional NMPC is the large state dimension (10^6 is not unusual) of an oil reservoir model (Binder et al., 2001). The size of the problem dictates that the ensemble Kalman filter is used for state and parameter estimation (history matching) and that single shooting optimization is used for computing the solution of the optimal control problem (Capolei et al., 2013; Jansen, 2011; Jørgensen, 2007; Sarma et al., 2005a; Suwartadi et al., 2012; Völcker et al., 2011).

In this paper, we focus on the formulation of the optimization problem in the NMPC for CLRM. In the study of different optimization formulations, we leave out data assimilation (history matching) as well as the effect of feedback from a moving horizon implementation and consider only the predictions and computations of the manipulated variables in the open-loop optimization of NMPC. This can be regarded as an optimal control study. The reason for this is twofold. First, in the initial development of a field, no production data would be available and the production optimization would be an open-loop optimal control problem. Secondly, the ability of different optimization strategies to mitigate the effect of the significant uncertainties present in reservoir models is better understood if investigated in isolation.

In conventional production optimization, the nominal net present value (NPV) of the oil reservoir is maximized (Brouwer and Jansen, 2004; Capolei et al., 2013, 2012b; Foss, 2012; Foss and Jensen, 2011; Nævdal et al., 2006; Sarma et al., 2005b; Suwartadi et al., 2012). To compute the nominal NPV, nominal values for the model's parameters are used. In certainty equivalent production optimization, the expected reservoir model parameters are used in the maximization, while robust production optimization uses an ensemble of reservoir models to maximize the expected NPV (Capolei et al., 2013; Van Essen et al., 2009). The purpose of the robust production optimization is to (indirectly) mitigate the effect of the significant uncertainties in the parameters of the reservoir model. However, by the certainty equivalent and the robust production optimization methods, the trade-off between return (expected NPV) and risk (variance of the NPV) is not addressed directly. Fig. 1 illustrates risk versus expected return (mean) for different optimization and operation strategies. This is a sketch that shows the qualitative behavior of the results in this paper. As is evident in the sketch, a significant risk is typically associated with the certainty equivalent optimization and the RO strategy. The implication is that the RO strategy may improve current operation, but you cannot be sure due to the significant risk arising from the uncertain reservoir model. This is probably one of the reasons that NMPC for CLRM has not been widely adopted in the operation of oil reservoirs. The optimization problem in production optimization can be compared in some sense to Markowitz portfolio optimization problem in finance (Markowitz, 1952; Steinbach, 2001) or to robust design in topology optimization (Beyer and Sendhoff, 2007; Lazarov et al., 2012). The key to mitigate risk is to optimize a bi-criterion objective function including both return and risk for the ensemble of possible reservoir models. In this way, we can use a single parameter to compute an ef-

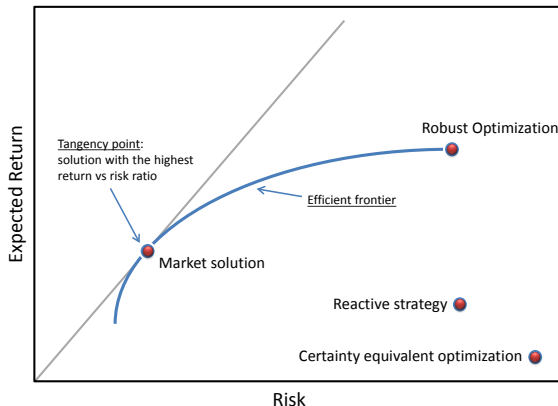


Figure 1: A sketch of the trade-off between risk and expected return in different optimization methods implemented in the optimizer for model based production optimization.

ficient frontier (the blue Pareto curve in Fig. 1) of risk and expected return. The robust optimization is one limit of the efficient frontier and the other limit is the minimum risk minimum return solution. By proper balancing the risk and the return in the bi-criterion objective function, we can tune the optimizer in the controller such that an optimal ratio of return vs risk is obtained; such a solution is called the market solution and is illustrated in Fig. 1.

The mean-variance optimization is based on a bi-criterion objective function. Previously in the oil literature, multi-objective functions have been used in production optimization to trade-off long- and short-term NPV (Van Essen et al., 2011), to robustify a non-economic objective function (Alhuthali et al., 2008), and to trade-off oil production, water production and water injection using a combination of mean value and standard deviation for each term (Yasari et al., 2013). These approaches pointed to the fact that a multi-objective function may be used to trade-off risk for performance, but did not explicitly address the risk-return relationship studied in the present paper using a mean-variance optimization strategy. Furthermore, these papers did not provide a systematic method for selection of the risk adverse parameter. The main contribution of the present paper is to demonstrate, that a return-risk bi-criterion objective function is a valuable tool for the profit-risk trade-off and provide a systematic method for selection the risk-return trade-off parameter. We do this for the open loop optimization and do not consider the effect of feedback.

The paper is organized as follows. Section 2 defines the reservoir model. Section 3 states the constrained optimal control problem and describes the mean-variance optimization strategy. The computation of economical and production key performance indicators is explained in Section 4. Section 5 describes the numerical case study. Conclusions are presented in Section 6.

2. Reservoir Model

We assume that the reservoirs are in the secondary recovery phase where the pressures are above the bubble point pressure of the oil phase. Therefore, two-phase immiscible flow, i.e. flow without mass transfer between the two phases, is a reasonable assumption. We focus on water-flooding cases for two-phase (oil and water) reservoirs. Further, we assume incompressible fluids and rocks, no gravity effects or capillary pressure, no-flow boundaries, and isothermal conditions. The state equations in an oil reservoir Ω , with boundary $\partial\Omega$ and outward facing normal vector \mathbf{n} , can be represented by pressure and saturation equations. The pressure equation is described as

$$\mathbf{v} = -\lambda_t \mathbf{K} \nabla p, \quad \nabla \cdot \mathbf{v} = \sum_{i \in \mathcal{I}, \mathcal{P}} q_i \cdot \delta(\mathbf{r} - \mathbf{r}_i) \quad \mathbf{r} \in \Omega \quad (1a)$$

$$\mathbf{v} \cdot \mathbf{n} = 0 \quad \mathbf{r} \in \partial\Omega \quad (1b)$$

\mathbf{r} is the position vector, \mathbf{r}_i is the well position, \mathbf{v} is the Darcy velocity (total velocity), \mathbf{K} is the permeability, p is the pressure, q_i is the volumetric well rate in barrels/day, δ is the Dirac's delta function, \mathcal{I} is the set of injectors, \mathcal{P} is the set of producers, and λ_t is the total mobility. The total mobility, λ_t , is the sum of the water and oil mobility functions

$$\lambda_t = \lambda_w(s) + \lambda_o(s) = k_{rw}(s)/\mu_w + k_{ro}(s)/\mu_o \quad (2)$$

The saturation equation is given by

$$\phi \frac{\partial}{\partial t} S_w + \nabla \cdot (f_w(S_w) \mathbf{v}) = \sum_{i \in \mathcal{I}, \mathcal{P}} q_{w,i} \cdot \delta(\mathbf{r} - \mathbf{r}_i) \quad (3)$$

ϕ is the porosity, s is the saturation, $f_w(s)$ is the water fractional flow which is defined as $\frac{\lambda_w}{\lambda_t}$, and $q_{w,i}$ is the volumetric water rate at well i . We use the MRST reservoir simulator to solve the pressure and saturation equations, (1) and (3), sequentially (Lie et al., 2012). Specifically, MRST first computes the total mobility using the initial water saturation. Secondly, the pressure equation is solved explicitly using the initial water saturation and the computed total mobility value. Thirdly, with the obtained pressure solution, the velocity is computed and is used in an implicit Euler method to solve the saturation equation. This procedure is repeated until the final time is reached. Wells are implemented using the Peaceman well model (Peaceman, 1983)

$$q_i = -\lambda_t W I_i (p_i - p_i^{bhp}) \quad (4)$$

p_i^{bhp} is the wellbore pressure, and $W I_i$ is the Peaceman well-index. The volumetric water flow rates at injection and production wells are

$$q_{w,i} = q_i \quad i \in \mathcal{I} \quad (5a)$$

$$q_{w,i} = f_w q_i \quad i \in \mathcal{P} \quad (5b)$$

The volumetric oil flow rates at production wells are

$$q_{o,i} = (1 - f_w) q_i \quad i \in \mathcal{P} \quad (6)$$

3. Optimal Control Problem

In this section, we present the continuous-time constrained optimal control problem and its transcription by the single shooting method to a finite dimensional constrained optimization problem. First we present the continuous-time optimal control problem; then we parameterize the control function using piecewise constant basis functions; and finally we convert the problem into a constrained optimization problem using the single shooting method.

Consider the continuous-time constrained optimal control problem in the Lagrange form

$$\max_{x(t), u(t)} J = \int_{t_a}^{t_b} \Phi(x(t), u(t)) dt \quad (7a)$$

subject to

$$x(t_a) = x_0, \quad (7b)$$

$$\frac{d}{dt} g(x(t)) = f(x(t), u(t), \theta), \quad t \in [t_a, t_b], \quad (7c)$$

$$u(t) \in \mathcal{U}(t). \quad (7d)$$

$x(t) \in \mathbb{R}^{n_x}$ is the state vector, $u(t) \in \mathbb{R}^{n_u}$ is the control vector, and θ is a parameter vector in an uncertain space Θ (in our case the permeability field). The time interval $I = [t_a, t_b]$ as well as the initial state, x_0 , are assumed to be fixed. (7c) represents the dynamic model and includes systems described by index-1 differential algebraic equations (DAE) (Capolei et al., 2012a,b; Völcker et al., 2009). (7d) represents linear bounds on the input values, e.g. $u_{\min} \leq u(t) \leq u_{\max}$. In our formulations we do not allow nonlinear state or output constraints. Suwartadi et al. (2012) provide a discussion of output constraints.

3.1. Production Optimization

Production optimization aims at maximizing the net present value (NPV) or oil recovery, for the life time of the oil reservoir. The stage cost, Φ , in the objective function for a NPV maximization can be expressed as

$$\Phi(x(t), u(t)) = \frac{-1}{(1 + \frac{d}{365})^{\tau(t)}} \left[\sum_{i \in \mathcal{I}} r_{wi} q_i(u(t), x(t)) + \sum_{i \in \mathcal{P}} (r_o q_{o,i}(u(t), x(t)) - r_{wp} q_{w,i}(u(t), x(t))) \right] \quad (8)$$

r_o , r_{wp} , and r_{wi} represent the oil price, the water separation cost, and the water injection cost, respectively. $q_{w,i}$ and $q_{o,i}$ are the volumetric water and oil flow rate at producer i ; q_i is the volumetric well injection rate at injector i ; d is the annual interest rate and $\tau(t)$ is the integer number of days at time t . The discount factor $(1 + \frac{d}{365})^{-\tau(t)}$ accounts for a daily compounded value of the capital. Note that from the well model (4), it follows that the flow rates q are negative for the producer wells and positive for the injector wells. Hence, the negative sign in front of the square bracket in the stage cost Φ . Note that in the special case when the discount factor is zero ($d = 0$) and the water injection and separation costs are zero as well, the NPV is equivalent to the quantity of produced oil.

3.2. Control Vector Parametrization

Let T_s denote the sample time such that an equidistant mesh can be defined as

$$t_a = t_0 < \dots < t_s < \dots < t_N = t_b \quad (9)$$

with $t_j = t_a + jT_s$ for $j = 0, 1, \dots, N$. We use a piecewise constant representation of the control function in this equidistant mesh, i.e. we approximate the control vector in every subinterval $[t_j, t_{j+1}]$ by the zero-order-hold parametrization

$$u(t) = u_j, u_j \in \mathbb{R}^{n_u}, t_j \leq t < t_{j+1}, j \in 0, \dots, N-1 \quad (10)$$

The optimizer maximizes the net present value by manipulating the well bhp's. A common alternative, is to use the injection rates as manipulated variables (Capolei et al., 2012b). The manipulated variables at time period $k \in \mathcal{N}$ are $u_k = \{p_{i,k}^{bhp}\}_{i \in \mathcal{I}}, \{p_{i,k}^{bhp}\}_{i \in \mathcal{P}}$ with \mathcal{I} being the set of injectors and \mathcal{P} being the set of producers. For $i \in \mathcal{I}$, $p_{i,k}^{bhp}$ is the bhp (bar) in time period $k \in \mathcal{N}$ at injector i . For $i \in \mathcal{P}$, $p_{i,k}^{bhp}$ is the bhp (bar) at producer i in time period $k \in \mathcal{N}$.

3.3. Single-Shooting Optimization

We use a single shooting algorithm for solution of (7) (Capolei et al., 2012b; Schlegel et al., 2005). Alternatives are multiple-shooting (Bock and Plitt, 1984; Capolei and Jørgensen, 2012) and collocation methods (Biegler, 1984, 2013). Despite the fact that the multiple shooting and the collocation methods offer better convergence properties than the single-shooting method (Biegler, 1984; Bock and Plitt, 1984; Capolei and Jørgensen, 2012), their application in production optimization is restricted by the large state dimension of such problems. The use of multiple-shooting is prevented by the need for computation of state sensitivities. Application of the collocation method is challenging due to the state vector's high dimension and requires advances in iterative methods for solution of large-scale KKT systems to be computationally attractive. Heirung et al. (2011) apply the collocation method for production optimization of a small-scale reservoir.

In the single shooting optimization algorithm, we define the function

$$\begin{aligned} \psi(\{u_k\}_{k=0}^{N-1}, x_0, \theta) = \\ \left\{ \begin{aligned} J &= \int_{t_a}^{t_b} \Phi(x(t), u(t)) dt : \\ x(t_0) &= x_0, \\ \frac{d}{dt} g(x(t)) &= f(x(t), u(t), \theta), t_a \leq t \leq t_b, \\ u(t) &= u_k, t_k \leq t < t_{k+1}, k = 0, 1, \dots, N-1 \end{aligned} \right\} \end{aligned} \quad (11)$$

such that (7) can be expressed as the optimization problem

$$\max_{\{u_k\}_{k=0}^{N-1}} \psi = \psi(\{u_k\}_{k=0}^{N-1}, \bar{x}_0, \theta) \quad (12a)$$

$$s.t. \quad c(\{u_k\}_{k=0}^{N-1}) \leq 0 \quad (12b)$$

Gradient based optimization algorithms for solution of (12) require evaluation of $\psi = \psi(\{u_k\}_{k=0}^{N-1}; \bar{x}_0, \theta)$, $\nabla_{u_k} \psi$ for $k \in \mathcal{N}$, $c(\{u_k\}_{k=0}^{N-1})$, and $\nabla_{u_k} c(\{u_k\}_{k=0}^{N-1})$ for $k \in \mathcal{N}$. For the cases studied in this paper, the constraint function defines linear bounds. Consequently, the evaluation of these constraint functions and their gradients is trivial. Given an iterate, $\{u_k\}_{k=0}^{N-1}$, ψ is computed by solving (7c) marching forwards. $\nabla_{u_k} \psi$ for $k \in \mathcal{N}$ is computed by the adjoint method (Capolei et al., 2012a,b; Jansen, 2011; Jørgensen, 2007; Sarma et al., 2005a; Suwartadi et al., 2012; Völcker et al., 2011).

To solve (12), we use Matlab's `fmincon` function (MATLAB, 2011). `fmincon` provides an interior point and an active-set solver. We use the interior point method since we experienced the lowest computation times with this method. An optimal solution is reported if the KKT conditions are satisfied to within a relative and absolute tolerance of 10^{-6} . The current best but non-optimal iterate is also returned in cases when the optimization algorithm uses more than 200 iterations. The current best, non-optimal iterate is returned in case of a relative change less than 10^{-8} in the cost function or the step size. Furthermore, the cost function is normalized to improve convergence. We use 4 different initial guesses when running the optimizations. These initial guesses are constant bhp trajectories with the bhp close to the maximal bhp for the injectors and the bhp close to the minimal bhp for the producers. About half of the simulations ended because they exceeded the maximum number of iterations but without satisfying the KKT conditions at the specified tolerance level. In these cases, the relative changes in the cost function and step size were of the order of 10^{-6} . Even if these solutions do not reach our specified tolerances for the KKT conditions, the solutions are sufficiently close to optimality to demonstrate qualitatively the behavior of the mean-variance (MV) optimization. This closeness to optimality is assessed by re-simulation of some of these scenarios with a tolerance limit of 10^{-8} . In these cases, the optimizer converged to a KKT point in about 300 iterations; and we did not observe important differences in these control trajectories compared to the already computed control trajectories.

3.4. Control Constraints

The bhp's are constrained by well and reservoir conditions. To maintain the two phase situation, we require the pressure to be above the bubble point pressure (290 bar). To avoid fracturing the rock, the pressure must be below the fracture pressure of the rock (350 bar). To maintain flow from the injectors to the producers, the injection pressure is maintained above 310 bar and the producer pressures are kept below 310 bar. With these bounds, we did not experience that the flow was reversed. Without these pressure bounds, state constraints must be included to avoid flow reversion.

3.5. Certainty-Equivalent, Robust, and Mean-Variance Optimization

In reservoir models, geological uncertainty is generally profound because of the noisy and sparse nature of seismic data, core samples, and borehole logs. The consequence of a large

number of uncertain model parameters (θ) is the broad range of possible models that may satisfy the seismic and core-sample data. Obviously, the optimal controls, $\{u_k\}_{k=0}^{N-1} = \{u_k(x_0, \theta)\}_{k=0}^{N-1}$, computed as the solution of the finite dimensional optimization problem (12) with the objective function (11) depend on the values of the uncertain parameters, θ . In practice, the initial states, x_0 , will also be uncertain, but in this paper we assume that all uncertainty is contained within θ . When θ is deterministic, the objective function $\psi = \psi(\{u_k\}_{k=0}^{N-1}; x_0, \theta)$ is deterministic and the optimization problem (12) is well defined. In contrast, when θ is stochastic, $\psi = \psi(\{u_k\}_{k=0}^{N-1}; x_0, \theta)$ is stochastic and the optimization problem (12) is not well defined. To define the optimization problem (12) for the stochastic case, a deterministic objective function for (12) must be constructed. The Certainty Equivalent (CE) optimization obtains a deterministic objective function by using the expected value of the uncertain parameters

$$\psi_{CE} = \psi(\{u_k\}_{k=0}^{N-1}; x_0, E_\theta[\theta]) \quad (13)$$

The MV optimization strategy is obtained by using the bi-criterion function

$$\psi_{MV} = \lambda E_\theta[\psi] - (1 - \lambda)V_\theta[\psi] \quad \lambda \in [0, 1] \quad (14)$$

as the objective function in (12). The term $E_\theta[\psi]$ is related to maximizing return while the term $V_\theta[\psi]$ is related to minimizing risk.

Van Essen et al. (2009) introduce Robust Optimization (RO) for production optimization to reduce the effect of geological uncertainties compared to the CE optimization. The RO objective is

$$\psi_{RO} = E_\theta[\psi] \quad (15)$$

The RO objective, ψ_{RO} , is a special case of the MV objective, ψ_{MV} , i.e. $\psi_{RO} = \psi_{MV}$ for $\lambda = 1$.

We use a Monte Carlo approach for computation of the expected value of parameters, $E_\theta[\theta]$. The expected value of the return, $E_\theta[\psi]$, and the variance of the return, $V_\theta[\psi]$, are also computed by the Monte Carlo approach. A sample is a set of realizations of the stochastic variables, θ :

$$\Theta_d = \{\theta^1, \theta^2, \dots, \theta^{n_d}\} = \{\theta^i\}_{i=1}^{n_d} \quad (16)$$

This sample is also called an ensemble and is generated by the Monte Carlo method. The objective function values, ψ^i , corresponding to this ensemble are

$$\psi^i = \psi(\{u_k\}_{k=0}^{N-1}; x_0, \theta^i) \quad i = 1, \dots, n_d \quad (17)$$

The sample estimators of the means and the variance are

$$\hat{\theta} = \frac{1}{n_d} \sum_{i=1}^{n_d} \theta^i \quad (18a)$$

$$\hat{\psi} = \frac{1}{n_d} \sum_{i=1}^{n_d} \psi^i \quad (18b)$$

$$\sigma^2 = \frac{1}{n_d - 1} \sum_{i=1}^{n_d} (\psi^i - \hat{\psi})^2 \quad (18c)$$

$\hat{\theta}$ is an estimator for $E_\theta[\theta]$ and $\hat{\psi}$ is an estimator for $E_\theta[\psi]$. σ^2 is an unbiased estimate of $V_\theta[\psi]$. Therefore, σ is an unbiased estimator of the standard deviation $\sigma_\theta[\psi] = \sqrt{V_\theta[\psi]}$.

The CE objective function, ψ_{CE} , is computed using the sample estimator $\hat{\theta} \approx E_\theta[\theta]$, i.e.

$$\psi_{CE} = \psi(\{u_k\}_{k=0}^{N-1}; x_0, \hat{\theta}) \quad (19)$$

Similarly, the MV objective function, ψ_{MV} , is computed using the sample estimators $\hat{\psi} \approx E_\theta[\psi]$ and $\sigma^2 \approx V_\theta[\psi]$, i.e.

$$\psi_{MV} = \lambda \hat{\psi} - (1 - \lambda)\sigma^2 \quad \lambda \in [0, 1] \quad (20)$$

ψ_{MV} is computed by computation of ψ^i for each parameter, $i = 1, \dots, n_d$, and subsequent computation of the sample estimators, $\hat{\psi}$ and σ^2 . The gradient based optimizer used in this paper needs the objective, ψ_{MV} , and the gradients, $\nabla_{u_k} \psi_{MV}$ for $k \in \mathcal{N}$. Appendix A provides an explicit derivation of these gradients. The computation of the objectives and the gradients, ψ^i , $\{\nabla_{u_k} \psi_{MV}\}_{k=0}^{N-1}$, can be conducted in parallel for $i = 1, 2, \dots, n_d$. The RO objective based on the sample estimator, $\hat{\psi} \approx E_\theta[\psi]$, is

$$\psi_{RO} = \hat{\psi} \quad (21)$$

The computational effort in computing ψ_{MV} is similar to the computational effort in computing ψ_{RO} . Therefore, no computational penalty is adopted by using the MV approach rather than the RO approach. The CE optimization needs one function and gradient evaluation in each iteration, while the MV optimization needs n_d function and gradient evaluations in each iteration. However, these n_d function and gradient evaluations can be conducted in parallel.

4. Key Performance Indicators

In this section, we present the key performance indicators (KPIs) used to evaluate the optimal control strategies. The KPIs are divided into economic KPIs and production related KPIs.

4.1. Profit, Risk and Market Solution

Given a control sequence, $\{u_k\}_{k=0}^{N-1}$, computed by some strategy, the NPV may be computed for each realization of the ensemble, $\psi^i = \psi(\{u_k\}_{k=0}^{N-1}; x_0, \theta^i)$ for $i = 1, \dots, n_d$. This gives a set of NPVs, $\{\psi^i\}_{i=1}^{n_d}$. By itself, these NPVs and their distribution is of interest. Economic KPIs such as NPV mean, NPV standard deviation, ratio of NPV mean to NPV standard deviation, and the minimum and maximum NPV in the finite set are used to summarize and evaluate the performance of a given control strategy, $\{u_k\}_{k=0}^{N-1}$. Given $\{\psi^i\}_{i=1}^{n_d}$, the expected mean NPV may be approximated using (18b), $E_\theta[\psi] \approx \hat{\psi}$. Similarly, the standard deviation of the mean may be approximated using (18c), $\sigma_\theta[\psi] \approx \sigma$. The ratio of return and risk is called the Sharpe ratio and is defined as (Sharpe, 1994)

$$S_h = \frac{E_\theta[\psi]}{\sigma_\theta[\psi]} \approx \frac{\hat{\psi}}{\sigma} \quad (22)$$

The ensemble, $\{\psi^i\}_{i=1}^{n_d}$, is finite. Therefore, the minimum and maximum NPV may be computed by

$$\psi_{\min} = \min \{\psi^i\}_{i=1}^{n_d} \quad (23a)$$

$$\psi_{\max} = \max \{\psi^i\}_{i=1}^{n_d} \quad (23b)$$

Given an optimal control sequence, $\{u_k\}_{k=0}^{N-1}$, ψ_{\min} is the lowest NPV in the ensemble of permeability fields and ψ_{\max} is the highest NPV in the ensemble of permeability fields.

The economic KPIs, $\{\hat{\psi}, \sigma, S_h, \psi_{\min}, \psi_{\max}\}$, provide a set of values that may be used to quickly evaluate and compare different control strategies, $\{u_k\}_{k=0}^{N-1}$, in terms of return and risk. Subsequently, selected solutions, $\{u_k\}_{k=0}^{N-1}$, may be evaluated in detail by inspection of the distribution of $\{\psi^i\}_{i=1}^{n_d}$ and by inspection of the solution trajectories, $\{u_k\}_{k=0}^{N-1}$. The idea in the mean-variance model is to compute the optimal solution for different values of the return-risk trade-off parameter, $\lambda \in [0, 1]$, and select the parameter λ to obtain the best trade-off between return and risk (Markowitz, 1952; Steinbach, 2001). As part of the mean-variance optimization, the NPV of each realization of the ensemble is computed for various values of λ in the mean-variance objective function (20). This gives $\{\psi^i(\lambda)\}_{i=1}^{n_d}$ and $\{u_k(\lambda)\}_{k=0}^{N-1}$ for a range of values of the mean-variance trade-off parameter, $\lambda \in [0, 1]$. For each value of λ , the set of ensemble NPVs and (18b) are used to approximate the expected NPV as function of λ , $E_\theta[\psi(\lambda)] \approx \hat{\psi}(\lambda)$. Similarly, the set of ensemble NPVs and (18c) are used to approximate the standard deviation of the NPV as function of λ , $\sigma_\theta[\psi(\lambda)] \approx \sigma(\lambda)$. The expected NPV, $E_\theta[\psi(\lambda)]$, and the risk $\sigma_\theta[\psi(\lambda)]$, may be plotted and tabulated as a function of λ . This gives some overview of the behaviour of key economic performance indicators such as expected profit and risk as a function of λ . Also a phase plot of risk versus return, $\{\sigma_\theta[\psi(\lambda)], E_\theta[\psi(\lambda)]\}$ for $\lambda \in [0, 1]$, illustrates the risk-return relationship of the mean-variance model. The efficient frontier is the curve that yields the maximal return as function of risk. By itself, the efficient frontier does not provide a unique solution to the production optimization problem. The efficient frontier provides only efficient pairs of return and risk; the preferred solution depends on the risk preferences of the decision maker. One way to choose a solution among the efficient risk-return pairs is to choose the solution that maximizes the Sharpe ratio (22) (Sharpe, 1994). The solution that maximizes the Sharpe ratio is called the market solution.

4.2. Cumulative Productions Indicators

In addition to the economic KPIs, we also consider production related KPIs. The production related KPIs are the expected cumulative oil production, the expected cumulative water injection, and the production efficiency.

The cumulative oil production, $Q_o(t)$, and the cumulative wa-

ter injection, $Q_{w,inj}(t)$, at time t are given by

$$Q_o(t) = \int_0^t \left(\sum_{i \in \mathcal{P}} q_{o,i} \right) dt \quad (24a)$$

$$Q_{w,inj}(t) = \int_0^t \left(\sum_{i \in \mathcal{I}} q_i \right) dt \quad (24b)$$

We approximate the cumulative oil production (24a) and water injection (24b) at final time t_b by using the right rectangle (implicit Euler) integration method

$$Q_o = Q_o(t_b) = \sum_{k=0}^{N-1} \left(\sum_{i \in \mathcal{P}} q_{o,i}(x_{k+1}, u_k) \right) \Delta t_k \quad (25a)$$

$$Q_{w,inj} = Q_w(t_b) = \sum_{k=0}^{N-1} \left(\sum_{i \in \mathcal{I}} q_i(x_{k+1}, u_k) \right) \Delta t_k \quad (25b)$$

and we compute the expected values of the cumulative productions (25a)-(25b) as the sample averages

$$E_\theta[Q_o] = \frac{1}{n_d} \sum_{i=1}^{n_d} Q_o^i \quad (26a)$$

$$E_\theta[Q_{w,inj}] = \frac{1}{n_d} \sum_{i=1}^{n_d} Q_{w,inj}^i \quad (26b)$$

Superscript i refers to the quantity computed using realization i . The production efficiency, ξ , is defined and computed as the volumetric ratio of the produced oil and the injected water

$$\xi = \frac{E_\theta[Q_o]}{E_\theta[Q_{w,inj}]} \quad (27)$$

5. Simulated Test Cases

The mean-variance optimization strategy is studied for two test cases. The same reservoir permeability fields and petrophysical parameters are used for the two test cases. Fig. 2 illustrates the ensemble of permeability fields used to represent the uncertain reservoir. Fig. 3 illustrates the mean permeability field of the ensemble of permeability fields. As illustrated by Fig. 4 and reported in Table 1, the difference between the two test cases are the well configurations and the economical parameters. Test Case I contains more injector wells than Test Case II. Furthermore, the water injection costs and the water separation costs are higher in Test Case I than in Test Case II. This implies that a reactive strategy that injects water at a maximal rate is penalized in Test Case I due to the high water injection and water separation costs. Test Case I is used to illustrate a complicated well configuration benefitting from intelligent coordination of wells and penalizing conventional reactive strategies. Test Case II is simpler and the value of feedback becomes more important than predictive coordination of the wells. This means that in Test Case II a feedback based reactive strategy will be able to do better than a model based open loop strategy. Combined, the two test cases illustrates that the shape and geometry of the efficient frontier is case dependent, that the value

Table 1: Petro-physical and economical parameters for the two phase model and the discounted state cost function used in the case studies. TC I = Test Case I. TC II = Test Case II.

	Description	Value	Unit
ϕ	Porosity	0.2	-
c_r	Rock compressibility	0	Pa^{-1}
ρ_o	Oil density (300 bar)	700	kg/m^3
ρ_w	Water density (300 bar)	1000	kg/m^3
μ_o	Dynamic oil viscosity	$3 \cdot 10^{-3}$	$\text{Pa} \cdot \text{s}$
μ_w	Dynamic water viscosity	$0.3 \cdot 10^{-3}$	$\text{Pa} \cdot \text{s}$
S_{or}	Residual oil saturation	0.1	-
S_{ow}	Connate water saturation	0.1	-
n_o	Corey exponent for oil	2	-
n_w	Corey exponent for water	2	-
P_{init}	Initial reservoir pressure	300	bar
S_{init}	Initial water saturation	0.1	-
r_o	Oil price	120	USD/bbl
r_{wp}	Water separation cost (TC I)	25	USD/bbl
r_{wp}	Water separation cost (TC II)	20	USD/bbl
r_{wi}	Water injection cost (TC I)	15	USD/bbl
r_{wi}	Water injection cost (TC II)	10	USD/bbl
d	Discount factor	0	-

of feedback in a reactive strategy compared to an open-loop optimization strategy is dependent on the well configuration, and that the mean-variance objective formulation is an efficient way to trade off risk and return.

5.1. Uncertain Parameters

In our study, the permeability field is the uncertain parameters. We generate 100 permeability field realizations of a 2D reservoir in a fluvial depositional environment with a known vertical main-flow direction. Fig. 2 illustrates such an ensemble of permeability fields. These permeability realizations are equal to the permeabilities used by Capolei et al. (2013). To generate the permeability fields, we first create a set of 100 binary (black and white) training images by using the sequential Monte Carlo algorithm ‘SNESIM’ (Liu, 2006). Then a Kernel PCA procedure is used to preserve the channel structures and to smooth the original binary images (Schölkopf et al., 1998). The realizations obtained by this procedure are quite heterogeneous. The values of the permeabilities are in the range 6 – 2734 mD.

5.2. Description of the Test Cases

We consider a conventional horizontal oil field that can be modeled as two phase flow in a porous medium (Chen, 2007). The reservoir size is $450 \text{ m} \times 450 \text{ m} \times 10 \text{ m}$. By spatial discretization this reservoir is divided into $45 \times 45 \times 1$ grid blocks. The permeability field is uncertain, $\theta = \ln K$. We assume that the ensemble in Fig. 2 represents the range of possible geological uncertainties.

Table 1 lists the reservoir’s petro-physical and economical parameters. The initial reservoir pressure is 300 bar everywhere

in the reservoir. The initial water saturation is 0.1 everywhere in the reservoir. This implies that initially, the reservoir has a uniform oil saturation of 0.9. The manipulated variables are the bhrs over the life of the reservoir. In this study, we consider a zero discount factor, d , in the cost function (8). This means that we maximize NPV at the final time without short term production considerations (Capolei et al., 2012b).

In both test cases, we consider a prediction horizon of $t_N = 4 \cdot 365 = 1460$ days divided in $N = 60$ control periods (i.e. the control period is $T_s \approx 24$ days). We control the reservoir using three strategies: a reactive strategy, a CE strategy, and a MV strategy. The RO strategy is considered a special MV strategy with $\lambda = 1$. In the reactive strategy, we develop the field at the maximum production rate by setting the producers at the lowest allowed bhp value (290 bar) and the injectors at the maximum allowed bhp value (350 bar). When a production well is no longer economical it is shut in. A production well is uneconomical when the value of the produced oil is less than the separation cost of the produced water. The CE strategy is based on solving problem (12) using the CE cost function ψ_{CE} (19). It uses the mean (Fig. 3) of the ensemble (Fig. 2) as its permeability field. The MV strategy is based on solving problem (12) using the cost function ψ_{MV} (20) for different values of the parameter λ .

5.3. Test Case I

Fig. 4a illustrates the well configuration for Test Case I. Test Case I has 9 injection wells and 4 producer wells. Table 1 contains the petro-physical as well as the economic parameters. From the oil price and the water separation cost for Test Case I, it is apparent that a producer well becomes uneconomical when the fractional flow, f_w , exceeds $r_o/(r_o + r_{wp}) = 120/(120 + 25) = 0.828$.

Fig. 5 shows the optimal bhp trajectories for the producer wells while Fig. 6 shows the optimal bhp trajectories for the injector wells. These trajectories are computed using the reactive, the MV, the RO, and the CE optimization strategy. $\lambda = 0.59$ gives the market solution for this case, and this value of λ is used in the MV strategy. Compared to the RO and the market MV strategy, the CE trajectories do not contain sudden large changes in the bhp. This is due to the fact that the mean permeability field used by the CE strategy does not have sharp edges. It is also apparent that the bhp trajectories of the RO strategy have larger sudden changes than the trajectories of the market MV strategy. For some realizations of the permeability field, the RO trajectories would perform very well because they utilize the sharp channel structure in the permeability field. However, sudden large changes in the manipulated variables is an indication of solutions that are sensitive to process noise and model uncertainties. As sensitivity to noise is related to high risk, the trajectories of the bore hole pressures indicate that the RO strategy is more risky than the market MV strategy. Fig. 7 confirms this observation.

Fig. 7 illustrates the profit, ψ^i , for each realization of the permeability field using the reactive strategy as well as the CE, the RO, and the market MV optimal control strategies. The average profit over the realizations is a measure of the expected

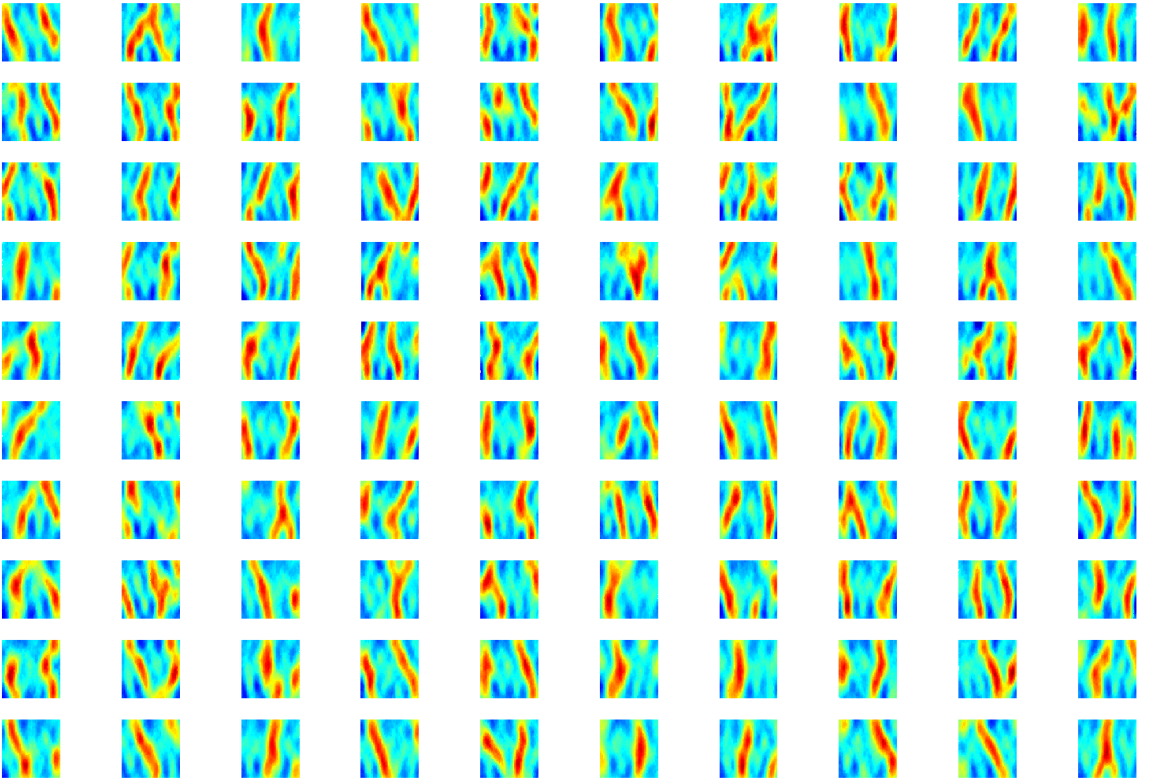


Figure 2: Plots of the permeability fields used to describe the uncertain reservoir. An ensemble of 100 realizations is used. The realizations are quite heterogeneous. The permeability values are in the range 6 – 2734 mD. The logarithm of the permeability is plotted for better visualization.

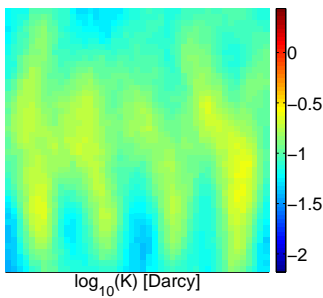


Figure 3: A plot of the mean permeability field for the ensemble of permeability fields in Fig. 2. The mean is a smoothed version of the ensembles. Due to the heterogenous nature of the ensembles, the mean does not necessarily reflect the channel structure of any of the ensemble members.

return, while the fluctuations are a measure of risk. For each control strategy, the bigger the fluctuations in profit, the bigger the related risk. It is evident that the CE strategy has the lowest expected return and the biggest risk. The CE strategy also has the lowest worst case return. The reactive strategy has a mean return that is higher than the mean return of the CE strategy but lower than the mean returns of the RO and the MV strategies. The risk for the reactive strategy is lower than the risk for the CE strategy but higher than the risks for the RO and the MV strategies. Comparing the market MV and the RO strategies, the RO strategy has a slightly higher mean profit than the market MV strategy but at the price of a significantly higher risk.

Table 2 reports KPIs for each control strategy. The economical KPIs are the expected NPV, the standard deviation NPV, the Sharpe ratio, and the minimum and maximum NPV for the ensemble. The production related KPIs are the mean oil production, the mean water injection, and the production efficiency (27) for the ensemble. The mean oil production and the mean water injection are scaled by the pore volume of the reservoir. Interestingly, the MV market strategy ($\lambda = 0.59$) has the highest minimum ensemble NPV value, ψ_{\min} . This means that

Table 2: Key Performance Indicators (KPIs) for Test Case I. The economic KPIs are the expected profit, the standard deviation of the profit, the Sharpe ratio, and the minimum and maximum profit for the ensemble. The reported production related KPIs are the expected oil production, the expected water injection, and the production efficiency, ξ . The productions are normalized by the pore volume. All improvements are relative to the reactive strategy.

Strategy	$\hat{\psi}$		σ		S_h	ψ_{\min}		ψ_{\max}		$E_o[Q_o]$		$E_o[Q_{w,inj}]$		ξ
	10 ⁶ USD, %	%	10 ⁶ USD, %	%		10 ⁶ USD, %	%	10 ⁶ USD, %	%	,	%	,	%	
Reactive	39.04,	/	9.01,	/	4.34	17.62,	/	60.47,	/	0.39,	/	1.04,	/	37.8
CE	28.57,	-26.8	18.93,	+110.2	1.51	-23.86,	-235.4	60.25,	-0.40	0.32,	-18.4	0.88,	-15.3	36.4
MV														
$\lambda = 1$ (RO)	50.40,	+29.1	8.17,	-9.3	6.17	28.11,	+67.2	69.90,	+15.6	0.26,	-34.0	0.44,	-57.4	58.5
$\lambda = 0.75$	48.00,	+25.0	6.13,	-32.0	7.83	34.68,	+96.8	64.52,	+6.7	0.24,	-38.9	0.39,	-62.5	61.6
$\lambda = 0.59$	47.09,	+20.6	4.89,	-45.7	9.63	35.44,	+101	57.747,	-4.5	0.23,	-40.9	0.38,	-63.6	61.5
$\lambda = 0.5$	45.58,	+16.7	5.15,	-42.8	8.85	33.13,	+88.0	57.84,	-4.3	0.23,	-41.0	0.39,	-62.4	59.3
$\lambda = 0.25$	45.09,	+15.5	4.76,	-47.1	9.47	32.39,	+83.8	56.3,	-6.9	0.22,	-42.5	0.37,	-64.0	60.3
$\lambda = 0.125$	44.00,	+12.7	4.61,	-48.8	9.54	31.73,	+80.1	54.67,	-9.6	0.22,	-44.1	0.36,	-65.1	60.5
$\lambda = 0$	41.57,	+6.5	5.02,	-44.2	8.28	29.47,	+67.2	52.40,	-13.3	0.21,	-45.6	0.36,	-64.9	58.6

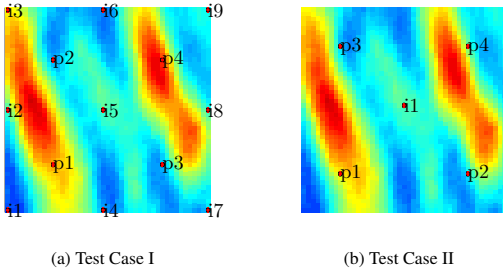


Figure 4: The well configuration for Test Case I and II. The permeability field in this plot is the permeability field in the upper left corner of Fig. 2. Producer wells are indicated by the letter p, and injector wells are indicated by the letter i. In addition to the injector and producer wells in Test Case II, Test Case I has a number of injector wells at the boundary of the field.

in this case, the market solution has a better worst case profit, ψ_{\min} , compared to all other control strategies including the MV strategies with lower standard deviation. Compared to the CE strategy and the reactive strategy, all MV control trajectories give higher expected NPV and lower NPV standard deviation. In that sense, the MV solutions are said to dominate the CE solution and the solution given by the reactive strategy. The RO solution has the highest maximum NPV and also the highest expected NPV. However, among the MV solutions, it is also the solution with the lowest minimum NPV. This implies that the RO solution is very risky and this is confirmed by its high NPV standard deviation. Among the MV solutions, the RO solution has the highest NPV standard deviation. Fig. 8 summarizes the economic KPIs of the MV solutions. Fig. 8a shows the expected NPV as well as the worst and best NPV for the ensemble as function of the mean-variance trade-off parameter, λ .

It is easily observed that the market MV solution, coincidentally, is also the max-min solution, i.e. the solution yielding the highest worst case NPV. Similarly, the high risk of the RO solution is evident. Fig. 8b illustrates the standard deviation of the NPV as function of the mean-variance trade-off parameter, λ . The standard deviation of the NPV is a measure of risk. The risk is a non-monotonous function of the mean-variance trade-off parameter, λ . Measured by NPV standard deviation, the minimum risk solution is obtained for $\lambda = 0.125$. However, this solution is inferior to the market MV solution, as the market MV solution has a higher worst case NPV, a higher mean NPV, and a higher best case NPV (see Fig. 8a). Fig. 8c plots the Sharpe ratio as function of the mean-variance trade-off parameter, λ . This plot indicates that the maximal Sharpe ratio, i.e. the market solution, is obtained for $\lambda = 0.59$. The Sharpe ratio is not a concave function of λ in this case. Another local maximum with almost the same Sharpe ratio as the global maximum is obtained for $\lambda = 0.125$, i.e. for the minimum risk solution. As we noted previously, this solution is inferior to the market solution. Also note that the RO solution has the lowest Sharpe ratio. Fig. 8d illustrates the risk-return relations for the different MV strategies as well as the CE, the RO (MV with $\lambda = 1$), and the reactive strategy. This figure clearly illustrates the superiority of the market MV strategy over the reactive strategy and the CE strategy. It also shows the reduced risk of the market MV strategy compared to the RO strategy at the cost of slightly reduced mean profit. The risk-return curve for the MV optimization strategies has two arcs. The efficient frontier arc is the blue curve in Fig. 8d; the red curve is the inefficient frontier. In the efficient frontier, an increased risk is associated with an increased mean return. The MV strategy contains some risk-return points that are feasible but not on the efficient frontier, i.e. points that for a given risk level does not produce the maximal expected return.

For Test Case I, the production related KPIs in Table 2 demonstrate that the reactive strategy produces much more oil compared to the other control strategies. However, it also injects and produces much more water, i.e. $E_o[Q_o] = 0.39$ pore

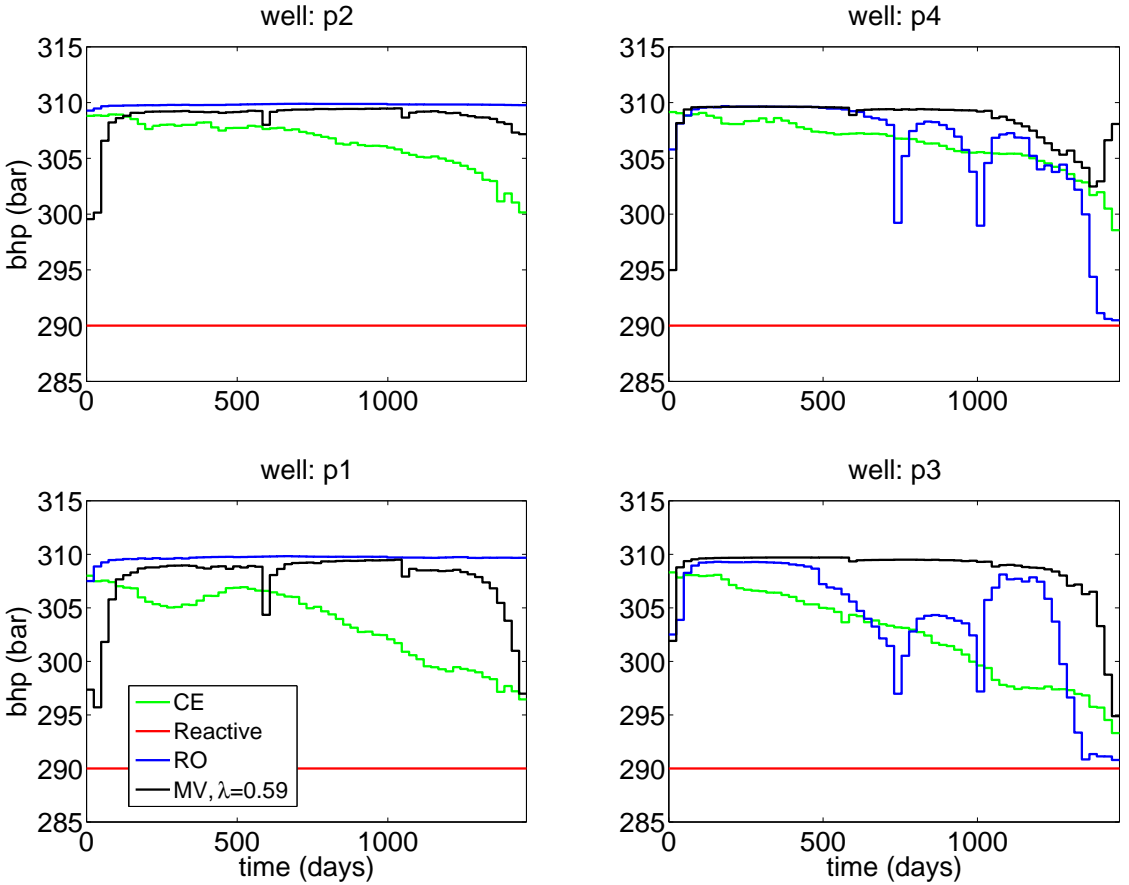


Figure 5: Test Case I. Trajectories of the bhp at producer wells using different optimization strategies. In the reactive strategy, the producer wells are shut in when production becomes uneconomical. The shut in time is different for each realization and is not indicated in the plot.

volume and $E_{\theta}[Q_{w,inj}] = 1.04$ pore volume. From a pure production point of view, the most efficient MV solution does not coincide with the market solution nor with the RO solution. It occurs for $\lambda = 0.75$ and has a production efficiency of $\xi = 61.6\%$, i.e. 61.6 barrels of oil is produced for 100 barrels of injected water.

5.4. Test Case II

Fig. 4b indicates the well configuration of Test Case II. Table 1 reports the petro-physical and economical parameters used for the simulations. The economic parameters imply that a producer well becomes non-economical when the fractional water flow, f_w , exceeds $r_o/(r_o + r_{wp}) = 120/(120 + 20) = 0.857$. Compared to Test Case I, Test Case II has fewer injection wells and the water separation cost is lower.

Fig. 9 and Table 3 report the economic KPIs for Test Case II. They summarize and provide an overview of the performance

of different control strategies for Test Case II. The Sharpe ratio curve in Fig. 9c indicates that the market MV solution is obtained for $\lambda = 0.125$. As illustrated by the efficient frontier in the risk-return plot in Fig. 9d, the RO solution and the CE solution both have higher expected return as well as significantly higher risk (NPV standard deviation) than the MV market solution. Comparing with the sketch in Fig. 1, the efficient frontier illustrated in Fig. 9d is a textbook example of the relation between risk and return. At the price of a low reduction in the expected return, the MV market solution decreases the risk significantly compared to the RO solution and the CE solution. Also the worst case NPV is much higher for the MV market solution than the corresponding values for the RO solution and the CE solution. The worst case NPV, ψ_{min} , is even negative for the CE solution.

Test Case II has been included to demonstrate the value of information and feedback. While the optimization based strate-

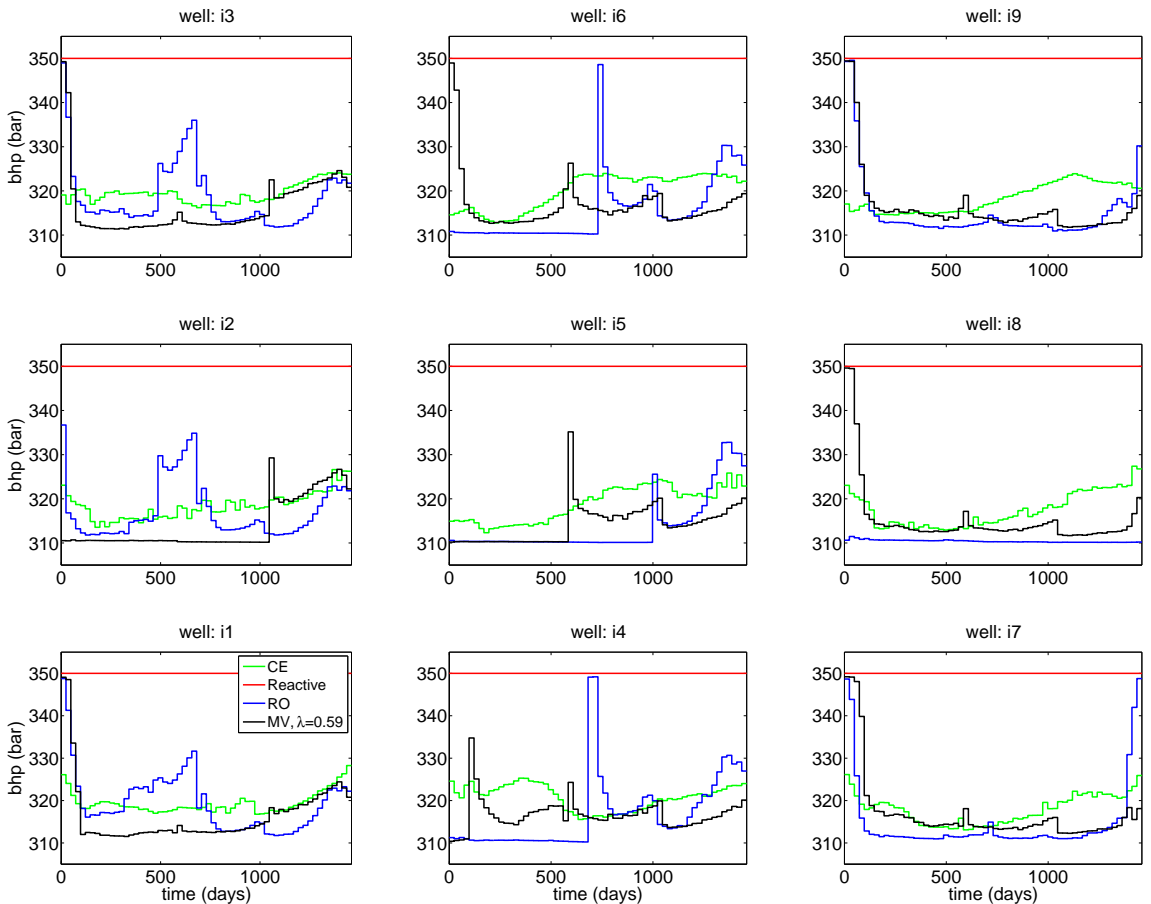


Figure 6: Test Case I. Trajectories of bhp for injector wells using different optimization strategies.

gies studied in this paper are open-loop strategies that do not use feedback, the reactive strategy is a feedback controller. As reported in Fig. 9d and Table 3, the reactive strategy has both a higher expected NPV and a lower risk (NPV standard deviation) than the RO solution as well as the CE solution. Consequently, the reactive solution is superior to the open-loop CE and RO strategies. Furthermore, the worst case NPV of the reactive strategy is higher than the worst case NPVs of the CE solution and the RO solution. The worst case NPV of the reactive strategy is even better than the mean NPV of the CE strategy. Fig. 9d illustrates that the reactive strategy has a significantly higher return than the MV market solution. However, the reactive strategy also has a higher risk measured by the NPV standard deviation. Nevertheless, the reactive strategy is still superior to the MV market solution as the worst case NPV of the reactive strategy is larger than the best case NPV of the market MV solution. This illustrates that even though a control strategy may have a larger standard deviation than another control strategy, it may still be superior as all its possible profits are

larger than the profits of the other control strategy.

Interestingly and perhaps surprising, Fig. 9a as well as Table 3 indicate that the Market MV solution is in some sense inferior to the MV solution obtained for $\lambda = 0.25$. The MV solution for $\lambda = 0.25$ has a worst case NPV, a mean NPV, and a best case NPV, that are all higher than the corresponding values for the market solution. Even though the market solution has lower risk in terms of standard deviation of the NPV, this becomes in some sense irrelevant as both the mean NPV and the worst case NPV of the MV solution with $\lambda = 0.25$ are higher than the corresponding values of the market solution. A more detailed comparison of the two MV strategies would require the distribution of the NPVs for the two strategies and not only the just discussed statistics.

In addition to economic KPIs, Table 3 also reports the production related KPIs. The reactive strategy has the highest oil recovery but also the highest water injection such that its production efficiency, ξ , is the lowest among all strategies. The most efficient solution measured by the production efficiency,

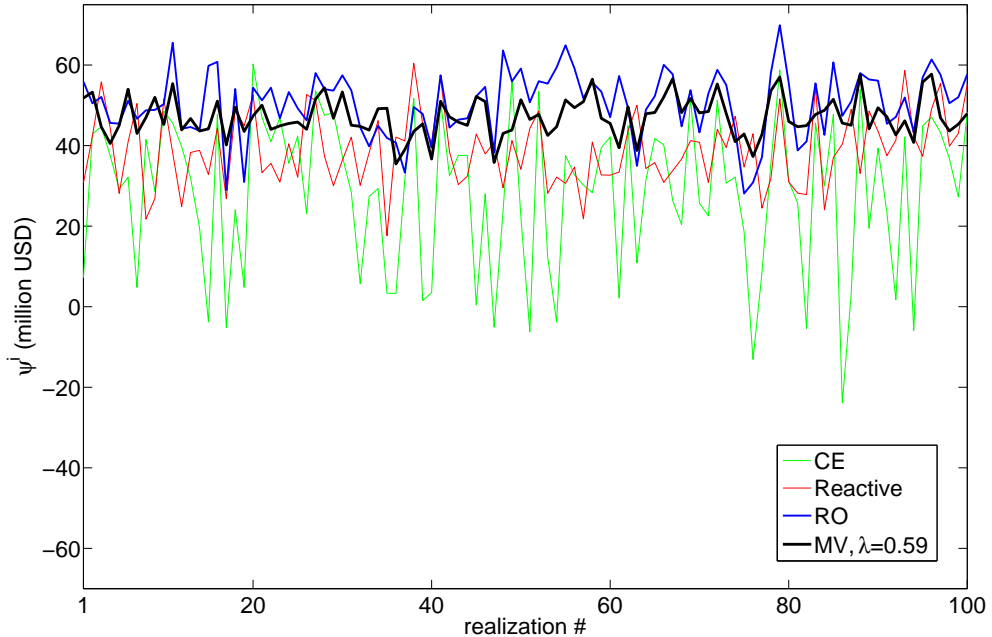


Figure 7: Test Case I. The net present value (NPV) of the optimal solution for each realization of the ensemble. The optimal solution is computed using a CE objective, a RO objective, and a MV objective with a mean-variance trade-off corresponding to the market solution ($\lambda = 0.59$). We also show the NPVs for the reactive strategy.

ξ , would be the minimum variance solution obtained for $\lambda = 0$. This solution would have a production efficiency of $\xi = 81.9\%$. In economic terms, this solution would still be inferior to the reactive strategy.

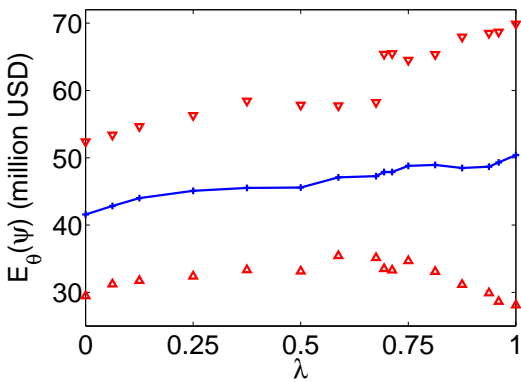
5.5. Discussion

Using two test cases, we demonstrated production optimization of an uncertain oil reservoir by open-loop optimal control using a mean-variance objective function. We compared optimal control using a mean-variance objective function to open-loop optimal control with a CE objective function and an RO objective function, respectively. For uncertain reservoirs, the market solution of the mean-variance objective provides better and more well-behaved bhp trajectories with less risk (standard deviation) of the NPV. This reduced risk typically comes at the price of reduced profit. The simulations revealed that for the reservoirs in this paper, the reduction in expected NPV is modest compared to the risk reduction. Risk mitigation by the mean-variance objective can be regarded as a regularization of the RO objective and has the same regularizing effect on the solution, i.e. the bhp trajectories, as the effect of e.g. a Tikhonov regularizer in least squares problems (Hansen, 1998).

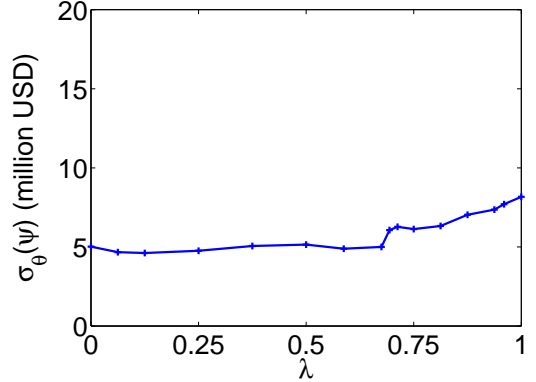
The analysis, evaluation and discussion of control performance in uncertain oil reservoirs is facilitated by Fig. 8 and

Fig. 9. In practice a dash board of risk-return relations similar to Fig. 8 and Fig. 9 will be very valuable for reservoir management and risk mitigation. A closed-loop reservoir management system, should compute MV optimal control solutions for $\lambda \in [0, 1]$. This would give the expected NPV, the NPV standard deviation, the Sharpe ratio, and the efficient frontier in a risk-return diagram. The range of possible NPVs are subsequently computed by simulating each of the optimal control solutions for each of the permeability fields in the ensemble. Reservoir engineers and managers could then analyze the diagrams as well as selected bhp trajectories. Based on this analysis, they should select a mean-variance trade-off parameter, λ . This could be the market solution, but it could also be another value. A set of optimal injector and producer well bhp trajectories corresponds to the selected value of λ . The bhp values in the first control period are implemented in the reservoir. Test Case II demonstrated the importance of feedback. To incorporate measurements obtained one control period later, a history matching procedure should be used to update the ensemble of permeability fields. Based on this updated ensemble of permeability fields, the mean-variance open-loop optimal control computations are repeated and the first part of the selected optimal bhps are implemented (Capolei et al., 2013).

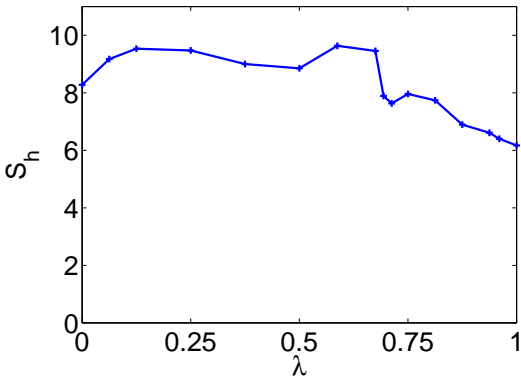
In the analysis and discussion of the performance of different



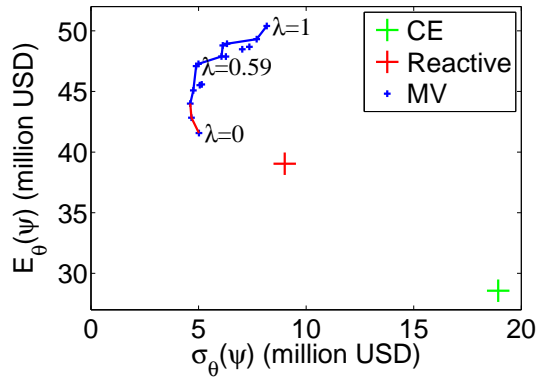
(a) Expected profit, max profit, and min profit.



(b) Risk measured as the standard deviation of profit.



(c) The Sharpe ratio.



(d) A risk-return plot. The expected NPV vs standard deviation of NPV.

Figure 8: Mean-variance relations for Test Case I. Profit (a), risk (b), and Sharpe Ratio (c) for different mean-variance trade-offs, λ . (d) is a phase plot of expected profit vs risk measured as the standard deviation of profit. The blue curve is the efficient frontier. The red curve is the inefficient frontier. Also the CE solution and the reactive solution are indicated.

control strategies, worst case analysis is beneficial and informative. In this study, we analyzed worst case performance by simulation using a bhp trajectory obtained by open-loop MV optimization; i.e. as part of solving the mean-variance optimal control problem, we computed the NPV, ψ^i , for each member of the ensemble, and the set $\{\psi^i\}_{i=1}^{n_d}$ was used to determine $\psi_{\min} = \min \{\psi^i\}_{i=1}^{n_d}$ and $\psi_{\max} = \max \{\psi^i\}_{i=1}^{n_d}$. In a future study, it would be interesting to compare the MV solution to a max-min solution, i.e. to compute the optimal control trajectories by solution of

$$\max_{\{u_k\}_{k=0}^{N-1}} \min_{i \in \{1, 2, \dots, n_d\}} \psi = \psi(\{u_k\}_{k=0}^{N-1}; x_0, \theta^i) \quad (28a)$$

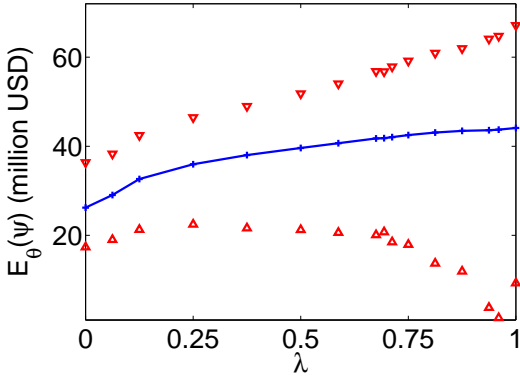
$$s.t. \quad c(\{u_k\}_{k=0}^{N-1}) \leq 0 \quad (28b)$$

Subsequently, KPIs such as the mean, the standard deviation, and the Sharpe ratio may be computed. These KPIs can be used

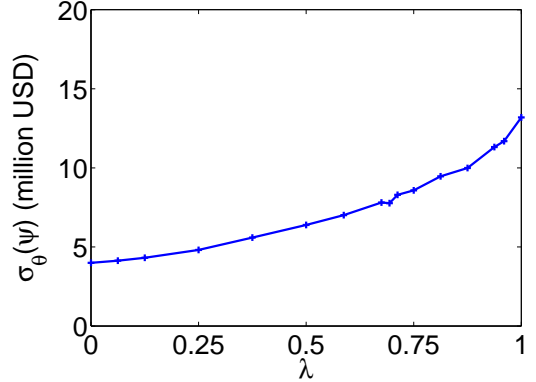
to evaluate and compare the max-min solution to the mean-variance solutions.

6. Conclusions

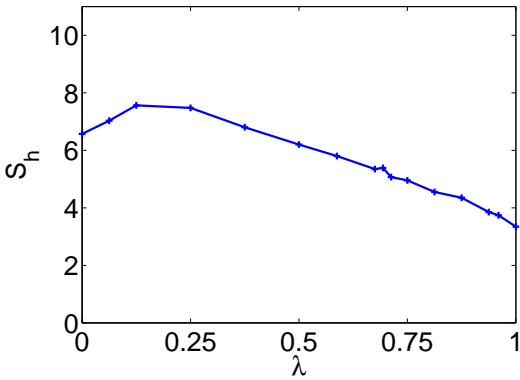
In this paper, we describe a mean-variance approach to risk mitigation in production optimization by open-loop optimal control. The mean-variance approach to risk mitigation is well known in finance and design optimization, but have to our knowledge not been used previously for production optimization of oil reservoirs. By simulation, we demonstrate a computationally tractable method for mean-variance optimal control calculations of a reservoir model consisting of an ensemble of permeability fields. Compared to the RO strategy and the CE strategy, the MV strategy based on the market value of the mean-variance trade-off parameter, λ , is able to reduce risk significantly. This comes at the price of slightly reduced mean



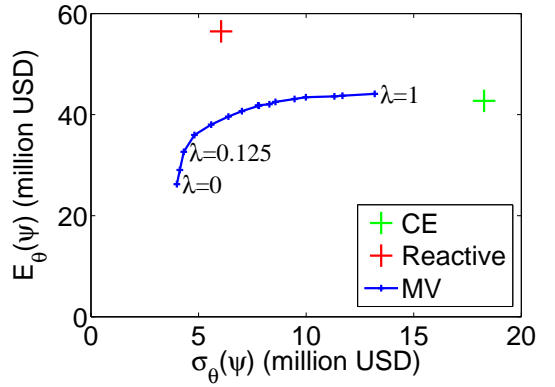
(a) Expected profit, max profit, and min profit.



(b) Risk measured as the standard deviation of profit.



(c) The Sharpe ratio.



(d) A risk-return plot. The expected NPV vs standard deviation of NPV.

Figure 9: Mean-variance relations for Test Case II. Profit (a), risk (b), and Sharpe Ratio (c) for different mean-variance trade-offs, λ . (d) is a phase plot of expected profit vs risk measured as the standard deviation of profit. The blue curve is the efficient frontier. Also the CE and reactive strategy are indicated.

profits. In Test Case II we indicated the importance of feedback. Therefore, future studies should investigate the mean-variance optimal control strategy in a moving horizon closed-loop fashion. Implemented in closed-loop using the moving horizon principle, the optimal control problem for production optimization of an oil reservoir is an example of an Economic Nonlinear Model Predictive Controller (Economic NMPC). Therefore, we believe that the mean-variance objective function introduced in this paper will be of interest to not only production optimization for closed-loop reservoir management but also for Economic NMPC in general. In the future, the mean-variance approach for production optimization should be compared to other methods for stochastic optimization, e.g. conditional-value-at-risk and two-stage stochastic programming, as well as the modified MV strategy that can shut in uneconomical wells (Capolei et al., 2013).

Acknowledgements

This research project is financially supported by the Danish Research Council for Technology and Production Sciences. FTP Grant no. 274-06-0284 and the Center for Integrated Operations in the Petroleum Industry at NTNU.

Appendix A. Computation of the MV Objective and its Gradients

The mean-variance objective function for an ensemble is defined as

$$\psi_{MV} = \lambda \hat{\psi} - (1 - \lambda)\sigma^2 \quad (\text{A.1})$$

Table 3: Key Performance Indicators (KPIs) for Test Case II. The economic KPIs are the expected profit, the standard deviation of the profit, the Sharpe ratio, and the minimum and maximum profit for the ensemble. The reported production related KPIs are the expected oil production, the expected water injection, and the production efficiency, ξ . The productions are normalized by the pore volume. All improvements are relative to the reactive strategy.

Strategy	$\hat{\psi}$		σ		S_h	ψ_{\min}		ψ_{\max}		$E_{\theta}[Q_o]$		$E_{\theta}[Q_{w.inj}]$		ξ
	10 ⁶ USD,	%	10 ⁶ USD,	%		10 ⁶ USD,	%	10 ⁶ USD,	%	,	%	,	%	
Reactive	56.47,	/	6.05,	/	9.33	43.92,	/	70.104,	/	0.35,	/	0.86,	/	39.5
CE	42.72,	-24.35	18.27,	+202.0	2.34	-38.40,	-187.4	72.21,	+3.01	0.26,	-26.0	0.64,	-27.4	40.3
MV														
$\lambda = 1$ (RO)	44.11,	-21.9	13.19,	+118.0	3.34	9.28,	-78.9	67.14,	-4.2	0.23,	-34.9	0.47,	-45.8	47.5
$\lambda = 0.75$	42.52,	-24.7	8.58,	+41.8	4.96	17.93,	-59.2	59.16,	+15.6	0.19,	-44.9	0.33,	-61.9	57.2
$\lambda = 0.5$	39.62,	-29.8	6.39,	+5.6	6.20	21.24,	-51.6	51.82,	-26.1	0.17,	-52.0	0.26,	-70.6	64.6
$\lambda = 0.25$	35.97,	-36.3	4.81,	-20.5	7.48	22.46,	-48.9	46.45,	-33.7	0.15,	-58.0	0.21,	-76.3	70.0
$\lambda = 0.125$	32.64,	-42.2	4.32,	-28.7	7.56	21.29,	-51.5	42.46,	-39.4	0.13,	-62.5	0.18,	-79.6	72.7
$\lambda = 0$	26.23,	-53.5	3.99,	-34.0	6.57	17.37,	-60.5	36.38,	-48.1	0.10,	-71.2	0.12,	-86.1	81.9

with the mean and variances computed by

$$\hat{\psi} = \frac{1}{n_d} \sum_{i=1}^{n_d} \psi^i \quad (\text{A.2a})$$

$$\sigma^2 = \frac{1}{n_d - 1} \sum_{i=1}^{n_d} (\psi^i - \hat{\psi})^2 \quad (\text{A.2b})$$

The gradient, $\nabla_{u_k} \psi_{MV}$ for $k \in \mathcal{N}$, is computed as

$$\nabla_{u_k} \psi_{MV} = \lambda \nabla_{u_k} \hat{\psi} - (1 - \lambda) \nabla_{u_k} \sigma^2 \quad k \in \mathcal{N} \quad (\text{A.3})$$

with the gradient of the mean, $\nabla_{u_k} \hat{\psi}$, computed as

$$\nabla_{u_k} \hat{\psi} = \frac{1}{n_d} \sum_{k=1}^{n_d} \nabla_{u_k} \psi^i \quad (\text{A.4})$$

The gradient of the variance, $\nabla_{u_k} \sigma^2$, is

$$\begin{aligned} \nabla_{u_k} \sigma^2 &= \frac{1}{n_d - 1} \sum_{i=1}^{n_d} \left[\nabla_{u_k} (\psi^i - \hat{\psi})^2 \right] \\ &= \frac{2}{n_d - 1} \sum_{i=1}^{n_d} \left[(\psi^i - \hat{\psi}) \nabla_{u_k} (\psi^i - \hat{\psi}) \right] \\ &= \frac{2}{n_d - 1} \sum_{i=1}^{n_d} \left[(\psi^i - \hat{\psi}) (\nabla_{u_k} \psi^i - \nabla_{u_k} \hat{\psi}) \right] \end{aligned} \quad (\text{A.5})$$

$\nabla_{u_k} \sigma^2$ can be computed by (A.5). To compute $\nabla_{u_k} \sigma^2$ more efficiently we express $\nabla_{u_k} \sigma^2$ as

$$\nabla_{u_k} \sigma^2 = \frac{2}{n_d - 1} \left(\sum_{i=1}^{n_d} \left[(\psi^i - \hat{\psi}) \nabla_{u_k} \psi^i \right] - \sum_{i=1}^{n_d} \left[(\psi^i - \hat{\psi}) \nabla_{u_k} \hat{\psi} \right] \right) \quad (\text{A.6})$$

and note that

$$\begin{aligned} \sum_{i=1}^{n_d} \left((\psi^i - \hat{\psi}) \nabla_{u_k} \psi^i \right) &= \left(\sum_{i=1}^{n_d} (\psi^i - \hat{\psi}) \right) \nabla_{u_k} \hat{\psi} \\ &= \underbrace{\left(\sum_{i=1}^{n_d} \psi^i - n_d \hat{\psi} \right)}_{=0} \nabla_{u_k} \hat{\psi} = 0 \end{aligned}$$

Consequently, the gradient of the variance can be computed efficiently by

$$\nabla_{u_k} \sigma^2 = \frac{2}{n_d - 1} \sum_{i=1}^{n_d} (\psi^i - \hat{\psi}) \nabla_{u_k} \psi^i \quad (\text{A.7})$$

References

- Alhuthali, A.H., Datta-Gupta, A., Yuen, B., Fontanilla, J.P. Optimal rate control under geologic uncertainty. In: SPE/DOE Symposium on Improved Oil Recovery. Tulsa, Oklahoma, USA; volume 3; 2008. p. 1066–1090. SPE-113628-MS.
- Beyer, H.G., Sendhoff, B. Robust optimization - a comprehensive survey. Computer Methods in Applied Mechanics and Engineering 2007;196:3190–3218.
- Biegler, L.T. Solution of dynamic optimization problems by successive quadratic programming and orthogonal collocation. Computers and Chemical Engineering 1984;8:243–248.
- Biegler, L.T. A survey on sensitivity-based nonlinear model predictive control. In: 10th IFAC International Symposium on Dynamics and Control of Process Systems. Mumbai, India; 2013. p. 499–510.
- Binder, T., Blank, L., Bock, H.G., Burlisch, R., Dahmen, W., Diehl, M., Kronseder, T., Marquardt, W., Schlöder, J.P., von Stryk, O.. Introduction to model based optimization of chemical processes on moving horizons. In: Grötschel, M., Krumke, S., Rambau, J., editors. Online Optimization of Large Scale Systems. Berlin: Springer; 2001. p. 296–339.
- Bock, H.G., Plitt, K.J.. A multiple shooting algorithm for direct solution of optimal control problems. In: Proceedings 9th IFAC World Congress Budapest. Pergamon Press; 1984. p. 243–247.
- Brouwer, D.R., Jansen, J.D.. Dynamic optimization of waterflooding with smart wells using optimal control theory. SPE Journal 2004;9(4):391–402. SPE-78278-PA.
- Capolei, A., Jørgensen, J.B.. Solution of constrained optimal control problems using multiple shooting and ESDIRK methods. In: 2012 American Control Conference. 2012. p. 295–300.
- Capolei, A., Stenby, E.H., Jørgensen, J.B.. High order adjoint derivatives using esdirk methods for oil reservoir production optimization. In: EC-MOR XIII, 13th European Conference on the Mathematics of Oil Recovery. 2012a. .
- Capolei, A., Suwardati, E., Foss, B., Jørgensen, J.B.. Waterflooding optimization in uncertain geological scenarios. Computational Geosciences 2013;17(6):991–1013.
- Capolei, A., Völcker, C., Frydendall, J., Jørgensen, J.B.. Oil reservoir production optimization using single shooting and ESDIRK methods. In: Proceedings of the 2012 IFAC Workshop on Automatic Control in Offshore Oil and Gas Production. Trondheim, Norway; 2012b. p. 286–291.

- Chen, Z.. Reservoir Simulation. Mathematical Techniques in Oil Recovery. Philadelphia, USA: SIAM, 2007.
- Chierici, G.L.. Economically improving oil recovery by advanced reservoir management. *Journal of Petroleum Science and Engineering* 1992;8(3):205–219.
- Foss, B.. Process control in conventional oil and gas fields - Challenges and opportunities. *Control Engineering Practice* 2012;20:1058–1064.
- Foss, B., Jensen, J.P.. Performance analysis for closed-loop reservoir management. *SPE Journal* 2011;16(1):183–190. SPE-138891-PA.
- Hansen, P.C.. Rank-Deficient and Discrete II-Posed Problems: Numerical Aspects of Linear Inversion. SIAM, Philadelphia, 1998.
- Heirung, T.A.N., Wartmann, M.R., Jansen, J.D., Ydstie, B.E., Foss, B.A.. Optimization of the water-flooding process in a small 2d horizontal oil reservoir by direct transcription. In: *Proceedings of the 18th IFAC World Congress*. 2011. p. 10863–10868.
- Jansen, J.. Adjoint-based optimization of multi-phase flow through porous media - A review. *Computers & Fluids* 2011;46:40–51.
- Jansen, J.D., Bosgra, O.H., Van den Hof, P.M.J.. Model-based control of multiphase flow in subsurface oil reservoirs. *Journal of Process Control* 2008;18:846–855.
- Jansen, J.D., Douma, S.D., Brouwer, D.R., Van den Hof, P.M.J., Bosgra, O.H., Heemink, A.W.. Closed-loop reservoir management. In: *2009 SPE Reservoir Simulation Symposium*. The Woodlands, Texas, USA; 2009. p. 856–873. SPE 119098-MS.
- Jørgensen, J.B.. Adjoint sensitivity results for predictive control, state- and parameter-estimation with nonlinear models. In: *Proceedings of the European Control Conference 2007*. Kos, Greece; 2007. p. 3649–3656.
- Lazarov, B., Schevenels, M., Sigmund, O.. Topology optimization with geometric uncertainties by perturbation techniques. *International Journal for Numerical Methods in Engineering* 2012;90(11):1321–1336.
- Lie, K.A., Krogstad, S., Ligaarden, I.S., Natvig, J.R., Nilsen, H.M., Skaffestad, B.. Open source matlab implementation of consistent discretisations on complex grids. *Computational Geosciences* 2012;16(2):297–322.
- Liu, Y.. Using the snesim program for multiple-point statistical simulation. *Computers & Geosciences* 2006;32(10):1544–1563.
- Markowitz, H.. Portfolio selection. *The Journal of Finance* 1952;7(1):77–91.
- MATLAB, . version 7.13.0.564 (R2011b). Natick, Massachusetts: The Math-Works Inc., 2011.
- Nævdal, G., Brouwer, D.R., Jansen, J.D.. Waterflooding using closed-loop control. *Computational Geosciences* 2006;10:37–60.
- Peaceman, D.W.. Interpretation of well-block pressures in numerical reservoir simulation with nonsquare grid blocks and anisotropic permeability. *SPE Journal* 1983;23:531–543.
- Ramirez, W.F.. *Application of Optimal Control Theory to Enhanced Oil Recovery*. Elsevier Science Ltd, 1987.
- Sarma, P., Aziz, K., Durlafsky, L.J.. Implementation of adjoint solution for optimal control of smart wells. In: *SPE Reservoir Simulation Symposium*, 31 January-2 February 2005, The Woodlands, Texas. 2005a. p. 67–83.
- Sarma, P., Durlafsky, L., Aziz, K.. Efficient closed-loop production optimization under uncertainty. In: *SPE Europe/EAGE Annual Conference*. Madrid, Spain; 2005b. p. 583–596.
- Schlegel, M., Stockmann, K., Binder, T., Marquardt, W.. Dynamic optimization using adaptive control vector parameterization. *Computers and Chemical Engineering* 2005;29:1731–1751.
- Schölkopf, B., Smola, A., Müller, K.R.. Nonlinear component analysis as a kernel eigenvalue problem. *Neural Computation* 1998;10(5):1299–1319.
- Sharpe, W.F.. The sharpe ratio. *The Journal of Portfolio Management* 1994;21(1):49–58.
- Steinbach, M.C.. Markowitz revisited: Mean-variance models in financial portfolio analysis. *SIAM Review* 2001;43(1):31–85.
- Suwartadi, E., Krogstad, S., Foss, B.. Nonlinear output constraints handling for production optimization of oil reservoirs. *Computational Geosciences* 2012;16:499–517.
- Van Essen, G.M., Van den Hof, P.M.J., Jansen, J.D.. Hierarchical long-term and short-term production optimization. *SPE Journal* 2011;16(1):191–199. SPE-124332-PA.
- Van Essen, G.M., Zandvliet, M.J., Van den Hof, P.M.J., Bosgra, O.H., Jansen, J.D.. Robust waterflooding optimization of multiple geological scenarios. *SPE Journal* 2009;14(1):202–210. SPE-102913-PA.
- Völcker, C., Jørgensen, J.B., Stenby, E.H.. Oil reservoir production optimization using optimal control. In: *50th IEEE Conference on Decision and Control and European Control Conference*. Orlando, Florida; 2011. p. 7937–7943.
- Völcker, C., Jørgensen, J.B., Thomsen, P.G., Stenby, E.H.. Simulation of subsurface two-phase flow in an oil reservoir. In: *Proceedings of the European Control Conference 2009*. Budapest, Hungary; 2009. p. 1221–1226.
- Yasari, E., Pishvaie, M.R., Khorasheh, F., Salahshoor, K., Kharrat, R.. Application of multi-criterion robust optimization in water-flooding of oil reservoir. *Journal of Petroleum Science and Engineering* 2013;109:1–11.

Bibliography

- [1] BP, “Bp statistical review of world energy june 2013,” <http://www.bp.com/statisticalreview>, Tech. Rep., 2013.
- [2] S. Thomas, “Enhanced oil recovery - an overview,” *Oil & Gas Science and Technology*, vol. 63, pp. 9–19, 2008.
- [3] Z. Chen, *Reservoir Simulation. Mathematical Techniques in Oil Recovery*. Philadelphia, USA: SIAM, 2007.
- [4] J. Jansen, “Adjoint-based optimization of multi-phase flow through porous media - A review,” *Computers & Fluids*, vol. 46, pp. 40–51, 2011.
- [5] C. Völcker, “Production optimization of oil reservoirs,” Ph.D. dissertation, Department of Informatics and Mathematical Modeling, Technical University of Denmark, 2011.
- [6] C. Völcker, J. B. Jørgensen, P. G. Thomsen, and E. H. Stenby, “Simulation of subsurface two-phase flow in an oil reservoir,” in *Proceedings of the European Control Conference 2009*, Budapest, Hungary, August 23-26 2009, pp. 1221–1226.
- [7] —, “Explicit singly diagonally implicit Runge-Kutta methods and adaptive stepsize control for reservoir simulation,” in *ECMOR XII - 12th European Conference on the Mathematics of Oil Recovery*, Oxford, UK, 6-9 September 2010 2010.
- [8] C. Völcker, J. B. Jørgensen, and E. H. Stenby, “Oil reservoir production optimization using optimal control,” in *50th IEEE Conference on Decision and Control and European Control Conference*, Orlando, Florida, December 12-15 2011, pp. 7937–7943.

- [9] K. A. Lie, S. Krogstad, I. S. Ligaarden, J. R. Natvig, H. M. Nilsen, and B. Skaflestad, "Open source matlab implementation of consistent discretisations on complex grids," *Computational Geosciences*, vol. 16, no. 2, pp. 297–322, 2012.
- [10] E. Suwartadi, "Gradient-based methods for production optimization of oil reservoirs," Ph.D. dissertation, Department of Engineering Cybernetics, Norwegian University of Science and Technology, 2012.
- [11] D. Brouwer, G. Nævdal, and J. Jansen, "Improved reservoir management through optimal control and continuous model updating," in *SPE Annual Technical Conference and Exhibition*, Houston, Texas, September 2004.
- [12] D. R. Brouwer and J. D. Jansen, "Dynamic optimization of waterflooding with smart wells using optimal control theory," *SPE Journal*, vol. 9, no. 4, pp. 391–402, 2004.
- [13] P. Sarma, L. Durlofsky, and K. Aziz, "Efficient closed-loop production optimization under uncertainty," in *SPE Europec/EAGE Annual Conference*, Madrid, Spain, June 2005.
- [14] G. Nævdal, D. R. Brouwer, and J.-D. Jansen, "Waterflooding using closed-loop control," *Computational Geosciences*, vol. 10, pp. 37–60, 2006.
- [15] J.-D. Jansen, O. H. Bosgra, and P. M. J. Van den Hof, "Model-based control of multiphase flow in subsurface oil reservoirs," *Journal of Process Control*, vol. 18, pp. 846–855, 2008.
- [16] J. D. Jansen, S. D. Douma, D. R. Brouwer, P. M. J. Van den Hof, O. H. Bosgra, and A. W. Heemink, "Closed-loop reservoir management," in *2009 SPE Reservoir Simulation Symposium*, no. SPE 119098, The Woodlands, Texas, USA, 2–4 February 2009.
- [17] R. J. Lorentzen, A. Shafieirad, and G. Nævdal, "Closed loop reservoir management using the ensemble Kalman filter and sequential quadratic programming," in *2009 SPE Reservoir Simulation Symposium*, no. SPE 119101, The Woodlands, Texas, USA, 24 February, 2009 2009.
- [18] B. Foss and J. P. Jensen, "Performance analysis for closed-loop reservoir management," *SPE Journal*, vol. 16, no. 1, pp. 183–190, 2011.
- [19] A. Capolei, E. H. Stenby, and J. B. Jørgensen, "High order adjoint derivatives using esdirk methods for oil reservoir production optimization," in *ECMOR XIII, 13th European Conference on the Mathematics of Oil Recovery*, 2012.
- [20] P. M. J. Van den Hof, J. D. Jansen, and A. Heemink, "Recent developments in model-based optimization and control of subsurface flow in oil reservoirs," in *Proceedings of the 2012 IFAC Workshop on Automatic Control in Offshore*

- Oil and Gas Production*, Trondheim, Norway, May 31 - June 1, 2012 2012, pp. 189–200.
- [21] A. Capolei, C. Völcker, J. Frydendall, and J. B. Jørgensen, “Oil reservoir production optimization using single shooting and ESDIRK methods,” in *Proceedings of the 2012 IFAC Workshop on Automatic Control in Offshore Oil and Gas Production*, Trondheim, Norway, May 31 - June 1, 2012 2012, pp. 286–291.
- [22] B. Foss, “Process control in conventional oil and gas fields - Challenges and opportunities,” *Control Engineering Practice*, vol. 20, pp. 1058–1064, 2012.
- [23] J. B. Rawlings and D. Q. Mayne, *Model Predictive Control: Theory and Design*. Madison, WI: Nob Hill Publishing, 2009.
- [24] L. Grüne and J. Pannek, *Nonlinear Model Predictive Control. Theory and Algorithms*. London, GB: Springer, 2011.
- [25] M. Grötschel, S. O. Krumke, and J. Rambau, Eds., *Online Optimization of Large Scale Systems*. Heidelberg, Germany: Springer, 2001.
- [26] F. Allgöwer and A. Zheng, Eds., *Nonlinear Model Predictive Control*, ser. Progress in Systems and Control Theory. Basel, Switzerland: Birkhäuser, 2000, vol. 26.
- [27] R. Findeisen, F. Allgöwer, and L. T. Biegler, Eds., *Assessment and Future Directions of Nonlinear Model Predictive Control*, ser. Lecture Notes in Control and Information Sciences. Heidelberg, Germany: Springer, 2007, vol. 358.
- [28] L. Magni, D. M. Raimondo, and F. Allgöwer, Eds., *Nonlinear Model Predictive Control. Towards New Challenging Applications*, ser. Lecture Notes in Control and Information Sciences. Heidelberg, Germany: Springer, 2009, vol. 384.
- [29] M. Lazar and F. Allgöwer, Eds., *4th IFAC Nonlinear Model Predictive Control Conference (NMPC'12)*. Noordwijkerhout, NL: IFAC, August 23-27, 2012 2012.
- [30] G. Evensen, *Data Assimilation: The Ensemble Kalman Filter*, 2nd ed. Springer, 2009.
- [31] L. T. Biegler, O. Ghattas, M. Heinkenschloss, and B. van Bloemen Waanders, Eds., *Large-Scale PDE-Constrained Optimization*. Springer, 2003.
- [32] L. T. Biegler, O. Ghattas, M. Heinkenschloss, D. Keyes, and B. van Bloemen Waanders, Eds., *Real-Time PDE-Constrained Optimization*. SIAM, 2007.
- [33] D. E. Ciaurri, T. Mukerji, and L. J. Durlofsky, “Derivative-free optimization for oil field operations,” in *Computational Optimization and Applications in Engineering and Industry Studies in Computational Intelligence*. Springer, 2011.

- [34] Y. Chen, D. S. Oliver, and D. Zhang, "Efficient ensemble-based closed-loop production optimization," *SPE Journal*, vol. 14, no. 4, pp. 634–645, 2009.
- [35] H.-J. Su and D. S. Oliver, "Smart well production optimization using an ensemble-based method," *SPE Reservoir Evaluation & Engineering*, vol. 13, pp. 884–892, 2010.
- [36] J. B. Jørgensen, "Moving horizon estimation and control," Ph.D. dissertation, Technical University of Denmark, Department of Chemical Engineering, 2005.
- [37] A. F. Bennett, *Inverse Modelling of the Ocean and Atmosphere*. Cambridge University Press, 2002.
- [38] J. R. Valstar, D. B. McLaughlin, C. B. M. T. Stroet, and F. C. van Geer, "A representer-based inverse method for groundwater flow and transport applications," *Water Resources Research*, vol. 40, 2004.
- [39] G. Chavent, M. Dupuy, and P. Lemonnier, "History matching by use of optimal theory," *SPE Journal*, vol. 15, pp. 74–86, 1975.
- [40] Z. Wu, A. Reynolds, and D. Oliver, "Conditioning geostatistical models to two-phase production data," *SPE Journal*, vol. 4, pp. 142–155, 1999.
- [41] O. Talagrand and P. Courtier, "Variational assimilation of meteorological observations with the adjoint vorticity equation. i: Theory," *Quarterly Journal of the Royal Meteorological Society*, vol. 113, pp. 1311–1328, 1987.
- [42] P. Courtier, "Dual formulation of four-dimensional variational assimilation," *Quarterly Journal of the Royal Meteorological Society*, vol. 123, pp. 2449–2461, 1997.
- [43] R. E. Kalman, "A new approach to linear filtering and predictions problems," *Journal of Basic Engineering*, vol. 82, pp. 35–45, 1960.
- [44] G. Evensen, "The ensemble kalman filter: theoretical formulation and practical implementation," *Ocean Dynamics*, vol. 53, no. 4, pp. 342–367, 2003.
- [45] C. Chen, Y. Wang, G. Li, and A. C. Reynolds, "Closed-loop reservoir management on the Brugge test case," *Computational Geosciences*, vol. 14, no. 4, pp. 691–703, 2010.
- [46] L. Peters, R. J. Arts, G. K. Brouwer, C. R. Geel, S. Cullick, R. Lorentzen, Y. Chen, K. Dunlop, F. C. Vossepoel, R. Xu, P. Sarma, A. H. Alhuthali, and A. C. Reynolds, "Results of the Brugge benchmark study for flooding optimization and history matching," *SPE Reservoir Evaluation & Engineering*, vol. 13, no. 3, pp. 391–405, 2010.

- [47] X.-H. Wen and W. H. Chen, "Some practical issues on real-time reservoir model updating using ensemble Kalman filter," *SPE Journal*, vol. 12, no. 2, pp. 156–166, June 2007.
- [48] M. Ehrendorfer, "A review of issues in ensemble-based Kalman filtering," *Meteorologische Zeitschrift*, vol. 16, no. 6, pp. 795–818, December 2007.
- [49] S. I. Aanonsen, G. Nævdal, D. S. Oliver, A. C. Reynolds, and B. Vallés, "The ensemble Kalman filter in reservoir engineering - a review," *SPE Journal*, vol. 14, no. 3, pp. 393–412, 2009.
- [50] D. Simon, *Optimal State Estimation. Kalman, H_∞ , and Nonlinear Approaches*. Hoboken, New Jersey, USA: Wiley, 2006.
- [51] J. B. Rawlings and B. R. Bakshi, "Particle filtering and moving horizon estimation," *Computers and Chemical Engineering*, vol. 30, pp. 1529–1541, 2006.
- [52] X.-H. Wen and W. H. Chen, "Real-time reservoir model updating using ensemble Kalman filter with confirming option," *SPE Journal*, vol. 11, no. 4, pp. 431–442, 2006.
- [53] P. Sarma and W. Chen, "Preventing ensemble collapse and preserving geostatistical variability across the ensemble with the subspace enkf," in *ECMOR XIII - 13th European Conference on the Mathematics of Oil Recovery*, Biarritz, France., 2012.
- [54] P. Sarma and W. H. Chen, "Robust and efficient handling of model constraints with the kernel-based ensemble kalman filter," in *Reservoir Simulation Symposium*, The Woodlands, Texas, USA, 2011.
- [55] P. Sarma and W. Chen, "Generalization of the ensemble kalman filter using kernels for nongaussian random fields," in *SPE Reservoir Simulation Symposium*, The Woodlands, Texas, 2009.
- [56] A. Capolei, E. Suwartadi, B. Foss, and J. B. Jørgensen, "Waterflooding optimization in uncertain geological scenarios," *Computational Geosciences*, September 2013, published online.
- [57] E. Suwartadi, S. Krogstad, and B. Foss, "Nonlinear output constraints handling for production optimization of oil reservoirs," *Computational Geosciences*, vol. 16, pp. 499–517, 2012.
- [58] G. M. Van Essen, M. J. Zandvliet, P. M. J. Van den Hof, O. H. Bosgra, and J. D. Jansen, "Robust waterflooding optimization of multiple geological scenarios," *SPE Journal*, vol. 14, no. 1, pp. 202–210, 2009.
- [59] H. Markowitz, "Portfolio selection," *The Journal of Finance*, vol. 7, no. 1, pp. 77–91, 1952.

- [60] M. C. Steinbach, "Markowitz revisited: Mean-variance models in financial portfolio analysis," *SIAM Review*, vol. 43, no. 1, pp. 31–85, 2001.
- [61] B. Lazarov, M. Schevenels, and O. Sigmund, "Topology optimization with geometric uncertainties by perturbation techniques," *International Journal for Numerical Methods in Engineering*, vol. 90, no. 11, pp. 1321–1336, 2012.
- [62] H. G. Beyer and B. Sendhoff, "Robust optimization - a comprehensive survey," *Computer Methods in Applied Mechanics and Engineering*, vol. 196, pp. 3190–3218, 2007.
- [63] W. W. Hager, "Runge-kutta methods in optimal control and the transformed adjoint system," *Numerische Mathematik*, vol. 87, pp. 247–282, 1999.
- [64] A. Sandu, "On the properties of Runge-Kutta discrete adjoints," in *International Conference for Computational Science*. Springer-Verlag Berlin Heidelberg, 2006, pp. 550–557.
- [65] P. Sarma, K. Aziz, and L. J. Durlofsky, "Implementation of adjoint solution for optimal control of smart wells," in *SPE Reservoir Simulation Symposium, 31 January-2 February 2005, The Woodlands, Texas, 2005*.
- [66] Y. Cao, S. Li, L. Petzold, and R. Serban, "Adjoint sensitivity analysis for differential-algebraic equations: The adjoint DAE system and its numerical solution," *SIAM Journal on Scientific Computing*, vol. 24, no. 3, pp. 1076–1089, 2002.
- [67] D. Kourounis, D. Voskov, and K. Aziz, "Adjoint methods for multicomponent flow simulation," in *12th European Conference on the Mathematics of Oil Recovery*, Oxford, UK, 2010.
- [68] S. K. Nadarajah and A. Jameson, "Optimum shape design for unsteady flows with time-accurate continuous and discrete adjoint methods," *AIAA Journal*, vol. 45, no. 7, pp. 1478–1491, 2007.
- [69] Y. Chen and D. S. Oliver, "Ensemble-based closed-loop optimization applied to Brugge field," *SPE Reservoir Evaluation & Engineering*, vol. 13, no. 1, pp. 56–71, 2010.
- [70] A. H. Alhuthali, A. Datta-Gupta, B. Yuen, and J. P. Fontanilla, "Optimal rate control under geologic uncertainty," in *SPE/DOE Symposium on Improved Oil Recovery*, Tulsa, Oklahoma, USA, April 2008.
- [71] E. Yasari, M. R. Pishvaie, F. Khorasheh, K. Salahshoor, and R. Kharrat, "Application of multi-criterion robust optimization in water-flooding of oil reservoir," *Journal of Petroleum Science and Engineering*, vol. 109, pp. 1–11, 2013.

- [72] K. Aziz and A. Settari, *Petroleum reservoir simulation*. Applied Science Publishers, 1979.
- [73] Z. Chen, G. Huan, and Y. Ma, *Computational Methods for Multiphase Flows in Porous Media*. SIAM, 2006.
- [74] E. D. Holstein, Ed., *Petroleum Engineering Handbook, Volume V: Reservoir Engineering and Petrophysics*. Society of Petroleum Engineers, 2007.
- [75] D. W. Peaceman, "Interpretation of well-block pressures in numerical reservoir simulation with nonsquare grid blocks and anisotropic permeability," *SPE Journal*, vol. 23, pp. 531–543, 1983.
- [76] J. T. Betts, *Practical Methods for Optimal Control Using Nonlinear Programming*. SIAM, 2001.
- [77] D. E. Kirk, *Optimal Control Theory: An Introduction*. Dover Publications, 2004.
- [78] M. Schlegel, K. Stockmann, T. Binder, and W. Marquardt, "Dynamic optimization using adaptive control vector parameterization," *Computers and Chemical Engineering*, vol. 29, pp. 1731–1751, 2005.
- [79] A. Capolei and J. B. Jørgensen, "Solution of constrained optimal control problems using multiple shooting and ESDIRK methods," in *2012 American Control Conference*, 2012, pp. 295–300.
- [80] H. G. Bock and K. J. Plitt, "A multiple shooting algorithm for direct solution of optimal control problems," in *In Proceedings 9th IFAC World Congress Budapest*. Pergamon Press, 1984, pp. 243–247.
- [81] L. T. Biegler, "Solution of dynamic optimization problems by successive quadratic programming and orthogonal collocation," *Computers and Chemical Engineering*, vol. 8, pp. 243–248, 1984.
- [82] J. Nocedal and S. J. Wright, *Numerical Optimization*. Springer, 2000.
- [83] S. Boyd and L. Vandenberghe, *Convex Optimization*. Cambridge University Press, 2004.
- [84] R. H. Byrd, J. Nocedal, and R. A. Waltz, "KNITRO: An integrated package for nonlinear optimization," in *Large Scale Nonlinear Optimization*, 2006.
- [85] MATLAB, *version 7.13.0.564 (R2011b)*. Natick, Massachusetts: The MathWorks Inc., 2011.
- [86] T. Kailath, A. H. Sayed, and B. Hassibi, *Linear Estimation*, T. Kailath, Ed. Prentice Hall, 2000.

- [87] A. H. Jazwinski, *Stochastic Processes and Filtering Theory*. Academic Press, 1970.
- [88] G. Burgers, P. J. van Leeuwen, and G. Evensen, "Analysis scheme in the ensemble kalman filter," *Monthly Weather Review*, vol. 126, no. 6, pp. 1719–1724, 1998.
- [89] X. H. Wen and W. Chen, "Real-time reservoir model updating using ensemble Kalman filter," in *SPE Reservoir Simulation Symposium*, The Woodlands, Texas, 2005.
- [90] Y. Gu and D. S. Oliver, "History matching of the punq-s3 reservoir model using the ensemble kalman filter," *SPE Journal*, vol. 10, no. 2, pp. 217–224, 2005.
- [91] R. Alexander, "Diagonally implicit runge-kutta methods for stiff O.D.E's," *SIAM Journal on Numerical Analysis*, vol. 14, pp. 1006–1021, 1977.
- [92] A. Kværnø, "Singly diagonally implicit runge-kutta methods with an explicit first stage," *BIT Numerical Mathematics*, vol. 44, n. 3, pp. 489–502, 2004.
- [93] M. R. Kristensen, M. G. Gerritsen, P. G. Thomsen, M. L. Michelsen, and E. H. Stenby, "Efficient integration of stiff kinetics with phase change detection for reactive reservoir processes," *Transport in Porous Media*, vol. 69, no. 3, pp. 383–409, 2007.
- [94] M. H. Carpenter, S. A. Viken, and E. J. Nielsen, "The efficiency of high order temporal schemes," *41st Aerospace Sciences Meeting and Exhibit*, 2003.
- [95] M. Tabesh and D. W. Zingg, "Efficient implicit time-marching methods using a newton-krylov algorithm," *47th AIAA Aerospace Sciences Meeting Including The New Horizons Forum and Aerospace Exposition*, 2009.
- [96] J. B. Jørgensen, Kristensen, M. R., Thomsen, and P. G., "A family of esdirk integration methods," *Submitted to SIAM Journal on Scientific Computing*, 2008.
- [97] M. R. Kristensen, J. B. Jørgensen, P. G. Thomsen, and S. B. Jørgensen, "An esdirk method with sensitivity analysis capabilities," *Computers and Chemical Engineering*, vol. 28(12), pp. 2695–2707, 2004.
- [98] M. R. Kristensen, J. B. Jørgensen, P. G. Thomsen, M. L. Michelsen, and S. B. Jørgensen, "Sensitivity analysis in index-1 differential algebraic equations by ESDIRK methods," in *16th IFAC World Congress*, Prague, 2005.
- [99] L. O. Jay, "Inexact simplified newton iterations for implicit runge-kutta methods," *SIAM Journal on Numerical Analysis*, vol. 38, no. 4, pp. 1369–1388, 2001.
- [100] W. F. Feehery, J. E. Tolsma, and P. I. Barton, "Efficient sensitivity analysis of large-scale differential-algebraic systems," *Applied Numerical Mathematics*, vol. 25, pp. 41–54, 1997.

- [101] H. G. Bock, "Numerical treatment of inverse problems in chemical reaction kinetics," *Modelling of Chemical Reaction Systems*. (Ebert, K.H. Deuffhard, P., Jäger, W. Eds) *Springer Series in Chemical Physics*, vol. 18, 1981.
- [102] K. Gustafsson, "Control of error convergence in ode solvers," Ph.D. dissertation, Department of automatic control, Lund Institute of Technology, 1992.
- [103] K. E. Brenan, S. L. Campbell, and L. R. Petzold, *Numerical Solution of Initial-Value Problems in Differential-Algebraic Equations*. Siam, 1996.
- [104] A. Capolei, E. Suwartadi, B. Foss, and J. B. Jørgensen, "A mean-variance objective for robust production optimization in uncertain geological scenarios," *Journal of Petroleum Science and Engineering*, 2013, in preparation.
- [105] W. F. Sharpe, "The sharpe ratio," *The Journal of Portfolio Management*, vol. 21, no. 1, pp. 49–58, 1994.
- [106] Y. Liu, "Using the snesim program for multiple-point statistical simulation," *Computers & Geosciences*, vol. 32, no. 10, pp. 1544–1563, 2006.
- [107] B. Schölkopf, A. Smola, and K.-R. Müller, "Nonlinear component analysis as a kernel eigenvalue problem," *Neural Computation*, vol. 10, no. 5, pp. 1299–1319, Jul. 1998.
- [108] V. Dehdari and D. S. Oliver, "Sequential quadratic programming for solving constrained production optimization – case study from Brugge field," *SPE Journal*, vol. 17, pp. 874–884, September 2012.
- [109] P. C. Hansen, *Rank-Deficient and Discrete Ill-Posed Problems: Numerical Aspects of Linear Inversion*. SIAM, Philadelphia, 1998.
- [110] *General Purpose Research Simulator*, SUPRI-B: RESERVOIR SIMULATION research group at Stanford University Std., 2013.
- [111] R. Klöfkorn, "Numerics for evolution equations - a general interface based design concept," Ph.D. dissertation, Albert-Ludwigs-Universität Freiburg, 2009.
- [112] J. Kraaijevanger, P. Egberts, J. Valstar, and H. Buurman, "Optimal waterflood design using the adjoint method," in *SPE Reservoir Simulation Symposium*. Houston, Texas, U.S.A.: Society of Petroleum Engineers, February 2007.
- [113] D. S. Oliver, A. C. Reynolds, and N. Liu, *Inverse Theory for Petroleum Reservoir Characterization and History Matching*. Cambridge University Press, 2008.
- [114] J. B. Jørgensen, "Adjoint sensitivity results for predictive control, state- and parameter-estimation with nonlinear models," in *Proceedings of the European Control Conference 2007*, Kos, Greece, 2007, pp. 3649–3656.